MERCURY CYCLING IN THE ROCKY MOUNTAINS: SOURCES, FATES, AND CLIMATE CHANGE IMPACTS

by

HANNAH ROSE MILLER

B.A., Bowdoin College, 2017

A thesis submitted to the

Faculty of the Graduate School of the

University of Colorado in partial fulfillment

of the requirement for the degree of

Doctor of Philosophy

Department of Ecology and Evolutionary Biology

2025

Committee Members:

Eve-Lyn S. Hinckley

Sarah E. Janssen

Charles T. Driscoll

Scott A. Taylor

Julian Resasco

Miller, Hannah Rose (Ph.D., Ecology and Evolutionary Biology)

Mercury Cycling in the Rocky Mountains: Sources, Fates, and Climate Change Impacts

Thesis directed by Associate Professor Eve-Lyn S. Hinckley

Humans have dramatically accelerated mercury (Hg) cycling in ecosystems across the globe due to anthropogenic activities. Depending on the speciation and concentration of Hg, exposure to this metal can cause a variety of health problems, which has led to significant research and regulation efforts to reduce the use and release of Hg. Despite these global and regional efforts, Hg will continue cycling at elevated levels for thousands of years due to its persistent nature. Continued cycling of Hg following its initial release is now of significant concern since around two-thirds of annual Hg emissions are from remobilized pools of Hg.

The goal of my research is to advance understanding of how mountain ecosystems cycle Hg and how that may change under a warming climate. First, I synthesized the recent literature on Hg cycling in mountain ecosystems with a focus on the U.S. Rocky Mountains. I identified primary Hg sources, storage, transformations, and losses, as well as impacts from climate change. I also highlighted important knowledge gaps and proposed future research priorities. Based on the gaps that I identified in my synthesis, I next characterized Hg inputs, storage, and bioaccumulation along an elevation gradient in the Colorado Rocky Mountains. Similar to past work conducted in the eastern U.S. Himalaya, and Tibetan Plateau, I found that elevation and tree cover are important drivers of Hg inputs and storage in mountain ecosystems. Unlike those past studies, however, I found that precipitation, rather than litterfall, dominated atmospheric inputs of Hg and was the primary driver of Hg bioaccumulation in terrestrial wildlife. Next, to

assess the impact of climate change on the toxicity and bioavailability of Hg, I measured rates of methylmercury (MeHg) formation in alpine and subalpine wetlands under increasing sulfate concentrations. I found that MeHg formation in subalpine peatlands in the North Boulder Watershed of the Colorado Rocky Mountains are sulfate-limited. This watershed has experienced a 200 % increase in sulfate concentrations over the past 30 years—a pattern observed in over 100 high elevation watersheds globally—due to climate-driven sulfate weathering associated with thawing permafrost and rock glacier features. This increased export of sulfate may accelerate MeHg production and bioaccumulation in sulfate-limited high elevation watersheds. Finally, synthesizing information on Hg inputs, storage, and losses, I characterized the sink-source behavior of alpine and subalpine zones in the North Boulder Watershed to better constrain the role that mountain ecosystems play in cycling legacy Hg pools. I found that these regions act as sinks for Hg, however, major uncertainties exist with regards to losses via evasion. This factor is particularly relevant for the coniferous subalpine zone. My findings highlight the importance of better constraining losses of Hg in evasion from soil and snow surfaces to more accurately quantify the sink-source nature of mountains regions currently, as well as under future warming conditions. Altogether, the results of this body of research advance our understanding of the critical role that mountain ecosystems play in the global Hg cycle and underscore key priorities for future research to address remaining uncertainties, particularly in the context of climate change.

DEDICATION

To the land that raised me

ACKNOWLEDGMENTS

So much of where I am today is thanks to my sibling Kait Miller who carved out a path for both of us from unschooling to college, and then strongly encouraged me to take an oceanography course my first year of undergrad. That class changed how I see the Earth and welcomed me into the world of biogeochemistry.

I have so many gratitudes for the people, places, and experiences that have brought me growth and joy during my dissertation. First, thank you to Eve for providing guidance, encouragement, and friendship, as well as space for me to develop as a whole human during my dissertation. I am particularly grateful for our time getting lost on bikes together in France, your hand-knit sweater with the hood, and Snow Mountain Ranch skis.

To my committee members: Sarah thank you for welcoming me with open arms into the U.S. Geological Survey Mercury Research Lab and providing me unending knowledge regarding mercury analysis and data interpretation. Charley, thank you for your steady guidance and warm encouragement throughout this whole process. Your "snowball's chance in hell" quote will stay with me forever. Scott, thank you for allowing me to sample chickadees with your group and for being someone who has helped make the academic space feel more welcoming and safe to me. Julian, thank you for sharing your insect knowledge and ecological perspective. I am honored to have worked with all of you.

This research would not have been possible without substantial lab and field assistance from numerous colleagues and friends. Thank you to all of the UGSG Mercury Research Lab scientists including Sarah Janssen, David Krabbenhoft, Jacob Ogorek, Michael Tate, Tylor Rosera, Laura Flucke, and Grace Armstrong. My dissertation simply would not have happened without the opportunity to analyze my samples at your lab and without your tireless trouble shooting and question

answering. Thank you to Wendy Roth for lab assistance at CU Boulder and for always keeping snacks and tea for the graduate students. Thank you to Molly Huber, Clifford Adamchak, Edward Riccio, Phil Guerry Thornton, Sammy Yevak, Jenna Maddock, Doug Castro, Luca Raulerson, and Sarah Abramson for fieldwork help ranging from repetitive soil sampling to full days chasing birds across the tundra (mostly unsuccessfully).

Thank you to all of my collaborators and co-authors. The Niwot Ridge LTER community was particularly crucial in helping with my fieldwork. Jen Morse, Kris Hess, Sammy Yevak, Sander Aplet, and Austin Willbern, I have so much gratitude for all your help transporting field equipment, checking on samplers for me, and helping me navigate longs days in the alpine safely. In addition, thank you to the other graduate students and field technicians who made the Niwot Ridge community a engaging, fun place to conduct my research. Thank you to the Boulder Open Space and Mountain Parks, particularly Ann Lezberg, for helping me with sample collection. Thank you to Laura Alison Nash for her incredible writing support. I learned so much from you and will continue to carry your science enthusiasm and writing smarts with me into the future.

This work would not have been half as successful or fun without my EeeBeeGeebies: Anna Hermes, Joel Singley, Molly Huber, Jessica Rush, Laura Rea, Clifford Adamchak, Douglas Castro, and Zachary Shwartz. You all brought so much laughter, learning, and ridiculousness into my graduate experience that means the world to me. Anna and Joel, thank you for welcoming me warmly into graduate school and continuing to provide me with advice 6 years later. Molly, there is no one else I would've wanted to start this whole adventure with—thank you for all the skin care advice and long shared lab and field days. Cliff, it has been such a pleasure working with you from your senior honors thesis in undergrad to now

having you as my mercury, beaver believer buddy. Zach, thank you for your constant bits and also the kindness and openness you bring into the spaces you exist in. Dougdoug, it was a lucky day when you joined our group, and I am so deeply grateful for your smarts, friendship, and dad jokes. Laura, thank you for always keeping the tea kettle warm and for your goofiness. And Jesse, thank you for being my fellow book-worm and keeping our group in line in the office and the lab.

Many dear friends have provided unending support, humor, and care throughout this process: Jenna Maddock who read my class readings aloud to me my first semester while I was recovering from a concussion and for spending hours clearing a field of snow to find buried soil sample bags; Sam Walkes for helping me develop my love of science and research in undergrad and then sharing work zooms and book chats over the past 6 years; Sam Shaheen for being a wonderful biogeochemistry and cross country skiing buddy; Chris Swomley and Jayce Moe for welcoming me into their lives while I plugged away at lab work in Madison, WI; Stacie DeSousa for your humor and down-to-earth approach to life—I couldn't have gotten this far without our poop conversations; and finally to my Picklebric Family who has given me a secure home base and taught me what it is to love, and be loved, well.

Thank you to Jaci Hull, Olivia Shay, Elizabeth Schmidt, Jay Harpp, and Germaine Weaver for caring for my body and soul throughout this whole process.

To Mama, you tuned my eye to the small beauties of this world from an unusual cloud formation to a tree growing directly from a boulder. These are joys I still carry with me and helped spark my curiosity in the natural world. Biogeochemistry helps me trust that the love I send you planting Cosmos each spring reaches you in falling autumn leaves from the old Maple. To my dad, thank you for always supporting my random interests from dairy farming to wood carving

and giving me the time and skills needed to develop my love and comfort of playing outside. To Daryl, thank you for being a rock I can lean on for unconditional support and love. Thank you to the Lanphers / Doanes / Blakelys, Chris Swomley, Jayce Moe, and Luca Raulerson for being my splendid chosen family.

To Michèle LaVigne, Eve-Lyn Hinckley, Sarah Janssen, and Tamar Barkay, thank you for setting stunning examples of being kickass biogeofeminists and for helping me feel like I belong here.

This research was funded by a number of grant awards, including National Science Foundation (NSF) DGE 2040434 and DEB 2224439. A number of awards from the University of Colorado Boulder Environmental Studies Program, Ecology and Evolutionary Biology Department, and Graduate School made research supplies and travel possible. Additional funding was awarded from the National Geographic Society Early Career Award, Geological Society of America Graduate Student Research Grant, and the American Water Resources Association.

Finally, I acknowledge that this research occurred on the traditional, ancestral, and contemporary occupied lands of Indigenous peoples and that mercury pollution is the direct result of colonization. Thank you to the researchers, activists, and politicians who are centering anti-colonialism and the many ways of knowing and connecting to the Earth systems of which are a part.

CONTENTS

CHAPTER

TABLES

FIGURES

CHAPTER I

INTRODUCTION AND BACKGROUND

Human activities have dramatically accelerated the cycling of mercury (Hg) in ecosystems globally (UN Environment, 2019). A geogenic metal, Hg is released naturally during bedrock erosion and volcanic activity (Selin, 2009). Since the industrial-era, the release of Hg from anthropogenic sources such as coal combustion, mining, and other industrial practices has increased significantly (Streets et al., 2019). As a result, concentrations of gaseous elemental Hg in the atmosphere and ocean are 450% and 230% higher than pre-industrial levels, respectively (Outridge et al., 2018). Depending on the form and concentration of Hg, exposure to this metal can cause a variety of health problems for humans and ecosystems (Basu et al., 2022; Chételat et al., 2020), which has led to a rich history of research and regulation to reduce the use and release of Hg globally (Bank, 2020). Despite these efforts, Hg contamination remains a serious issue for ecosystems globally; due to its persistent nature, Hg can cycle within Earth's ecosystems for thousands of years before sequestration in deep ocean sediments or stable soil pools (Amos et al., 2013; Selin et al., 2008).

This continued cycling of Hg following its initial release is now of significant concern. Approximately two-thirds of annual Hg emissions to the atmosphere are from remobilization of existing or "legacy" pools of Hg in soil and waterbodies (Amos et al., 2013; Outridge et al., 2018). Thus, constraining the source-sink behavior of Hg and potential for production of methylmercury (MeHg) within different ecosystems is critically important to better understand not only baseline Hg cycling and health risks for communities, but also how Hg cycling and contamination will shift with ongoing climate change and other drivers that affect its fate.

Mercury occurs in a variety of forms with different levels of toxicity and ecosystem mobility. Gaseous elemental Hg (Hg(0)) is the most abundant form of Hg in the atmosphere with a lifetime of about 0.5–1 year (Gustin et al., 2015). Due to its long residence time, Hg(0) can undergo long-range transport and reach remote ecosystems far from the original source (Dastoor et al., 2022). Atmospheric deposition of Hg can occur via dry or wet deposition. Dry atmospheric deposition is dominated by stomatal Hg(0) uptake by vegetation and transfer to soils via litterfall (Zhou et al., 2021). Oxidization and partitioning of Hg into divalent (Hg(II)) and particulate forms (Hg(P)), respectively, also contribute to transfer of Hg from the atmosphere to the biosphere. Oxidized Hg is more soluble in water compared to Hg(0), and, therefore, typically dominates Hg transfer in precipitation (Lyman et al., 2020). Additionally, due to its ionic character, oxdized Hg can sorb directly onto vegetation and soil surfaces, thereby contributing additional dry deposition to the land surface.

Soils make up the largest global Hg pool followed by the oceans and the atmosphere (Outridge et al., 2018). Mercury in soils is comprised mostly of Hg(II) which binds tightly to soil organic matter helping to retain Hg within the soil matrix (Bishop et al., 2020; C. I. Olson et al., 2022). While this form of Hg has relatively low toxicity, when it is transported via runoff to—or is directly deposited into—portions of the landscape that experience wetting and drying cycles, or are anoxic (e.g., soils and waters of lakes and wetlands), it can be methylated into its organic form, methylmercury (MeHg; Bishop et al., 2020). A potent neurotoxin, MeHg bioaccumulates and biomagnifies in food webs and is the form of Hg that typically drives exposure in humans and wildlife (Chételat et al., 2020).

Methylmercury contamination has caused acute, localized impacts as well as long-term, global effects on human communities and ecosystems, shaping research

and policy efforts over the past half a century. The period from the 1950s–1970s was characterized by point source, industrial contamination with multiple high profile poisoning incidents that drew the world's attention to the risks associated with Hg exposure. In the 1950s, MeHg released from the Chisso Corporation chemical factory in Minamata Japan caused high levels of Hg poisoning in the community that relied heavily on fish in their diet (Ekino et al., 2007). In the 1970s, rural communities in Iraq were exposed to high levels of MeHg by ingesting grains imported from the U.S. that were treated with an organomercurial pesticide (Woolf, 2022). Between 1946–1970, Allied Chemical and Dye Company discharged 165,000 pounds of Hg into Onondaga Lake on the lands of the Onondaga Nation and Haudenosaunee Confederacy, which is sacred ceremonial and fishing grounds. The discharged Hg was subsequently converted to MeHg within Onondaga giving this lake the reputation as the most polluted body of water in the U.S. (C. Miller, 2021; O'Toole, 2012). The communities in these examples—as well as many other communities—experienced neurological conditions, including damage to visual, auditory, and sensory faculties, and, in more extreme cases, mental retardation, cerebral palsy, deafness, and blindness (Ekino et al., 2007; Woolf, 2022). Offspring from pregnant people in these communities experienced even more serious effects. These high-profile poisoning events catalyzed global awareness of the harm associated with exposure to Hg and ushered in an era of research and regulation.

In the U.S., several regulations during the 1970s had direct and indirect impacts on Hg contamination (US EPA, 2015). Scrubbers and electrostatic precipitators installed on power plants as part of the Clean Air Act (CAA) indirectly reduced Hg emissions by capturing particulates and gases from which Hg is associated. The Clean Water Act (CWA) directly addressed Hg discharge into water bodies from industrial sources such as chlor-alkali plants and metal refineries. In

addition to the CAA and CWA, the toxic substances control act of 1976 phased out, or reduced, the use of Hg in many industrial processes and products including fungicides, batteries, and paints. More recently, the CAA amendments of the 1990s identified hazardous air pollutants, including Hg, and developed maximum achievable control technology standards for Hg emissions from specific industries. In 2011, the Mercury and Air Toxics Standards directly regulated Hg emissions from coal and oil-fired power plants which was the largest domestic source of Hg at the time (Everett, 2014).

As a result of these regulations, point-source Hg contamination in atmospheric deposition declined in the U.S., as in many other parts of the developed world (C. I. Olson et al., 2020). Mercury emissions, particularly from coal combustion and artisanal small gold mining, continued to enlarge the global atmospheric Hg pool, though, resulting in atmospheric deposition becoming the dominant pathway for Hg contamination into most ecosystems (Driscoll et al., 2013). This source shift in contamination highlighted the far-reaching extent of Hg pollution and the need for global efforts to reduce contamination.

To address the ubiquitous nature of Hg contamination, the United Nations Environmental Program (UNEP) convened in 2003 to evaluate the global impact of Hg contamination and the pressing need for international cooperation. By 2009, the governing council of UNEP began negotiations for a legally binding treaty, culminating in the adoption of the Minamata Convention on Mercury by 128 countries in 2013 (Bank, 2020). The primary goals of this convention, named after the Minamata disaster in Japan, include reducing Hg releases from industrial sources, phasing out products containing Hg (e.g., thermometers, fluorescent lamps), and promoting environmentally sustainable alternatives in artisanal and

small-scale gold mining, which remains the largest source of global Hg emissions (UN Environment, 2019).

Due to these regional and global efforts, the release of Hg has abated and in more developed regions, local and regional emissions have decreased significantly (C. I. Olson et al., 2020; Yanxu. Zhang et al., 2016). Note, however, that the environmental injustices of Hg pollution persist. In developed countries where Hg emissions have decreased significantly, the communities that remain close to—and disproportionately impacted by—Hg emissions are marginalized communities that lack political capital to advocate for more stringent environmental protections (Dai et al., 2023; Marchese et al., 2024). In addition to proximity to Hg contamination sources, many minority and underserved communities—such as indigenous peoples—rely more regularly on fish in their diet, increasing exposure to MeHg. This has led to devastating outcomes in communities worldwide including Grassy Narrows in Ontario, Canada, the Yanomami People of the Amazon, and Munduruku people of Brazil. On the global scale, developing countries depend heavily on coal-fired power plants to achieve economic growth and industrialization on trajectories that mirror those of already developed nations (Alhassan et al., 2024). This reliance on coal creates an environmental burden of associated environmental and health hazards including Hg exposure, and these countries often lack the resources to adopt cleaner technologies or enforce strict regulations, exacerbating vulnerability to pollution. While these environmental injustices persist, affected communities have come together in powerful and impactful ways to fight for protection against Hg contamination adding local momentum to ongoing global efforts.

Despite significant regional and global progress in limiting Hg emissions, the persistent nature of Hg means this contaminant will continue cycling through

Earth's spheres for thousands of years with compounding impacts from climate change (Y. Zhang et al., 2023). Thus, the goals of the Minamata Convention still stand today, including to better quantify and characterize new and legacy cycling of Hg within ecosystems, as well as the factors influencing MeHg formation under warming conditions.

Mountain ecosystems mark an important area for this research as they cover significant portions of Earth's surface, provide important water and food resources to downstream communities, and are disproportionately impacted by climate change (Hock & Rasul, 2019). Because of the long-lived nature of Hg(0) in the atmosphere, it can travel far distances to remote mountain ecosystems where high rates of atmosphere deposition lead to elevated loads of Hg compared to lower elevations (H. Zhang et al., 2013). Mountain ecosystems are disproportionately impacted by climate change with warming air temperatures, changes in hydrology, and shifts in vegetation cover (Coppola et al., 2018; Dong et al., 2019; Hock & Rasul, 2019; Trant et al., 2020). These climate-driven shifts may change how Hg cycles in mountain regions making it critically important to characterize the drivers of Hg cycling. While significant research has been conducted in mountain ecosystems globally (Gerson et al., 2017; R. Sun et al., 2021; H. Zhang et al., 2013), major knowledge gaps remain regarding inputs, storage, and losses of Hg, particularly in semi-arid mountain ecosystems. Thus, characterizing Hg cycling is critical to better predict and constrain future changes and potential contamination risk with a warming climate.

1.1 Dissertation Overview

With this dissertation, I address the overarching question: How does Hg cycle in high-elevation mountain ecosystems? My research advances the state of

knowledge regarding Hg biogeochemistry, specifically: (1) the patterns and drivers of Hg inputs and cycling within high-elevation ecosystems, and (2) how climate change may influence the toxicity and mobility of Hg in the coming decades. To do so, I combined data synthesis, field methods, biogeochemical laboratory analyses, and experiments to quantify Hg cycling in the Colorado Rocky Mountains. These studies provide insights into the patterns and drivers of Hg cycling in high-elevation, semi-arid mountain ecosystems, which are applicable to similar areas globally. My dissertation is divided into four chapters. Chapters II-V include conceptual and methodological advice, as well as field and analytical assistance by coauthors and committee members who I have recognized in the Acknowledgements section. These chapters are at various stages of journal publications; I published Chapter II in *Biogeochemistry* in 2023, Chapter III is in prep for submission to *JGR Biogeosciences* in Spring 2025*,* Chapter IV is in review with *Environmental Research Letters*, and I will submit Chapter V to *Proceedings of the National Academy of Sciences* in Spring 2025. In the final chapter (Chapter VI), I summarize the findings from Chapters II–V and provide recommendations for future Hg research in high-elevation mountain ecosystems globally.

Chapter II: Mercury cycling in the U.S. Rocky Mountains: a review of past research and future priorities

While significant past work has been conducted in mountain ecosystems of the Eastern U.S., as well as glacial regions of the Himalaya and Tibetan Plateau, Hg cycling in the semi-arid mountain ecosystems of the Western U.S. remains limited. Thus, a comprehensive assessment of knowns and knowledge gaps regarding Hg cycling in Western U.S. mountain ecosystems is needed to guide and prioritize future research directions. I synthesized the literature on Hg cycling in the U.S. Rocky Mountains between 2000–2023 to identify the state of knowledge

regarding Hg sources, storage, transformations, and losses, as well as the impacts of climate change—specifically changes in hydrology and wildfire—on Hg bioavailability. I highlighted important knowledge gaps throughout the text and proposed future research priorities. This chapter is published (Miller et al., 2023) in *Biogeochemistry*.

Chapter III: Mercury Cycling in a U.S. Semi-Arid Mountain Ecosystem: Patterns, Drivers, and Bioaccumulation

Major gaps remain in our understanding of inputs, storage, and bioaccumulation of Hg across elevation gradients in mountain ecosystems. Studies from the Eastern U.S. and Asia identify broad patterns in Hg cycling at different elevations due to shifts in tree cover, as well as precipitation volume and quality. Studies from semi-arid, coniferous forest-dominated mountain ecosystems—such as the Rocky Mountains—remain limited despite evidence that coniferous forests receive greater loads of Hg from atmospheric deposition compared to deciduous forest regions and efficiently produce MeHg in underlying soils. Here, I quantify Hg inputs (concentrations and fluxes), storage (concentrations and pools), and bioaccumulation (concentrations) from the plains to the alpine. I synthesize these data to assess the drivers of Hg cycling in a semi-arid mountain elevation gradient and compare the findings to other mountain regions.

Chapter IV: Climate-driven sulfate export in alpine watersheds may stimulate methylmercury production

Mountain ecosystems are experiencing elevated climate-driven sulfate export, wetland expansion, and enhanced atmospheric deposition of Hg which increase the potential for MeHg formation. Ambient rates of MeHg production, as well as sulfate limitations on those reactions, are unknown in high-elevation wetlands of the Rocky Mountains. I assessed the potential of increasing sulfate export in alpine streams to

stimulate MeHg production in subalpine peatlands—areas of major storage of both organic carbon and inorganic Hg in mountain ecosystems globally. I amended peatland soils with sodium sulfate to mimic enhanced sulfate export from accelerated mineral weathering and measured net MeHg production rates for different sulfate treatments. This chapter is currently under review with *Environmental Research Letters*.

Chapter V: Alpine and subalpine environments of the Colorado Rocky Mountains act as sinks for mercury, but this character may shift with ongoing climate change

The Minamata Convention on Mercury highlights the importance of characterizing the sink-source behavior of Hg in different ecosystems, particularly those most impacted by climate change, such as remote mountain regions. While efforts are being made to expand our understanding of Hg cycling in mountain areas, limited mass balance studies exist and those that do lack a comprehensive characterization of depositional pathways, as well as estimates of Hg loss via evasion. Here, I present a mass balance of Hg within alpine and subalpine zones of the North Boulder Watershed, Colorado by quantifying inputs via wet and dry deposition, storage in soils and vegetation, and losses via runoff and evasion.

MERCURY CYCLING IN U.S. ROCKY MOUNTAINS: A REVIEW OF PAST RESEARCH FUTURE PRIORITIES

Adapted from:
Miller, H. R., Driscoll, C. T., & Hinckley, E. L. S. (2024). Mercury cycling in the US Rocky Mountains: a review of past research and future priorities. *Biogeochemistry*, *167*(1), 1-20. DOI: https://doi.org/10.1007/s10533-023-01108-w.

2.1 Abstract

Mercury cycles at levels three- to five-fold higher today than the pre-Industrial era, resulting in global contamination of ecosystems. In the western United States (U.S.), mercury mobilization has led to widespread production of methylmercury (MeHg), a potent, bioaccumulating neurotoxin, which has resulted in fish consumption advisories across all states. Mountain regions are particularly sensitive to continued mercury contamination as they receive higher rates of atmospheric deposition, compared to lower elevations, and have aquatic ecosystems on the landscape conducive to MeHg production. In this paper, we focus on the U.S. Rocky Mountain region and synthesize: (1) current knowledge regarding the mercury cycle; (2) impacts of climate change on the mercury cycle connected to hydrology and wildfire; and (3) future research priorities for informing mercury research and regulation. Studies on the interactions between mercury contamination and climate change in mountain ecosystems is still nascent. We use the findings from this synthesis to summarize the following research needs: (1) quantify sources of mercury in wet and dry deposition, as these pathways dictate mercury exposure and toxicity, and are shifting with climate change; (2) investigate MeHg in mountain aquatic ecosystems, which are important pathways of human mercury exposure and provide food resources and habitat to local wildlife; and (3) examine the disproportionate impact of mercury contamination on Indigenous

communities through community-led research. Although we focus on the Rocky Mountains for this review, the findings are applicable to semi-arid mountain ecosystems globally and must be prioritized to promote the health of ecosystems and people everywhere.

2.2 Introduction

Mercury is a geologically sourced, bioaccumulating trace metal, and its release, global transport, and exposure have been greatly accelerated by human activities (UNEP, 2018). Catastrophic poisoning events, and the global extent of contamination, have provided international motivation to curb the extraction, use, and distribution of mercury. These efforts have been primarily led by the United Nations' Minamata Convention on Mercury (UN Environment, 2019). Now signed and ratified by 147 parties, this treaty has made historic progress in expanding our understanding of the mercury cycle, and mitigating exposure. However, mercury contamination remains a serious global threat to human and ecosystem health due to its continued use, release, and persistent nature (C. Y. Chen et al., 2018; UNEP, 2018). When emitted into the atmosphere, mercury can be transported long distances and deposited onto remote landscapes (Selin, 2009). Following initial deposition to the Earth surface, mercury may be subsequently reemitted to the atmosphere by evasion, or mobilized via water to aquatic ecosystems. This cycle can repeat several times before mercury is permanently sequestered in sediments (Amos et al., 2014). In aquatic ecosystems, mercury can be converted to methylmercury (MeHg), a bioaccumulating neurotoxin, that is responsible for widespread contamination in wildlife and fish consumption advisories in all fifty states of the United States (U.S.). The mercury cycle is highly manipulated by human activities with 3–5 times more mercury cycling today than during the pre-

Industrial era; coal combustion, artisanal gold mining, and other industrial practices are the major activities that have led to the rapid mobilization and bioavailability of this element (F. Li et al., 2020; UNEP, 2018).

The increased cycling of mercury in the biosphere and associated harmful human health impacts have provided motivation for research and regulation over the past several decades. The long atmospheric residence time of mercury allows for long range transport to remote regions such as high latitude and altitude ecosystems (Selin, 2009). With concentrations of mercury above background levels predicted to persist for centuries, due to reemission from legacy pools (Amos et al., 2013), it is important to understand the response of remote regions to continued mercury contamination, especially in the context of ongoing global change. Over the past 10 years, mercury research in remote ecosystems has largely focused on Arctic, as well as mountain systems in the Himalaya and eastern U.S. (Blackwell & Driscoll, 2015; Chai et al., 2022; Demers et al., 2007; Gerson et al., 2017; Tripathee et al., 2019; Q. Zhang et al., 2019). In mountain ecosystems of the western U.S., research on mercury cycling has historically been limited and relatively narrow in scope. This paucity of studies marks an important knowledge gap. Mountain ecosystems make up a large portion of the western U.S. and are experiencing increasing mercury deposition, as well as climate change, which likely alter baseline mercury cycling (Eagles-Smith, Wiener, et al., 2016; Mast et al., 2005; Packer et al., 2020). As such, we seek to assess the state of research regarding mercury cycling in mountain ecosystems of the western U.S. to identify unknowns and priorities for future research.

In this Synthesis and Emerging Ideas paper, we focus on the U.S. Rocky Mountains region (hence-forward, "Rocky Mountains"). The consequences of elevated mercury deposition to the Rocky Mountains are still poorly understood

despite this region covering over one-third of the conterminous western U.S. land area. In general, processes in semi-arid mountain ecosystems, such as the Rocky Mountains, remain inadequately constrained with regards to mercury cycling. Specifically, studies are lacking on mercury uptake, release, and evasion in shrub/grassland and forest environments; storage in high-elevation soils; and transformations in aquatic ecosystems such as mountain wetlands, reservoirs, and lakes. We synthesize the state of knowledge regarding mercury cycling in the Rocky Mountains with relevant comparisons to other mountain regions, evaluate how mercury cycling processes may evolve with continued climate change, and highlight important areas for future research.

2.3 Mercury Cycling in the U.S. Rocky Mountains

2.3.1 Background

The Rocky Mountains of the U.S. are >800,000 km in total area, spanning ~3,000 km from New Mexico to the Canadian Border; they cross Colorado, Utah, Wyoming, Idaho, and Montana (Fig. 2-1). The region is characterized by extreme gradients in climate, elevation, and land cover, which drive patterns of mercury cycling (Eagles-Smith, Wiener, et al., 2016). The Rocky Mountains range from~1500–4300 m in elevation and are comprised of desert, grassland, shrubland, and forested land covers. Approximately 70% of the annual water supply to the region is tied to mountain snowpack, with over 200 reservoirs greater than 0.1 km3 storage located within the alone (Lehner et al., 2011). Ongoing climate change has the potential to shift mercury cycling in ecosystems and landscapes of the Rocky Mountains with consequences that are both local and regional in scale. In the following sections, we summarize the research investigating sources, storage,

transport, and transformations of mercury within the Rocky Mountains and how it is impacted by climate change (Table 2-1). We focus on two specific drivers associated with a changing climate that are having a profound effect on ecosystems of the mountainous western U.S.: shifts in hydrologic regimes and wildfire activity.

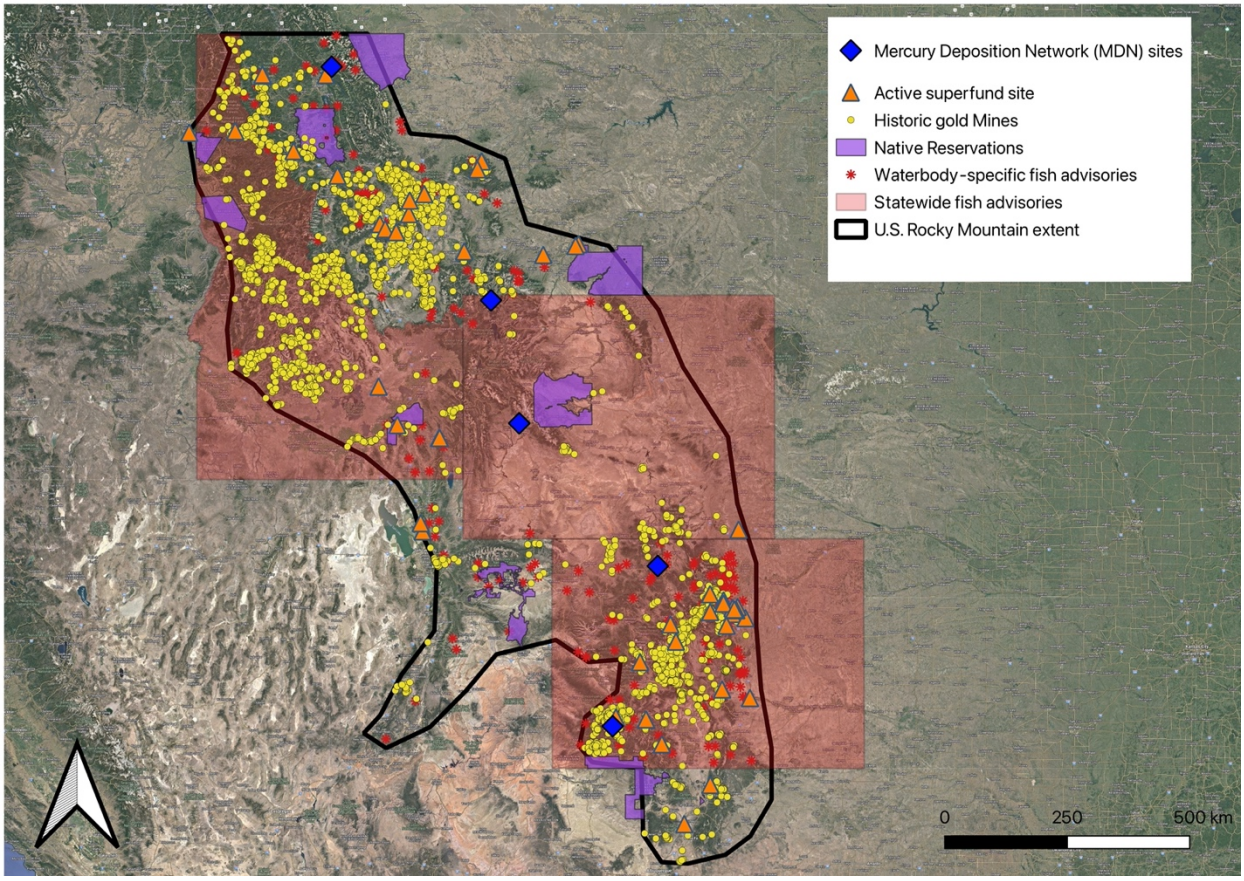

Figure 2-1: Map of study area showing MDN sites (blue diamond), active superfund sites (orange triangle), historic gold mines locations (yellow circle), Native American Reservations (purple shading), waterbody-specific fish advisories (red star), and statewide fish advisories (red shading) within the Rocky Mountains. Statewide fish advisories in Idaho, Wyoming, and Colorado are for all waterbodies for specific species of fish (see manuscript text for more information).

2.3.2 Sources and Atmospheric Deposition

Mercury is transferred from the atmosphere to the Earth surface in oxidized (Hg(II)) and elemental (Hg(0)) forms, and deposited through both wet and dry

atmospheric deposition (Selin, 2009). Globally, dry deposition dominates the atmospheric flux, accounting for 60–90% of terrestrial atmospheric mercury deposition (Zhou et al., 2021). Wet atmospheric mercury deposition occurs during periods of precipitation and fog and is typically comprised of soluble Hg(II) dissolved in water or adsorbed on the surface of water particles. Dry mercury deposition occurs primarily from the uptake of atmospheric Hg(0) by plants and deposition of particle-bound Hg(II) to foliar and land surfaces (F. Li et al., 2020; Selin, 2009). Studies from across the western U.S., including sites in the Rocky Mountains, show that most of atmospheric mercury deposition in this region is derived from the well-mixed global pool of Hg(0), as opposed to local sources (C. I. Olson et al., 2020; Selin & Jacob, 2008). There are periods—typically in the spring—of greater sourcing directly from east-Asian industrial activities. Long-distance transport of mercury from Asia occurs across the Pacific in the free troposphere (Huang & Gustin, 2015; Lin et al., 2012; P. Weiss-Penzias et al., 2006).

Table 2-1: Total mercury and methylmercury concentrations for previously studied ecosystem compartments of the Rocky Mountains

Compartment	Total mercury	Methylmercury	Description	Region	Reference
Atmosphere	16.1 ± 45 pg m^{-3} (PBM), 20.4 ± 28 pg m^{-3} (GOM), 1.9 ± 0.9 ng m^{-3} (GEM)		Average values from 2008 to 2018	Salt Lake City, Utah (AmNet UT97)	Zhang et al., 2016, https://nadp.slh.wisc.edu/sites/amnet-UT97/
Soil	Conifer forests: 58.4 – 208 ng/g (μ = 108 ng/g); deciduous forests: 25.2 – 37.5 ng/g (μ = 31.7 ng/g)		O horizon	Wyoming Rocky Mountains	Biswas et al., 2007
	< 10 – 1320 ng g^{-1} (μ = 30 ng g^{-1})	0.17 – 0.43 ng g^{-1}	A horizon	U.S. Rocky Mountains	Olson et al., 2022*
	< 10 – 520 ng g^{-1} (μ = 25 ng g^{-1})		C horizon	U.S. Rocky Mountains	Olson et al., 2022*
	40.4 – 118.1 ng g^{-1} (μ = 81.7 ng g^{-1})	0.32 – 1.50 ng g^{-1} (μ = 0.89 ng g^{-1})	Wetland soils	Wetlands near Great Salt Lake, UT	Fleck et al., 2016*
	5.7 – 24,732.4 ng g^{-1} (μ = 776.9 ng g^{-1})	U.S – 77.00 ng g^{-1} (μ = 2.97 ng g^{-1})	Lake sediments	U.S. Rocky Mountains	Fleck et al., 2016*
	1.59 – 466 ng g^{-1} (μ = 111.1 ng g^{-1})	U.S= 1.9 ng g^{-1} (μ = 0.6 ng g^{-1})	Stream sediment	U.S. Rocky Mountains	Fleck et al., 2016*

	29.0 – 45.8 ng/g (μ = 39.2 ng/g)	0.09 – 0.12 ng/g (μ =0.104 ng/g)	Reservoir sediment (0-9 cm)	CO (Narraguinnep Reservoir)	Gray et al., 2014
Water	0.27-14.09 ng L^{-1}	0.01-0.73 ng L^{-1}	Lake surface water	90 high-altitude lakes in the western U.S.	Krabbenhoft et al., 2002
	0.5-13.5 ng g^{-1}	0.04-0.048 ng L^{-1}	Alpine stream	U.S. Rocky Mountains	Mast et al., 2005, Packer et al., 2020, Shanley et al., 2008
	filtered = 0.17-0.43 ng L^{-1}, particulate = 0.22-0.83 ng L^{-1}	filtered = 0.005-0.114 ng L^{-1}, particulate = 0.003-0.102 ng L^{-1}	Reservoir surface water	Idaho	Baldwin et al., 2022
Fish	30.3-3992 ng g^{-1} wet weight (μ = 670 ng g^{-1})		Salmonidae family in lake	U.S. Rocky Mountains	USGS, unpublished data
		36.6-488 ng g^{-1}	Centrarchids in reservoir	Idaho	Baldwin et al., 2022
Dragonflies	5 – 1769 ng g^{-1} (μ = 219 ng g^{-1})		Aeshnidae family	U.S. Rocky Mountains	Eagles-Smith et al., 2020*

* Rocky Mountain sites extracted from larger dataset

Regulation in the U.S. through the 2011 Mercury and Air Toxins Standards (MATS), in addition to control technologies for other pollutants such as sulfur dioxide and nitrogen oxides, have resulted in a >75 % decrease in mercury emissions from U.S. coal-fired utilities (Yanxu. Zhang et al., 2016). As a result of these emission declines, wet atmospheric mercury deposition has been decreasing over the past several decades in the eastern U.S., which is downgradient of major mercury emission sources in the Midwestern U.S. (Fig. 2-2; Olson et al. 2020).

This decreasing trend of wet atmospheric mercury deposition, however, is not mirrored in the western U.S. where National Atmospheric Deposition Program (NADP) sites show mostly non-significant, increasing mercury concentrations in wet deposition since 2008 (P. S. Weiss-Penzias et al., 2016). Specifically in the Rocky Mountains, NADP sites show increasing mercury concentrations since 2000 in wet deposition with the highest concentrations occurring between 2010 and 2015 (Fig. 2-2). Additionally, wet deposition rates are significantly higher at sites above 3000 m elevation compared to lower elevation sites (9.90 ± 2.44 ng m−2 yr1 versus 5.36 ± 1.28 ng m^{-2} yr^{-1}, $p < 0.01$; Fig. 2-2). These contrasting patterns are likely due to East Coast monitoring sites, such as in New England, falling within the planetary boundary layer (<2 km elevation), which is primarily influenced by local mercury sources. The Rocky Mountain sites, alternatively, fall within the free troposphere (>2 km elevation), which reflects global background mercury concentrations. As a result, higher elevation sites in the Rocky Mountains, that reflect the augmenting global pool of atmospheric mercury, show increasing patterns, whereas lower elevation sites in New England show decreasing trends due to reductions in regional mercury emissions (Lin et al. 2012; Weiss-Penzias et al. 2016; Olson et al. 2020).

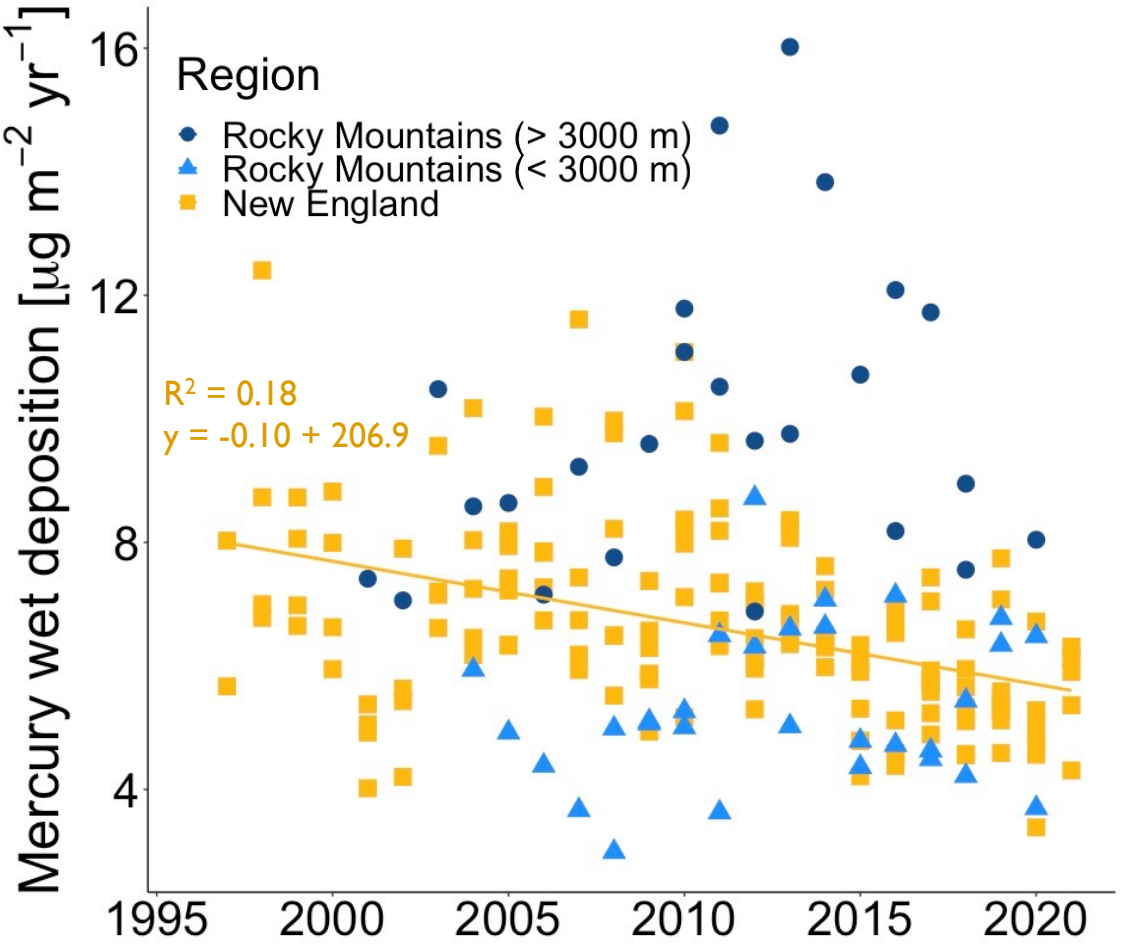

Figure 2-2: National Atmospheric Deposition Program (NADP) mercury wet deposition rates for eight sites in New England (yellow squares), two sites below 3000 m elevation in the Rocky Mountains (light blue triangles), and two sites above 3000 m elevation in the Rocky Mountains (dark blue circles). The lower-elevation Rocky Mountain data, and log-transformed higher-elevation Rocky Mountain and New England data, are normally distributed (Shapiro–Wilk test, $p > 0.05$). The New England sites show significant decreasing trends in atmospheric mercury deposition (Pearson correlation coefficient, $p<0.01$) likely due to decreases in regional mercury emissions. Rocky Mountain sites, alternatively, show non-significant increasing trends at both the high-elevation sites (Pearson correlation coefficient, $p=0.19$) and lower-elevation sites (Pearson correlation coefficient, $p=0.33$) likely due to the augmenting global pool of mercury. Additionally, mercury wet deposition rates increase with elevation with significantly higher deposition rates at Rocky Mountain sites over 3000 m in elevation compared to sites below 3000 m (t-Test, $p<0.01$). These higher rates of atmospheric deposition are likely due to the location of higher-elevation sites within the free troposphere, which has higher atmospheric Hg concentrations compared to lower-elevation air masses (Huang and Gustin 2015).

Wet atmospheric mercury deposition rates range from 2.9 to 16.0 μg m^{-2} yr^{-1} in the Rocky Mountains, as calculated from five active Mercury Deposition Network sites (MDN; Fig. 2-2). The highest wet mercury deposition occurs at the two Colorado sites which are both located over 3,000 m elevation (Fig. 2-2). These rates are comparable to other mountain regions globally with rates varying from 1.75 to 8.20 μg m^{-2} yr^{-1} in the Tibetan Plateau (Chai et al., 2022; Gu et al., 2020; Huang et al., 2012) and from 4.2 to 13.0 μg m^{-2} yr^{-1} in the Adirondacks and Green Mountains of the eastern U.S. (Gerson et al., 2017, p. 20; Shanley et al., 2008).

Direct dry deposition (the flux of mercury in the absence of precipitation) is more difficult to measure and often estimated by using atmospheric mercury species concentrations combined with model estimated deposition velocities, eddy covariance techniques, or by sampling vegetation litterfall and throughfall (Wright et al., 2016). The Atmospheric Mercury Network (AMNet) includes measured concentrations of atmospheric mercury species with model calculations of dry mercury deposition. This network is sparse; all sites west of the Mississippi were discontinued by 2018, and only two of those sites were located within the Rocky Mountains in Utah. The estimated dry deposition at these two Utah AMNet sites ranged from 9.5 to 14.0 μg m^{-2} yr^{-1}. These rates are comparable to wet deposition rates, but do not include mercury fluxes via litterfall and throughfall, suggesting that dry deposition dominates in the region, consistent with global patterns (Fig. 2-3; Zhang et al. 2016). Comparisons of direct dry deposition to other mountain regions are challenging due to the lack of direct and accurate measurements; however, one study found mercury fluxes up to 35.3 μg m^{-2} yr^{-1} in the Tibetan Plateau (Chai et al., 2022; R. Sun et al., 2021) and fluxes ranging from 5.2 to 16.9 μg m^{-2} yr^{-1} in eastern U.S. mountain ecosystems (Shanley et al. 2008; Wright et al. 2016).

Eckley and colleagues (2016) estimated vegetation uptake of mercury (a proxy for dry deposition) across the western U.S. They used previously published litterfall and throughfall data from other regions in the U.S., as well as studies from Europe and China, and found that uptake of mercury by vegetation varies by ecoregion. Their estimates ranged from 1.6 ± 0.1 μg m^{-2} yr^{-1} in desert ecosystems to 10.9±0.1 μg m^{-2} yr^{-1} in marine West Coast forests (Eckley et al., 2016). As far as we are aware, there have been no studies investigating rates of vegetation-derived deposition specifically in the Rocky Mountains. However, modeled estimates from the Great Plains (comparable to Rocky Mountains foothills vegetation) average 3.7 ± 0.1 μg m^{-2} yr^{-1}, estimates from northwestern U.S. forested mountains (comparable to montane and subalpine vegetation of the Rocky Mountains) average 8.8 ± 0.1 μg m^{-2} yr^{-1}, and measurements from the Alaskan tundra (comparable to high alpine vegetation of the Rocky Mountains) average 8.0 μg m^{-2} yr^{-1} (Fig. 2-3; Eckley et al. 2016; Olson et al. 2019). In the absence of local data, these rates help to constrain atmospheric deposition rates in the Rocky Mountains. Extensive dry deposition measurements across the Rocky Mountains, however, are needed to better quantify mercury inputs to this region. Increasing monitoring efforts is especially urgent in the context of increasing wildfire intensity and frequency; wildfire mobilizes mercury from vegetation and surface soils for subsequent deposition back to the land surface (Kumar et al., 2018).

Studies from the Tibetan Plateau and eastern U.S. show that mercury cycling varies significantly along mountain elevation gradients due to shifts in atmospheric mercury deposition and vegetation cover (Blackwell & Driscoll, 2015; Gerson et al., 2017; X. Li et al., 2022; H. Zhang et al., 2013; L. Zhang et al., 2013). Steep elevation gradients in the Rocky Mountains also likely play an important role in atmospheric mercury deposition but have not yet been investigated. Precipitation generally

increases with elevation in the Rocky Mountains, from ~190 mm yr^{-1} at 1600 m to ~1500 mm yr^{-1} at 3500 m, suggesting that mercury inputs through wet atmospheric deposition likely increase with elevation as well (assuming continual transport of mercury into the area; Heindel et al., 2020; USDA n.d.). Alternatively, particulate deposition through dust generally decreases with elevation in the Rocky Mountains, likely due to greater contributions of dust from urban and agricultural practices at lower elevations, and atmospheric suspension of soil due to climate induced decreases in soil moisture. This pattern could potentially result in a negative correlation between direct dry deposition of particulate mercury with altitude (Heindel et al., 2020). Changes in precipitation and temperature with elevation also drive dramatic shifts in plant communities in the Rocky Mountains, going from, for example, Tallgrass prairie in the plains, to open *Pinus ponderosa* forests in the foothills, to more dense mixed stands of *Pseudotsuga menziesii* and *Pinus contorta* in the montane and subalpine, to sparse krummholz and open tundra in the alpine. Differences in plant community structure play an important role in determining patterns of mercury dry deposition through plant uptake and transfer to soils (see above) but these impacts have not yet been quantified in the Rocky Mountains. The absence of these data was corroborated by the synthesis study of Eagles-Smith et al. (2016). They reported that currently, data on mercury uptake by shrubs, grasslands, and herbaceous plant functional groups is lacking relative to forested ecosystems, thereby making it challenging to properly characterize mercury cycling in areas where these plant communities dominate (Gerson et al. 2022; Zhou et al. 2021).

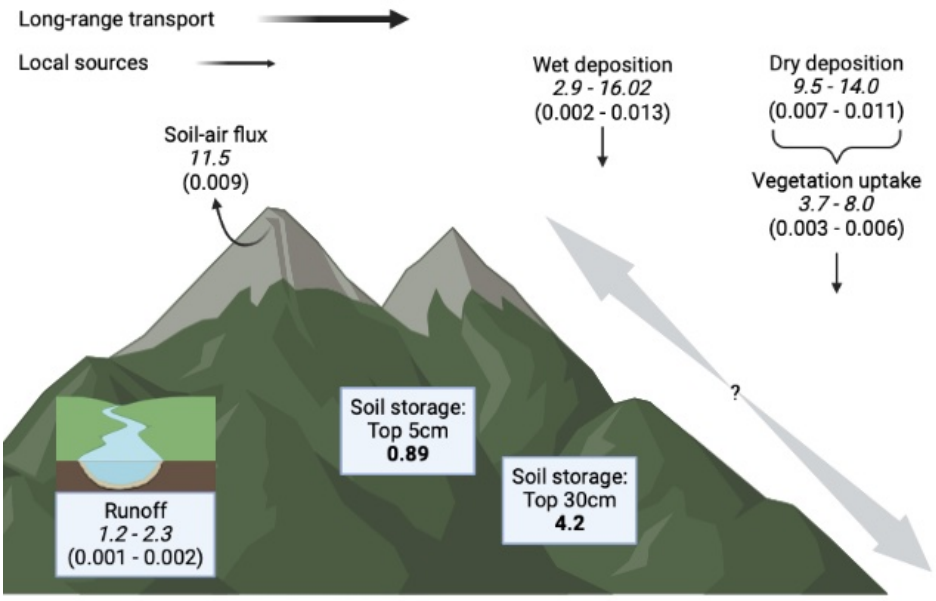

Figure 2-3: The mercury cycle in the Rocky Mountains (~ 807,075 km^2). Fluxes are in italics (ug m^{-2} yr^{-1}), annual area fluxes are in parentheses (Gg yr^{-1}), and soil pools are bolded (Gg). Gray arrows represent uncertainty along mountain elevation gradients.

2.3.3 Soil Storage and Evasion

Across the ~807,000 km of the Rocky Mountains, approximately 4.2 Gg of mercury is stored in the upper 0.3 m of soil, with approximately 0.89 Gg in the top 5 cm (derived from Olson et al. 2022; Fig. 2-3). Mercury concentrations are highest in the soil O horizon when present (70 – >200 ng g^{-1}) followed by the A horizon (30.2 ± 61 ng g^{-1}) and the C horizon (25.5 ± 32 ng g^{-1}). The presence and depth of an O horizon is highly heterogenous across the Rocky Mountains and is driven by changes in elevation, temperature, aspect, slope, vegetation cover, and disturbance history (Hoffmann et al., 2014). The concentration of mercury within an O horizon also varies markedly depending on the type of parent litter and period of decomposition. Some areas may have an older, thinner O horizon composed of high mercury concentration material (e.g., moss, lichen); in contrast, other areas may be composed of newer, thicker O horizon comprised of lower mercury concentration

material (e.g. deciduous leaves; Pokharel & Obrist, 2011). Soil mercury concentrations in the A horizon are broadly driven by soil organic matter content, land cover, and ecoregion (Olson et al. 2022). Although mercury concentrations in the O horizon are typically higher than the A horizon, mercury pools are typically larger in the A horizon due to higher soil bulk density (Olson et al. 2022). Across the U.S., the soil A horizon has significantly higher mercury concentrations compared to the C horizon (34.0 ± 0.5 ng g^{-1} versus 27.0 ± 0.4 ng g^{-1}, $p < 0.01$). Olson and colleagues (2022) attributed this difference to enrichment of surface soils by external inputs such as atmospheric deposition. Yet, this pattern is not evident in the Rocky Mountains where there is no significant difference between the A and C horizons ($p > 0.05$; Olson et al. 2022). The lack of horizonal variation in non-aquic soils may be a result of lower organic carbon content, lower precipitation rates, and higher incident solar radiation that drives photoreduction in surface soils; however, further analysis would be needed to determine the driving influences.

Watersheds in the Rocky Mountains with historic mercury, gold, or silver mining typically have elevated mercury concentrations that can exceed 100,000 ng g^{-1} total mercury and 20 ng g^{-1} MeHg in soils (Fleck et al., 2016). Within the Rocky Mountains, there are over 7,300 historic sites where gold was mined either as a primary, secondary, or tertiary commodity (Fig. 2-1; Mason et al., 1996). Most of the mines are located within central Colorado, western Montana, and central Idaho which coincide with the highest density of waterbody-specific fish advisories (Fig. 2-1). Fewer downstream impacts are associated increasing watershed size and greater natural vegetation land cover (Domagalski et al., 2016).

In mountains of the eastern U.S. and China, researchers have found that soil mercury concentrations are positively correlated with altitude due to shifts in land cover, atmospheric mercury deposition, and soil storage capacity (Gerson et al.

2017; Zhang et al. 2013). Studies from the central Himalaya, however, have found an inverse relationship between total mercury concentrations and elevation associated with decreasing soil carbon content (Tripathee et al. 2019). Soil mercury concentrations and pools along elevational gradients in the Rocky Mountains have yet to be investigated marking an important knowledge gap regarding the factors that drive mercury soil storage in this region, and how these factors may change in the future with ongoing global change.

Across the western U.S., an estimated 35,100 kg yr^{-1} of mercury is emitted from soils to the atmosphere, primarily in the elemental Hg(0) form due to its high volatility. Fluxes vary widely across the west ranging from 7.7 ± 0.2 μg m^{-2} yr^{-1} in the Great Plains to 29.7 ± 1.9 μg m^{-2} yr^{-1} in the Mediterranean ecosystems of California (Eagles-Smith et al. 2016; Eckley et al. 2016). Comparing estimates of mercury inputs and losses across the entire western U.S. (inclusive of the Rocky Mountains) indicates that, on average, this region is a mercury sink (Eagles-Smith et al. 2016). Within the Rocky Mountains, the source-sink behavior of mercury likely varies across elevation gradients, land and plant cover, variability in atmospheric deposition rates, leaching in runoff, and evasion to the atmosphere. In Rocky Mountain National Park, researchers found that less than 20% of atmospherically deposited mercury was lost in annual runoff, suggesting that the alpine zone acts as a sink for mercury (Mast et al. 2005; Shanley et al. 2008). However, this estimate was made without soil flux measurements and intense solar radiation at high-elevations likely promotes high evasion rates (Eckley et al. 2016). Soil evasion measurements using dynamic flux chambers from northwestern forested mountains average 11.5 ± 0.4 μg m^{-2} yr^{-1} and provide an estimate for rates in forested montane and subalpine regions of the Rocky Mountains (Eckley et al. 2016). However, measurements from across a diverse subset of Rocky Mountain

land covers will be necessary to better constrain the overall source or sink nature of mercury.

2.3.4 Transport, Transformations, and Bioaccumulation

If deposited or transported into areas of permanent or temporary saturation, inorganic mercury can be readily transformed into MeHg if conditions are conducive for microbial methylation. Across the western U.S., MeHg concentrations in aquatic sediments have large spatial variability that are driven by landscape and land-use characteristics. Importantly, Fleck and colleagues (2016) found some of the areas with the highest MeHg concentrations occurred in areas with relatively low total mercury concentrations, particularly in areas of the Rocky Mountains. The production of MeHg in aquatic regions of the Rocky Mountains, however, has received little attention despite over 6000 km^2 of lakes and ponds, 3000 km^2 of reservoirs, 700 km^2 of streams, and 650 km^2 of wetlands.

There is evidence, however, from dragonfly larvae used as biosentinels that lakes, streams, and wetlands in the Rocky Mountains have MeHg concentrations at levels of concern for human and ecosystem health (Eagles-Smith et al. 2020). Eagles-Smith and colleagues (2020) conducted a survey of >450 sites spanning 100 U.S. National Park service units to create integrated impairment indices for fish, wildlife, and humans based on mercury concentrations of dragonfly larvae. Data extracted from the seven sites sampled within the Rocky Mountains shows 10 % of samples were below any of the deleterious effect benchmarks, 16% had low hazard risk, 35 % had moderate hazard risk, 22 % had high hazard risk, and 5 % had severe hazard risk. The percentage of sites within the high hazard and severe hazard risk categories in the Rocky Mountains was higher than in the U.S. as a whole, where only 11 and 1 % of sites fell into those categories, respectively (Eagles-

Smith et al., 2020). Despite the Rocky Mountains having areas with high- to severe-risk for MeHg contamination, we did not find any studies that quantify the processes driving these concentrations, such as studies on mercury methylation and demethylation rates. Indeed, methylmercury production in lake, stream, and wetland environments of the Rocky Mountains has received little to no attention, with most studies previously reporting total mercury MeHg concentrations from high altitude lake ecosystems (e.g., Krabbenhoft et al., 2002). This knowledge gap is important to address, as these aquatic regions act as gateways for the transport of water from high-elevations downstream, and provide habitat and forage for local wildlife.

Despite limited investigation of MeHg production in mountain regions, the atmospheric deposition and methylation of mercury across the western U.S. has resulted in widespread mercury contamination and mercury bioaccumulation within fish populations of the Rocky Mountains (Lepak et al. 2016). There are over 200 waterbody-specific fish consumption advisories for mercury in the region (Fig. 2-1). These advisories likely underestimate the extent of the mercury contamination, as waterbody-specific advisories are limited to sites where fish mercury concentrations have been tested. In addition, there are state-wide consumption advisories for specific fish species and fish lengths for all locations in Idaho (<8 meals per month of Smallmouth (*Micropterus dolomieu*) and Largemouth (*Micropterus salmoides*) bass), Colorado (<1 meals per month of Smallmouth Bass (*Micropterus dolomieu*) <38 cm, Largemouth Bass (*Micropterus salmoides*) > 38 cm, Tiger Muskie (*Esox masquinongy*); and <2 meals per month of Cutthroat Trout (*Oncorhynchus clarkia*) and *Micropterus dolomieu* >38 cm), and Wyoming (avoid *Oncorhynchus clarkia* >38 cm, *Micropterus* >30 cm, Black Crappie (*Pomoxis nigromaculatus*) >25 cm, Burbot (*Lota lota*) >51 cm, Channel Catfish (*Ictalurus*

punctatus) >51 cm, Sauger (*Sander canadensis*) and Walleye (*Sander vitreus*) >30 cm, and Northern Pike (*Esox Lucius*) and Muskellunge (*Esox masquinongy)*; Fig. 2-1). These advisories are for general populations and more stringent recommendations exist for pregnant people and children.

Of the waterbody-specific advisories in the Rocky Mountains, over half of the locations are found above 1500 m in elevation, with the majority in constructed waterbodies such as reservoirs. Alternatively, lotic, or moving freshwater environments, generally, have lower mercury bioaccumulation in fish. Day et al., (2020) found that only 13 % of over 2,300 samples exceeded fish health benchmarks in their study of the Upper Colorado River Basin. This pattern suggests that high-elevation reservoirs may be particularly important hot spots for mercury bioaccumulation and exposure with implications for downstream ecosystems and human populations.

In addition to mercury bioaccumulation in aquatic food webs, evidence from other mountain and steppe regions suggest that terrestrial bioaccumulation of mercury is also an area of concern. The impacts, however, of MeHg bioaccumulation on behavior, reproduction, and survival is poorly understood for most terrestrial taxa in mountainous regions (Rimmer et al., 2010; Rodenhouse et al., 2019). Although terrestrial ecosystems typically produce low concentrations of MeHg, aquatic MeHg can pass into terrestrial food webs and enhance mercury bioaccumulation (Cristol et al., 2008; Janssen et al., 2023). Additionally, terrestrial food webs can have higher trophic levels compared to aquatic food webs resulting in greater MeHg bioaccumulation in top consumers (Bartrons et al., 2015; Janssen et al., 2023). Elevated mercury concentrations, specifically in terrestrial mountain food webs, have been observed across trophic levels from arthropods (Rimmer et al., 2010) to birds (Ackerman et al., 2016; Jackson et al., 2016; Sauer et al., 2020) to top

predators (Y. Ma et al., 2023). These studies generally found organism tissue MeHg concentrations to be highest in mid- to high-elevation zones because of elevated atmospheric mercury deposition and increased MeHg bioavailability (Rodenhouse et al., 2019; Sauer et al., 2020; Townsend et al., 2014).

The human impact of mercury exposure is widespread throughout the world, causing a variety of neurological health consequences, primarily through consumption of fish and shellfish (USEPA 2018). Many of the fish species with advisories are popular for anglers who feed themselves and their families with locally caught fish. Indeed, for many communities and families experiencing financial hardship, eating locally caught fish is an essential protein source (Quimby et al., 2020). Additionally, catching and consuming fish is a sovereign right for the Tribal Nations marking an essential social practice and source of economic sustenance for Indigenous communities (Cantzler & Huynh, 2016). Thus, the widespread mercury contamination of fish populations across the U.S. marks a stark environmental justice issue (Barbo et al., 2023; Chiapella et al., 2021; Dai et al., 2023; Eagles-Smith, Ackerman, et al., 2016; Houde et al., 2022; Roe, 2003). The disproportionate impact of mercury contamination on Indigenous peoples has been studies most extensively in the Arctic where adverse health outcomes have been observed across all life stages (see Basu et al. 2022). The effect of mercury contamination on native communities outside the Arctic is much less studied. One 2003 study examined the disproportionate impact of mercury contamination in food sources for Indigenous communities across the U.S. and found 59 reservations are at moderate risk, 70 at high risk, and 19 at severe risk for mercury exposure. Additionally, across 655 watersheds containing a native community (>10 % native population), the mean fish mercury concentration was 0.32 ppm, just above the EPA's guidance value for safe fish consumption at the time (Roe 2003). There are

eleven reservations with native communities within the Rocky Mountains (Fig. 2-1), and Indigenous peoples make up ~2–10 % of the total population within each of the states that include the Rocky Mountains (Fig. 2-1). These communities are likely to be impacted by continued mercury contamination; however, information is not currently available regarding the disproportionate exposure of MeHg to these groups. This deficiency marks an important need for community-driven research, education, and outreach to better understand the scope of this issue and effective means for counteracting mercury exposure while maintaining cultural traditions.

2.4 How Does Climate Change Impact Mercury Cycling in the Rocky Mountains?

2.4.1 Background

Climate change is impacting high-elevation ecosystems more rapidly and intensely than lowland regions (Hock & Rasul, 2019; Kittel et al., 2015). Since these ecosystems are highly sensitive to mercury contamination, it is important to consider how future change will impact mercury transport, bioavailability, and toxicity. In the Rocky Mountains, climate change is causing increased warming (McGuire et al., 2012), drought conditions (Tague & Dugger, 2010), and growing season length (Hu et al., 2010), all of which have important implications for mercury cycling in local and distant ecosystems. Here, we focus specifically on the effects of shifting hydrology and wildfire on mercury mobilization and ecosystem exposure (Fig. 2-4).

2.4.2 Shifts in Hydrology

Drought and warming temperatures are causing shifts in hydrology that impact the availability and transport of inorganic mercury, as well as the potential for MeHg production in the Rocky Mountains through a variety of mechanisms (Fig. 2-4). As the Rocky Mountains warm, snowmelt is occurring earlier and more precipitation is falling as rain than snow (Halofsky & Peterson, 2018; Larson et al., 2011). Clow (2010) found that between 1978 and 2007, increasing springtime air temperatures and declining snowpack shifted snowmelt 2 to 3 weeks earlier in the Colorado Rocky Mountains. Hydrologic simulation experiments using reconstructed snowpacks, also from the Colorado Rocky Mountains, predicted an earlier melt-out of 31 days on average, spanning the years 2001–2014 (Badger et al., 2021). Additionally, more precipitation is occurring as rain than snow across the Northern Hemisphere where snow occurs, with periods of heavy precipitation intensifying (McCabe & Wolock, 2010; Rocca et al., 2014). In mountain environments, more precipitation as rain is also causing well documented increases in rain-on-snow events (Cache et al., 2023; Musselman et al., 2018). These changes increase erosion and transport of sediment downstream, and these responses are predicted to worsen with continued climate change (Cache et al., 2023; Pelletier, 2009). Using a landscape evolution model, Cache and colleagues (2023) demonstrated that under the most extreme climate scenario (RCP8.5), sediment yield in a small Swiss Alps catchment increased by 6 % due to more precipitation falling as rain and intensification of heavy precipitation events. Increased flushing and erosion of surface soils results in greater export of soil-bound mercury downstream to lentic ecosystems where anoxic conditions and availability of organic carbon and terminal electron acceptors favor conversion of inorganic mercury to MeHg (Halofsky & Peterson, 2018; X. Sun et al., 2022). Earlier snowmelt, decreasing snowpack, coupled with subsequent drought and more intense periodic rainfall lead to more

extreme wetting and drying cycles that can accelerate MeHg production. Reservoirs are particularly sensitive to this phenomenon; earlier, more intense spring runoff causes reservoir stage to decrease earlier and fluctuate more dramatically among years (Cohen et al., 2020). Across the western U.S., a 3.2-fold increase in fish mercury concentrations was observed across −30 to +50 % variations in interannual reservoir water levels (Willacker et al., 2016). Fish in reservoirs that experienced their lowest water stage at the beginning of the summer (May, June, or July) had fish mercury concentrations up to 11-fold higher than in reservoirs with water minimums at other times of the year (Willacker et al., 2016). Elevated MeHg production under these conditions is likely driven by accelerated decomposition of organic matter in littoral sediments experiencing water-level fluctuations. This wet-dry cycle enhances mercury methylation by liberating inorganic mercury into bioavailable forms during low stage, as well as increasing reducing conditions and dissolved organic carbon needed for microbial methylation during high stage conditions (Eckley et al., 2017).

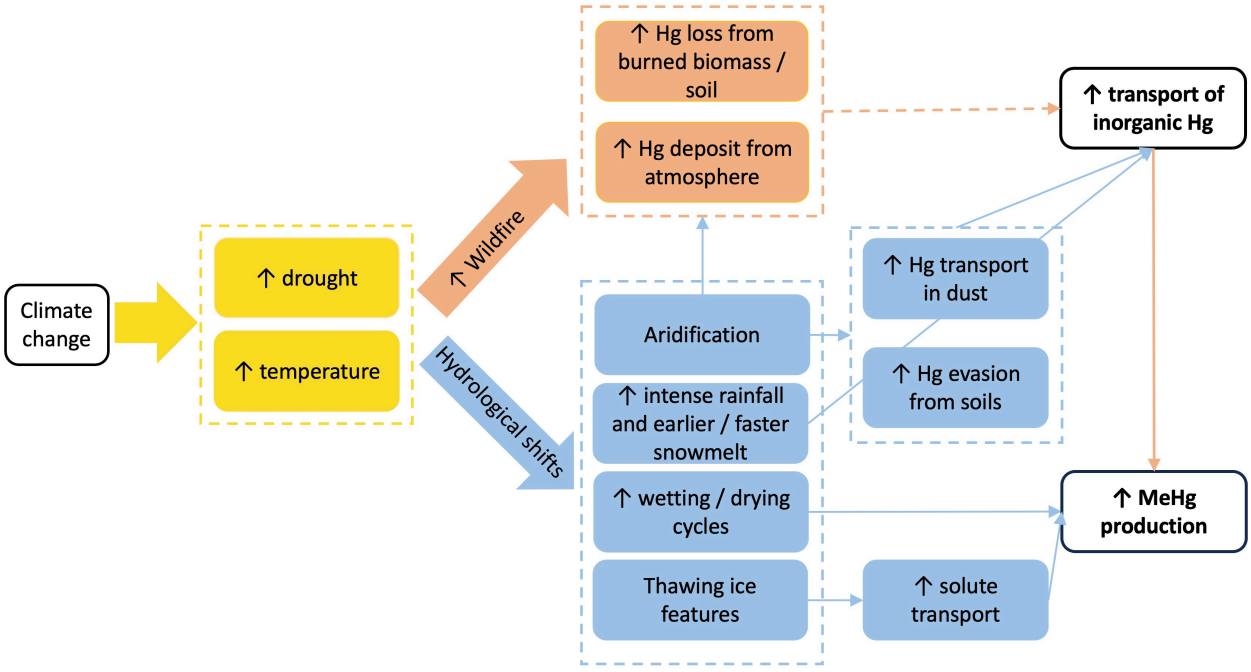

Figure 2-4 Schematic illustrating the climate change driven impacts of changing wildfire (red) and hydrology (blue) on inorganic mercury transport and MeHg production in the Rocky Mountains.

Changes in selective water withdrawal can also impact temperature and oxygen conditions within reservoirs. These changes have implications for MeHg production in reservoirs with past studies documenting increased MeHg production and uptake in aquatic food webs at the Hells Canyon Complex (Snake River, Idaho-Oregon) because of increased thermal stratification and anoxia (Baldwin et al. 2022). Climate and land-use changes are driving widespread increases in seasonal anoxia and thermal stratification, which combined with increased wetting and drying cycles has the potential to exacerbate MeHg production across a variety of mountain aquatic ecosystems (Jane et al., 2021). This marks an important knowledge gap and area for future research to better quantify the impact of climate-driven hydrologic shifts on MeHg production in reservoirs, as well as other natural water bodies, within the Rocky Mountains.

Thawing ice features in high-elevation regions may also impact hydrology and the potential for MeHg production in mountain regions across the globe. Over the past three decades, chemistry in high-elevation streams from multiple sites in the Rocky Mountains, western Canada, the European Alps, the Icelandic Shield, and the Himalayas demonstrate consistent and widespread patterns of increasing sulfate and base cation concentrations or fluxes (Crawford et al., 2019). In the Rocky Mountains, despite decreasing trends in atmospheric sulfate deposition, sulfate concentrations in runoff have increased by 300% over the past 30 years. This trend is likely the result of accelerated weathering of pyrite associated with thawing ice features (Crawford et al., 2019). It is unknown whether the MeHg production in the Rocky Mountains is sulfate limited; however, it is possible that increases in sulfate export could stimulate MeHg production by sulfate reducing bacteria in downstream aquatic environments, such as mountain reservoirs and wetlands (Jeremiason et al., 2006).

Aridification also impacts mercury cycling in the Rocky Mountains by changing inputs and losses of dust-bound mercury through wind erosion, and soil mercury evasion (Duniway et al., 2019; Huang et al., 2020; Overpeck & Udall, 2020; Scott & Black, 2020). Aridification and land use changes are increasing desertification and dust storms in many regions of the globe, particularly the Asian and African continents (Han et al., 2021; Z. Yang et al., 2022; C. Zhang et al., 2019; L. Zhang et al., 2013; Zhu et al., 2022). The western U.S. receives a significant percentage of annual dust loads from these regions with 49–77 % coming from Asia and 15–34 % coming from Africa (Duncan et al., 2007; L. Zhang et al., 2013). Multiple studies from western Chinese mountain ecosystems, the Atlantic Ocean, and Antarctic snowpack, demonstrate that wind-transported dust from Asia and

Africa are important sources of mercury to downwind regions, such as the western U.S. (Huang et al., 2020; Witherow & Lyons, 2008).

In addition to receiving dust-bound mercury from afar, the western U.S. is also experiencing aridification and intensifying dust storms that can transport dust-bound mercury to the Rocky Mountains (Duniway et al. 2019; Overpeck and Udall 2020). Historical data from glaciers and high-elevation lake sediments cores in the Rocky Mountains demonstrate that dust is an important source of mercury to mountain ecosystems (Carling et al., 2017; Mast et al., 2010). Future studies that determine the concentration of mercury in dust, rates of deposition, and how these factors are shifting with global change are needed to better understand the relative importance of this mercury source. Inputs through dust, though, likely play an important role in the mercury cycle in the Rocky Mountains, as work from the Arctic demonstrates how elevated dust increases mercury concentrations in vegetation with implications for litterfall, soil, and local wildlife (C. L. Olson et al., 2019).

With continued drought, the Rocky Mountains may also become a global source of mercury through wind erosion and soil-air evasion (Eckley et al., 2016; Goudie, 2018; Scott & Black, 2020). To our knowledge, no studies have investigated mercury export in aeolian erosion from this region, particularly in the context of the total mercury transport flux. Future work must determine if the Rocky Mountains are a sink or source for dust-bound mercury and what the global and regional implications are for mercury transport and bioaccumulation. Aridification also impacts mercury evasion from soils back to the atmosphere by reducing waterbody and vegetation extent, thereby exposing more bare soil surfaces (Bodner & Robles, 2017; Hannoun & Tietjen, 2022). In general, bare soils receive greater solar radiation and have drier surfaces, two factors known to be positively correlated with

greater soil-air mercury fluxes (Eckley et al. 2016). Eckely and colleagues (2016) demonstrated across the western U.S. that sparsely vegetation regions have larger net ecosystem mercury emissions compared to forested and other heavily vegetation regions. This suggests that continued aridification of the west may contribute to greater net losses of mercury from these ecosystems over time.

2.4.3 Increased Wildfire Activity

Warmer air temperatures and increased drought are driving more frequent and intense wildfires across the western U.S (Abatzoglou & Williams, 2016). Ash released from wildfires can have a variety of consequences for local mercury cycling. When biomass is burned, mercury previously stored in above ground plant tissues such as grasses, shrubs, and trees, as well as surface soils (<5 cm), is released back to the atmosphere in elemental and oxidized forms that act as a substantial release of mercury from terrestrial ecosystems (Homann et al., 2015; Webster et al., 2016). Remobilized mercury is then available for further transformations and uptake by organisms once it is redeposited onto the landscape (Kumar & Wu, 2019; X. Li et al., 2022). Webster and colleagues (2016) report that across the western U.S., ~3100 ± 1900 kg yr^{-1} of mercury is released annually from wildfires; this value is likely to increase because of more frequent and intense wildfires. Additionally, enrichment of mercury in terrestrial ecosystems, due to increasing atmospheric mercury emissions, is projected to increase mercury wildfire emissions across North America by 19% in 2050 (Kumar et al. 2018). The amount of mercury released from an ecosystem during wildfire depends on the vegetation structure and fire severity. In general, across forests of the western U.S., Aspen forests (*Populus tremuloides*) tend to release the lowest amount of mercury during a burn event, averaging 0.9 g ha^{-1}, while Hemlock-Sitka Spruce forests (*Picea sitchensis*) release the most averaging,

7.8 g ha^{-1} (Webster et al., 2016). In the Wyoming Rocky Mountains, wildfire was found to release 3.6–12.9 g ha^{-1} of mercury in deciduous forests and 7.4–25.3 g ha^{-1} in coniferous forests (Biswas et al., 2007).

Wildfire in grasslands is also likely an important vector for mercury loss within the Rocky Mountains. Long-term records demonstrate increasing wildfire activity in these ecosystems over the past 30 years (Donovan et al., 2017). The quantity of mercury stored and released in grassland ecosystems, however, has received little attention. One study from the Rocky Mountains reported a loss of ~4.1 g ha^{-1} of mercury during wildfire (Biswas et al. 2007). This research suggests that grasslands can act as a source of mercury during wildfire, similar to forested regions, but additional studies are needed. In addition to vegetation cover, soil development also impacts the amount of mercury released during wildfire with soil O horizons releasing more mercury than A horizons (Homann et al. 2015). Since the Rocky Mountains are characterized by extreme gradients in soil development and vegetation cover with changes in elevation and aspect, better measurements of mercury release from wildfire across these different regions will be critical in assessing the mercury sink/source nature of the region.

Most of the mercury released during wildfire is in its particulate, oxidized form with a relatively short residence time. Thus, a large fraction of ash is redepositing on the landscape close to the source (Seigneur et al., 2004). When ash falls to the surface of Earth, it acts as a vector for the movement of mercury into an ecosystem where it can have a variety of fates and consequences. Ash-bound mercury typically has a relatively low methylation potential, resulting in low bioavailability (Ku et al., 2018). However, wildfire ash has also been shown to leach labile organic matter which provides an important energy source to mercury methylating microbes, thereby indirectly increasing MeHg production (Li et al.

2022). Li and colleagues (2022) showed that wildfire ash efficiently sorbs inorganic mercury onto its surface, helping to store mercury within ecosystems.

These various fates of ash-bound mercury illustrate the uncertainties regarding the impact of increased wildfire activity on mercury contamination, specifically for the Rocky Mountains. In addition to local wildfires, the Rocky Mountains also intercept smoke plumes from more distant wildfires such as those occurring in California (Brey et al., 2018; Val Martin et al., 2013). These distal sources of smoke may increase inputs of mercury into the Rocky Mountains through wet and dry atmospheric deposition. It will be important for future studies to quantify the sources, concentrations, and species of mercury in smoke plumes to better predict how continued wildfire activity will impact mercury transport, bioavailability, and exposure of biota.

2.5 Summary of Research Opportunities

With continued atmospheric mercury deposition to the Rocky Mountains, there is a need for research that addresses important knowledge gaps both for this region, as well as semi-arid mountains globally. We examined these gaps in the text above and summarize research priorities here (Table 2-2).

First, it is important to quantify the inputs and losses of mercury through atmospheric deposition and evasion, particularly in the context of increasing wildfire activity and aridification. Quantifying net mercury budgets is critical to constrain the source or sink nature of the Rocky Mountains and to improve understanding of the role of this region in the global mercury cycle. Constraining the sources and pathways of mercury inputs through wet and dry deposition is also important as the proportions of each are likely to change with increased wildfire

and wind erosion, as well as shifts in global primary emission sources, which will dictate mercury exposure and toxicity. It will be particularly critical to characterize and quantify the role of vegetation in mediating the atmosphere-land exchange of mercury.

Second, it is important to constrain how the mercury cycle shifts along elevation gradients to determine the zones with the highest contamination risk, and how higher-elevation sites may impact downstream regions. Assessing mercury inputs, storage, and transformations with changes in precipitation and vegetation cover along elevation gradients in the Rocky Mountains will help determine the factors controlling mercury cycling in western U.S. mountain ecosystems. Additionally, it will strengthen our ability to compare the Rocky Mountains to other mountain regions of the world where research has provided a better understand of mercury dynamics along mountain elevation gradients, such as in the Himalaya and eastern U.S.

Third, methylmercury production in mountain aquatic regions such as reservoirs, wetlands, and streams needs to be assessed to determine contamination risk for humans and local wildlife. Reservoirs are an important area of focus since they make up a large percentage of waterbodies in the Rocky Mountains and are susceptible to MeHg production due to increases in wet-dry cycles and low stage conditions. Additionally, reservoirs are important pathways of human exposure to mercury through fish consumption. Investigating MeHg production in streams and wetlands is also important. These aquatic expanses provide important food resources and habitat to local ecosystems, as well as pathways for water supply downstream. Shifts in hydrologic conditions due to climate change in these areas will likely exacerbate net MeHg production.

Fourth, there is a need to examine the disproportionate impact of mercury contamination on indigenous communities within the Rocky Mountains—and U.S., more broadly—through community-lead research, education, and outreach. Such efforts will require integration of Indigenous representatives into scientific studies; such inclusion must occur at the beginning of the research process to ensure that the priorities and standards of indigenous communities lead and are represented in the research.

Finally, it is important to assess the impact of climate change on mercury cycling in mountain regions. Shifts in hydrology and wildfire connected to global change have the potential to increase the availability of mercury, production of MeHg, and exposure to humans and wildlife in mountain regions making this a critical area of research. Quantifying the impacts of climate change on mercury cycling will require a combination of long-term observations and modeling efforts to understand the consequences of different climate-related forcings (Table 2-2).

Although we have focused on existing research and knowledge gaps in the U.S. Rocky Mountains region, the topic of mercury cycling is applicable to other semi-arid mountain ecosystems of the world. Indeed, due to the ubiquity of mercury in environments globally, it is truly a topic that concerns everyone, and must be prioritized in the research agenda to promote the health of ecosystems and people everywhere.

Table 2-2: Summary of knowledge gaps and future research priorities.

Knowledge gap	Future research priority for western mountain regions
Concentrations and flux of atmospheric mercury dry deposition	Increase number of AMNet sites. Collect litterfall and throughfall data. Assess the impact of plant cover along elevation gradients on dry deposition rates.
Concentrations and pools of mercury in soils along mountain elevation gradients	Conduct studies similar to past work done in the eastern U.S. and China to determine patterns of total and methylmercury concentrations and pools along elevation gradients. This will provide insights into regions with the greatest risk for mercury exposure to humans and wildlife.
Rates of mercury evasion from soils along mountain elevation gradients	Use consistent, reproducible methods (e.g., dynamic flux chambers) for measuring mercury evasion rates across different land covers and elevation zones.
Methylmercury production in mountain reservoirs, lakes, and wetlands	Measure concentrations and mercury methylation efficiencies in different aquatic landforms to determine regions that are hotspots for MeHg production and exposure to local wildlife and downstream ecosystems. Use dragonflies as biosentinels to put ecosystems into larger contamination risk index.
The disproportionate impact of mercury contamination on indigenous communities	Use community-driven research, education, and outreach to better understand the scope of mercury exposure and effective measures for counteracting health concerns while maintaining cultural traditions.
Impacts of climate change on mercury cycling in mountain regions	

Rates of mercury transport downstream as a result of earlier and faster snowmelt	Measure mercury concentrations in runoff and use stable isotopes to determine mercury source (atmospheric versus terrestrial).
Methylmercury production in reservoirs, lakes, and wetlands that are experiencing increasing wetting / drying cycles	Measure concentrations and methylation rates in aquatic mountain regions to determine areas that act as MeHg hotspots. Conduct wetting / drying incubation experiments. Measure soils *in situ* following wetting / drying events and compare to baseline conditions.
Mercury transport in dust from increased aridification and dust storms	Collect dust from persistent snowpack / glacial regions to determine mercury inputs via dust over time. Collect bulk deposition and air samples in areas exposed to dust plumes.
Mercury evasion from soils with increased aridification	Combine measurements of soil evasion rates across moisture and plant cover gradients with model predictions of aridification.
The sources, concentrations, and species of mercury transported in wildfire plumes	Collect air samples within wildfire plumes to determine source, concentrations, and species of mobilized mercury. Use these data to determine the bioavailability of mobilized mercury and source / sink nature of regions that are burning.

2.6 Acknowledgements

The authors thank Connor I. Olson for providing subset soil data of mercury concentrations and pools for the Rocky Mountains. Writing of this manuscript was supported by NSF (DGE-2040434 and EAR-1945388).

2.7 Author Contributions

The initial literature review and synthesis was conducted by HRM with inputs from coauthors. The first draft of the manuscript was written by HRM and all authors contributed text to subsequent versions of the manuscript. All authors read and approved the final manuscript.

2.8 Funding

Funding support was provided by the National Science Foundation (DGE 2040434) and EAR-1945388.

CHAPTER III

MERCURY CYCLING ACROSS A U.S. SEMI-ARID MOUNTAIN ELEVATION GRADIENT: PATTERNS, DRIVERS, AND BIOACCUMULATION

H. R. Miller, S. E. Janssen, S.A. Taylor, J. R. Gerson, Tyler L McIntosh, and E. S. Hinckley

3.1 Abstract

Mercury (Hg) cycling in high-elevation ecosystems remains poorly understood despite significant implications for ecosystem and human health. These landscapes receive higher atmospheric Hg deposition compared to lower-elevation sites. Due to slow soil carbon turnover and temperature-regulated biological processes, high-elevation regions have the potential to serve as sinks for atmospheric Hg, but the degree to which they act as sinks or sources is underexplored, particularly in the western United States. In this study, we quantify Hg inputs, storage, and bioaccumulation along a ~2,000 m semi-arid elevation gradient in the Colorado Rocky Mountains, encompassing plains, foothills, montane, subalpine, and alpine zones. Over a three-year period, we investigated Hg fluxes and pools in atmospheric deposition, vegetation, soil, and terrestrial biota. Contrary to predictions, atmospheric Hg concentrations and precipitation fluxes were significantly higher at lower elevations ($p < 0.05$), likely reflecting local emissions and meteorological pooling. Hg storage in soils was more strongly linked to organic matter content ($R^2 = 0.49$) and water retention ($R^2 = 0.45$) rather than elevation ($R^2 = 0.21$). In alpine regions, slower organic matter turnover and accumulation led to significantly higher Hg concentrations compared to lower elevations (66.3 ± 25.3 vs. $<41.0 \pm 12.7$ ng g^{-1}, $p < 0.01$). We also found methylmercury concentrations in chickadee feathers

peaked at mid-elevation (205 ± 155 ng g^{-1}), coinciding with increased coniferous canopy cover and throughfall fluxes. These results indicate that vegetation type and climatic factors drive Hg cycling patterns more than elevation alone. Our findings establish a baseline for understanding Hg cycling and bioaccumulation in mountain ecosystems, offering critical insights into how climate change may disrupt these landscapes' roles as Hg sinks.

3.2 Introduction

Mercury (Hg) cycling has been dramatically accelerated by human activities over the past century with consequences for human and ecosystem health globally (Selin, 2009). Due to a relatively long residence time in the atmosphere (up to two years), inorganic Hg can undergo long range transport reaching remote landscapes, such as mountainous regions, far from industrial sources (Lovett & Kinsman, 1990; Weathers et al., 2006). There, Hg can enter the landscape via precipitation, dry deposition, and litterfall, then accumulate in soil, enter streams, or oxidize back to the atmosphere (Driscoll et al., 2007). Additionally, if inorganic Hg enters anoxic, high carbon (C) environments, such as wetlands, it can be transformed into the neurotoxic substance methylmercury (MeHg) by anaerobic microbes (Benoit et al., 2002). This organic form of Hg can then bioaccumulate and biomagnify in the local ecosystem and is currently responsible for fish consumption advisories in every state of the United States (U.S.) (US EPA, 2014) and many waterbodies globally. Such consequences are concerning in mountain and high latitude regions where Indigenous groups, in particular, rely on fish as a major food source (Basu et al., 2022).

Despite making up 27 % of Earth's land surface area (H. Zhang et al., 2013), high-elevation ecosystems have received limited attention with respect to Hg

inputs, cycling, and contamination. Abrupt changes in meteorological, orographic, and biological factors along mountain elevation gradients drive unique patterns of Hg cycling that have been studied in several environments (e.g., Blackwell and Driscoll 2015) but remain poorly constrained. Additionally, mountain landscapes are disproportionately impacted by climate change (Beniston, 2006; Hock & Rasul, 2019), which will likely shift baseline Hg cycling and highlights the importance of characterizing and quantifying Hg contamination in these regions. Quantifying MeHg bioaccumulation in terrestrial mountain wildlife is particularly important, as they are understudied relative to aquatic end points and often rely on aquatic food sources with elevated MeHg concentrations (Janssen et al., 2023). Therefore, understanding the inputs, transformations, and fates of Hg across mountain elevation gradients is critically important to assess current and future contamination risk.

Recent studies highlight broad trends in Hg cycling at different elevations along mountain landscapes. Generally, greater Hg inputs and storage occur at higher elevations, which researchers have attributed to higher quantities of precipitation, shifts in tree cover from deciduous to coniferous stands, and slower soil carbon turnover (Fisher & Wolfe, 2012; Stankwitz et al., 2012; Szopka et al., 2011; Townsend et al., 2014; H. Zhang et al., 2013). Hardwood versus coniferous tree cover type is a particularly important driver of Hg cycling. Studies in the Adirondack Mountains, NY, showed that coniferous stands receive higher inputs of Hg compared to hardwood stands due to greater needle surface area, have higher losses of Hg via drainage, and result in greater bioaccumulation in downstream fish populations compared to deciduous stands (Blackwell et al., 2014; Drenner et al., 2013). This pattern is likely due to the efficient production of MeHg within coniferous forests, with Zhou et al. (2018) finding a 444 % increase in MeHg

concentrations within montane coniferous forest litter over a one-year incubation. Multiple investigators have documented the subsequent bioaccumulation of MeHg along several mountain elevation gradients. For example, Townsend and colleagues (2014) found a linear increase in Hg concentrations in *Catharus* thrushes and the salamander (*Plethodon cinereus*) with elevation, while Ma et al. (2021) and Sauer et al. (2020) observed the highest Hg concentrations in biota (small mammals and *Catharus* thrushes, respectively) in mid-elevation areas between 3,500–3,800 m and 1,000–1,300 m, respectively.

While these studies provide a helpful preliminary assessment of mountain Hg cycling, they are mostly based in the eastern U.S. or Himalayan Mountains. The semi-arid, mountainous western U.S. marks a particularly relevant knowledge gap, as it is dominated by coniferous forests that have the potential to efficiently transfer Hg into terrestrial and aquatic ecosystems and act as water resources for millions of people in lowland communities (Colorado State Forest Service, n.d.; NatureServe Explorer, n.d.). Some studies of Hg cycling across the western U.S. have included sampling sites within mountain regions that provide a snapshot of Hg concentrations in soil, precipitation, and wildlife (Eagles-Smith, Wiener, et al., 2016; Obrist et al., 2016; C. I. Olson et al., 2020). There are, however, notable data gaps, such as Hg fluxes via litterfall and dry deposition, which contribute significantly to Hg budgets, as reported in studies in the eastern U.S. and elsewhere (Blackwell et al., 2014; NADP, 2025; Zhou et al., 2021). To date, no studies have simultaneously comprehensively assessed inputs, storage, and fates within a semi-arid mountain environment, making it challenging to piece together a complete assessment of the relative importance of different pathways of Hg in ecosystems, as well as to compare cycling across mountain regions.

The goal of our study was to quantify the inputs and fates of Hg across a western U.S. semi-arid mountain elevation gradient to determine the primary drivers of Hg contamination. To do this, we examined precipitation, throughfall, litterfall, vegetation, soil, and terrestrial biota across a ~2,000 m elevation gradient in the Colorado Rocky Mountains during the 2021–2023 growing seasons. Our research aimed to address the following questions: 1) What are the patterns and drivers of atmospheric Hg inputs and soil storage? and 2) How do elevational patterns influence MeHg bioaccumulation across mountain ecosystems? Broadly, we expected increasing inputs and storage of THg with elevation due to increasing precipitation and litterfall volume and slower rates of soil mineralization, following results from prior studies (Stankwitz et al., 2012; H. Zhang et al., 2013). We also hypothesized that as atmospheric THg inputs increase, there would be an increase in soil THg storage and potential for Hg bioaccumulation because of greater inorganic Hg availability. This comprehensive study covers a major knowledge gap for baseline Hg cycling in high-elevation and arid ecosystems. Such studies are critically important when assessing response to reductions in Hg emissions if policies enacted by the Minamata Treaty are effective, as well as long-term variations in Hg deposition from climate-change related factors, such as increased wildfire and changing precipitation and water cycle patterns (Abatzoglou & Williams, 2016; Kittel et al., 2015; UN Environment, 2019).

3.3 Materials and Methods

3.3.1 Study Area

Our study area covers ~2,000 m of elevation gradient in the headwaters of the Boulder Creek Watershed of the Colorado Rocky Mountains. Following Marr

(1961), we categorized our sampling sites into five elevation zones based on approximate elevation ranges: the plains (1,450–1,800 m, 39.961°N, -105.264 °W), foothills (1,800–2,350 m, 40.015°N, -105.338°W), montane (2,350–2,800 m, 40.013°N, -105.460°W), subalpine (2,800–3,350 m, 40.036°N, -105.548°W), and alpine (3,350–4,200 m, 40.053°N, -105.590°W) zones (Fig. 3-1). For consistency, all sites along the elevation gradient were selected on east-facing aspects. There are several long-term monitoring sites co-located with our study sites that we used for flux calculations of precipitation and litterfall. A National Atmospheric Deposition Program (NADP) National Trends Network (NTN) monitoring site within the subalpine and alpine sites, a National Ecological Observatory Network (NEON) litterfall site within the subalpine and alpine sites, and National Oceanographic and Atmospheric Administration (NOAA) and NEON precipitation sites with all five sampling sites.

The headwaters of the Boulder Creek Watershed are dominated by granitic rocks, biotitic gneiss, schist, and migmatite with intrusions of Laramide rocks. From the plains to the alpine zone, there is a decrease in average daily minimum air temperatures (10°C to -6°C) and an increase in mean annual precipitation (~500 to 1,100 mm yr^{-1}; Murphy et al., 2015, 2003). The tree cover along the elevation gradient is dominated by coniferous forests with primarily Ponderosa Pine (*Pinus ponderosa*) woodlands in the plains and foothills, mixed conifer forests in the montane, and Lodgepole Pine (*Pinus contorta*) and subalpine fir (*Abies lasiocarpa*) forests in the subalpine (Barry, 1973). Plant cover varies from grasslands in the plains to shrublands in the foothills, montane, and subalpine, with very limited growth under tree canopy; alpine tundra species occur above tree line (Barry, 1973).

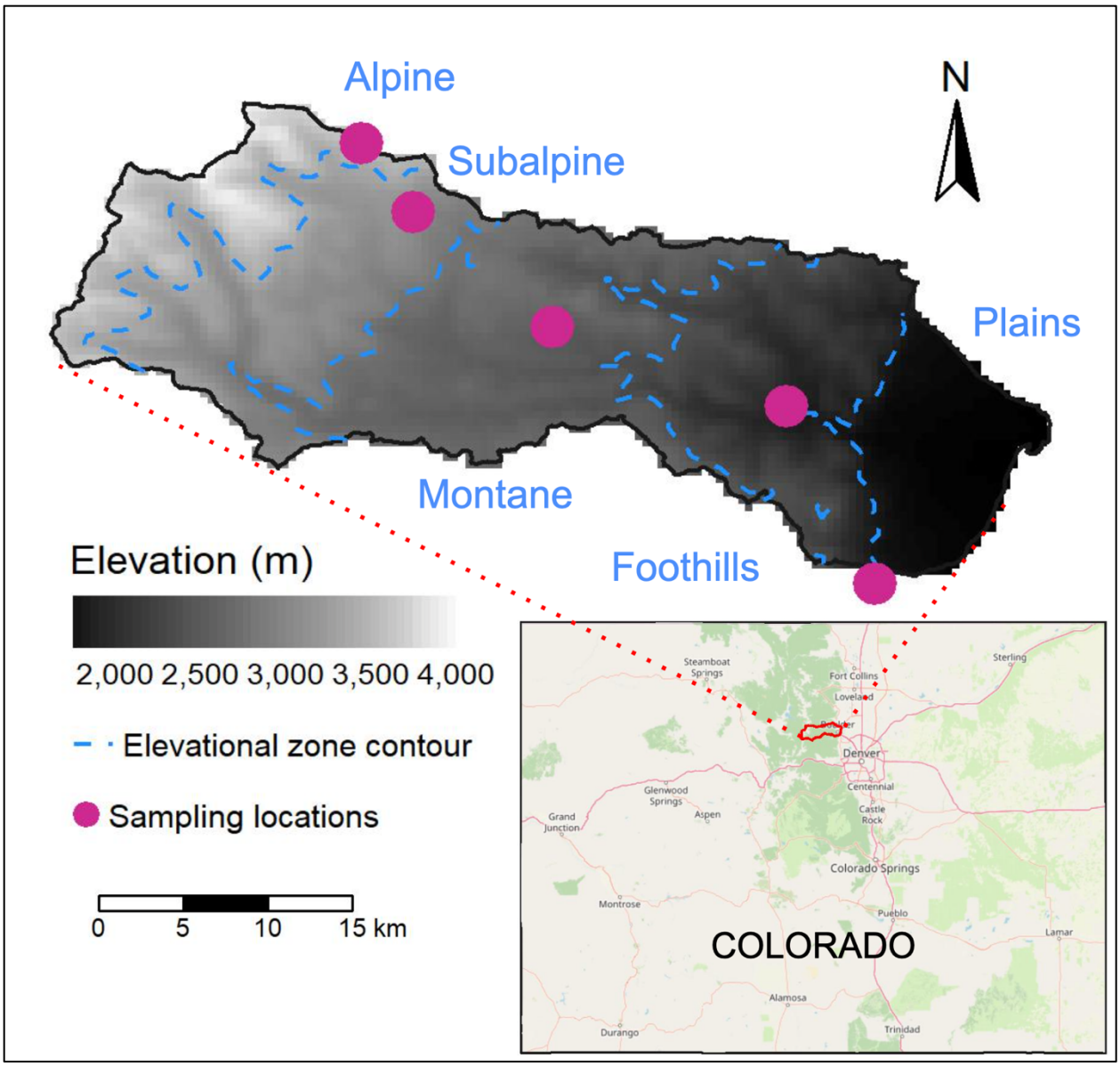

Figure 3-1: Outline of the Headwaters Boulder Creek Watershed (Hydrologic Unit Code 10; (Seaber, 1988) with sampling locations (pink circles) and elevation zones (dashed blue lines) overlaid on a digital elevation model.

3.3.2 Sample and Data Collection

We collected bulk air samples for total gaseous Hg (TGM), which is predominantly gaseous elemental Hg (GEM), as well as Hg stable isotope (δ^{202}Hg) analysis at three locations (plains, subalpine and alpine) (Tate et al., 2023). Air was pumped through a sample train consisting of a 0.45 um polytetrafluoroethylene

(PTFE) filter, soda lime trap, and two chlorinated activated carbon traps using a diaphragm pump with a flow rate of ~900 mL min^{-1}. Two-week integrated samples were collected from May–August, 2023. All air samplers were installed ~1.5 m from the ground surface with free air flow to the sampler. Following collection, all air samplers were shipped to the U.S. Geological Survey Mercury Research Lab (MRL) for analyses.

Litterfall was collected monthly at each site in 0.44m^2 mesh-lined baskets that were deployed in late June and retrieved in late October 2022. Each site had four replicate baskets strapped to trees ~1 m above the ground surface. Samples were handled with clean nitrile gloves, placed in plastic bags, and transported in coolers to the laboratory where they were frozen for further processing. For alpine sites where there is no tree cover, bulk aboveground biomass was collected for THg concentration analysis. Litterfall samples (n=100) were weighed before and after lyophilization to determine percent moisture (% water) and then homogenized.

Direct precipitation and throughfall were collected in triplicate every ~two weeks depending on precipitation volume throughout the growing season (early June – early September 2023) within each elevation zone (only direct precipitation in the alpine due to no tree cover). The sampler was comprised of an acid washed 0.011 m^2 glass funnel attached to c-flex tubing, Teflon tubing, and a PTFE 250 ml sample bottle all housed within black piping to prevent exposure to solar radiation. The tubing was looped with a zip tie to prevent evaporation and the sample bottle was pre-acidified with 2.5 ml 50% hydrochloric acid (HCl) to prevent microbial growth and Hg volatilization. At each collection time point, the tubing was rinsed thoroughly with ultra-high purity water and the sample bottle was replaced with a new, pre-acidified bottle. Field blanks were collected at weekly intervals for one

month to determine if any Hg sorbing from the atmosphere occurred through the exhaust hole of the sample bottle.

Four replicate soil cores were collected for Hg and physiochemical analyses at each elevation zone in 2021 using a 4 cm x 10 cm bulb corer. In addition to the soils collected from the five east-facing sites, we also collected soil samples from north- and south-facing slopes in the foothills, montane, and subalpine. All samples were handled with clean nitrile gloves, placed in plastic bags, and transported to the laboratory in coolers where they were frozen for further processing. Bulk density samples were collected at each site using a mini bulk corer (5 cm x 5 cm) for the A horizon. For the O horizon, we used a 10 cm x 10 cm square plus measured the depth with a ruler.

Within each elevation zone, plant leaves were collected from herbaceous, graminoid, and shrub species in Summer 2022. Bulk aboveground biomass samples were also collected in Summer 2023 by harvesting all standing live and dead plant material from a 0.5 m x 0.5 m square at each site. Since plant species composition varies along the elevation gradient, we also sampled the upper 4–8 leaves of *Achillea millefolium* the week after bloom at each site along the elevation gradient to assess variation in Hg uptake in vegetation unrelated to plant species composition. Samples were transported to the lab, dried for 24 h in a 60°C oven, and weighed. A subset of each sample was then ground for Hg analysis.

We collected Black Capped Chickadee (*Poecile atricapillus*) and Mountain Chickadee (*Poecile gambeli*) feathers from 12-day-old chicks across the elevation gradient in collaboration with the Boulder Chickadee Study. These organisms were chosen since they are present at all elevations, which made it possible to assess drivers of bioaccumulation along the elevation gradient. Additionally, chicks are fed by adults that forage <500 m from the nest on primarily terrestrial insects (e.g.,

Lepidoptera sp., Hymenoptera sp., and *Hemiptera sp*), and, therefore, MeHg concentrations within juvenile birds provide a reliable signal for terrestrial Hg contamination within the elevation zone from which they were sampled. Composite feather samples were collected by combining 10–15 breast feathers from each chick (n = 2–8) within each nest.

3.3.3 Laboratory Analysis for Hg Concentrations

All samples were analyzed at the U.S. Geological Survey Mercury Research Lab (USGS MRL) following established methods and quality assurance criteria noted below. We analyzed litterfall, aboveground biomass, and soil for THg concentrations using atomic adsorption followed by direct combustion on a Nippon MA-3000 Mercury analyzer. The instrument was calibrated using National Institute of Standards and Technology (NIST) certified reference material (CRM) 1575a (pine needles, 39.9 ± 0.7 ng g^{-1}) for litterfall and aboveground biomass, and International Atomic Energy Agency (IAEA) certified reference material (CRM) 456 (coastal sediment, THg concentration = 77 ± 5 ng g^{-1}) for soil with a detection limit of 0.02 ng Hg. Analytical quality control was verified by an instrument calibration linearity >0.995, as well as a method blank (<0.05 ng/boat), CRM (80–120% recovery), and triplicate (<15 % relative standard deviation) every 10 samples.

Soil MeHg concentrations were determined by distillation and isotope dilution per the USGS Techniques and Methods 5A-7 (Hintelmann & Evans, 1997; U.S. EPA, 1998). Soils were enriched with a MeHg spike, acidified with potassium chloride/cupric sulfate solution, and distilled by heating them to 120–125°C while being purged with N_2 gas. The resulting distillate was then buffered with sodium acetate/acetic acid, ethylated with sodium tetraethylborate (NaTEB), and analyzed on the Brooks-Rand "MERX-M" automated MeHg analytical system coupled to the

Thermo iCAP inductively coupled plasma-mass spectrometer (ICPMS) with a detection limit of 0.014 ng g^{-1}. MeHg concentrations were calculated using isotopic dilution. We performed analytical quality control with a mass bias correction (<5 %) and isotope dilution correction (<5 %) at instrument calibration, as well as an instrument calibration check standard every six samples (85 – 115% recovery), a method triplicate (<25 % relative standard deviation of MeHg concentration) every 15 samples, and a CRM IAEA 405 (estuarine sediment, MeHg concentration = 5.49 ± 0.53 ng g^{-1}, 80–120% recovery) every 15 samples.

Total Hg concentrations in direct precipitation and throughfall were determined by cold vapor atomic fluorescence spectroscopy (CVAFS) with the Brooks-Rand "MERX-T" automated Hg analytical system. Briefly, bromine monochloride (BrCl) was added to each sample and then samples were heated to 50°C for 5 d to release matrix-bound Hg and oxidize all forms of Hg to the Hg^{2+} oxidation state. Just prior to analysis, the BrCl was neutralized by the addition of hydroxylamine hydrochloride (HAH) and the oxidized Hg is then reduced by addition of stannous chloride ($SnCl_2$). Volatile Hg^0 is purged from the sample and captured onto a gold sand trap, desorbed, and detected by CVAFS. Analytical quality control was verified by a duplicate (<10 % difference between duplicates), instrument spike (recovery within 85–115 % of known addition), and instrument blank for every 10 samples analyzed. Instrument calibration linearity (>0.995) and a daily detection limit (three times the standard deviation of the calibration blanks) was calculated every day of analysis.

For chickadee feathers, MeHg concentrations were determined by cold vapor atomic fluorescence detection with the Brooks-Rand "MERX-M" automated Hg analytical system. Samples were weighed into Teflon vials and digested in 4.5 M nitric acid at 60 °C for 8 h. The sample extract was then added to reagent water,

titrated with an equivalent volume of 5 M potassium hydroxide, and buffered with sodium acetate / acetic acid to a pH of 4.5–5.0. Oxidized Hg species (Hg^{2+} and $MeHg^{+}$) were ethylated by addition of sodium tetraethylborate (NaTEB). The ethylated species, as well as elemental Hg, were then purged from the sample with argon gas, retained on Tenax traps, thermally desorbed back into the sample stream, and separated by mass with a gas chromatography column. The elemental and ethylated Hg species were then released from the column into the sample stream, thermally oxidized to elemental Hg, and detected by CVAFS. Analytical quality control was performed with a mass bias correction (<5 %) and isotope dilution correction (<5 %) at instrument calibration, as well as an instrument calibration check standard every 10 samples (85 – 115% recovery), a method triplicate (<15 % relative standard deviation of MeHg concentration) every 15 samples, and a CRM (IAEA 452) every 10 samples (80–120 % recovery of certified value).

Total Hg concentrations were determined for chickadee feathers using the same digestate as for the MeHg analyses. Samples were then treated with BrCl and heated to 50°C for 5 d to oxidize all forms of Hg. An aliquot of the digest was added to an analytical vial, and immediately prior to analysis the BrCl was neutralized by the addition of HAH. Following neutralization, $SnCl_2$ is added to the sample to reduce Hg from Hg^{2+} to Hg^{0}. The volatile Hg^{0} is purged from the sample and captured onto a gold sand trap, desorbed, and detected by CVAFS. Analytical quality control was performed with a mass bias correction (<5 %) and isotope dilution correction (<5 %) at instrument calibration, as well as an instrument calibration check standard every 10 samples (90–110% recovery), a method triplicate (<15 % relative standard deviation of THg concentration) every 15 samples, and a CRM (IAEA 452) every 10 samples (80–120% recovery of certified

value). Instrument calibration linearity (>0.995) was calculated every day of analysis.

3.3.4 Soil Physicochemical Analyses

Soil samples were analyzed for a suite of soil physicochemical variables including sulfate, loss on ignition (LOI), total carbon (C), total nitrogen (N), pH, and water content. For physicochemical analysis, soils were divided into subsamples based on drying technique: one subsample was dried at 105°C to calculate gravimetric water content and loss on ignition, one subsample was dried at 60°C to determine total C, and the remaining soil was air-dried and used to measure pH and extractable sulfate. Loss on ignition (LOI) was used as a proxy for total soil organic matter. Briefly, dried soils were combusted at 550°C for 4 h following methods outlined by (Heiri et al., 2001). To measure pH, ~10 g of air-dried soil was suspended in 20 mL of 0.01M calcium chloride ($CaCl_2$) for 1 h and pH of the solution was measured with a benchtop pH probe. Extractable inorganic sulfate (SO_4^{2-}) concentrations were determined by shaking ~30g of air-dried soil in 100mL of 0.006 M calcium dihydrogen phosphate ($Ca(H_2PO_4)^2$*H2O) solution and measuring the filtrate using ion chromatography (Metrohm 930 Compact IC Flex; detection limit 0.1 mg L-1 SO_4^{2-}) (Tan et al., 1994). For total C and N, dried soil was packed into tins and measured at the University of Wyoming Stable Isotope Facility on a Thermo Finnigan elemental analyzer.

3.3.5 Flux Calculations for Litterfall, Open Precipitation, and Throughfall

Growing season litterfall fluxes were calculated by multiplying litterfall THg concentrations (aboveground biomass for the alpine site) by litterfall masses for

each sampling time point, summing the quadruplicate average concentration over the sampling period and dividing by the total area of the four collectors. Litterfall masses were used from NEON litterfall sites for the alpine (NEON site 047) and subalpine (NEON sites 040 and 057) (NEON, 2025). For the montane and foothills, litterfall masses were used from NEON litterfall sites in Rocky Mountain National Park at the same elevation and with comparable tree cover. Direct litterfall collection masses from our collectors were used for the plains site.

Fluxes in open precipitation for the sampling period were determined by multiplying the concentration of THg in open precipitation by the volume of precipitation and summing the triplicate average from each sampling time point. Precipitation volumes were extracted from NADP and NOAA precipitation gauges (NADP, 2025; NOAA Physical Sciences Laboratory, 2024). We used NADP CO02 for the alpine, NADP CO90 for the subalpine, NOAA Nederland 2.8 NE for the montane, NOAA Boulder 4.5 W for the foothills, and NOAA 3.5 S, CO (CoCoRaHS) for the plains.

Growing season throughfall THg fluxes were calculated by multiplying monthly throughfall volumes by throughfall THg concentrations and summing the triplicate average from each sampling time point. In cases where throughfall collectors overflowed, a throughfall coefficient was used to determine volume by multiplying open precipitation volumes by this coefficient. The interception coefficient was calculated by dividing throughfall volumes by open precipitation volumes during the sampling period and then averaging this ratio across the elevation zone. This calculation resulted in a throughfall coefficient of 0.48 (Table S3-1).

To calculate total fluxes of Hg into each elevation zone (open precipitation, throughfall, and litterfall aggregated), we assumed that open precipitation

represented total fluxes of Hg in atmospheric deposition in areas with no forest canopy cover (i.e. bare ground and non-forest vegetation) and that throughfall combined with litterfall represented total fluxes in areas with canopy cover. We used NASA MODIS vegetation continuous fields (VCF) data (DiMiceli et al., 2021, 2022) to calculate percent canopy cover within each elevation zone and then scaled total fluxes by canopy cover coefficients to weight THg fluxes through different atmospheric deposition pathways. Past research has assumed forested areas represent 100% canopy cover, which is reasonable for regions such as the Adirondack Mountains, but is less accurate for semi-arid mountain ecosystems where canopy cover can be as low as 15 % within, for example, open Ponderosa Pine woodlands. As far as we are aware, this is the first study to take into account percent canopy cover to weight total fluxes of Hg by percent open area (open precipitation fluxes) and percent canopy covered areas (throughfall combined with litterfall).

In addition, we geospatially modeled THg fluxes across the headwaters of the Boulder Creek Watershed based on remotely sensed canopy cover and elevation. We first created spatially explicit maps of Hg fluxes across the watershed by interpolating between our *in-situ* sampling locations. Between each sampling location, we linearly interpolated flux values based on elevation; for locations above the highest elevation sampling site and below the lowest elevation sampling site, we used the values of those sampling locations to avoid extrapolation beyond sampling bounds (Fig 3–8 C). Due to minimal canopy cover in the alpine (i.e., on isolated northern aspects and along the lower elevational bounds of the bands), our sampling structure lacked throughfall and litterfall flux measurements in this elevational band. We extrapolated subalpine forest throughfall and litterfall values to the alpine sampling site based on observed similarities between alpine and

subalpine precipitation Hg values and site-specific knowledge that forest characteristics in the alpine and subalpine regions of the watershed are similar. For each pixel location across the watershed of interest, we weighted the interpolated flux values by the remotely sensed vegetation continuous fields percent cover data (Fig 3–8 B), resulting in spatially explicit surfaces of estimated annual, growing season, and non-growing season THg fluxes (Fig. 8 D–F).

3.3.6 Statistical Analyses

We conducted statistical analyses using R 2023.03.0+386 (R Core Team, 2023). When necessary, we log-transformed the data to meet distributional assumptions of statistical analyses. All concentrations below the detection limit were assigned a concentration of 0. Influential data points were determined using Cook's distance with a threshold of 4 divided by the number of observations. Outliers greater than 3 on the studentized residual plot were removed when performing regression analyses. All model residuals were tested for normality using the Shapiro-Wilk test, homogeneity of variance across groups using a Bartlett (normal distribution) or Levene (non-normal distribution) test, heteroskedasticity in regression models using a White Test. Results from ANOVA analyses are reported as trends by elevation zone. Comparisons among factors were performed using Tukey's post hoc adjustment. Reported p values reflect main effect comparisons within factors at an alpha value of 0.05. All linear models were checked for multicollinearity and all variance inflation factor (VIF) values were <5. All reported values in the results section reflect the average ± standard deviation.

For comparisons across sample types (e.g., chickadees and soil versus atmospheric deposition), we compiled a datasheet by taking four replicate soil samples and then using a running average for the remaining variables to create

four replicates for those other values as well. This approach yielded a datasheet with four replicates for every elevation zone that also had no missing values.

3.4 Results

3.4.1 Atmospheric Hg Concentrations

Gaseous elemental Hg concentrations ranged from 0.69–1.41 ng m^{-3} across the growing season (May–August). Unlike past work (e.g., Zhang et al., 2013), Hg concentrations in the plains (1.19 ± 0.18 ng m^{-3}, n = 5) were significantly higher than concentrations in the subalpine (0.83 ± 0.12 ng m^{-3}, n = 5) and alpine (0.92 ± 0.14 ng m^{-3}, n = 5, $p < 0.01$, Fig. S3-1). After adjusting for the sampling month, there was a significant negative relationship between elevation and TGM air concentrations ($p = 0.04$), and TGM concentrations in September were significantly lower than May ($p = 0.04$, Fig. S3-1 B); however, the overall model was not significant ($p > 0.05$). δ^{202}Hg ranged from 0.12 – 0.70 ‰ across the elevation gradient and was significantly higher in the subalpine (0.58 ± 0.12 ‰) compared to the plains (0.19 ± 0.06 ‰) and alpine (0.35 ± 0.13 ‰) ($p < 0.05$, Fig. S3-1 C–D).

3.4.2 Mercury in Atmospheric Deposition: Open Precipitation, Throughfall, and Litterfall

Open precipitation THg concentrations ranged from 10.1 to 34.0 ng L^{-1} across the elevation gradient, and the foothills (24.8 ± 2.9 ng L^{-1}) was significantly higher than the subalpine (19.7 ± 2.9 ng L^{-1}) and alpine (19.0 ± 4.1 ng L^{-1}) during the sampling period (Fig. 3-2A; $p < 0.05$). Contrary to our hypothesis, we observed a significant negative linear relationship between elevation and open precipitation THg concentrations ($p < 0.01$, AIC = 336, Table S3-2).

Throughfall THg concentrations ranged from 14.7 to 98.7 ng L^{-1} and were higher than open precipitation concentrations at all elevation zones (Fig. 3-2A). Throughfall THg concentrations in the subalpine (36.6 ± 16.3 ng L^{-1}) were significantly lower than montane (58.6 ± 22.2 ng L^{-1}, $p < 0.05$) and no other sites were significantly different from each other ($p > 0.05$). Again, contrary to our hypothesis, we observed a non-linear, quadratic relationship between elevation and throughfall THg concentrations ($p = 0.02$, $R^2 = 0.13$; S3-2), and no linear relationship was observed ($p > 0.05$).

Litterfall THg concentrations ranged from 7.5 ng g^{-1} to 110.0 ng g^{-1} (Fig. 3-2B). Averaged across all collection time points, the alpine (15.6 ± 7.3 ng g^{-1}) was significantly lower than the subalpine (49.6 ± 31.0 ng g^{-1}), montane (40.6 ± 21.8 ng g^{-1}), and foothills (34.8 ± 20.2 ng g^{-1}), but not the plains (27.5 ± 15.2 ng g^{-1}) and the subalpine was significantly higher than the plains ($p < 0.05$).

Our litterfall THg concentrations aligned most with past studies (e.g., Fisher and Wolfe, 2012; Gerson et al., 2017; Li et al., 2022) and supported our hypotheses. The strongest predictor of litterfall THg concentrations was a quadratic relationship of elevation with the interaction of month ($p < 0.01$; $R^2 = 0.21$; Table S3-2). The quadratic component of elevation alone predicted litterfall THg concentrations ($p < 0.01$; $R^2 = 0.09$), and was strengthened by including the interaction between elevation and month ($p < 0.01$, $R^2 = 0.27$). A linear relationship was observed between elevation, month, and litterfall THg concentrations but the relationships were all weaker ($p < 0.05$; $R^2 < 0.22$). When only assessing sites below treeline (removing the alpine site), the strongest predictor of litterfall THg concentrations was the linear interaction between month and elevation ($p < 0.01$; $R^2 = 0.41$). We also found a weak significant positive linear relationship between THg litterfall

concentrations and elevation ($p < 0.01$; $R^2 = 0.09$), as well as when adding month as a predictor ($p < 0.01$; $R^2 = 0.22$; Table S3-2).

In June, litterfall THg concentrations were significantly higher in the subalpine (84.3 ± 11.1 ng g^{-1}) compared to the plains (22.8 ± 15.0 ng g^{-1}; $p < 0.05$) and marginally higher than the foothills (28.1 ± 17.7 ng g^{-1}; p-value = 0.06). In July, litterfall THg concentrations were significantly higher in the subalpine (80.4 ± 23.8 ng g^{-1}) compared to the plains (25.6 ± 9.0 ng g^{-1}) and alpine (22.4 ng g^{-1}, $p < 0.05$). No other significant differences were observed among elevation zones for other sampling months ($p > 0.05$, Fig. S3-1).

Within each elevation zone, no significant differences were observed for litterfall THg concentrations across sampling months except in the subalpine, where June (84.3 ± 11.1 ng g^{-1}) and July (80.4 ± 23.8 ng g^{-1}) were significantly higher than August (36.7 ± 19.4 ng g^{-1}), September (23.7 ± 4.3 ng g^{-1}), and October (22.8 ± 6.3 ng g^{-1}; $p < 0.05$). In general, litterfall THg concentrations in the spring increased with elevation. However, by September and October, the concentrations were generally highest in the mid-elevation zones (Fig. S3-2).

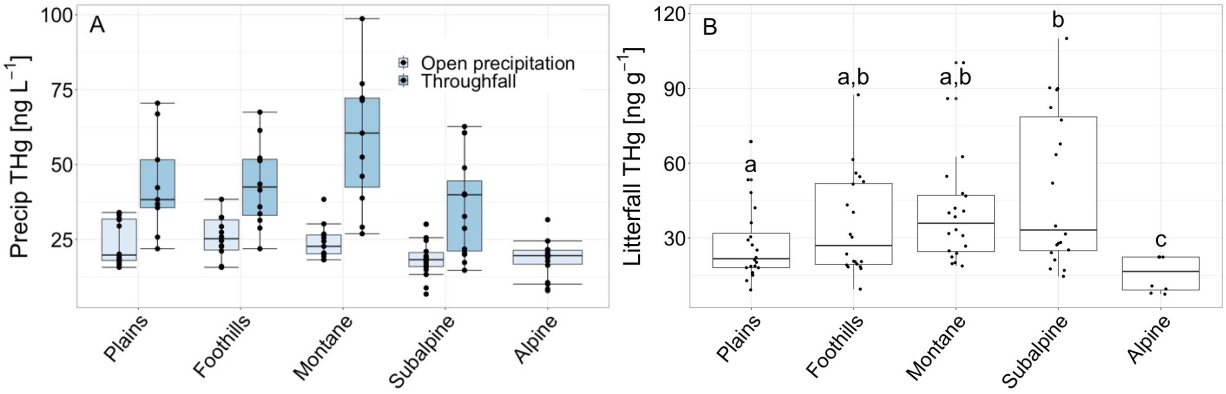

Figure 3-2: Concentrations of total mercury (THg) in open precipitation and throughfall (A) and litterfall (B) along the elevation gradient during the growing season.

3.4.3 Vegetation

Bulk aboveground vegetation THg concentrations ranged from 4.2 to 28.7 ng g^{-1} across the elevation gradient and were significantly higher in the alpine (22.3 ± 7.6 ng g^{-1}) compared to the plains (4.2 ± 0.1 ng g^{-1}; $p < 0.01$; Fig. 3-3A). Pools of THg in bulk vegetation ranged from 0.05 μg m^{-2} to 2.8 μg m^{-2} and were significantly higher in the alpine (2.5 ± 0.4 μg m^{-2}) compared to the plains, montane, and subalpine (0.1 – 1.0 μg m^{-2}; $p < 0.05$; Fig. 3-3B). Across the elevation gradient, THg concentrations were highest in the leaf tissues of herbaceous plant species (10.0 ± 4.2 ng g^{-1}) compared to graminoid and shrub species (7.2 ± 1.6 ng g^{-1} and 6.7 ± 2.3 ng g^{-1}, respectively; Fig. 3-3A), although the differences were not statistically significant ($p > 0.05$). Averaged across all three functional groups, THg concentrations were significantly higher in the foothills (11.6 ± 4.2 ng g^{-1}) compared to the alpine (4.7 ± 0.3 ng g^{-1}) and on average higher than the montane (8.5 ± 1.6 ng g^{-1}), plains (8.3 ± 2.1 ng g^{-1}), and subalpine (6.7 ± 1.9 ng g^{-1}). Average THg concentrations in combined herbaceous, graminoid, and shrub tissues along the elevation gradient had a strong positive relationship with open precipitation concentrations ($p = 0.03$; $R^2 = 0.75$). *Achillea millefolium* THg concentrations ranged from 6.0 to 13.2 ng g^{-1} and generally increased with elevation; we observed significantly higher concentrations in the alpine compared to the plains ($p < 0.05$; Fig. 3-3D).

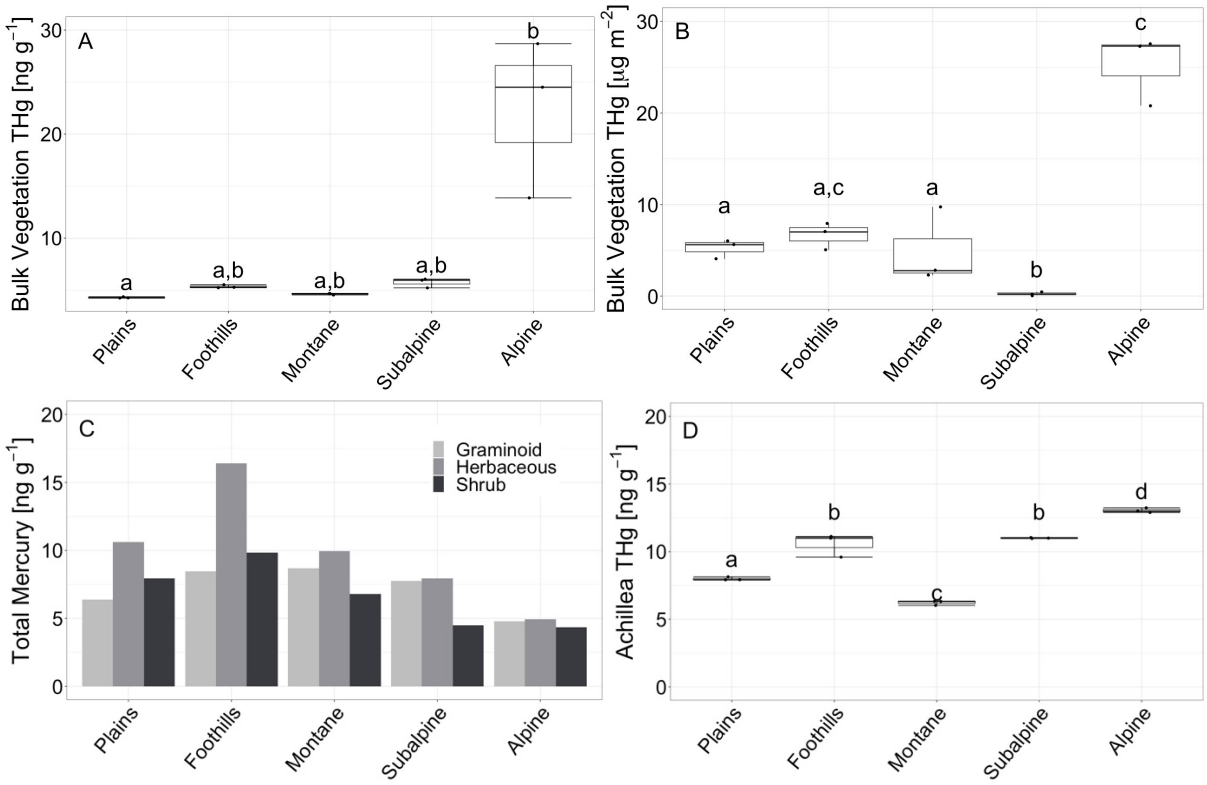

Figure 3-3: Bulk vegetation concentrations (A) and pools (B), as well as concentrations of THg in graminoid, herbaceous, and shrub functional groups (C), and concentrations in *Achillea millifolium* (D).

3.4.4 Soil

Soil litter layer THg concentrations ranged from 32.2 to 47.7 ng g^{-1} and were significantly lower in the plains (33.5 ± 1.7 ng g^{-1}) compared to the foothills (39.4 ± 0.0 ng g^{-1}), subalpine (41.1 ± 0.4 ng g^{-1}), and alpine (44.7 ± 3.5 ng g^{-1}; $p < 0.05$; Fig. S3-3A). Soil litter THg concentrations in the subalpine and alpine were also significantly higher than the montane concentrations (34.3 ± 1.0 ng g^{-1}). Litter THg concentrations have a positive relationship with elevation ($p < 0.01$; $R^2 = 0.57$; Fig. S3-3B; Table S3-2), as well as with *Achillea millifolium* THg concentrations ($p < 0.01$; $R^2 = 0.64$).

Soil O horizons on east-facing slopes were only present in the plains and subalpine sites so patterns could not be analyzed across the entire elevation gradient. THg concentrations at these sites ranged from 73 to 120 ng g^{-1}.

Soil THg concentrations in the A horizon ranged from 19.9 to 92.0 ng g^{-1} with significantly higher concentrations in the alpine (66.3 ± 25.3 ng g^{-1}) compared to the foothills (26.1 ng g^{-1}; $p < 0.05$; Fig. 3-4A). THg concentrations in the A horizon were most strongly correlated with percent N ($p < 0.01$; $R^2 = 0.69$), SOM ($p < 0.01$; $R^2 = 0.49$), percent water content ($p < 0.01$; $R^2 = 0.45$), and sulfate concentrations ($p = 0.01$; $R^2 = 0.29$; Table S3-2). Supporting our hypothesis, we found a weak significant relationship between soil THg concentrations and elevation ($p < 0.05$; $R^2 = 0.21$; Fig. S3-3) and soil litter layer THg concentrations ($p < 0.01$; $R^2 = 0.11$). Combined, percent water, SOM, and percent N significantly predicted THg concentrations (p-value = 0.01; $R^2 = 0.61$). When adding elevation as a predictor, the linear model was no longer significant ($p > 0.05$). Soil THg concentrations had a significant positive relationship with open precipitation fluxes ($p = 0.02$; $R^2 = 0.24$), but no relationship with throughfall THg concentrations or throughfall fluxes ($p > 0.05$). Interestingly, soil A horizon THg concentrations had a slightly negative relationship with litterfall fluxes ($p = 0.05$; $R^2 = 0.14$) and open precipitation concentrations ($p < 0.01$; $R^2 = 0.3$). Finally, soil THg concentrations were positively related to vegetation THg pools along the elevation gradient ($p < 0.05$; $R^2 = 0.26$).

Soil THg pools in the top 5 cm of the A horizon ranged from 0.9 to 3.5 mg m^{-2} across the elevation gradient, and were highest in the alpine, although no sites were significantly different from each other ($p > 0.05$; Fig. 3-4B). Similar to soil THg concentrations, THg pools were best predicted by percent N ($p < 0.01$; $R^2 = 0.63$), SOM ($p < 0.01$; $R^2 = 0.41$), and percent water content ($p < 0.05$; $R^2 = 0.23$; Table S3-2). There was no significant relationship between THg pools and elevation ($p > 0.05$)

or sulfate concentrations ($p = 0.09$, $R^2 = 0.12$). Open precipitation fluxes weighted by canopy cover had a significant positive relationship with soil THg pools ($p = 0.02$; $R^2 = 0.21$), but we did not observe a significant relationship with litterfall or throughfall concentrations or fluxes ($p > 0.05$).

Soil THg normalized to SOM ranged from 0.15 to 0.52 μg Hg g SOM^{-1} and is highest in the mid-elevation zones, with the montane zone (0.43 ± 0.03 μg g^{-1}) marginally higher than the plains (0.25 ± 0.09 μg g^{-1}; $p = 0.09$; Fig. 3-3–3-4C). Elevation did not significantly predict THg:LOI across the gradient ($p > 0.05$), nor did the other predictors including % water content, % nitrogen, sulfate concentrations, or C:N. ($p > 0.05$).

Soil MeHg concentrations along the elevation gradient range from below detection to 0.6 ng g^{-1} (Fig. 3-4D), while soil MeHg concentrations normalized to SOM were highest in the mid-elevation zones (Fig. S3-4). In both instances, none of the sites were significantly different from each other ($p > 0.05$).

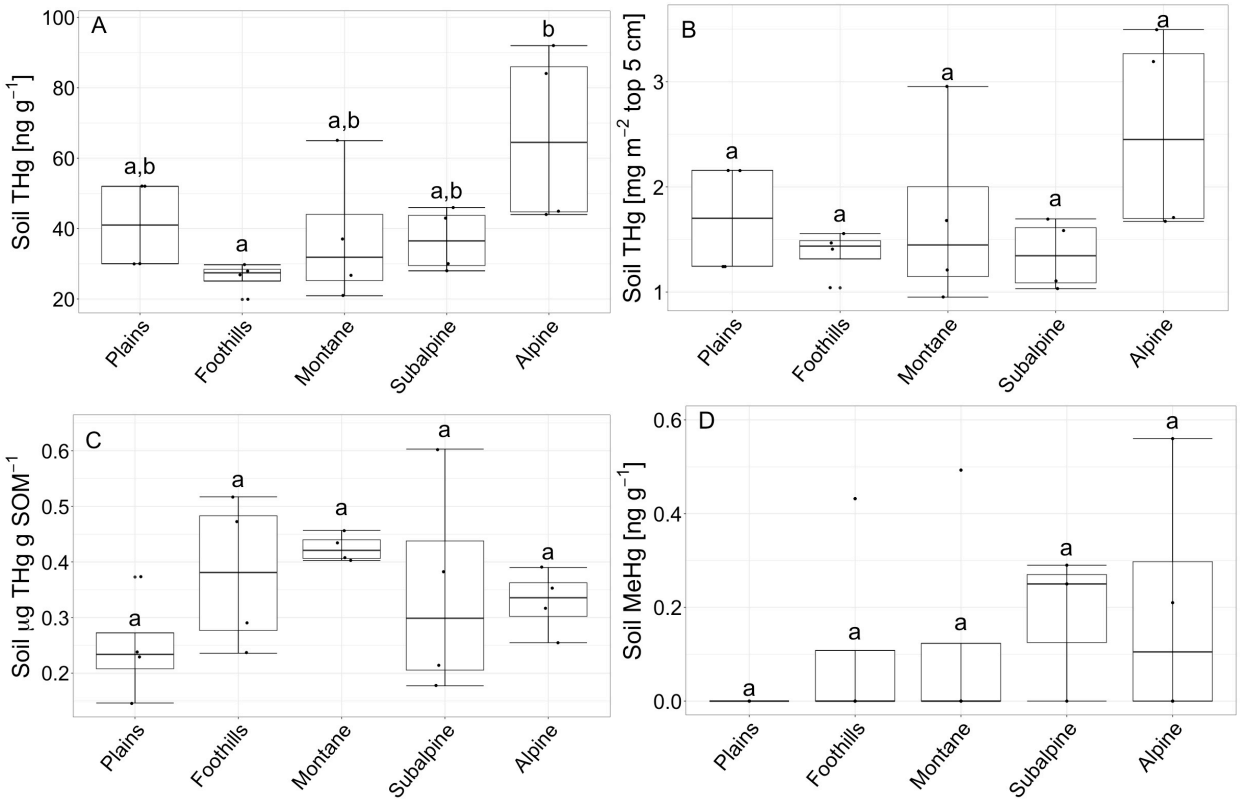

Figure 3-4: Elevation gradient soil total mercury (THg) concentrations (A), THg pools (B), THg normalized to organic matter (C), and soil methylmercury (MeHg) concentrations (D). Lowercase letters show significance among the different sites.

Soil THg concentrations in the top 10 cm of the soil (A and O horizons combined when present) ranged from 16.0 to 280 ng g^{-1} and are significantly higher on north-facing slopes (30.0–280 ng g^{-1}) compared to east- and south-facing slopes (16–83 ng g^{-1}; $p < 0.05$; Fig. 3-5A). Soil THg concentrations normalized to SOM ranged from 0.15 to 0.52 μg Hg g^{-1} SOM and generally decreased from the foothills

to the subalpine but are not significantly different across aspects ($p > 0.05$; Fig. 3-5B).

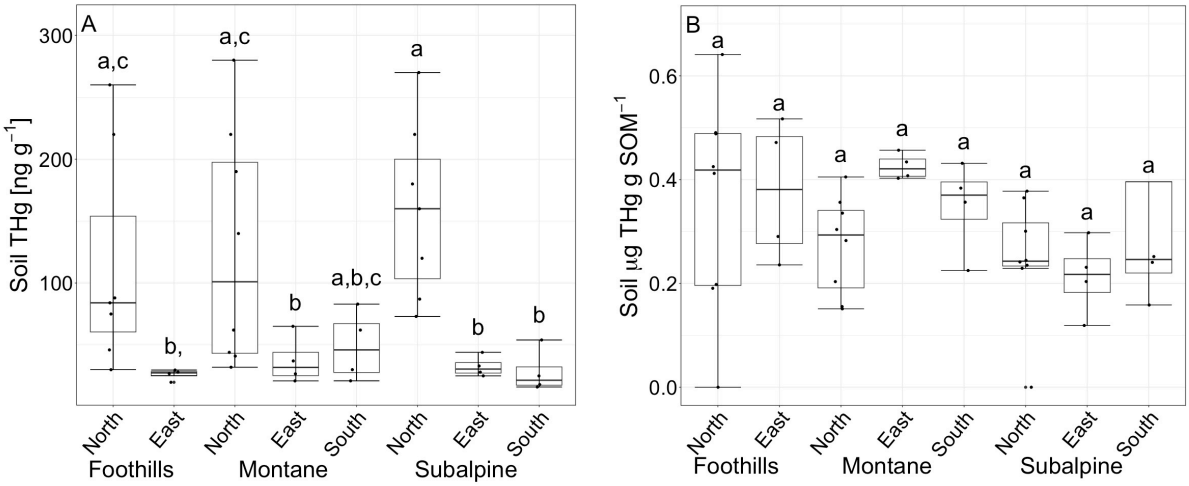

Figure 3-5: Total mercury (THg) concentrations (A) and THg normalized to SOM (B) for combined A and O horizons for different aspects in Foothills, Montane, and Subalpine elevation zones.

3.4.5 Terrestrial Hg Fluxes

Average open precipitation Hg fluxes during the growing season were higher in the plains (5.5 ± 0.1 ug m^{-2}), foothills (5.9 ± 0.2 ug m^{-2}), and montane (5.8 ± 0.4 ug m^{-2}) compared to the subalpine (3.6 ± 0.2 ug m^{-2}) and alpine (4.3 ± 0.3 ug m^{-2}; Fig. 3-6A and Table 3-1). Due to greater precipitation volumes at high elevation sites during the winter months, annual THg fluxes were highest in the subalpine (13.6 ± 0.5 ug m^{-2}) although the differences among sites were not large; they all fell between 12.1 ± 0.4–13.6 ± 0.5 ug m^{-2} (Fig. 3-6B; Table 3-1). No significant relationship was found between elevation and growing season or annual open precipitation THg fluxes ($p > 0.05$).

Average growing season throughfall THg fluxes were highest in the montane (4.3 ± 0.7 ug m^{-2}) and foothills (3.9 ± 0.6 ug m^{-2}) and had a marginally significant quadratic relationship with elevation ($p = 0.05$, Fig. 3-6A, Table 3-1). Average annual throughfall THg fluxes were highest in the montane (13.6 ± 1.6 ug m^{-2}) and

subalpine (12.7 ± 1.7 ug m^{-2}) and no significant relationship was found with elevation (($p > 0.05$; Fig. 3-6B; Table 3-1).

Average growing season litterfall THg fluxes were highest in the subalpine (5.2 ± 0.8 ug m^{-2}), lowest in the alpine (0.2 ± 0.0 ug m^{-2}) and gradually decreased from the montane to the plains (Fig. 3-6A). A similar pattern was observed for average annual litterfall Hg fluxes with the greatest fluxes in the subalpine (6.5 ± 0.8 ug m^{-2}) and a gradually decreasing trend from the montane (3.6 ± 0.5 ug m^{-2}) to the plains (2.8 ± 0.8 ug m^{-2}; Fig. 3-6B). No significant relationship was found between elevation and growing season or annual litterfall THg fluxes ($p > 0.05$). A marginally significant relationship was found between both growing season ($p = 0.08$; $R^2 = 0.7$) and annual ($p = 0.06$; $R^2 = 0.8$) litterfall fluxes and elevation when removing the alpine site.

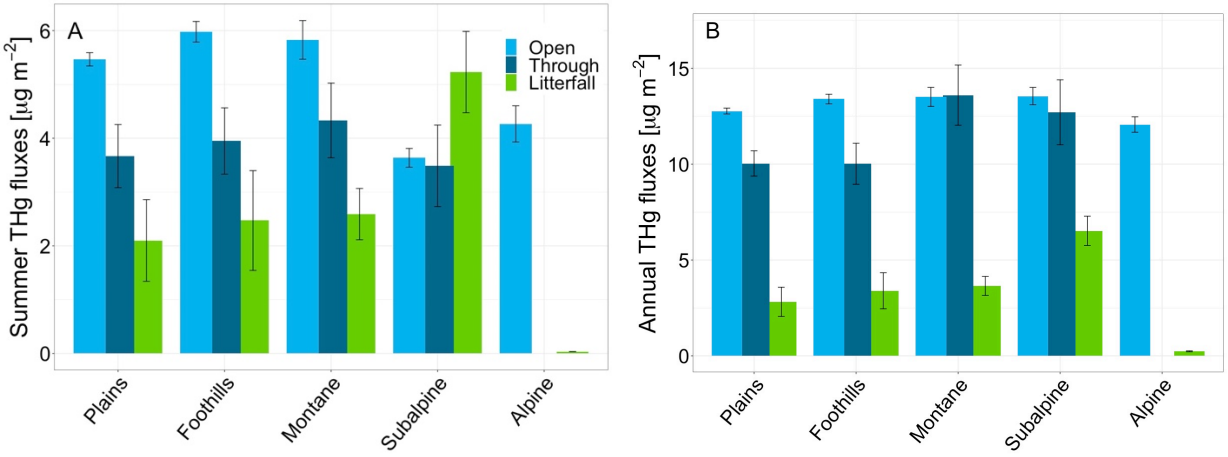

Figure 3-6: Fluxes of THg in litterfall, open precipitation, and throughfallfor the growing season (A) and year (B) along the elevation gradient.

Percent canopy within each elevation zone was determined from analysis of MODIS VCF data to be 13% in the plains, 32% in the foothills, 35% in the montane, and 40% in the subalpine (Table S3-3). Growing season fluxes of THg weighted by canopy cover were highest in the montane (6.2 ug m^{-2}) and foothills (6.1 ug m^{-2}; Fig. 3-7A); whereas, annual fluxes of THg were highest in the subalpine (15.8 ug m^{-2})

and montane (14.9 ug m^{-2}; Fig. 3-7B). Both growing season and annual fluxes of THg were dominated by open precipitation, which made up 38 %–99 % of total fluxes. When considering only the growing season, litterfall and throughfall fluxes made up similar contributions to total fluxes, except for the subalpine. There, litterfall was 37 % and throughfall only 25 % of total THg fluxes. When considering annual fluxes, throughfall contributions (9–32 %) increased relative to litterfall contributions (1–16 %). The quadratic component of elevation significantly predicts average growing season and annual THg fluxes along the elevation gradient ($p < 0.01$).

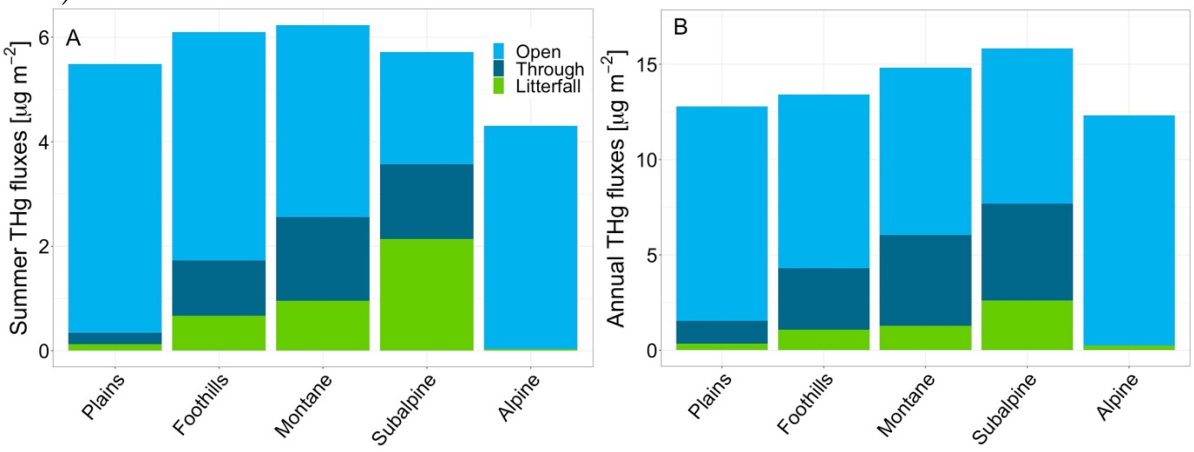

Figure 3-7: Canopy-weighted proportions of total mercury (THg) fluxes for the growing season (A) and year (B) with the contribution of each flux indicated by sample type color.

Average spatially modeled THg fluxes within each elevation zone were nearly identical to canopy-weighted calculations, with the difference due to elevational flux interpolation between sampling locations within the watershed (Table 3-1). Loads of THg within each elevation zone ranged from 0.8 g Hg in the alpine to 2.7 g Hg in the montane for the growing season (Fig. 3-8E), and 2.5 g Hg in the alpine to 6.5 g Hg in the montane for the whole year (Fig. 3-8D; Table 3-1). Total loads of Hg into the Boulder Creek Watershed were 8.8 g for the growing season and 21.9 g annually (Table 3-1). Although modeled average fluxes at the elevational-zone scale were

nearly identical to non-spatial calculations, our modeling demonstrated significant within-zone spatial variation in Hg flux, primarily driven by variation in canopy cover.

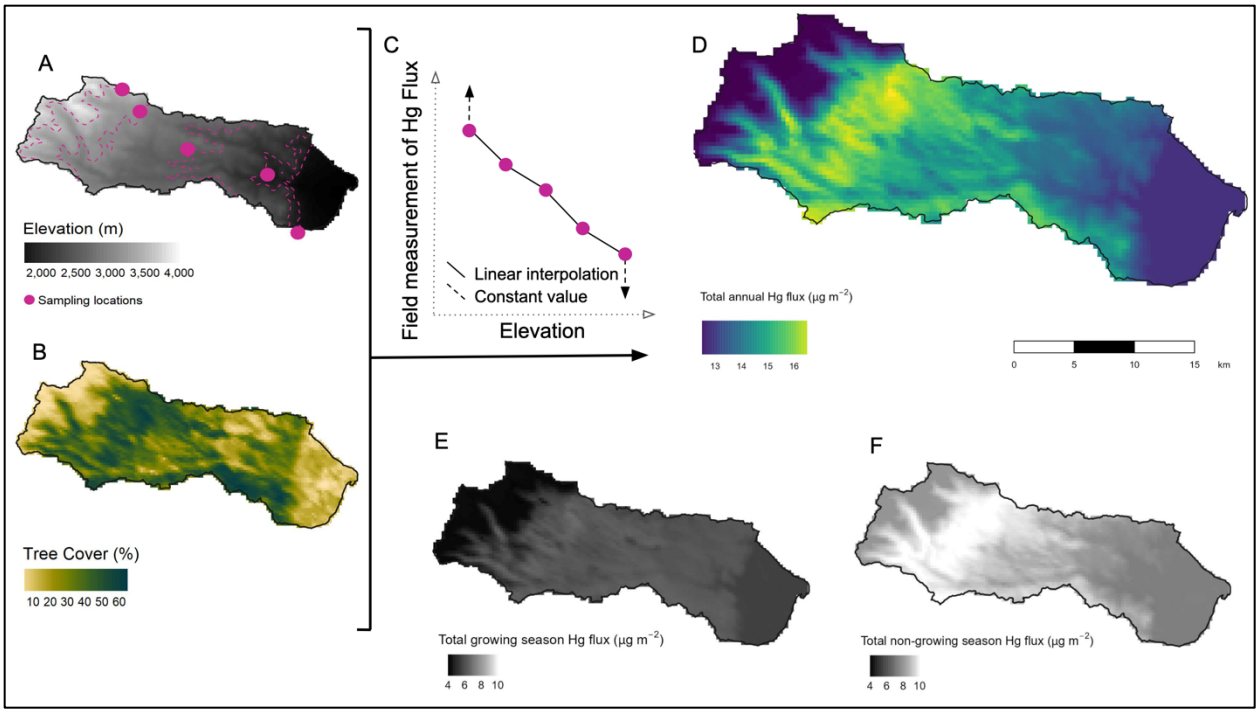

Figure 3-8: Flux modeling schematic. (A) The Headwaters Boulder Creek Watershed with sampling locations (pink circles) and elevation contours (pink dashed lines) used for interpolation and spatial analysis. (B) Percent canopy cover within the Headwaters Boulder Creek Watershed based on the MODIS VCF data product. (C) Schematic illustrating the approach used for interpolation of mercury (Hg) fluxes across elevation bands. Modeled annual (D), growing season (E), and non growing season (F) Hg fluxes across the Headwaters Boulder Creek Watershed based on interpolated fluxes and canopy cover.

Table 3-1: Open precipitation, throughfall, and litterfall fluxes (μg m^{-2}, unless otherwise stated) for both the growing season and full year. "Unweighted" values represent fluxes not taking into consideration percent canopy cover while "canopy-weighted" values are adjusted to account for percent canopy cover.

Elevation Zone	Open precipitation unweighted growing season fluxes	Open precipitation canopy-weighted growing season fluxes	Open precipitation % total growing season inputs	Open precipitation unweighted annual fluxes	Open precipitation canopy-weighted annual fluxes	Open precipitation % total annual inputs
Plains	5.5 ± 0.1	4.8	87%	12.8 ± 0.2	11.2	88%
Foothills	5.9 ± 0.2	4.1	66%	13.4 ± 0.3	9.1	68%
Montane	5.8 ± 0.4	3.8	61%	13.5 ± 0.5	8.8	59%
Subalpine	3.6 ± 0.2	2.2	38%	13.6 ± 0.5	8.1	51%
Alpine	4.3 ± 0.3	4.3	99%	12.1 ± 0.4	12.1	98%

	Throughfall unweighted growing season fluxes	Throughfall canopy-weighted growing season fluxes	Throughfall % total growing season inputs	Throughfall unweighted annual fluxes	Throughfall canopy-weighted annual fluxes	Throughfall % total annual inputs
Plains	3.6 ± 0.8	0.5	8%	10.3 ± 0.7	1.2	9%
Foothills	3.9 ± 0.6	1.3	21%	10.0 ± 1.1	3.2	24%

Montane	4.3 ± 0.7	1.5	24%	13.6 ± 1.6	4.8	32%
Subalpine	3.5 ± 0.8	1.4	25%	12.7 ± 1.7	5.1	32%
Alpine						

	Litterfall unweighted growing season fluxes	Litterfall canopy-weighted growing season fluxes	Litterfall % total growing season inputs	Litterfall unweighted annual fluxes	Litterfall canopy-weighted annual fluxes	Litterfall % total annual inputs
Plains	2.1 ± 0.8	0.3	5%	2.8 ± 0.8	0.3	3%
Foothills	2.5 ± 0.9	0.8	13%	3.4 ± 0.9	1.1	8%
Montane	2.6 ± 0.5	0.9	15%	3.6 ± 0.5	1.3	9%
Subalpine	5.2 ± 0.8	2.1	37%	6.5 ± 0.8	2.7	16%
Alpine	0.2 ± 0.0	0.2	1%	0.2 ± 0.0	0.2	2%

	Total canopy-weighted growing season fluxes	Modeled total canopy-weighted growing season fluxes	Total canopy-weighted annual fluxes	Modeled total canopy-weighted annual fluxes	Growing season THg loads (g)	Annual total Hg loads (g)
Plains	5.5	5.5	12.8	13.0	1.1	2.7
Foothills	6.1	6.1	13.4	12.9	2.2	4.6

Montane	6.2	6.1	14.9	14.6	2.7	6.5
Subalpine	5.7	5.5	15.8	16.2	1.9	5.6
Alpine	4.5	4.2	12.3	12.6	0.8	2.5

3.4.6 Chickadees

Methylmercury concentrations in chickadee feathers ranged from 38.9 to 551.4 ng g^{-1} across the elevation gradient and were significantly higher in the mid-elevation zones (205 ± 155 ng g^{-1}) compared to other elevations ($p < 0.01$; Fig. 3-9 and S5). The quadratic component of a GLM with elevation as a predictor was significant ($p < 0.01$; AIC = 36), but the linear component was not (Table S3-1). Chickadee MeHg concentrations were best predicted by a positive relationship with throughfall THg fluxes (GLM; $p < 0.01$; AIC = 7) and had a significant positive relationship with precipitation fluxes ($p = 0.01$; AIC = 20) and throughfall concentrations ($p = 0.03$; AIC = 21). A model combining the quadratic component of elevation and all input concentrations and fluxes provided a model fit with an AIC of -9 and all components were significant ($p < 0.05$).

3.5 Discussion

In this study, we provide a comprehensive evaluation of Hg cycling across a semi-arid mountain elevation gradient in the Colorado Rocky Mountains. The findings from this research demonstrate that in addition to elevation, environmental gradients in vegetation cover, precipitation, and aspect play important roles in Hg cycling. Here, we discuss the primary patterns and drivers of Hg distribution in our study and the implications for MeHg bioaccumulation. We end by characterizing the Hg cycling role of different elevation zones within semi-arid western U.S. mountain ecosystems and highlight areas for future research. This work pieces together a coherent assessment of the relative important of different pathways of Hg cycling and compares our observations in the Colorado Rocky Mountains to mountain regions elsewhere.

3.5.1 Air Mass Source and Tree Cover Mediate Terrestrial Inputs of Hg in Mountain Environments

Contrary to past studies in mountain environments (e.g., (Blackwell and Driscoll, 2015; Fu et al., 2016; Gerson et al., 2017; Table S5), we found elevated TGM and THg fluxes in open precipitation at lower elevations along our study gradient (Fig. S3-1A and Fig. 3-2A), likely due to local Hg sources from the Denver Metropolitan Area. Local point sources combined with meteorological conditions in the Colorado Front Range can drive pooling of pollutants in lower elevation regions, particularly in the summer (Flocke et al., 2020). This is supported by the more depleted δ^{202}Hg observed at our plains site compared to other regions, which is indicative of industrial Hg sources (Fu et al., 2016; Tate et al., 2023, Fig. S3-1C). Indeed, elevated TGM concentrations and open precipitation Hg fluxes are likely driven by five coal-fired power plants within a 250 km radius of our study site, as well as a variety of other pollution sources from oil and gas processing and vehicular emissions (Hornbrook et al., 2017).

Smoke intrusions from Canadian wildfires and above average precipitation volumes may also have contributed to elevated TGM and open precipitation THg fluxes at lower elevations. During spring 2023 (particularly May 18–24th), the city of Boulder, CO recorded air PM2.5 of 140 μg m^{-3} from a smoke plume transported south from Canada (UCAR, 2023). Wildfire smoke is known to transport high concentrations of Hg in various forms, including TGM (McLagan et al., 2021). The 2023 plume only reached our lower elevation sites (i.e., <2,500 m) and was not observed at our higher elevation sites, potentially contributing to the pattern of greater Hg in the air and open precipitation at lower elevations. This again is supported by lower δ^{202}Hg observed in our plains site, particularly during the month of May, which is associated with Hg transported in smoke plumes (Richter et

al., 2023). In addition to higher Hg concentrations at lower elevations, Spring 2023 was characterized by intense precipitation events <2,500 m in Boulder County that increased precipitation volumes by 170 and 260 % compared to the past 30-year average in May and June, respectively (NOAA Physical Sciences Laboratory, 2024; Table S3-3). Comparatively, precipitation in the alpine and subalpine zones was lower than average. The higher-than-average lower elevation precipitation volumes likely contributed to the higher fluxes of THg in open precipitation that we observed during our sampling period.

We expect that changes in forest structure and composition drove patterns of THg fluxes in litterfall along the elevation gradient. The transition from sparse Ponderosa Pine forests in the plains to dense Engelmann Spruce and Subalpine Fir forests in the subalpine likely drive significant increasing trends in litterfall THg concentrations and fluxes with elevation, with the highest litterfall loads in the subalpine (Table S3-3). Despite comparable THg concentrations to past studies, litterfall THg fluxes in our study (3.3 ± μg m^{-2} yr^{-1}) were generally lower than rates found in the Adirondack Mountains (7.0 ± 0.8 μg m^{-2} yr^{-1}), Tibetan Plateau (4.1 – 38.5 μg m^{-2} yr^{-1}; Li et al., 2022), Swiss Alps (25.0 ± 0.28 μg m^{-2} yr^{-1}), and Great Smoky Mountains (10.3–29.3 μg m^{-2} yr^{-1}) due to lower litterfall masses in the mountain coniferous forests compared to these sites (Table S3-3). (Fisher & Wolfe, 2012; X. W. Fu et al., 2010; X. Li et al., 2022). Therefore, litterfall is less important for THg fluxes in the U.S. mountain west than other mountain environments previously studied.

Integrating open precipitation and tree cover characteristics, throughfall concentrations and fluxes were highest in mid-elevation zones. Elevated throughfall concentrations may be driven by greater dry deposition since open precipitation concentrations were not higher in this elevation zone. Greater dry deposition may

be the result of increasing canopy cover and shifts toward tree species that have denser canopies that can sorb more Hg onto their surfaces. The higher fluxes of THg in throughfall is likely due to both higher concentrations in throughfall, as well as increasing precipitation volumes.

Interestingly, throughfall concentrations in our study were notably higher than past studies (Blackwell et al., 2014; Fisher and Wolfe, 2012; Fu et al., 2010; Gerson et al., 2017; Lawson et al., 2003; Table S5). This difference is likely due to the episodic nature of rain events in the western U.S. Concentrations of Hg in throughfall increase with the duration of dry weather preceding the rain event (Choi et al., 2008 and Rea et al., 2002 from Blackwell 2014). For example, Blackwell and colleagues (2014) found that throughfall concentrations in the Adirondack Mountains were significantly higher in 2010 (~28 ng L^{-1}) when rain events were more episodic and intense compared to more consistently rainy conditions in 2009 (~14 ng L^{-1}). And although TGM concentrations were relatively low in our study, Hg(II) concentrations (which we did not measure) have been shown to increase during periods of warm air temperatures and dry weather (Han et al., 2004 from Blackwell 2014). Conifer needles with high needle surface area are highly efficient at sorbing Hg(II) onto their needle surfaces during these dry periods, which can lead to high concentrations of THg in throughfall. This result may also explain the quadratic relationship between throughfall THg concentrations and elevation since *Pinus contorta* forest cover within the mid-elevation zones have denser canopy structure than *Pinus ponderosa* forests at lower elevation leading to greater throughfall interception and Hg wash off in those mid-elevation regions (Battaglia et al., 2018).

Despite higher throughfall concentrations, fluxes of THg in throughfall fell within a similar range to past studies due to generally lower precipitation volumes

at our sites (Table S5). It is well documented that precipitation volumes under canopy is reduced due to canopy interception (Dohnal et al., 2014) and this effect may be exaggerated in semi-arid western U.S. mountain ecosystems where intense heat and sunlight prior to short, intense storms results in a considerable portion of the precipitation evaporating from foliar surfaces rather than passing through to the soil beneath (Andreasen et al., 2023). This reduced throughfall volume was observed anecdotally during our study, when direct precipitation collectors would fill completely during one afternoon storm event while throughfall collectors would receive negligible inputs during the same storm and take four times as long to fill in some instances. Only during sustained or closely coupled storms did the throughfall collectors receive inputs comparable to direct precipitation collectors. In regions like the eastern U.S. where storms persist for longer periods of time, throughfall volumes are more likely to mirror open precipitation volumes. However, in the Western U.S., storms are often of much shorter duration, so precipitation volumes in throughfall are likely to be much smaller than open precipitation and therefore significantly impact total input fluxes of Hg.

As far as we are aware, THg fluxes in open precipitation, throughfall, and litterfall have not previously been measured in parallel within a semi-arid Western U.S. mountain ecosystem. Our study, therefore, provides a first assessment of the dominant pathways for Hg inputs in this region. Total annual inputs of Hg—litterfall, open precipitation, and throughfall weighted by canopy cover—were on the lower end of the range of fluxes observed in the eastern U.S. (14–44 ug m^{-2} yr^{-1}, Blackwell and Driscoll, 2015; Table 3), and showed a similar pattern of increasing fluxes with elevation below treeline. In contrast to trends observed in hardwood forest ecosystems, Figures 6C-D and Figures 8 illustrate how open precipitation and throughfall were the dominant input of THg across the elevation gradient. Although

litterfall is often considered the largest input of Hg into forested ecosystems (Zhou et al., 2021), most of these studies are based in deciduous forests. Our data suggest that in semi-arid mountain regions, precipitation in the form of both open precipitation and throughfall are the dominant sources of Hg to terrestrial ecosystems, a finding supported by Blackwell and colleagues (2014) from coniferous stands of the Adirondack Mountains. Shifts in dominant fluxes from open precipitation at the lower elevations to throughfall combined with litterfall in the mid-elevations is likely a reflection of changes in tree cover density and type with increases in elevation.

Differences in the proportions of THg inputs in our study compared to past studies may also be attributed to assumptions around canopy cover extent. Past studies have assumed forested regions have 100 % canopy cover and thus calculate total Hg inputs by summing litterfall and throughfall fluxes. In our study, we accounted for the patchiness of canopy cover across the elevation gradient by weighting fluxes of open precipitation and fluxes of throughfall combined with litterfall to percent canopy cover. We contend that our approach provides a more accurate estimate of THg fluxes and the relative proportion of the different pathways. In doing so, we demonstrate that open precipitation is an important input of THg into semi-arid coniferous mountain ecosystems. Our result supports recent findings that bioaccumulation of Hg within dragonflies in arid regions of the Western U.S. is derived primarily from open precipitation rather than litterfall Hg sources (Janssen et al., 2024).

The results from our modeling approach further support the importance of accounting for the patchiness of canopy cover within Western U.S. mountain ecosystems. We observed that localized spatial variation of THg fluxes within each elevation zone was primarily controlled by forest canopy dynamics and patterning,

demonstrating the importance of integrating broad-scale data on terrestrial ecosystem dynamics with climatic and topographic controls on Hg inputs. Accurate modeling of THg fluxes at broad ecosystem scales will require further investigation of the impact of forest structure and species composition on Hg dynamics, in addition to the role of non-tree (e.g. shrub, herbaceous) throughfall and litterfall in Hg fluxes. Shifts in forested ecosystems driven by climate change and climate-related events, such as forest-to-shrubland state transitions initiated by disturbance events, will have long-term impacts on localized THg accumulation.

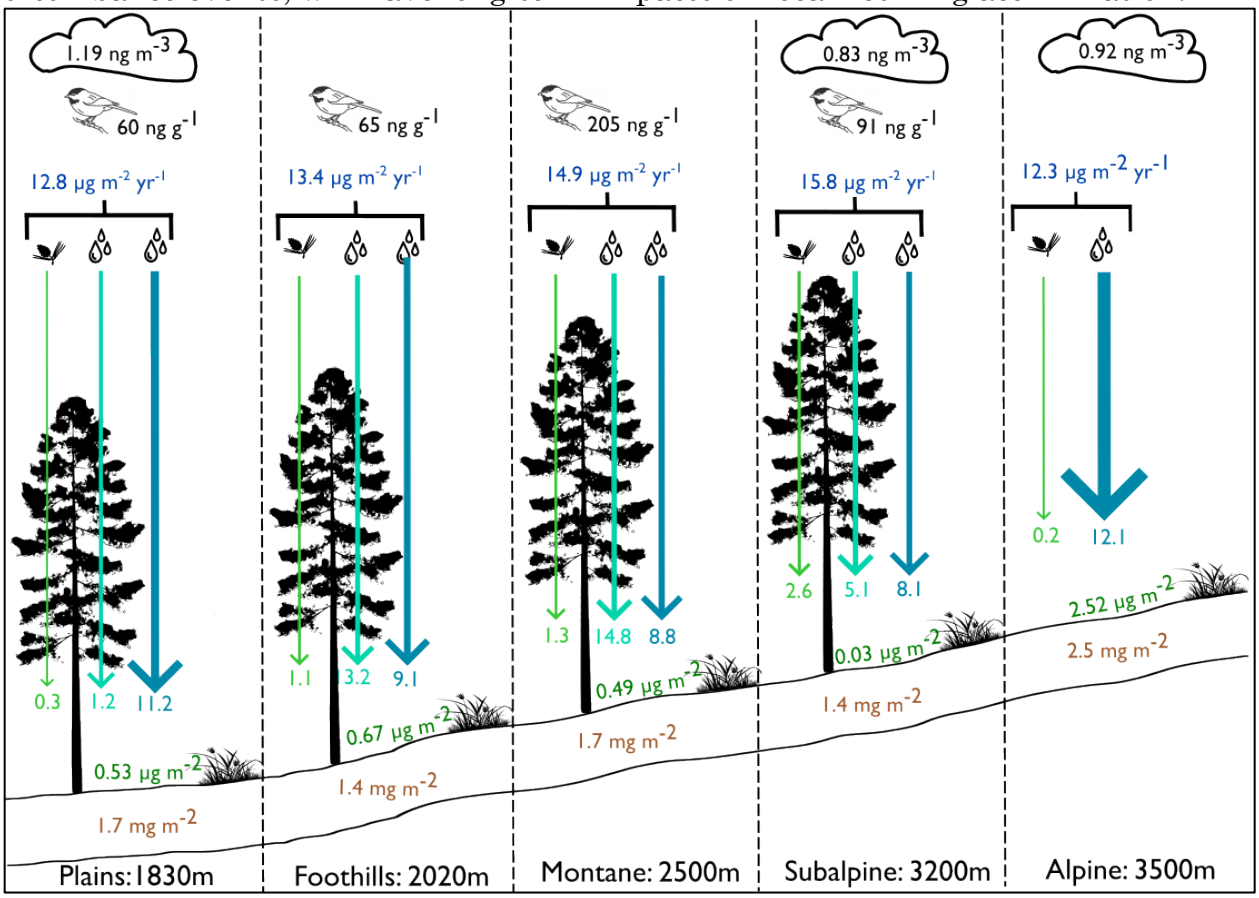

Figure 3-9: Schematic representing air THg concentrations, chickadee MeHg concentrations, annual THg fluxes (blue gradient), as well as the individual components of fluxes (litterfall (green gradient), thoughfall (teal gradient), and open precipitation (blue gradient)) bulk vegetation THg pools (green gradient), and soil THg pools (brown gradient). Darker colors and thicker arrows represent higher values.

3.5.2 Storage of Hg in Vegetation and Soil is Driven by Multiple Abiotic and Biotic Factors

The significantly higher concentrations and pools of THg in bulk vegetation from the alpine zone was unexpected, but is likely a result of shifts in plant species toward non-vascular, long-lived species, such as *Silene acaulis* and *Sedum lanceolatum*, that absorb high concentrations of Hg over time (Pleijel et al., 2021, Fig. 3-3A and Fig. 3-9). Similarly, in the Artic, Olson and colleagues (2019) found substantial Hg mass in aboveground biomass (29 μg m^{-2}) due to a high abundance of nonvascular vegetation. Greater aboveground biomass in the foothills, as well as slightly more elevated biomass THg concentrations, drove the significantly higher THg pools in the foothills region compared to the subalpine. We also observed elevated Hg in the foothills in the three main plant functional groups, which may be driven by the elevated TGM air concentrations observed at lower elevations since the primary mechanism for Hg accumulation in plants is through stomatal uptake of GEM during photosynthesis (Jiskra et al., 2015).

Increasing THg litterfall fluxes along the elevation gradient may explain the elevated THg concentrations observed in soil litter across this gradient. This did not translate to the A soil horizon, though, where instead we observed significantly higher THg concentrations and pools in the alpine and no clear patterns below treeline (Fig. 3-4A-B and Fig. 3-9). Elevated concentrations and pools of THg in alpine soils can be attributed to colder air temperatures driving slower soil C turnover compared to lower elevation sites and have been documented previously (Blackwell & Driscoll, 2015; H. Zhang et al., 2013). The lack of pattern in THg pools below treeline is likely due to a strong correlation between THg and % water

content, SOM, and % N along the gradient, all variables that do not vary significantly with elevation. Likely, this result was due to patterns in SOM whereby wetter areas promote slower C turnover leading to SOM accumulation, which is composed of N species and binds efficiently to THg in soils. This hypothesis is supported by the fact that no environmental predictors are significantly correlated with THg pools once normalized to SOM.

The importance of SOM for driving THg concentrations across mountain ecosystems extends beyond elevation patterns. Although our main study sites were on east-facing slopes, we also sampled on north- and south-facing slopes in the foothills, montane, and subalpine to assess the impact of aspect on THg concentrations within soil. Reduced solar radiation and higher soil moisture on north-facing slopes leads to greater forest and plant cover compared to east- and south-facing slopes (Littell et al., 2008). These differences lead to the development of soil O horizons on north-facing aspects which have much higher C content and are therefore more efficient at binding Hg within the soil. This pattern led to significantly higher concentrations of THg within the upper 10 cm of soil on north-facing slopes across all elevation gradients compared to south- and east-facing slopes (Fig. 3-5A). These aspect patterns are somewhat intuitive and have been observed in other mountain environments (e.g., H. Ma et al. 2022), but we highlight them here as they could have broader implications in the context of disturbance in western U.S. mountain ecosystems. For example, the western U.S. is experiencing increasing frequency and intensity of wildfire activity (Abatzoglou & Williams, 2016) and when a wildfire burns through a mountain ecosystem, the aspect where the burn occurs could dramatically alter the amount of Hg released from the surface soil layers. Moreover, difference in tree species across aspects also influences how much Hg is released from forested ecosystems during wildfire with coniferous

forests shown to release more Hg compared to deciduous, aspen forests (Biswas et al., 2007; Webster et al., 2016). This aspect dependence marks an important area for future research under increasing wildfire conditions.

The ultimate concern regarding THg within an ecosystem is its conversion to MeHg and bioaccumulation. Although only six of our 20 soil MeHg concentration samples fell above the detection limit of our instruments, the range of values (< DL–0.6 ng g^{-1}) was similar to values measured in the Adirondack Mountains of the eastern U.S. where concentrations were highest in mid-elevation coniferous zones (Gerson et al., 2017). While our sample size was too small for further analysis, the soil MeHg concentrations that were above detection were from the mid- and high-elevation zones. In general, this result suggests variable methylation potential within semi-arid upland mountain soils and a larger sampling design is needed for further investigation.

Table 3-2: Study Comparison of Air, Inputs, Vegetation, Soil, and Organism THg Concentrations, Fuxes, and Pools.

Site	References	Sample Type (average ± STD (range))						
		Air						
		Air THg concentration (ng m^{-3})						
Rocky Mountains, U.S.	This study	0.97 ± 0.20 (0.69 - 1.41)						
Miaoling Mountain Range, China	Fu et al., 2010	2.8 ± 1.51 (0.41 - 23.9)						
Mt Ailao, China	Li et al., 2022	1.7						
Rocky Mountains, U.S.	Obrist et al., 2008	1.51 ± 0.12 (1.06 - 2.15)						
Rocky [ountains, U.S.	Derry et al., 2024	1.25 ± 0.11						
		Inputs						
		Total fluxes (ug m^{-2} yr^{-1})	*Open precipitation THg concentration (ng L^{-1})*	*Open precipitation THg flux (ug m^{-2} yr^{-1})*	*Throughfall THg concentration (ng L^{-1})*	*Throughfall THg flux (ug m^{-2} yr^{-1})*	*Litterfall THg concentration (ng g^{-1})*	*Litterfall THg fluxes (ug m^{-2} yr^{-1})*
Rocky Mountains, U.S.	This study	14.2 ± 1.9	21.8 ± 5.2 (6.7 - 34.0)	13.1 ± 0.4	44.8 ± 18.8 (14.7 - 98.7)	11.5 ± 1.2	34.8 ± 24.1 (7.5 - 110)	3.3 ± 0.7
Adirondack Mountains, U.S.	Blackwell et al., 2014		5.3 ± 1.3 - 8.3 ± 1.6	(6.0 - 7.5)	13 ± 1.1 - 27.7 ± 3.2	(10.1 - 26.2)		
Adirondack Mountains, U.S.	Blackwell et al., 2015	14.1 - 44.0	(3.9 - 11.2)	(8.6 - 40.1)	(4.9 - 18.1)	(5.3 - 16.3)		

Great Smoky Mountains, U.S.	Fisher et al., 2012		6.03 ± 0.54		17.8 (9.8 - 22.6)	3.2 (1.6 - 5.6)	(37.2 - 62.9)	17.9 (10.3 - 29.3)	
Miaoling Mountain Range, China	Fu et al., 2010		4.0 (1.2 - 30.8)	6.1	8.9 (2.8 - 32.5)	10.5	91 (57 - 110)	39.5 (17.6 - 70.6)	
Adirondack Mountains, U.S.	Gerson et al., 2017	18 ± 3	8.1 ± 1.9	7.3 ± 0.3 (just the growing season)	12.4 ± 0.9	8.5 ± 0.7 (4.5 - 11.0)	(31 - 67)	7.0 ± 0.8	
Swiss alps	Huang et al., 2023						(10.5 - 350)	25.0 ± 0.28	
Green Mountains	Lawson et al., 2003				17.5 ± 6.6 (9.9 - 33.3)	16			
Mt Ailao, China	Li et al., 2022						48.7 ± 17.5 (15.8 - 118.9)	16.6 ± 7.8 (4.1 - 38.5)	
Shergyla Mountain, Tibetan Plateau	Liu et al., 2019						9.5 ± 3.3 (6.0 - 15.9)		
Southwest China	Zhou et al., 2018						85 ± 12 (71 - 108)	40.5	

	Vegetation and Soil							
	Bulk vegetation concentration (ng g^{-1})	*Bulk vegetation pools (ng m^{-2})*	*Soil litter layer THg concentration (ng g^{-1})*	*Soil O horizon THg concentrations (ng g^{-1})*	*Soil O horizon THg pools (mg m^{-2})*	*Soil A horizon THg concentration (ng g^{-1})*	*Soil A horizon THg pool (mg m^{-2})*	*Soil A Horizon MeHg conc (ng g^{-1})*

Rocky Mountains, U.S.	This study	8.5 ± 7.8 (4.2 - 28.7)	846 ± 923 (8.6 - 2754)	38.5 ± 4.8 (32.2 - 47.7)	98.0 ± 18.8 (73 - 120)		41.5 ± 19.8 (19.9 - 92.0)	1.7 ± 0.7 (0.9 - 3.5)	0.12 ± 0.2 (< DL - 0.6)
Adirondack Mountains, U.S.	Blackwell et al., 2014					13.9	84 ± 20	2.9	
Adirondack Mountains, U.S.	Blackwell et al., 2015						(72 - 598)		
Borneo Mountains	Brearley et al., 2023						227 (35.0 - 876)		
Serra do Mar Mountains, Brazil	Drummond et al., 2022						250.7 ± 79.4 (119.4 - 443.6)		
Adirondack Mountains, U.S.	Gerson et al., 2017				156 - 337	4.0 - 6.1			(0.17 - 0.39)
Shergyla Mountain, Tibetan Plateau	Liu et al., 2019						51.2 ± 15.9 (18.7 - 69.8)		
Qinling mountains, China	Ma et al., 2021						54.8 ± 31.2 (10.7 - 112.2)		
Qinling mountains, China	Ma et al., 2022			74 ± 33 (32 - 200)	71 ± 36 (30 - 166)		34 ± 17 (10 - 83)		
Catskill Mountains, U.S.	Townsend et al., 2014				(65 - 503)				
Himalayas, Nepal	Tripathee et al., 2019						35.8 ± 24.2 (3.8 - 105.7)		
Southwest China	Zeng et al., 2022			40.9 ± 20.8			(24.3 - 230)		

Southwest China	Zhang et al., 2013					190 (70 - 380)
Southwest China	Zhou et al., 2018			91 ± 1	220 ± 29	127 ± 4

Biota

		Organism type	*Organism MeHg concentration (ng g^{-1})*
Rocky Mountains, U.S.	This study	Chickadee blood equivalent	5.1 ± 3.0 (2.3 - 14.8)
Serra do Mar Mountains, Brazil	Drummond et al., 2022	Amphibian tissues	126.1 ± 85.4 (50.3 - 492.6)
Qinling mountains, China	Ma et al., 2021	Non-volant mammals	43.0 ± 35.0 (8.3 - 183.0)
Adirondack Mountains, U.S.	Sauer et al., 2020	Song bird blood Hg conc	(18 - 112)
Catskill Mountains, U.S.	Townsend et al., 2014	Thrushes blood Hg	(58 - 110)
Catskill Mountains, U.S.	Townsend et al., 2014	Whole salamander	169 ± 2.1

3.5.3 MeHg Bioaccumulation in Birds is Associaciated with Throughfall Concentrations

Although the storage of THg is greatest in high-elevation zones, we did not observe elevated bioaccumulation within the alpine zone. Rather, greater annual fluxes of THg, as well as greater contributions from throughfall and litterfall, appear to drive the elevated MeHg bioaccumulation observed in mid-elevation zones. This suggests that "fresher" Hg sources in atmospheric deposition are more important for driving terrestrial Hg bioaccumulation compared to Hg stored in soils, an observation that is supported by work from Bishop and colleagues (2020). As illustrated in Figure 9, more extensive canopy cover and larger proportions of atmospheric inputs from litterfall and throughfall likely make the soil conditions in the mid-elevation zones more conducive to MeHg formation by providing a labile source of C, as well as inorganic Hg to methylating microbes (Grigal, 2003). This pattern was also found by Sauer and colleagues (2020) who observed elevated MeHg concentrations in songbirds at mid-elevation zones in the Adirondack Mountains. They attributed this pattern to elevated atmospheric Hg deposition in these elevation zones, and conversion to MeHg within soils (Sauer et al., 2020).

While soil THg concentrations and pools did not predict MeHg concentrations in chickadees, THg normalized to SOM explained 21 % of the variation and was marginally significant (GLM, $p = 0.07$). A higher ratio of THg to SOM generally indicates more labile Hg that is available for methylation. Although most of our soil samples were below detection for MeHg concentrations, the samples that were above detection were in the mid- and higher elevation zones (Fig. 3-2). Therefore, it is possible that higher fluxes of THg in throughfall in mid-elevation zones drives

higher concentrations of bioavailable Hg and methylation in the soil, which leads to greater contamination and bioaccumulation within terrestrial wildlife, as seen in our chickadee MeHg concentration data.

To assess the broader extent of elevated THg:SOM in mid-elevation zones, we analyzed a subset of USGS soil THg data (C. I. Olson et al., 2022) from within the Rocky Mountain region. Although there were no significant patterns, the highest values of soil THg:SOM were in mid-elevation zones like our study (Fig. S3-6). These findings are important to consider in the context of Hg contamination for mountain wildlife since species richness tends to be highest in mid-elevation zones in mountain ecosystems for a variety of animals including reptiles, birds, and mammals (Y. Ma et al., 2021). Although our chickadee concentrations are not within levels of concern previously established for songbirds (Ackerman et al., 2016), this dataset is important to establish a baseline for environmental and montane fauna that can be monitored as changes from policies implemented by the Minamata Convention on Mercury intersect with climate change over the coming decades.

3.5.4 Synthesizing Hg Dynamics Across Ecosystems of Semi-Arid U.S. Elevation Gradients

Although elevation only explained a portion of the Hg patterns observed in our study, some general themes emerged for different elevation zones within semi-arid mountain ecosystems. In the alpine, significantly higher pools of THg within soils and vegetation highlight the role these regions play in storing Hg. Although inputs of Hg into alpine zones are lower than other elevation zones, the slow turnover of carbon in high-elevation soils results in the accumulation of Hg over

time. Additionally, longer-lived plants that do not shed leaves annually (e.g., *Silene acaulis*) allow for Hg to accumulate at higher concentrations within plant tissues providing another storage mechanism. Indeed, Mast and colleagues (2005) found that alpine regions of Rocky Mountain National Park act as a sink for Hg, storing up to 80 % of atmospherically deposited Hg annually. Although alpine zones store more THg compared to lower elevations, these regions appear to have minimal risk for contamination and bioaccumulation, likely due to the Hg being bound up within older, less labile organic carbon compounds. With continued climate change and warming, however, alpine regions are likely to experience increased thawing of permafrost features and greater mineralization of carbon within soils (D'Alò et al., 2021), which may lead to greater release of Hg downstream, as well as methylation and subsequent bioaccumulation within local wildlife. While this phenomenon is being studied extensively in the Arctic region (Schaefer et al., 2020), the release of Hg from previously recalcitrant soil pools in semi-arid mountain ecosystems is poorly understood and marks an important area for future research.

Mid-elevation zones within semi-arid mountain ecosystems appear to be the regions most at risk to Hg contamination with the greatest total annual inputs of THg, throughfall concentrations, fluxes of throughfall and litterfall, Hg:SOM ratios, and MeHg bioaccumulation in songbirds observed in this zone. Higher soil MeHg concentrations and bioaccumulation within mid-elevation zones has been documented across a range of mountain ecosystems (Y. Ma et al., 2021; Sauer et al., 2020) and may be due to cloud cap dynamics whereby the lower limit of clouds—which have the highest concentration of contaminants—tend to intercept mountain ranges at mid-elevations. This pattern has been documented for Hg (Brearley et al., 2023), as well as other compounds such as ammonium in the Colorado Front Range (Heindel et al., 2020). Although concentrations of MeHg in our chickadee feathers

are below previously established benchmarks for health risks in songbirds (Sauer et al., 2020), continued monitoring of songbirds, as well as other terrestrial species, within these mid-elevation zones will be important in the context of future climate change and policy implementation.

Finally, lowerelevation zones are dominated by atmospheric deposition via open precipitation and have the highest THg air concentrations, likely as a result of local pollution sources. This pattern is mirrored in plant THg concentrations but not in soil pools. This observation may be due to elevated evasion of THg from soils back to the atmosphere in lower altitude areas where there are warmer air temperatures and greater solar radiation. Both of these factors promote Hg volatilization and could reduce the long-term storage and bioaccumulation of Hg at lower-elevations (Eckley et al., 2016).

3.6 Conclusions

In this study, we provide a comprehensive evaluation of Hg cycling across a semi-arid mountain elevation gradient in the Colorado Rocky Mountains. Our findings reveal that elevation does not play the only role in determining Hg cycling within ecosystems across a mountain gradient. Fluxes of THg were highest in the mid-elevation zones and were dominated by open precipitation, with increasing contributions from litterfall and throughfall in the mid-to-upper elevations. Storage of Hg in soils did not mirror atmospheric deposition and instead was highest in the alpine zone due to strong correlations with SOM. Methylmercury concentrations in chickadee feathers peaked at mid-elevation, likely reflecting greater throughfall fluxes from increased coniferous canopy cover. The findings of this study underscore the complexity of Hg retention and cycling mechanisms in mountain environments,

where elevation and climatic factors interplay with ecological processes to dictate Hg storage and bioavailability.

While this work establishes a crucial baseline for understanding Hg cycling in high-elevation ecosystems, significant questions remain. Future studies should focus on quantifying soil-atmosphere TGM fluxes to address uncertainties in atmospheric re-emission rates. Investigations into Hg dynamics during extreme climate events, such as rapid snowmelt and wildfires, will enhance predictions of Hg mobility under changing environmental conditions. Additionally, the role of vegetation shifts in response to climate change, particularly the encroachment of subalpine vegetation into alpine zones, warrants further exploration to assess implications for Hg fluxes and storage patterns. By addressing these knowledge gaps, future research will enhance our understanding of mountain ecosystems as critical components of global Hg cycling, ultimately improving projections of Hg dynamics in the context of ongoing climatic change.

CHAPTER IV

CLIMATE-DRIVEN SULFATE EXPORT IN ALPINE WATERSHED MAY STIMULATE METHYLMERCURY PRODUCTION

Adapted from *Environmental Research Letters* submission:
Hannah R. Miller, Charles T. Driscoll, Sarah E. Janssen, Eve-Lyn Hinckley

4.1 Abstract

Climate change is increasing sulfate export and wetland extent in mountain regions. These changes may increase microbially-mediated production of the neurotoxic substance, methylmercury due to enhanced sulfate metabolism in mountain environments. Here, we assess methylmercury concentrations and formation rates across high-elevation wetlands in the Colorado Rocky Mountains. We also investigate sulfate controls on methylmercury production within subalpine peatlands by amending soils with sulfate additions to mimic increased stream export of sulfate from the alpine zone and measuring methylmercury formation rates for different sulfate treatments. We found that subalpine peatlands have significantly higher methylmercury concentrations and formation rates compared to alpine, mineral soil wetlands. We also found methylmercury production in subalpine peatlands increased significantly ($p < 0.05$) following sulfate additions; the highest rates occurred in sediments with intermediate extractable sulfate concentrations (~ 0.60–1.4 mg sulfate g^{-1} dry soil) and rates decreased above and below this range. Our study is the first to identify soil sulfate-related thresholds for methylmercury production and sulfate-limitation of methylmercury production in

subalpine peatlands. These findings highlight important linkages between climate-driven mineral weathering and Hg cycling in mountain regions globally.

4.2 Introduction

Mountain ecosystems are disproportionately influenced by climate change, which is causing increasing air temperatures and shifts in the amount and timing of precipitation events (Hock et al., 2019). Two lesser-known consequences of climate change in mountain regions include elevated sulfate export due to accelerated mineral weathering (Crawford et al., 2019) and changing wetland extent, both associated with thawing ice features (Dangles et al., 2017). Taken together, these trends may pose a notable risk of increased production of the neurotoxic substance methylmercury (MeHg, Fig. 4-1).

Globally, there is a well-documented increase in sulfate mobilization in runoff from mountain ecosystems (Crawford et al., 2019; Table S4-1) that results from climate-driven accelerated weathering of sulfide-bearing minerals, such as pyrite. These minerals are widespread in mountain settings (Craig & Vokes, 1993), as hydrothermal activity and metamorphism during mountain formation provide conditions conducive to the formation and concentration of sulfide deposits (Wilson et al., 1967). Some of the largest sulfide-rich ores in the world are located in high-elevation ecosystems such as the Cordillera Blanca of the Peruvian Andes Mountains (Santofimia et al., 2017) and are easily weathered when exposed to water and oxygen (Heil et al., 2022; R. Murphy & Strongin, 2009; Ross et al., 2018). This process produces sulfuric acid, which drives weathering and produces sulfate (Heil et al., 2022). The effects of climate change, including changes in precipitation and thawing of ice features, accelerate the exposure of fresh mineral surfaces, including sulfide-bearing minerals, and enhance weathering in mountain regions

(Calmels et al., 2007; Darmody et al., 2007; Todd et al., 2012). Compilation of sulfate export trends from over 150 high-elevation alpine streams and lakes (Fig. S4-1(a)) shows increasing trends ranging from 20–2000% over the past several decades as the result of a warming climate (Table S4-1). Sulfate concentrations at these sites range from 0.2–600 mg sulfate (SO_4^{2-}) L^{-1}.

Particularly in glaciated watersheds, increasing air temperatures are associated with the expansion of wetland extent and greater hydrologic connectivity to downstream regions (Dangles et al., 2017; Polk et al., 2017). Wetlands are found in mountain landscapes globally, and, generally, increase in areal extent and density with elevation (Cooper et al., 2012). As glaciers, permafrost, and other ice features thaw, more water is released downslope, and a more topographically heterogeneous landscape is exposed, promoting wetland development in the alpine (Dangles et al., 2017; Rühland et al., 2006). Alternatively, at lower-elevations in mountain environments, increasing air temperatures (Pepin et al., 2022) and changes in precipitation (Kittel et al., 2015) may reduce wetland extent, as has been predicted for subalpine peatlands of the Tibetan Plateau (J. Sun et al., 2023).

While wetlands provide critical habitat for local wildlife and act as gateways for the supply of water downstream (Cooper et al., 2012; Dahl, 2011), they also serve as important landscape features for transforming inorganic mercury (Hg) into the bioaccumulating and neurotoxic form, MeHg (St. Louis et al., 1994; J. Zhang et al., 2023). Mercury is a global pollutant and its cycling has been dramatically accelerated since the pre-industrial era by human activities such as mining, coal combustion, and other industrial practices (Streets et al., 2019). With a residence time in the atmosphere of up to one year (D. P. Krabbenhoft & Sunderland, 2013), Hg undergoes long-range transport reaching remote locations such as mountain ecosystems where it is deposited onto the landscape via dry and wet deposition

(Miller et al., 2023; Selin, 2009). There, anoxic environments within high-elevation wetlands can stimulate a phylogenetically diverse group of microorganisms containing the *hgcAB* genes and promote the microbial conversion of inorganic Hg to MeHg (Janssen et al., 2022; Parks et al., 2013). Sulfate reducing bacteria (SRB) can be particularly important—either through direct methylation or indirectly through synergistic relationships with other methylating microbes (Peterson et al., 2023); numerous studies in lowland wetland environments show a strong relationship between MeHg production and sulfate additions (Bergman et al., 2012; Coleman Wasik et al., 2012; Gilmour & Henry, 1991; Tjerngren et al., 2012). Subalpine peatlands, which are found in mountain ecosystems globally may be particularly suitable for MeHg formation. Specifically, they are high carbon (C) environments that promote microbial metabolism, and act as gateways for runoff as it moves from the alpine downslope (Brand et al., 2013; Chignell et al., 2019; French et al., 2016; Iqbal & Shang, 2020; Khan et al., 2020; van der Knaap et al., 2011). Thresholds for MeHg production with respect to sulfate concentrations have previously been established for low-elevation, agriculturally dominated peatlands such as the Florida Everglades (U.S.) (Gilmour et al., 1992; Jeremiason et al., 2006). However, these studies have limited applicability outside subtropical wetlands and our understanding of sulfate thresholds in soils from temperate and alpine environments is still lacking.

The objective of this study was to quantify MeHg accumulation across mountain wetlands, as well as to experimentally assess the impact of elevated sulfate loading on MeHg production rates in subalpine peatlands. To conduct this investigation, we sampled across a high-elevation (~3,000–3,900 m) watershed in the Colorado Rocky Mountains during the 2020–2022 growing seasons. Our research aimed to address the following questions: 1) How do concentrations of Hg

and rates of MeHg formation vary across high-elevation wetlands? and 2) How do elevated sulfate loads influence MeHg formation in subalpine peatlands? Broadly, we hypothesized that organic-rich soils with permanent inundation (e.g., subalpine peatlands) would have higher Hg concentrations, as well as rates of MeHg formation, compared to mineral soils with temporary inundation (e.g., alpine wetlands). We expected sulfate additions to increase MeHg formation in subalpine peatlands due to sulfate limitation. Ultimately, information derived from this study will inform our understanding of biogeochemical cycling of Hg in mountainous regions, critical information for effectively managing contamination of these sensitive ecosystems.

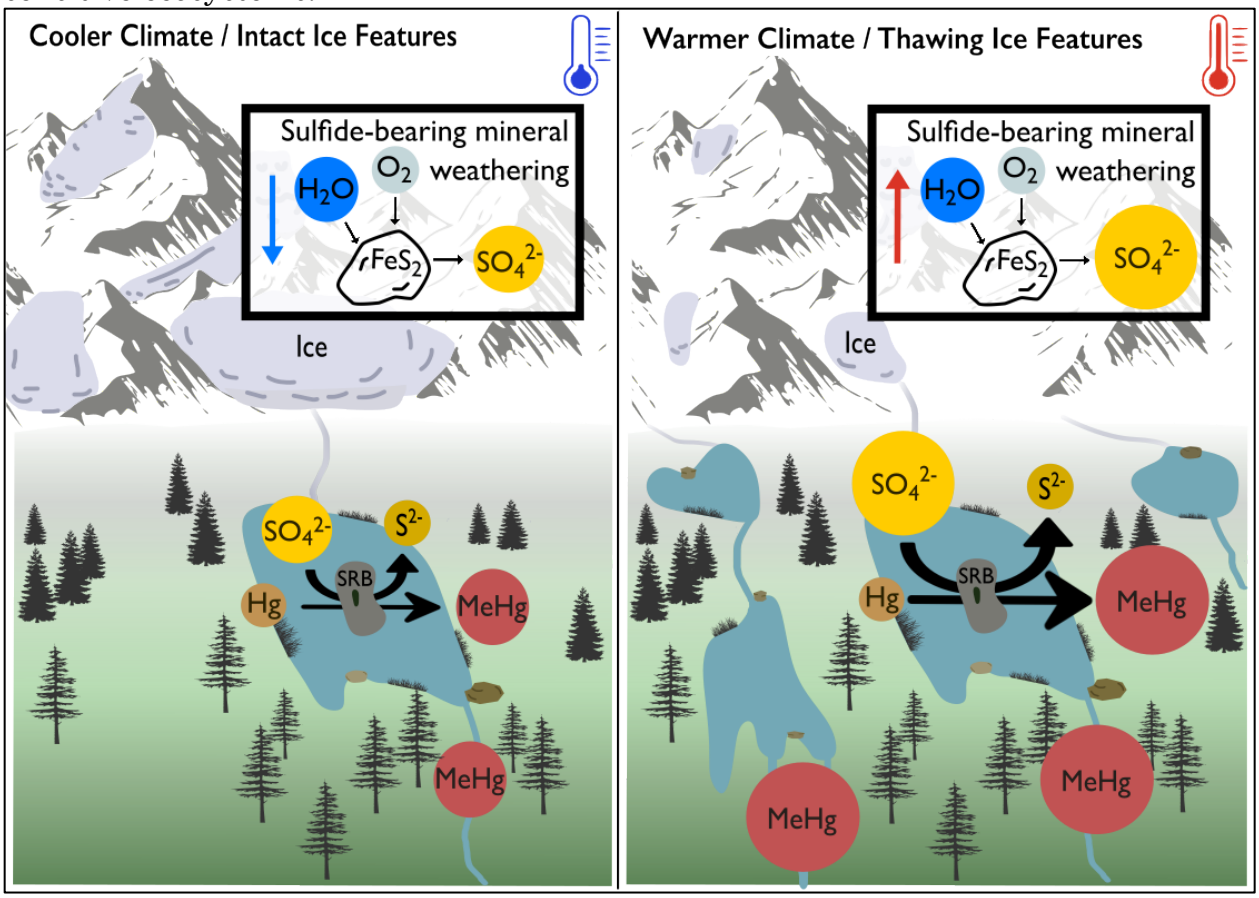

Figure 4-1: Schematic illustrating how warming air temperatures leads to thawing high-elevation ice features, accelerated weathering of sulfide (S^{2-})-bearing minerals, increased runoff of sulfate (SO_4^{2-}), and increased extent of mountain wetlands, all of

which can stimulate the activity of sulfate reducing bacteria (SRB) and production of MeHg downstream.

4.3 Methods

4.3.1 Sampling Sites

Here we use the North Boulder Watershed in the Colorado Rocky Mountains (Fig. S4-1(b)) to investigate MeHg concentrations and formation in high-elevation ecosystems. This watershed has ~10 % wetland cover dominated by mineral soil wetlands >3100 m elevation, and subalpine peatlands between 2900–3100 m elevation (Fig. S4-1(b)-(c)). The watershed has experienced increasing summer air temperatures of 0.43°C per decade since 1953 (McGuire et al., 2012) and increasing annual precipitation of 60 mm per decade since 1952 (Kittel et al., 2015). The climate-related air temperature and precipitation changes are comparable to other high-elevation ecosystems globally (Pepin et al., 2022). Importantly for this study, the North Boulder Watershed has also experienced a ~200% increase in sulfate export over the past 30 years (~10–30 kg SO_4^{2-} ha^{-1}), attributed to increased weathering of sulfide-bearing minerals (Crawford et al., 2020). Thus, this location provides a unique opportunity to investigate the relationship between elevated sulfate export and MeHg production in mountain wetlands.

4.3.2 Soil Sampling

Replicate surface soil samples were collected using trace metal clean procedures from an alpine dry meadow (n = 14), a range of mineral soil wetlands in the alpine zone (solifluction lobes (n = 10), wet meadows (n = 15), riparian shrub areas (n = 14)), and a subalpine peatland (n = 14) using a 5 cm x 10 cm soil corer.

All samples were handled with nitrile gloves, placed directly into plastic bags, sealed to maintain *in situ* redox status, and transported to the laboratory in coolers.

Based on MeHg, soil organic matter (SOM), and extractable sulfate conditions measured within the above-mentioned land cover types (i.e., "sites"), we also collected soil from an alpine dry meadow (low MeHg, extractable sulfate, and SOM), solifluction lobe (low MeHg and SOM, high extractable sulfate), and subalpine peatland (high MeHg and SOM, moderate extractable sulfate) to determine first-order rate constants of Hg methylation. At each site, clean soil coring devices and plastic spoons were used to fill acid washed mason jars until overflowing and were subsequently placed in coolers for transport to the lab.

4.3.3 Soil Laboratory Analyses

Details for soil analyses can be found in the supplementary methods of the Supporting Information. Briefly, soil samples from across the different sites were analyzed for a suite of soil physiochemical variables including bulk density, extractable sulfate, SOM, total C, total nitrogen (N), pH, and water content, as well as for THg and MeHg concentrations.

4.3.4 Methylmercury Production Assays

Details for the Hg methylation incubation experiment are provided in the Supporting Information. Briefly, soil samples from the alpine dry meadow, solifluction lobe, and subalpine peatlands were injected with a pre-equilibrated $^{201}Hg(II)$ tracer and frozen after 0, 24, 48, and 72 hour (h) incubation time. Additional soils from the subalpine peatland were amended with 5, 10, and 20 mg SO_4^{2-} L^{-1} of 0.5 M sodium sulfate to assess sulfate controls on MeHg production. These amendments resulted in a 50–280% increase in soil extractable sulfate

concentrations comparable to ~200 % increase in sulfate concentrations detected within the watershed (Crawford et al., 2020). A schematic of the incubation experiment can be found in Figure S4-2. Because the starting tracer was initially 100% inorganic Hg(II), any measured $Me^{201}Hg$ was assumed to be newly formed during the experiment making it possible to determine pseudo-first order Hg methylation rate constants based on the production of excess $Me^{201}Hg$ (Helmrich et al., 2022; Hintelmann & Evans, 1997). Any abiotic methylation that occurs because of incubation set-up were controlled for using t = 0 samples. Excess $Me^{201}Hg$ was quantified by isotope dilution after distillation, aqueous phase ethylation, trapping on Tenax (Buchem B.V.), isothermal gas chromatography separation, and detection by inductively coupled plasma mass spectroscopy (ICP-MS; iCAP, Thermo Scientific) (Hintelmann et al., 1995; Hintelmann & Evans, 1997; U.S. EPA, 1998). Excess $T^{201}Hg(II)$ was measured using BrCl oxidation, $SnCl_2$ reduction, and ICP-MS (Hintelmann & Evans, 1997; Olund et al., 2004; Peterson et al., 2023; U.S. EPA, 2002). First-order kinetics were assumed over the duration of the incubation and potential Hg methylation rates (K_{meth}) were determined according to:

$$K_{meth} = \frac{\text{excess } Me^{201}Hg_{t=24} - \text{excess } Me^{201}Hg_{t=0}}{\text{excess } T^{201}Hg \times \text{day}}$$

where excess $Me^{201}Hg_{t=24}$ is the $Me^{201}Hg$ concentrations (ng g^{-1}) produced in the sample at the end of the incubation, excess $Me^{201}Hg_{t=0}$ is the initial $Me^{201}Hg$ concentrations (ng g^{-1}), excess $T^{201}Hg$ is the concentration of $T^{201}Hg$ injected into each sample, and day is the number of days of the incubation. Because incubations were conducted on discrete samples that required destructive sampling at each time point, and there is variation in methylation among triplicates (average standard deviation among triplicates = 0.01 ng g^{-1} for alpine dry meadows, 0.02 ng g^{-1} for solifluction lobes, and 0.71 ng g^{-1} for subalpine peatlands), t = 24 h samples

occasionally had lower average concentrations of excess $Me^{201}Hg$ than the t = 0 h samples. This outcome resulted in negative K_{meth} values which is an impossible outcome; thus, we rounded all negative values to zero since there was likely no methylation occurring within these samples. Daily detection limits for excess $Me^{201}Hg$ were on average ≤0.002 ng g^{-1} for the alpine dry meadows, ≤0.003 ng g^{-1} for the solifluction lobes, and <0.2 ng g^{-1} for the subalpine peatlands. Excess $Me^{201}Hg$ for each sample surpassed the detection limit. Method detection limits for K_{meth} were calculated following methods proposed in Hintelmann and Evans (Hintelmann & Evans, 1997) and were found to range from 0.0002–0.0005 day^{-1} for the alpine dry meadows, 0.0008–0.0035 day^{-1} for the solifluction lobes, and 0.0196–0.0304 day^{-1} for the subalpine peatlands.

Because no previous studies have measured Hg methylation potentials within these types of ecosystems, we ran the experiment 72 h to ensure detectible excess $Me^{201}Hg$. Given that $Me^{201}Hg$ accumulation appeared linear over the first 48 h (Fig. S4-4(b)), but plateaued thereafter, we focus on the 24 h incubation results in the main text. Longer incubation times (48 and 72 h) may include the influence of demethylation but are included in Figures S4-4–S4-9. Since the bioavailability of spiked $T^{201}Hg$ may differ from naturally occurring inorganic THg within the sediment, we also measured ambient MeHg concentrations across the samples used for the sulfate amendments to verify that sulfate additions increased methylation of naturally present inorganic Hg. Quality assurance acceptance criteria for THg and MeHg analytical methods can be found in Tables S3-4.

4.3.5 Statistical Methods

Statistical analyses were performed using R version 4.3.1 (2023) (R Core Team, 2023). Ambient and sulfate-amended K_{meth} were normally distributed and

met the assumptions of homogeneity of variance and independence. Therefore, differences among treatments were assessed using an ANOVA test followed by a Tukey HSD post hoc test. Log-transformed concentrations of MeHg for wetland soils were not normally distributed. Therefore, differences among groups were assessed using a Kruskal-Wallis test followed by a post hoc Dunn's test. Monotonic relationships between MeHg, THg, SOM, extractable sulfate, C, N, and pH were determined using Spearman's Rank Correlation tests.

4.4 Results

4.4.1 Soil physiochemical conditions across site types

In line with our hypotheses, the elevated SOM subalpine peatlands had significantly higher MeHg concentrations (6.37 ± 2.28 ng g^{-1}) compared to alpine mineral soil wetlands (0.44–0.80 ng g^{-1}) and dry meadow soils (0.06 ± 0.04 ng g^{-1}; $p <$ 0.01; Fig. 4-2(a)). The solifluction lobe had an order of magnitude higher extractable sulfate concentrations (6.18 ± 5.43 mg SO_4^{2-}·g^{-1} dry soil) compared to the other sites (<0.40 mg SO_4^{2-}·g^{-1} dry soil; Fig. 4-2(b); Table S4-2). Across all sites, MeHg had a statistically significant, positive relationship with THg concentrations ($p < 0.01$), SOM ($p < 0.01$), total C ($p < 0.05$), and extractable sulfate concentrations <1.0 mg SO_4^{2-} g^{-1} ($p < 0.01$) (Fig. S4-3a – d). No positive relationship was observed with pHor total N ($p > 0.05$) (Fig. S4-3e – f). Additional environmental variables are summarized in Table S4-2.

4.4.2 Methylmercury production potential

We observed significantly higher K_{meth} over 24 h in the subalpine peatlands (0.027 ± 0.004 day^{-1}) compared to the solifluction lobe and dry meadow soils, which

had no detectible methylation ($p < 0.01$; Fig. 4-2(c)). This pattern persisted across the full incubation with consistently low excess $Me^{201}Hg$ in both the alpine dry meadow and solifluction lobe soils, indicating minimal methylation activity (Fig. S4-5(b)).

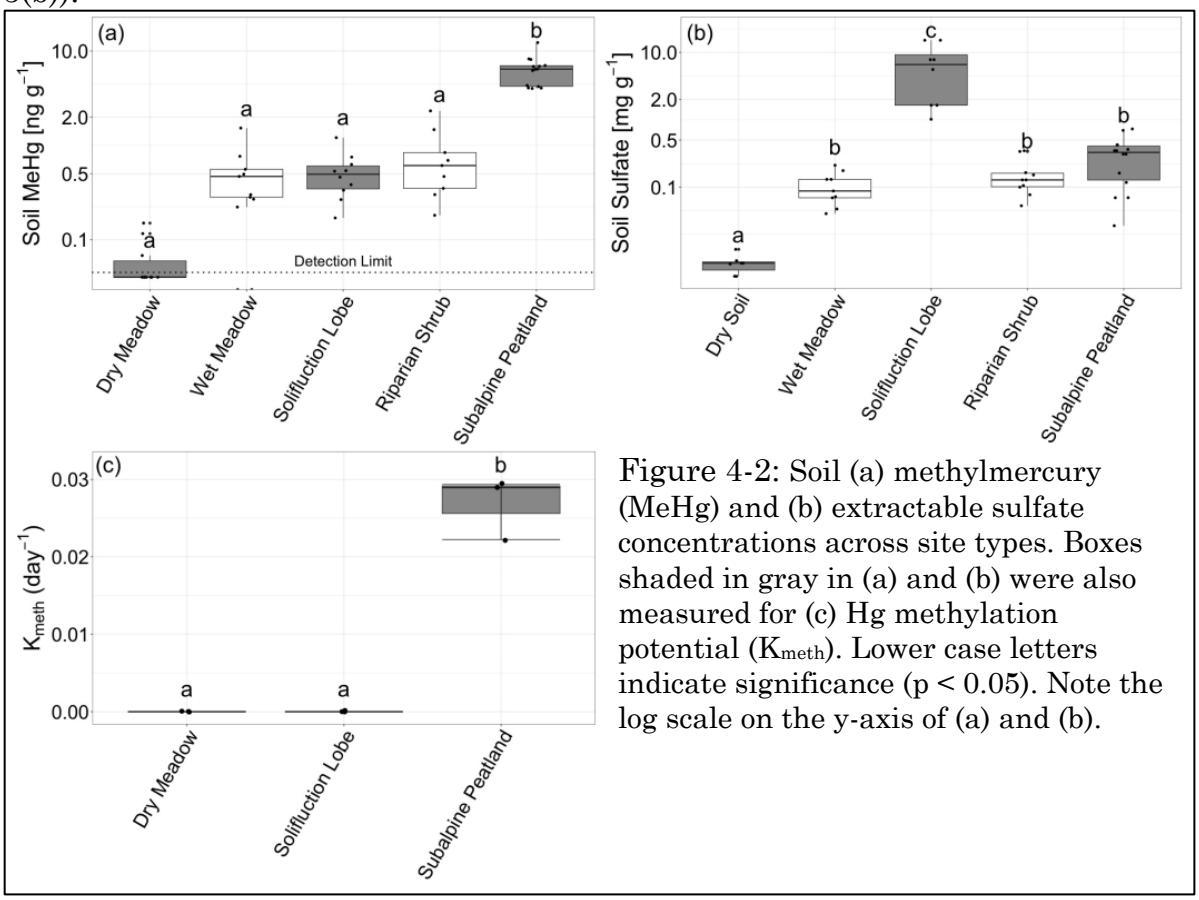

Figure 4-2: Soil (a) methylmercury (MeHg) and (b) extractable sulfate concentrations across site types. Boxes shaded in gray in (a) and (b) were also measured for (c) Hg methylation potential (K_{meth}). Lower case letters indicate significance ($p < 0.05$). Note the log scale on the y-axis of (a) and (b).

Subalpine peatland soil extractable sulfate concentrations at t = 0 h were 0.46 ± 0.21 mg SO_4^{2-}-g^{-1} dry soil for 0 mg SO_4^{2-} L^{-1} additions; the 5 mg SO_4^{2-} L^{-1} treatment was 0.70 ± 0.08 mg SO_4^{2-}-g^{-1} dry soil, the 10 mg SO_4^{2-} L^{-1} treatment was 1.33 ± 0.10 mg SO_4^{2-}-g^{-1} dry soil, and the 20 mg SO_4^{2-} L^{-1} treatment was 1.76 ± 0.10 mg SO_4^{2-}-g^{-1} dry soil (Fig. 4-3(a)). Sulfate amendments enhanced MeHg formation, supporting our hypothesis that these areas are sulfate limited with respect to MeHg production. Excess $Me^{201}Hg$ concentrations were significantly higher in the 5 mg SO_4^{2-} L^{-1} (2.4 ng g^{-1}) and 10 mg SO_4^{2-} L^{-1} (3.0 ng g^{-1}) additions compared to the 0 mg

SO_4^{2-} L^{-1} treatment (0.5 ng g^{-1}; $p < 0.01$; Fig. S4-4(b)). While the 20 mg SO_4^{2-} L^{-1} treatment (1.4 ng g^{-1}) had higher excess $Me^{201}Hg$ than the 0 mg L^{-1} addition, it was not significantly different from the other treatments ($p > 0.05$; Fig. 4-5(b)). A summary of soil extractable sulfate concentrations across the experiment is provided in Figure S4-9.

Sulfate additions of 10 mg SO_4^{2-} L^{-1} in subalpine peatland soil resulted in significantly higher K_{meth} over 24 h (0.023 ± 0.008 day^{-1}; $p < 0.05$; Fig. 4-3(b)) compared to the 0 mg SO_4^{2-} L^{-1} L^{-1} addition (0.004 ± 0.002 day^{-1}). The 5 and 20 mg SO_4^{2-} L^{-1} additions had mean K_{meth} values of 0.018 ± 0.006 and 0.014 ± 0.008 day^{-1}, respectively, which were on average higher than the 0 mg SO_4^{2-} L^{-1} $^{-1}$ addition, but the differences were not significant ($p > 0.05$; Fig. 4-3(b)). For the 48 and 72 h intervals, excess $Me^{201}Hg$ concentrations continued to increase (Fig. S4-4(b)), although K_{meth} across sulfate treatments were not significantly different (Fig. S4-7). Ambient MeHg concentrations also increased with sulfate additions (Fig. S4-8), suggesting the presence of a methylating environment, but methylation rates for ambient and spiked inorganic Hg are not directly comparable

4.5 Discussion

While the importance of peatland environments for cycling Hg is well established in high latitude environments (Fahnestock et al., 2019; Grigal, 2003), as far as we are aware, this study provides the first measurements of MeHg accumulation and formation within mountain peatland ecosystems. Our findings suggest that subalpine peatlands act as important regions for storing and producing MeHg in high-elevation ecosystems, with significantly higher MeHg concentrations and formation rates observed in the subalpine peatlands compared to the alpine, mineral soil wetlands in the North Boulder Watershed (Figs. 4-1(a) and 4-1(c)).

Given the widespread occurrence of similar mountain peatlands globally (Cooper et al., 2012; Gilmour & Henry, 1991; Khan et al., 2020, p. 20; J. Sun et al., 2023; Tjerngren et al., 2012; van der Knaap et al., 2011), our observations highlight the need to better constrain Hg pools and transformations in these ecosystems, as well as to assess the role of climatic drivers in altering the future extent of subalpine peatlands (J. Sun et al., 2023).

We also found evidence of sulfate limitation to MeHg production in subalpine peatlands of the North Boulder Watershed, an observation that provides important context for understanding how Hg cycling is changing in response to climate-driven alterations in mountain environments. As illustrated in Figure 4-3, MeHg formation was significantly higher when soil extractable sulfate concentrations were between ~1.24–1.45 mg SO_4^{2-}·g^{-1} dry soil (the 10 mg SO_4^{2-} L^{-1} addition shaded in green, Figs. 4-3(a) – (b)). Additionally, we found that methylation rates decreased above and below this sulfate range (equivalent to the 5 and 20 mg SO_4^{2-} L^{-1} sulfate additions shaded in yellow) but were still on average higher than the 0 mg SO_4^{2-} L^{-1} sulfate addition.

This differential response to sulfate levels, termed the "Goldilocks effect" by Gilmour and Henry (Gilmour & Henry, 1991), has been observed in other ecosystems whereby MeHg production is maximum—or "just right"—at intermediate sulfate concentrations due to complex relationships between sulfate and Hg cycles. Sulfate acts as a terminal electron acceptor for SRB, which can directly or indirectly promote MeHg production across different ecosystems (Gilmour et al., 1992; Peterson et al., 2023). Other anaerobic microbes, such as methanogens, fermenters, and iron reducers, are also capable of producing MeHg (Peterson et al., 2023); however, MeHg production in many ecosystems is highly sensitive to sulfate additions (Gilmour et al., 1992; Jeremiason et al., 2006). Such

results have led to the hypothesis that SRB can act as syntrophs to other Hg methylating microbes, whereby SRB consume metabolic biproducts of other microbes allowing for continued C metabolism and Hg methylation (Bae et al., 2014; Yu et al., 2018). Thus, if sulfate concentrations are too low, SRB metabolism will be less favored and will limit MeHg production either directly or indirectly. Alternatively, at elevated sulfate concentrations, sulfide can accumulate through sulfate reduction. Sulfide strongly binds inorganic Hg forming nanoparticulate mercuric sulfide, which immobilizes inorganic Hg, thereby limiting further transformations, such as methylation (Poulin et al., 2017). At moderate sulfate concentrations, however, an optimum range can be attained, whereby SRB have sufficient sulfate for metabolism, and inorganic Hg is still available for methylation. While our study lacks the benefit of microbial and sulfide analyses, this Goldilocks effect demonstrates the sensitivity of MeHg production in subalpine peatlands to climate-driven sulfate additions.

Indeed, our study provides evidence that continued increases in sulfate export from high-elevation watersheds may increase MeHg production in subalpine peatlands. Our sulfate additions increased soil extractable sulfate concentrations by 50–280% which is within the range of the ~200 % increase in sulfate export observed within runoff in the North Boulder Watershed over the past 30 years (Crawford et al., 2019). It is worth noting that while we only modified sulfate concentrations in this study, accelerated weathering can also result in increased release of other ions such as iron, as well as changes in pH (Mast et al., 1990, p. 199; Ross et al., 2018). Additionally, increased spatial extent of wetlands can enhance mobilization of dissolved organic matter, which can interact with inorganic Hg and influence MeHg formation (He et al., 2019). Simultaneous changes in solute export beyond sulfate concentrations could also influence MeHg production within

high-elevation watersheds and marks an important area for future research since these changes have implications for local wildlife, as well as for downstream ecosystems.

The observed sensitivity of subalpine peatlands to sulfate additions in our study also raises questions regarding the timeline of accelerated sulfate weathering. Mountain ecosystems are losing ice features at accelerating rates globally, but the degree to which they have lost ice extent varies significantly with the Southern Andes, Caucasus, European Alps, and Pyrenees experiencing the greatest mass losses of glaciers (-490 ± 100 kg m^{-2} yr^{-1}), and the high mountains of Asia showing the slowest mass losses (-150 ± 110 kg m^{-2} yr^{-1}, (Hock et al., 2019)). Mountain regions dominated by smaller glaciers, such as the North Boulder Watershed, are the most vulnerable to thawing ice features, with projected end-of-century mean mass losses of ~80 %, relative to 2015 (Hock et al., 2019). With the complete loss of ice features in a watershed, the rate of mineral weathering may abate as the exposure of new mineral surfaces slows, resulting in a decrease in sulfate concentrations (Manning et al., 2013). This shift may limit MeHg formation within high-elevation wetlands, which raises questions regarding the timescale of ecosystem recovery from elevated MeHg production around the globe—vital information for current international regulation efforts regarding atmospheric Hg releases and exposure. Limited studies have examined MeHg recovery from sulfate additions. Studies from boreal peatlands have found that MeHg concentrations decrease several years after the cessation of sulfate additions (Coleman Wasik et al., 2012). However, MeHg concentrations remain elevated compared to locations that have never experienced sulfate additions (Coleman Wasik et al., 2012).

While loss of ice features may slow mineral weathering, other climate-related changes may counteract this effect. Hydrologic shifts in mountain ecosystems due to

continued warming (e.g., reduced snowpack, earlier snowmelt) have resulted in the lowering of the water table (Zaremehrjardy et al., 2022). This process also exposes new mineral surfaces to weathering agents of oxygen and water and could result in continued accelerated mineral weathering in the absence of thawing ice features (Manning et al., 2013). Depending on the sulfate thresholds conducive to MeHg formation, sulfate concentrations may eventually reach levels at which Hg methylation is limiting, resulting in a decline in MeHg concentrations. These complexities highlight the need for long-term studies that investigate the MeHg production in high-elevation wetlands under increasing sulfate concentrations, the thresholds at which MeHg formation is optimal, and the potential for ecosystem recovery following the cessation of sulfate additions.

The sulfate thresholds identified in our experiment may also help explain differences in soil MeHg concentrations and formation rates observed across natural sulfate gradients in the North Boulder Watershed (Fig. 4-3). In the subalpine peatlands, we observed the highest K_{meth} when soil extractable sulfate concentrations were between 0.60–1.45 mg SO_4^{2-} g^{-1} dry soil and found K_{meth} decreased as extractable sulfate concentrations either increased or decreased beyond this range (Figs. 4-3(a)-(b)). Alpine dry meadows, alpine wet meadows, and riparian shrub zones all have relatively low extractable sulfate concentrations (< 0.2 mg $SO_4^{2-}$$g^{-1}$ dry soil), which may create sulfate-limiting conditions that decrease MeHg formation (Fig. 4-3(c)). Solifluction lobes, alternatively, have extractable sulfate concentrations an order of magnitude higher than the other sites (> 1.6 (6.2 ± 5.4) mg SO_4^{2-} g^{-1} dry soil, Fig. 4-2(b) and Fig. 4-3(c)), which may result in the buildup of sulfide compounds and inhibition of MeHg formation; these high sulfate concentrations are likely the result of the presence of a permanent ice lens beneath the solifluction lobe that prevents subsurface drainage and concentrates solutes

over time from evaporative losses (Huber, 2021). These observations suggest that mountain wetlands with sulfate concentrations between 0.02 – 1.6 mg SO_4^{2-} g^{-1} dry soil are most conducive to MeHg production in alpine and subalpine environments.

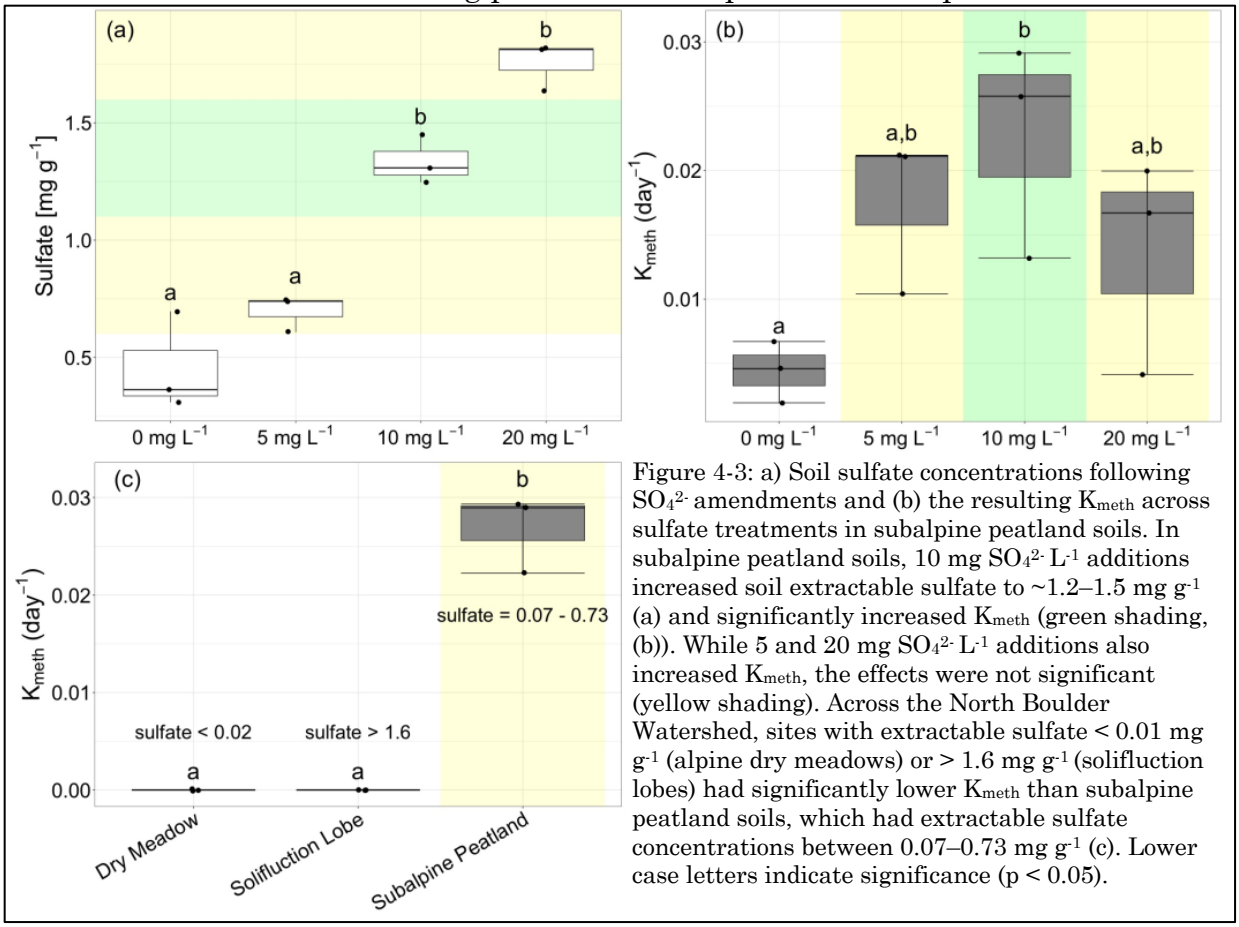

Figure 4-3: a) Soil sulfate concentrations following SO_4^{2-} amendments and (b) the resulting K_{meth} across sulfate treatments in subalpine peatland soils. In subalpine peatland soils, 10 mg SO_4^{2-} L^{-1} additions increased soil extractable sulfate to ~1.2–1.5 mg g^{-1} (a) and significantly increased K_{meth} (green shading, (b)). While 5 and 20 mg SO_4^{2-} L^{-1} additions also increased K_{meth}, the effects were not significant (yellow shading). Across the North Boulder Watershed, sites with extractable sulfate < 0.01 mg g^{-1} (alpine dry meadows) or > 1.6 mg g^{-1} (solifluction lobes) had significantly lower K_{meth} than subalpine peatland soils, which had extractable sulfate concentrations between 0.07–0.73 mg g^{-1} (c). Lower case letters indicate significance ($p < 0.05$).

In addition to sulfate gradients, other soil physiochemical properties also likely drive the slower Hg cycling observed in the alpine. Alpine dry meadows, wet meadows, riparian shrub zones, and solifluction lobes all have low SOM (Table S4-2), as well as variable hydrologic inundation, creating less favorable conditions for anaerobic metabolism (Parks et al., 2013). Subalpine peatlands, alternatively, are permanently hydrologically inundated creating anoxic, high SOM environments conducive to Hg methylation. While this study targets a single watershed in the Colorado Rocky Mountains, these alpine and subalpine wetlands are widespread

globally, making up, for example, >2,000 km^2 land area in the western U.S. alone (Fig. S4-10) suggesting the importance of better constraining Hg cycling across these landscape features.

4.6 Conclusions

Our study demonstrates how co-occurring climatic and biogeochemical stressors may accelerate Hg cycling in high-elevation ecosystems. We show that previously understudied subalpine peatlands in the Colorado Rocky Mountains play a critical role in Hg storage and transformation, exhibiting significantly higher MeHg concentrations and formation rates than alpine, mineral soil wetlands. Additionally, our findings reveal that sulfate additions enhance MeHg production in subalpine peatlands, highlighting potential links to global trends in accelerated mineral weathering. Given the global prevalence of alpine and subalpine wetlands, further research on sulfate thresholds for Hg methylation across environmental and climatic gradients is essential for assessing contamination risk. Such insights can inform both local watershed management and global policy efforts to mitigate Hg contamination in mountain ecosystems under climate change.

CHAPTER V

MERCURY SINK CHARACTERISTIC OF HIGH ELEVATIONS MAY SHIFT WITH ONGOING CLIMATE CHANGE

Hannah R. Miller, Clifford R. Adamchak, Jiahao Wen, Janice Brahney, Eve-Lyn S. Hinckley

5.1 Abstract

To determine future mercury contamination risk under a changing climate, it is critical to constrain the sink-source characteristic of different ecosystems. Mountain ecosystems are a particularly important area for this research since they receive high loads of mercury through atmospheric deposition and are disproportionately impacted by climate change. While past studies have found that mountain regions act as sinks for mercury, they lack measurements of mercury fluxes in dry deposition and land to air fluxes (evasion). In this study, we quantify mercury inputs in wet and dry deposition, pools in soil and vegetation, and losses via runoff and evasion. Unlike pasts studies from forested ecosystems, we found that open precipitation comprises the largest proportion of atmospheric mercury inputs both in the alpine and subalpine compared to litterfall and throughfall. Despite greater total mercury inputs in the subalpine compared to the alpine, the alpine had significantly higher pools of mercury in soil and vegetation, likely due to slower carbon turnover and longer-lived plant species. By subtracting atmospheric Hg deposition from pools of Hg in snowpack, as well as evasion estimates from the literature, we contend that evasion is an important pathway of mercury loss in both the alpine and subalpine, with more uncertainty associated with estimates for the

subalpine coniferous forest. Mercury loss in runoff was significantly higher in the subalpine compared to the alpine but did not account for the lower mercury pools in the soil. In sum, our findings demonstrate that mountain ecosystems are net sinks of mercury with 24–63 % of atmospherically deposited mercury retained on the landscape. If we had only included mercury losses in runoff, without the addition of evasion, our estimates would have range from 93–99 % retention. Our findings highlight the importance of including evasion in mercury mass balances of mountain ecosystems and the need for better constraints on the drivers of mercury volatilization. Broadly, our study indicates that mountain ecosystems act as complex regions for Hg cycling and highlight the critical need to constrain the sinks-source nature of these areas in the context of continued climatic change.

5.2 Introduction

Human activities have greatly accelerated mercury (Hg) cycling globally, increasing atmospheric concentrations by ~450 % since pre-industrial times (Outridge et al., 2018). Over the past half-century, international initiatives such as the Minamata Convention have aimed to mitigate Hg pollution by reducing emissions, managing waste, and restricting Hg trade (USEPA, 2018). While these efforts have slowed the growth of global Hg emissions and led to significant regional declines (Streets et al., 2019), Hg remains a persistent contaminant, capable of cycling for thousands of years through the atmosphere and biosphere, before permanent sequestration in deep ocean sediments or stable soil pools (Amos et al., 2013; Selin, 2009). Indeed, re-mobilization of Hg from temporary storage pools, such as soil, leaves, or water bodies, is now the largest source of Hg to the atmosphere; these fluxes account for approximately two-thirds of global emissions (Amos et al., 2013; Bishop et al., 2020). Climate change and human land disturbance have the

potential to exacerbate the magnitude of emissions from these "legacy" Hg pools and highlights the importance of investigating the sink-source behavior of different ecosystems globally.

Mountain ecosystems cover ~27 % of terrestrial land surfaces and may play a critical role in cycling legacy Hg. These regions receive elevated atmospheric deposition (Lovett & Kinsman, 1990), store Hg long-term in permafrost and glaciers (R. Sun et al., 2021), and transport Hg in runoff, particularly during snowmelt (Packer et al., 2020; Shanley et al., 2008; X. Sun et al., 2017). Limited studies have investigated the source-sink nature of mountain environments but those that exist have found these regions tend to act as net sinks (X. Li et al., 2022; Wang, Yuan, et al., 2020). For example, Mast and colleagues (2005) found ~80 % of annually deposited Hg was retained within the landscape each year in the Rocky Mountain National Park (Mast et al., 2005). Now 20 years old, this is the last time a comprehensive assessment of the fate of wet Hg deposition in the Colorado Rocky Mountains was conducted, despite continued alteration of Hg cycling under ongoing climate change. Additionally, these studies do not account for dry depositional pathways through vegetation and dust, nor losses of Hg back to the atmosphere via evasion (X. Li et al., 2022; Mast et al., 2005; Wang, Yuan, et al., 2020).

Climate change is disrupting Hg cycling dynamics in high-elevation ecosystems in ways that could shift the sink-source characteristic of mountain regions. Warming temperatures, permafrost thaw, and more rapid snowmelt threaten long-term Hg storage (Chai et al., 2022). Additionally, changes in precipitation, aridification, and shifts in vegetation cover may enhance deposition and re-emission to the atmosphere (Eckley et al., 2016; Wang, Luo, et al., 2020). Despite the importance of mountain ecosystems, baseline Hg cycling in these regions remains poorly constrained (Miller et al., 2023), with existing studies often

focusing on either mountain systems as sinks for atmospheric Hg (e.g., Wang, Luo, et al., 2020), or as sources for Hg in runoff (e.g., Domagalski et al., 2016; Shanley et al., 2008). Prior, less comprehensive studies leave important gaps in our understanding of mountain ecosystems' contributions to global Hg cycling, as well as the potential shifts that will occur with continued climate change. To assess the effectiveness of the Minamata Convention, as well as ongoing risks associated with legacy Hg contamination, it is critical to constrain the bi-directional transport of Hg within mountain ecosystems globally.

Here, we present a mass balance of Hg within Niwot Ridge Long-term Ecological Research Site, a high-elevation ecosystem of the Colorado Rocky Mountains that has been a location of climate and ecological research for over 40 years, as well as an indicator of patterns in high-elevation ecosystems globally (Campbell et al., 2022). Specifically, we ask the following questions: 1) what role do high-elevation ecosystems play in the global Hg cycle and what drives either sink or source behavior? and 2) how may climate change impact Hg cycling in mountain ecosystems based on the primary drivers of Hg cycling? Broadly, we hypothesize that Colorado Rocky Mountain ecosystems act as sinks for Hg due to high rates of atmospheric deposition and cold temperatures that cause slow rates of soil carbon (C) mineralization, and, therefore, Hg retention. By including estimated losses of Hg via evasion, however, we do expect the degree of the sink characteristic to be less than reported in previous studies. For the second question, we hypothesize that warming air and soil temperatures will promote greater soil mineralization and Hg loss via runoff and evasion over the coming years, which could push these ecosystems closer to—or into—a source status.

5.3 Methods

5.3.1 Study Area

We conducted this study between 2020–2023 at the Niwot Ridge Long-term Ecological Research (NWT-LTER) site (40.05 N, 105.59 W), a high-elevation, mountainous ecosystem in the Colorado Rocky Mountains. This region, broadly, is part of the traditional territories of the Cheyenne, Ute, and Arapaho Peoples. We sampled within the 0.26 km^2 alpine Saddle Catchment above tree line (~3,500 m elevation), as well as the 4.9 km^2 subalpine Como Creek Catchment (~3,000 m elevation), both of which drain into the larger Boulder Creek Watershed. The Saddle Catchment is comprised predominantly of dry meadow regions (> 80%) with the remaining ~20 % by a variety of alpine wetlands (Hermes et al., 2020). About 40–50% of the landscape is hydrologically connected to the stream channel in this catchment (Hermes et al., 2020). The Saddle Catchment has an annual mean temperature of 0.3°C (Greenland & Losleben, 2001) and is experiencing increasing summer air temperatures of ~0.43°C $decade^{-1}$ from 1953–2008 (McGuire et al., 2012). The subalpine Como Creek Catchment is comprised predominantly of subalpine forest with <10 % of the landscape covered by subalpine wetlands. The Como Creek Catchment has an annual mean temperature of 2.0°C (NEON, n.d.) and is experiencing increasing air temperatures of ~0.24°C $decade^{-1}$ and increasing precipitation of ~9 mm $decade^{-1}$ between 1970–2019 (J. L. Campbell et al., 2022). Annual precipitation is ~1000 mm in the alpine and ~800 mm in the subalpine (Kittel et al., 2015). Precipitation is dominated by snowfall (~80 %), however frequent summer convective thunderstorms contribute significant rainfall during the summer months (Hermes et al., 2020). Long-term records at NWT-LTER show that precipitation has increased by 60 mm per decade since 1952 in the alpine, however, no significant change is observed in the subalpine (Kittel et al., 2015).

Mast and colleagues (2005) estimated that annual bulk atmospheric Hg deposition to the Colorado Rocky Mountains was between 8.3 to 12.4 ug m^{-2}. Over the past several decades, wet atmospheric Hg deposition has been increasing in this region in comparison to the Eastern U.S. where atmospheric deposition rates have been decreasing (Miller et al., 2023).

5.3.2 Air Sampling

We collected bulk air samples for total gaseous Hg, which is predominantly gaseous elemental Hg (GEM) and Hg stable isotope (δ^{199}Hg, δ^{202}Hg) analysis in both the alpine and subalpine (Tate et al., 2023). Air was pumped through a sample train consisting of a 0.45 um PTFE filter, soda lime trap, and two chlorinated activated C traps using a diaphragm pump with a flow rate of ~900 mL min^{-1}. Two-week integrated samples were collected from May–August 2023. All air samplers were installed ~1.5 m from the ground surface with free air flow to the sampler. Following collection, all air samplers were shipped to the U.S. Geological Survey Mercury Research Lab (MRL) for Hg analyses.

5.3.3 Atmospheric Deposition Sampling

To estimate summer atmospheric wet Hg deposition, direct precipitation and throughfall were collected monthly in triplicate (only direct precipitation in the alpine due to lack of tree cover) from early June–early September 2023. The sampler was comprised of an acid-washed 0.011 m^2 glass funnel attached to c-flex tubing, Teflon tubing, and a PTFE 250 ml sample bottle all housed within black piping to prevent exposure to solar radiation. The tubing was looped with a zip tie to prevent evaporation, and the sample bottle was pre-acidified with 2.5 ml 50 % HCl to prevent microbial growth and Hg volatilization. At each collection time

point, the tubing was rinsed thoroughly with ulta-high purity water and the sample bottle was replaced with a new, pre-acidified bottle. Field blanks were collected at weekly intervals for one month to determine if any sorbing of Hg from the atmosphere occurred through the exhaust hole of the sample bottle.

To estimate summer atmospheric dry Hg deposition, dust (open areas) and litterfall (canopy) were collected. Dust samples were collected in the alpine and subalpine during Summer 2022 using National Atmospheric Deposition Program (NADP) dry deposition samplers and dust was recovered per Brahney et al., (2020) (Brahney et al., 2020). Litterfall was collected monthly in the subalpine in four replicate 0.44m^2 mesh-lined baskets that were deployed in late June and retrieved in late October 2022. Samples were handled with clean nitrile gloves, placed in plastic bags, and transported in coolers to the laboratory where they were frozen for further processing. For alpine sites where there is no tree cover, bulk aboveground biomass was collected for THg concentration analysis. Litterfall samples (n = 37) were weighed before and after lyophilization to determine wet and dry weights and then homogenized.

To estimate atmospheric bulk Hg winter deposition during the months that collectors were not deployed, full-depth snowpack samples were collected in early May 2021 just prior to the onset of snowmelt. Depth-integrated samples were collected from a freshly exposed face of each snow pit and placed into acid-washed Teflon bags for transport back to the lab. Five samples were collected in open areas representative of open precipitation and three snow throughfall samples were collected under canopy. All samples were then promptly melted, subsampled, and acidified to 1% hydrochloric acid solution for Hg analysis. Snow water equivalent (SWE) was also measured for each depth interval.

5.3.4 Soil Sampling

To estimate storage of Hg within the alpine and subalpine, we collected soil samples using trace metal clean procedures from different zones delineated by Hermes et al. (2020): "dry" zones (alpine dry meadows (n = 27) and subalpine forest floor (n = 11)), "wet to moist" snowmelt fed areas that dried down slowly throughout the growing season (riparian shrub zones, n = 27), "wet to dry" snowmelt-fed areas that dry down rapidly (alpine moist meadows (n = 4), alpine wet meadows (n = 16)), and persistently "wet" areas (solifluction lobes (n = 13) and subalpine peatlands (n = 14)). All samples were handled with clean nitrile gloves, placed in plastic bags, and transported to the laboratory in coolers for Hg analysis, as well as measurements for a suite of other environmental variables (see below).

5.3.5 Runoff Sampling

To measure Hg concentrations and fluxes in alpine and subalpine runoff, we collected unfiltered grab samples (n = 22) weekly at Saddle Stream (n = 10) and Como Creek (n = 12) from May – September 2021. Samples were collected into Nalgene PTEG bottles after rinsing them three times with sample water. All samples were handled using trace metal clean procedures and transported back to the laboratory in coolers where they were acidified to a 1% hydrochloric acid. Additional grab samples were collected in ashed glass bottles for analysis of dissolved organic carbon (DOC) and sulfate concentrations. Stream discharge was monitored continuously throughout the sampling period at Saddle Stream by the NWT-LTER and at Como Creek by NEON.

5.3.6 Total Hg Analysis

Total Hg concentrations in direct precipitation, throughfall, and runoff were determined by cold vapor atomic fluorescence spectrometry (CVAFS) with the Brooks-Rand "MERX-T" automated Hg analytical system (U.S. EPA, 2002). Briefly, bromine monochloride (BrCl) was added to each sample and then samples were heated to 50°C for 5 d to release matrix-bound Hg and oxidize all forms of Hg to the Hg^{2+} oxidation state. Just prior to analysis, the BrCl was neutralized by the addition of hydroxylamine hydrochloride and the oxidized Hg is then reduced by addition of stannous chloride ($SnCl_2$). Volatile Hg^0 is purged from the sample and captured onto a gold sand trap, desorbed, and detected by CVAFS. Analytical quality control was verified by a duplicate (<10 % difference between duplicates), instrument spike (recovery within 85–115 % of known addition), and instrument blank for every 10 samples analyzed. Instrument calibration linearity (>0.995) and a daily detection limit (three times the standard deviation of the calibration blanks) was calculated every day of analysis.

Soil and litterfall were analyzed for THg using atomic adsorption followed by direct combustion on a Nippon MA-3000 Mercury analyzer (U.S. EPA, 2007). Analytical quality control was verified by an instrument calibration linearity > 0.995, as well as a method blank (<0.05 ng/boat), National Institute of Standards and Technology (NIST) certified reference material (CRM) 1575a (Pine Needles, 39.9 ± 0.7 ng g^{-1}) for litterfall and IAEA-475 (Marine Sediment, THg concentration = 29.9 ± 1.5 ng g^{-1}) for soil, and a triplicate every 10 samples. The CRM IAEA-475 averaged 29.3 ± 0.5 ng g^{-1} and the relative standard deviation of the triplicates was <6 % across our analyses.

5.3.7 Calculations for THg Fluxes in Wet and Dry Atmospheric Deposition

Fluxes of THg in snow, open precipitation, throughfall, and litterfall weighted by month and tree cover were used to estimate total annual inputs of THg into the alpine and subalpine. Fluxes of THg in open precipitation were determined for the growing season (June–September) by multiplying Hg concentrations from open precipitation collectors by precipitation volumes measured in co-located NADP collectors in both the alpine (CO02) and the subalpine (CO90). Fluxes of THg in open precipitation during the period when collectors were not deployed was estimated by multiplying THg concentrations of open precipitation collected at the Mercury Deposition Network (MDN) collector at Buffalo Pass, CO by precipitation volumes at NWT-LTER. To verify Buffalo Pass as a proxy for unsampled months in the alpine and subalpine at NWT-LTER, THg concentrations and precipitation volumes were compared between Buffalo Pass and NWT-LTER during the period of overlapping data collection (June–September, 2023). The Buffalo Pass MDN site sits between the elevation of the NWT-LTER alpine and subalpine sampling sites and has been used previously as a comparison to verify THg deposition trends within the Front Range of the Colorado Rocky Mountains (Mast et al., 2005). Neither THg concentrations nor precipitation volumes were significantly different between Buffalo Pass and NWT-LTER in the alpine or subalpine (Figs. S5-1–S5-2).

Fluxes of THg in throughfall in the subalpine were determined the same way as for open precipitation except that the volume of precipitation was based either upon the volume of precipitation collected within the throughfall collectors, or in the cases when the collectors overflowed, a throughfall interception coefficient was used to determine throughfall volume. The interception coefficient was calculated by dividing throughfall volumes by open precipitation volumes during the sampling period and was determined to be 0.58 for the subalpine. During the winter months,

average snow concentrations from under canopy cover at NWT-LTER were multiplied by NWT-LTER precipitation volumes.

Fluxes of THg in litterfall in the alpine were determined by calculating THg concentrations in bulk vegetation samples by monthly litterfall rates measured by the National Ecological Observatory Network (NEON) at site NIWO_047 between June–September 2021. We assumed that no litterfall occurred in the alpine between October–May due to snow cover and plant dormancy. In the subalpine, THg fluxes in litterfall were determined by multiplying the concentration of litterfall THg by litterfall mass for each month. During the period that our collectors were not deployed (November–May), average THg concentrations were multiplied by litterfall masses at co-located NEON litterfall collector sites (NIWO 040 and 057).

Fluxes of THg in dust were calculated by multiplying THg concentrations in dust samples by total dust volumes during the sampling period. Since we only had dust samples for three months for each site, we then multiplied the sum from the sampling period by four to estimate fluxes for the full year.

To determine total fluxes of THg to the alpine, fluxes in open precipitation, dust, throughfall, and litterfall were summed over the year. To determine fluxes of THg to the subalpine, fluxes in open precipitation and dust were summed and multiplied by the percent no-canopy area (60 %), fluxes in throughfall and litterfall were summer and multiplied by the percent canopy area (40 %), and then finally canopy fluxes and no-canopy fluxes were summed over the year.

5.3.8 Calculations for THg Export in Runoff

Total fluxes of Hg in Saddle Stream and Como Creek runoff were calculated by multiplying the monthly discharge volume by the average THg concentration for

that month, summing THg export for each month over the entire year, and then normalizing to the watershed area.

5.3.9 Soil Storage Calculations

Storage of THg in alpine soils was determined by sampling within previously established soil moisture groups, as described above in the "Soil Concentrations" subsection, and multiplying the average THg pools (in the upper 5 cm of soil) within each group by the area of the watershed represented by that group. Within the watershed, "dry" regions made up 85.5 %, "wet to moist" areas made up 9.7 %, "wet to dry" areas made up 1.5 %, and "wet" areas made up 3.3 % of the landscape. In the subalpine zone, 94 % of the watershed was determined to be dry forest floor and 6 % percent was determined to be wetland (QGIS analysis); soil THg pools from those respective locations were weighted accordingly.

5.3.10 Evasion Estimates

Since we were unable to directly measure evasion rates of Hg from our sites, we instead used estimated values. For the summertime, per Eckley et al. (2016), we used "Southern Semi-Arid Highlands" evasion rates for the alpine. Fluxes measured in coniferous forests vary significantly in the literature from net deposition to net evasion. Additionally, studies show that coniferous forest soils shift seasonally from net loss during the growing season and net sink during snow-covered periods. We compiled a range of annual flux estimates for coniferous forests to represent a range of estimates for summertime. For the winter months, we subtracted THg pools measured in snowpack at NWT-LTER just prior to the onset of snowmelt from fluxes of THg during the same period to represent loss of Hg from snowpack back to the atmosphere. The fluxes of THg were calculated by multiplying THg

concentrations from Buffalo Pass by precipitation volumes from NWT-LTER during the winter months. During winter 2020–2021, snowfall began on October 14th at NWT-LTER and snowpack samples were collected on May 8th, 2021 (https://wcc.sc.egov.usda.gov/nwcc/view).

5.3.11 Statistical Analysis

All statistical analyses was conducted using R 2023.03.0+386 (R Core Team, 2023). Data were log transformed when necessary to meet distributional assumptions. All concentrations below the detection limit were assigned a concentration of 0. Influential data points were determined using Cook's distance with a threshold of 4 divided by the number of observations. All model residuals were tested for normality using Shapiro-Wilk test and homogeneity of variance across groups using a Bartlett (normal distribution) or Levene test (non-normal distribution).

5.4 Results

5.4.1 Air Concentrations and Stable Isotopes

Air concentrations of THg were not significantly different between the alpine (0.92 ± 0.15 ng m^{-3}) and subalpine (0.83 ± 0.12 ng m^{-3}). In the alpine, THg concentrations were highest in July (1.07 ng m^{-3}) and lower in September (0.76 ng m^{-3}) while in the subalpine, concentrations were highest in May (0.97 ng m^{-3}) and lowest in August (0.69 ng m^{-3}). δ^{202}Hg ranged from 0.19 – 0.70 ‰ and was on average lower in the alpine (0.35 ± 0.13 ‰) compared to the subalpine (0.58 ± 0.12 ‰), although the difference was not significant ($p > 0.05$).

5.4.2 Comparison of Buffalo Pass to NWT-LTER

Summer THg concentrations in open precipitation were not significantly different between Buffalo Pass (8.8–33.9 ng L^{-1}) and NWT-LTER (6.8–31.6 ng L^{-1}) between June to September (two-way permutation test; $p > 0.05$; Fig. S5-2A). Precipitation volumes during the same period were also not significantly different between Buffalo Pass (10.4–51.3 L) and NWT-LTER ($p > 0.05$; 14.3–64.8 L; Fig. S5-3). Additionally, average THg concentrations during winter months at the Buffalo Pass MDN collector (0.83–59.51 ng L^{-1}) were not significantly different than concentrations measured within snowpack at NWT-LTER ($p > 0.05$; 1.57–24.5 ng L^{-1}; Fig S5-2B). This result suggests that Buffalo Pass is a reliable proxy for NWT-LTER. As such, we used THg concentrations from Buffalo Pass to fill in unsampled months at NWT-LTER.

5.4.3 Atmospheric Sources of Hg

5.4.4 Open Precipitation

Total Hg concentrations in open precipitation collected in the alpine averaged 18.5 ± 6.1 ng L^{-1} during the summer months and 9.5 ± 13.1 ng L^{-1} during the winter months (Buffalo Pass concentrations). In the subalpine, open precipitation averaged 18.7 ± 6.2 ng L^{-1} during the summer months and 9.5 ± 13.1 ng L^{-1} during the winter months (Fig. 5-1A). Concentrations in the alpine and subalpine were both highest in July and lowest in the winter months (Buffalo Pass concentrations) and were not significantly different between the two elevation zones ($p > 0.05$; Fig. S5-1A). Due to higher annual precipitation volumes in the subalpine (832 mm) compared to the alpine (719 mm) during the sampling period, annual fluxes of THg were higher in

the subalpine 13.6 ± 0.5 ug m^{-2} yr^{-1} compared to the alpine 12.1 ± 0.4 ug m^{-2} yr^{-1} although the difference was not statistically significant ($p > 0.05$). Throughfall in the subalpine averaged 36.1 ± 14.0 ng L^{-1} in the summer months and 12.4 ± 8.3 ng L^{-1} in the winter months (Fig 5-1A). Annual fluxes of throughfall to the subalpine zone were 12.7 ± 1.7 ug m^{-2} yr^{-1}.

5.4.5 Throughfall

Throughfall in the subalpine averaged 36.1 ± 14.0 ng L^{-1} in the summer months and 12.4 ± 8.3 ng L^{-1} in the winter months (Fig 5-1A). Annual fluxes of throughfall to the subalpine zone were 12.7 ± 1.7 ug m^{-2} yr^{-1}.

5.4.6 Dust

Dust averaged 67.3 ± 19.7 ng g^{-1} in the alpine and 108.0 ± 17.0 ng g^{-1} in the subalpine and were not significantly different from each other ($p > 0.05$; Fig. 5-1B). Fluxes of dust averaged 0.12 in the alpine and 0.17 in the subalpine ug m^{-2} $yr^{-1}$and were not significantly different between the two elevation zones ($p > 0.05$).

5.4.7 Litterfall

Aboveground bulk biomass in the alpine (representative of litterfall) averaged 22.4 ± 6.2 ng g^{-1} and was significantly lower than litterfall concentrations in the subalpine which were 49.0 ± 22.0 ng g^{-1} ($p < 0.01$; Fig. 5-1B). Litterfall in the subalpine was highest in July and August (Fig S5-1B). Average annual fluxes of litterfall in the alpine (0.2 ± 0.02 ug m^{-2} yr^{-1}) were significantly lower than average litterfall fluxes in the subalpine (6.5 ± 0.8 ug m^{-2} yr^{-1}).

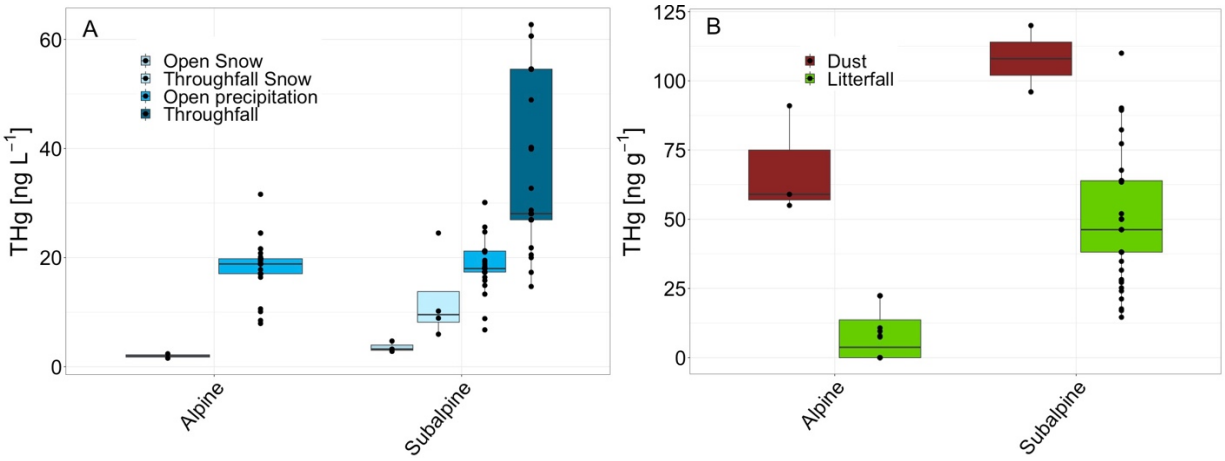

Figure 5-1: Total mercury (THg) concentrations in snow, open precipitation and throughfall (A) and dust and litterfall (B) in the alpine and subalpine.

5.4.8 Total Fluxes

Total fluxes of THg were 12.4 ug m^{-2} yr^{-1} in the alpine and 15.9 ug m^{-2} yr^{-1} in the subalpine (Fig. 5-2). In the alpine, the contribution to total fluxes was dominated by open precipitation which made up 97 % of total fluxes (12.1 ug m^{-2} yr^{-1}). Litterfall and dust made up 2 % (0.24 ug m^{-2} yr^{-1}) and 1 % (0.12 ug m^{-2} yr^{-1}) of the remaining deposition fluxes, respectively. Fluxes of THg in the subalpine were also dominated by open precipitation, which made up 51 % (8.13 ug m^{-2} yr^{-1}) of total fluxes. The remaining proportions were from throughfall (32 %; 5.1 ug m^{-2} yr^{-1}), litterfall (16 %; 2.1 ug m^{-2} yr^{-1}), and dust (1 %; 0.10 ug m^{-2} yr^{-1}).

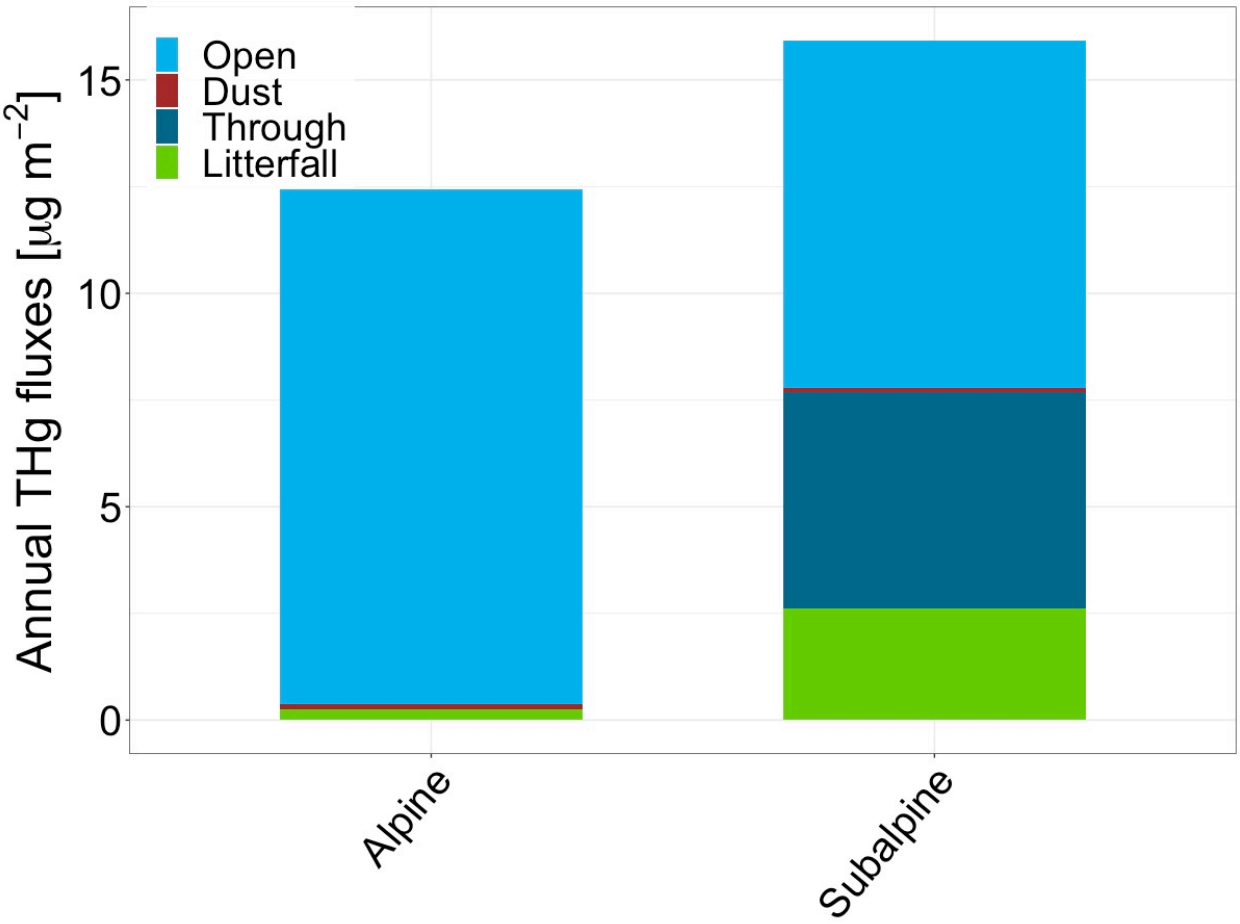

Figure 5-2: Canopy-weighted total mercury (THg) fluxes of open precipitation, dust, throughfall and litterfall in the alpine and subalpine.

5.4.9 Soil Concentrations and Pools of THg

Concentrations of THg within soils varied across moisture and soil organic matter gradients in the alpine and subalpine. In the alpine, THg concentrations averaged 52.2 ± 20.6 ng g^{-1} in dry areas, 75.8 ± 25.4 ng g^{-1} in persistently wet areas, 96.3 ± 29.5 ng g^{-1} in wet areas that dried down slowly and 58.2 ± 31.6 ng g^{-1} in areas that dried down rapidly (Fig. S5-4A). Wet areas that dried down slowly were significantly higher than dry and wet areas that dried down rapidly ($p < 0.05$). THg concentrations in the alpine were significant positively correlated with soil organic matter ($p < 0.01$; $R^2 = 0.35$) and soil moisture ($p < 0.01$; $R^2 = 0.21$).

Concentrations of THg normalized to soil organic matter in the alpine were 0.3 ± 0.1 μg Hg g organic matter^{-1} in dry areas, 0.8 ± 0.8 μg Hg g organic matter^{-1} in wet areas, 0.3 ± 0.2 μg Hg g^{-1} organic matter in wet areas that dry down slowly, and 0.3 ± 0.1 μg Hg g^{-1} organic matter in wet areas that dry down rapidly (Fig. S5-4B). Persistently wet areas were significantly higher than the other soil groups ($p < 0.05$).

Pools of THg within alpine soils varied across moisture groups averaging 2.0 ± 0.8 mg m^{-2} in upper 5 cm in dry areas, 4.0 ± 1.3 mg m^{-2} in upper 5 cm in persistently wet areas, 1.5 ± 0.6 mg m^{-2} in upper 5 cm in wet areas that dry down slowly, and 1.5 ± 1.0 mg m^{-2} in upper 5 cm in wet areas that dry down rapidly (Fig. S5-4C). Pools of THg were not significantly correlated with soil moisture or organic matter in the alpine ($p > 0.05$) but were significantly higher in the persistently wet areas compared to the other soil groups. The dry areas also had significantly higher pools compared to wet areas that dried down rapidly.

In the subalpine, THg concentrations were significantly lower in the dry forest floor (35.4 ± 8.1 ng g^{-1}) compared to wet regions (114.7 ± 34.2 ng g^{-1}; Fig. S5-5A). THg concentrations in the subalpine were significant positively correlated with soil organic matter ($p < 0.01$; $R^2 = 0.65$) and soil moisture ($p < 0.01$; $R^2 = 0.78$).

Concentrations of THg normalized to soil organic matter in the subalpine were 0.3 ± 0.2 μg Hg g^{-1} organic matter in dry forest soils and 0.2 ± 0.1 μg Hg g^{-1} organic matter in wet soils and were not significantly different from each other ($p > 0.05$, Fig. S5-5B).

In the subalpine, pools of THg averaged 1.3 ± 0.3 mg m^{-2} in upper 5 cm in dry forest soils and 0.9 ± 0.3 mg m^{-2} in upper 5 cm in wet regions and were not significantly different from each other ($p > 0.05$; Fig. S5-5C). Pools of THg in the

subalpine were weakly correlated with soil organic matter ($p = 0.04$; $R^2 = 0.15$) and water content ($p < 0.01$; $R^2 = 0.25$).

Accounting for percent land cover for each soil moisture group in the alpine and subalpine, the weighted average of THg pools was significantly higher in the alpine (2.0 ± 0.8 mg m^{-2} in upper 5 cm) compared to the subalpine (1.3 ± 0.8 mg m^{-2} in upper 5 cm; $p < 0.01$).

Soil pH in dry soils averaged 4.7 ± 0.2 in the alpine and 3.9 ± 0.3 in the subalpine. Across all soil types, pH averaged 4.6 ± 0.5 in the alpine and 4.4 ± 0.5 in the subalpine.

5.4.10 Stream Water

Past work from across the Rocky Mountains demonstrated that the majority of Hg is transported from high-elevation ecosystems in dissolved forms (Mast et al., 2005; Packer et al., 2020; Shanley et al., 2008). As such, we presume that the majority of Hg present in our samples is in the dissolved phase. Average THg concentrations in runoff were significantly lower in the alpine (1.1 ± 0.5 ng L^{-1}) compared to the subalpine (4.8 ± 2.5 ng L^{-1}). Stream THg concentrations and discharge were highest in June at both sites and decreased throughout the summer (Fig. 5-3A-B). DOC concentrations were 4.0 ± 3.6 mg L^{-1} in the alpine and 10.2 ± 3.7 mg L^{-1} in the subalpine. Sulfate concentrations were 1.7 ± 0.5 in the alpine and 1.9 ± 0.7 in the subalpine. The ratio of THg to DOC was 0.4 ± 0.2 in the alpine and 0.6 ± 0.3 in the subalpine.

Due to both lower THg concentrations and lower discharge volumes, average annual export of THg was significantly lower in Saddle Stream (0.11 ± 0.01 μg m^2 yr^{-1}) compared to Como Creek (1.13 ± 1.1 μg m^2 yr^{-1}; $p = 0.01$).

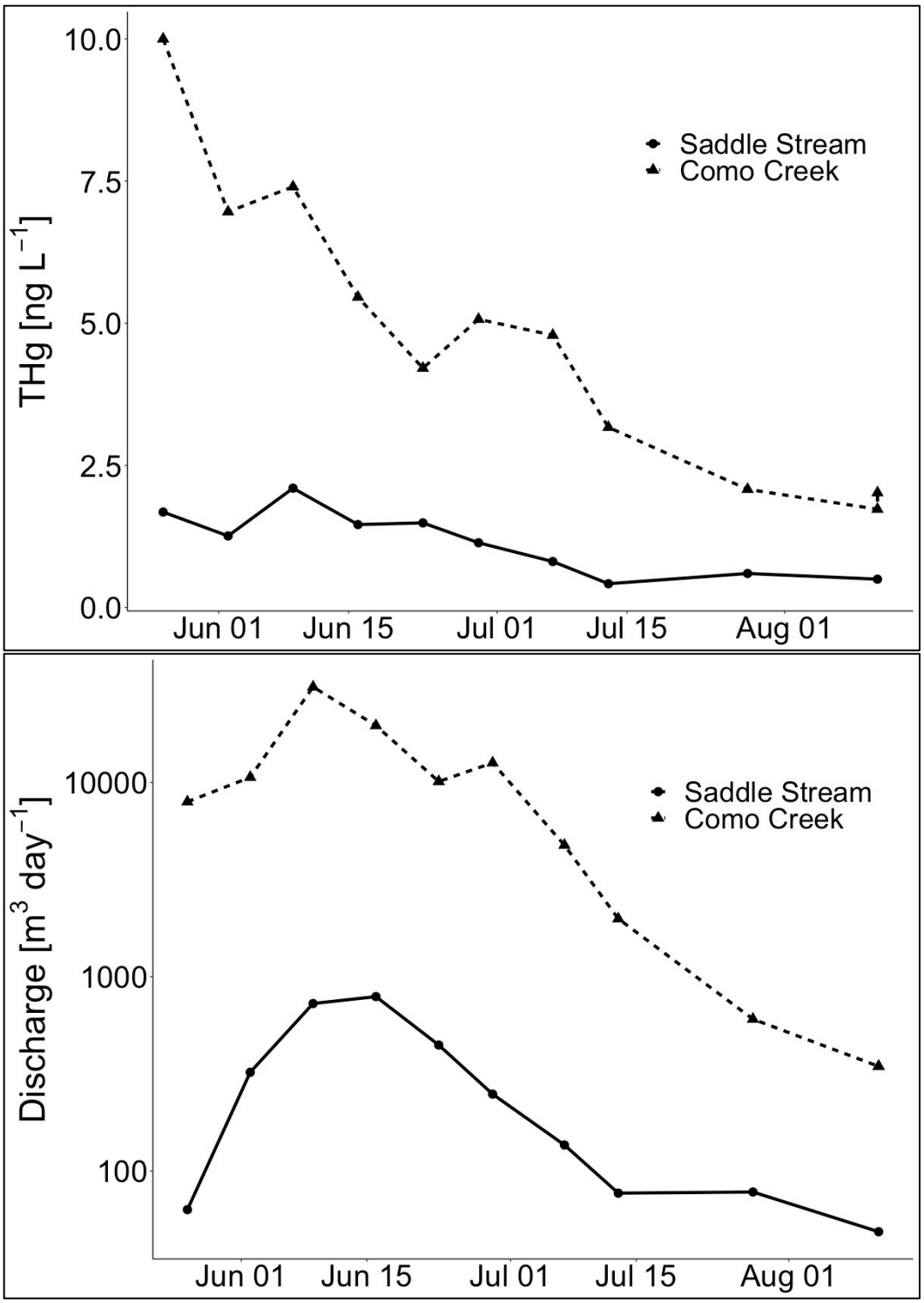

Figure 5-3: Total mercury (THg) concentrations (A) and total discharge (B) in Saddle Stream and Como creek during the sampling period. Note the y-axis log scale in B.

To better understand the drivers of Hg export across the alpine and subalpine, we examined correlations with Hg concentrations and fluxes in runoff (Fig. 5-4). In the alpine, THg concentrations were strongly correlated to discharge (r = 0.71, p = 0.02) and sulfate concentrations (r = 0.78; p = 0.01). DOC had no relationship with THg concentrations, but did have a significant positive correlation with THg fluxes (r = 0.71; p = 0.02), as well as discharge (r = 0.76; p = 0.01). In the subalpine, both THg concentrations (r = 0.60, p = 0.05) and fluxes (r = 0.97, p < 0.01) were positively correlated with discharge. Weak positive correlations were also observed with sulfate (r = 0.35), however the relationships were not significant (p = 0.32). Interestingly, DOC had a weak negative relationship were both THg and sulfate concentrations.

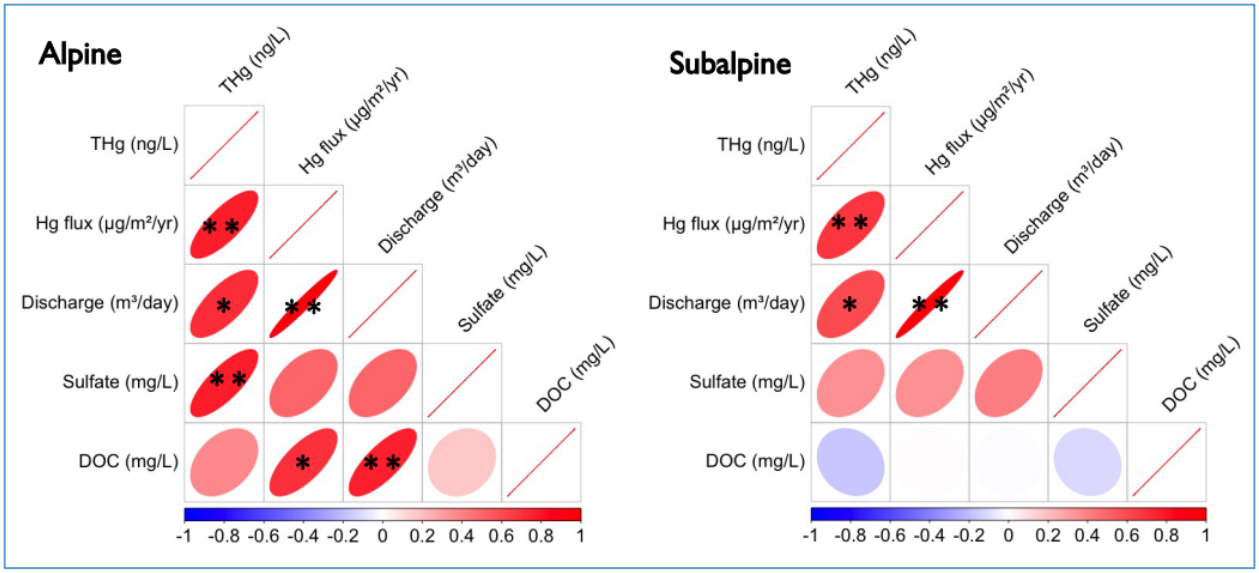

Figure 5-4: Pearson ranked correlation coefficients for total mercury (THg) concentrations, THg fluxes, discharge, sulfate, and dissolved organic carbon (DOC) across the alpine (left matrix) and subalpine (right matrix). Colors denote positive (red) or negative (blue) correlations and ellipse shape is a proxy for relationship strength. Asterisks denote significance level; * represents p < 0.05 and ** represents p < 0.01.

5.4.11 Evasion of THg

For the summer, we used soil THg evasion estimates of 10.5 ± 1.2 ug m^{-2} yr^{-1} for the alpine. Open precipitation fluxes estimated from Buffalo Pass THg concentrations and NWT-LTER precipitation volumes from October 2020–April 2021 were 6.3 ± 0.2 µg m^{-2} in the alpine and THg pools in NWT-LTER snowpack were 1.3 ± 1.0 µg m^{-2}. The difference in these values resulted in an estimated THg loss from snowpack of 5.0 ± 1.1 ug m^{-2} yr^{-1}. Total evasion rates were calculated by averaging the summer and winter estimates resulting in 7.75 ± 1.15 ug m^{-2} yr^{-1}.

Evasion of THg from forested ecosystems, particularly coniferous forests, have high levels of uncertainty associated with them (Blackwell et al., 2014; Landis et al., 2024). We identified several past studies with similar conditions to our subalpine site that had evasion rates ranging from -1.0 (Blackwell et al., 2014) to 11.5 ± 0.4 µg m^{-2} yr^{-1} (Eckley et al., 2016). We also calculated the difference between open precipitation fluxes (8.0 ± 0.4 µg m^{-2}, Buffalo Pass THg concentrations combined with NWT-LTER precipitation volumes) and snowpack THg pools (1.8 µg m^{-2}) to obtain an estimated loss of 6.3 ± 3.5 ug m^{-2} yr^{-1} THg during the winter months in the subalpine. We then separately averaged the low and high summer evasion estimates with winter evasion estimates to get a range of average annual evasion rates from the subalpine of 2.15 ± 3.3 to 8.9 ± 3.2 ug m^{-2} yr^{-1}.

5.4.12 Mass Balance of Hg Within the Alpine and Subalpine

We found that both the alpine and subalpine currently act as sinks for atmospherically deposited Hg (Fig. 5-5). The alpine retains ~46% of atmospherically deposited Hg with increases in soil Hg pools of 5.69 µg m^{-2} yr^{-1}. The subalpine retains 24–63 % of atmospherically deposited Hg, depending on evasion estimates, with increases in soil Hg pools of 5.87–12.12 µg m^{-2} yr^{-1}.

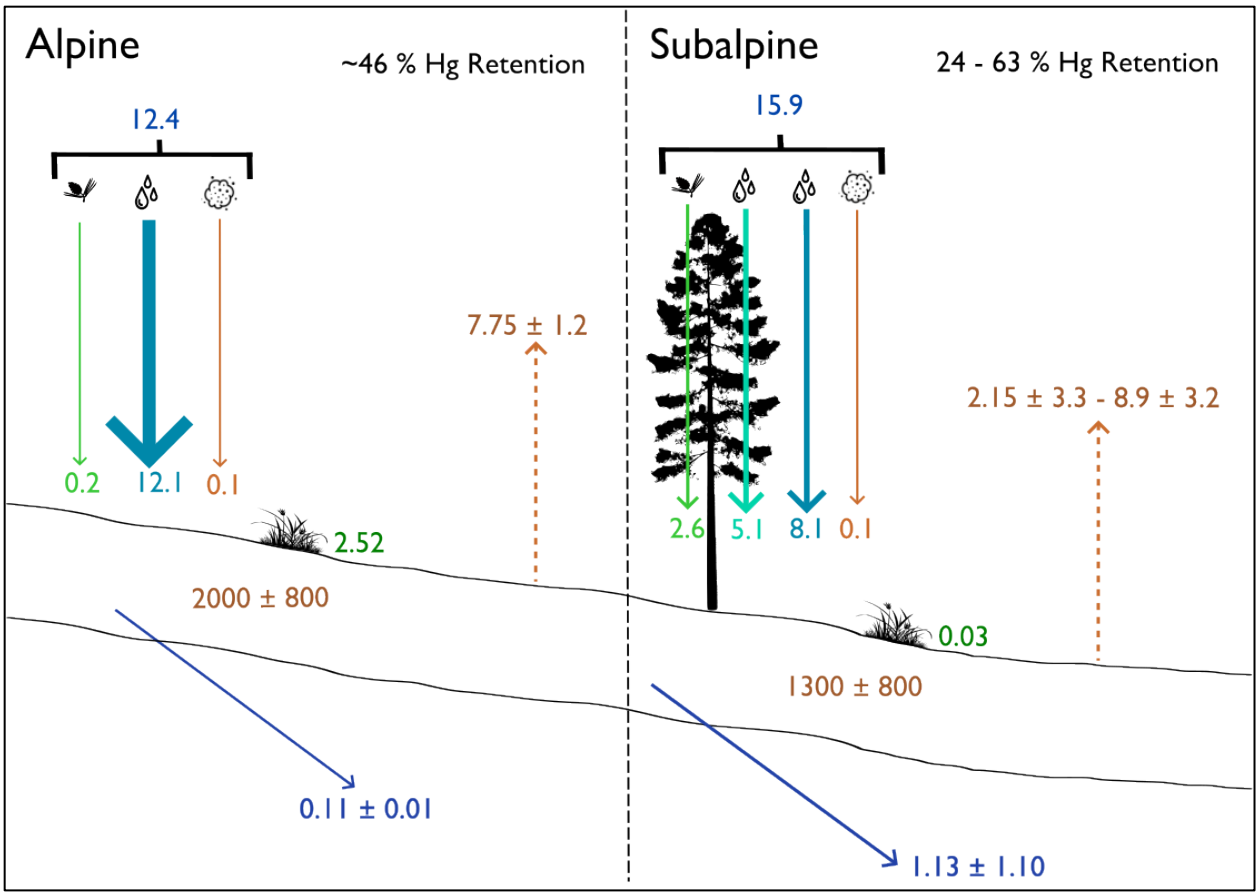

Figure 5-5: A mass balance of total mercury (THg) fluxes (μg m^{-2} yr^{-1}) and storage (μg m^{-2}) in the alpine and subalpine at NW-LTER. The needle with green arrows represent litterfall, the rain drops with blue arrows represent open precipitation when not passing through tree canopy and throughfall when passing through canopy, and dust with brown arrows represent dust fluxes. Blue arrows at the bottom represent runoff fluxes. Dashed yellow arrows represent estimated evasion fluxes. Brown text represents soil pools and green text represents vegetation pools.

5.5 Discussion

Our findings demonstrate that the Colorado Rocky Mountains currently act as sinks for Hg, similar to findings from other studies in high-elevation ecosystems (Mast et al., 2005; Wang, Yuan, et al., 2020). This sink character is driven by higher fluxes of inputs via atmospheric deposition compared to losses in runoff and evasion.

5.5.1 Inputs of Hg to High-Elevation Ecosystems are Dominated by Open Precipitation

In both the alpine and subalpine, open precipitation was the dominant input of THg from the atmosphere making up 97% and 53% of total inputs, respectively. This high contribution from open precipitation is surprising in the subalpine since forested areas typically have atmospheric deposition dominated by litterfall (Wang, Yuan, et al., 2020). Globally, vegetation Hg uptake is estimated to account for 60–90 % of terrestrial Hg deposition (Zhou et al., 2021). Studies focused on coniferous forests at high-elevation, however, are sparse, and, additionally, do not consider percent canopy cover within those forested regions. Factoring percent canopy cover can make a particularly big difference for areas like our site in the semi-arid western U.S. where there is only ~40 % canopy cover in the subalpine and no canopy cover in the alpine.

Considering percent canopy cover, our study in a high-elevation, coniferous-dominated forest shows that litterfall makes up only 16 % of total inputs and that atmospheric THg deposition is instead dominated by open precipitation and throughfall. This finding is similar to observations made by Blackwell et al. (2014) in coniferous forests of the Adirondack Mountains where litterfall fluxes accounted for as little as 21 % of total Hg deposition compared to deciduous forests where litterfall accounted for up to 65 % of total Hg deposition. Accounting for tree cover also resulted in considerably lower throughfall fluxes than past forest estimates. Without factoring in tree cover, our throughfall fluxes were 12.7 $\mu g\ m^2\ yr^{-1}$, which was comparable to throughfall fluxes observed by Blackwell et al., (2014) in the Adirondack Mountains. However, incorporating percent canopy cover results in fluxes that are much lower in the Colorado Rocky Mountains at ~5.1 $\mu g\ m^2\ yr^{-1}$.

The greater proportion of throughfall compared to litterfall Hg fluxes in the subalpine may also be due to the nature of climate and precipitation conditions in the Western U.S. In semi-arid ecosystems of the Rocky Mountains, precipitation typically occurs as pulsed events that are separated by periods of warm, dry conditions. For example, during the continental monsoon season of the summer, a storm front will typically build up during the day, peak in the mid-afternoon with a thunderstorm accompanied by rain, and then return to clear conditions until the following afternoon (Adams & Comrie, 1997). Because Hg(II) concentrations in the atmosphere are positively correlated with air temperature and solar radiation (Blackwell & Driscoll, 2015; Lindberg & Stratton, 1998), warmer, drier weather in the West likely promotes greater dry deposition to canopy surfaces, and, therefore, higher throughfall concentrations during periods of rainfall. This phenomenon was observed by Blackwell and colleagues (2014) in the Adirondack Mountain where they found significantly higher concentrations of Hg in throughfall during a dry year compared to a wetter year.

The importance of precipitation in the Western U.S. in transferring Hg from the atmosphere to the biosphere has also been observed with regards to bioaccumulation. Janssen and colleagues (2023) found dragonfly larvae from more arid regions, including Rocky Mountain National Park, had more positive δ^{200}Hg values (indicative of a greater proportion of Hg bioaccumulating from wet deposition) compared to areas with greater precipitation (e.g., Olympic National Park in Washington, U.S.), which had more negative δ^{200}Hg and Δ^{200}Hg isotope values (indicative of Hg source from dry deposition). Miller and colleagues (in prep) also found a significant, positive relationship between MeHg concentrations in chickadees and THg fluxes in precipitation along an elevation gradient in the Colorado Rocky Mountains.

Although atmospheric Hg contributions from dust were nominal, developing a baseline for Hg fluxes in dust is particularly important for the Western U.S., which is experiencing aridification and desertification at accelerating rates (Duncan et al., 2007; Duniway et al., 2019; Huang et al., 2020, p. 20; L. Zhang et al., 2013). Additionally, a long history of mining and industry may influence heavy metals loads in dust through erosion and extended dry seasons, such as demonstrated in the Great Salt Lake region of Utah (Blakowski et al., 2021; Lee et al., 2024). Wind remobilization of loess from soil and glacial deposits has been observed in the Arctic to distribute elements, including Hg, within dust (Witherow & Lyons, 2008). Olson and colleagues (2019) found Hg in vegetation was correlated with typical crustal elements, including Fe, Ti, V, and Ni, which indicate dust as a potential source of Hg in local vegetation (C. L. Olson et al., 2019). In addition to remobilization of soil through erosion, wildfire can release previously stored Hg from soils back to the atmosphere, providing another possible source of Hg through atmospheric deposition (McLagan et al., 2021).

In general, the presence of tree cover drove higher total inputs of THg into the subalpine compared to the alpine because of increased dry deposition through litterfall and throughfall. This finding suggests that in addition to changes in elevation, shifts in aspect, which drive strong gradients in tree cover and type, may influence inputs of Hg across mountain ecosystems marking an important area for future research. As tree line shifts with ongoing climate change (Cazzolla Gatti et al., 2019; Tourville et al., 2023), there is also potential for changes in atmospheric Hg fluxes.

5.5.2 Mercury in Runoff is Driven by Snowmelt and Atmospheric Deposition

The strong correlation in both the alpine and subalpine between THg concentrations and discharge suggests that spring snowmelt (and large precipitation events throughout the growing season) are the main drivers of THg in runoff, an observation supported by a number of past studies (Mast et al., 2005; Packer et al., 2020; Shanley et al., 2008). Unlike past research, we did not find a relationship between runoff THg concentrations and DOC concentrations when examining the alpine and subalpine independently (Fig. 5-4). This result was surprising since THg concentrations are typically strongly correlated to DOC concentrations in high-elevation streams (Mast et al., 2005; Packer et al., 2020; X. Sun et al., 2022). Past studies have attributed this result to flushing of soluble organic C that accumulates in soils over the winter. Instead, the strong correlation that we observed between THg concentrations and sulfate concentrations in the alpine—a constituent primarily derived from atmospheric deposition—suggests that preferential release of Hg stored in snowpack rather than soils drove changes in stream Hg concentrations (D. H. Campbell et al., 1995; Mast et al., 2005). The weak but significant positive relationship between DOC and THg concentration across both the alpine and subalpine suggests that greater soil development and flushing of those soils during snowmelt in the subalpine may contribute to higher loads of Hg, compared to the alpine, even if DOC alone is not the main driver within either of the sites individually. This finding suggests that DOC controls the baseline concentration of THg across these sites, but that seasonal changes within each site are influenced more by snowmelt and precipitation events rather than soil flushing.

Concentrations of DOC in our study were higher than past work by Mast and colleagues (2005) in the Rocky Mountains. They found peak concentrations of 3.4 mg DOC L^{-1} in the alpine and 7.1 mg DOC L^{-1} in the subalpine. Higher DOC concentrations in our study may indicate greater soil development and

mineralization with increasing average soil temperatures over the past two decades. Interestingly, higher DOC concentrations did not result in greater Hg export as we would have expected since DOC and Hg are typically correlated. Rather, fluxes of Hg in our study remain similar to past measurements in the Rocky Mountains, which explains why DOC and Hg are not strongly correlated. This decoupling of DOC and Hg raises questions as to the primary drivers of Hg transport, if not from flushing of surface soils, and highlights important areas for future research of THg export under a changing climate. For example, this decoupling may indicate that warming soils release more DOC, but that C-bound Hg is lost via evasion before it can be transported in runoff. It is worth noting that the lack of correlation between Hg and DOC may be the result of measuring unfiltered waters (Janssen et al., 2025) and future analysis of dissolved and particulate fractions may help explain drivers of Hg loss in runoff more clearly.

Interestingly, we did find that Hg pools in snowpack were greater than total Hg loads in runoff within both the alpine and subalpine. This pattern suggests that Hg fluxes in runoff could primarily be explained by atmospheric inputs and that contributions from surface soil flushing may be less important. We see additional evidence that supports this hypothesis in late June when a large precipitation event increased stream discharge and led to an increase in Hg concentrations within Como Creek. Earlier and faster snowmelt in the future, as well as reduced hydrologic connectivity, could contribute to less flushing of Hg from surface soils and greater contributions of Hg directly from atmospheric deposition.

5.5.3 Mercury Pools in Soil are Associated with Soil C

Despite greater inputs of Hg into the subalpine compared to the alpine, pools of Hg in soil were smaller and the offset cannot be fully explained differences in

runoff. The subalpine receives 3.5 μg m^{-2} yr^{-1} (15.9–12.4 μg m^{-2} yr^{-1}) greater inputs compared to the alpine, but only 1.02 μg m^{-2} yr^{-1} (1.13–0.11 μg m^{-2} yr^{-1}) greater losses in runoff, leaving ~2.48 μg m^{-2} yr^{-1} Hg loss that is unaccounted. This difference could be explained by higher evasion rates in the subalpine and highlights the importance of better constraining soil-atmosphere fluxes in these ecosystems. This is not the first time, though, that this discrepancy of elevated atmospheric deposition to coniferous forests combined with smaller than expected soil pools has been observed.

Landis and colleagues (2024) used fallout radionuclide chronometry to directly measure soil Hg accumulation rates in a variety of ecosystems globally. While they observed Arctic, boreal, temperate, and tropical soils are all efficient at retaining anthropogenic Hg, they did observe that there was significant GEM re-emission potential in a group of "low accumulating" soils that were all comprised of soils found in coniferous forests (Landis et al., 2024). Blackwell and colleagues (2014) also observed smaller soil pools of Hg in coniferous forest soils compared to deciduous forest soils in the Adirondack Mountains, despite enhanced deposition in coniferous stands. The authors from both of these studies proposed several possible explanations for this discrepancy including greater atmospheric re-emission (although Blackwell and colleagues (2014) found net storage of deposition), leaching to mineral soils, greater uptake of Hg by woody structures in conifer trees which have been shown to store significantly more Hg in roots and stems than hardwood species (Obrist et al., 2012), or greater export in runoff. Considering the latter hypothesis, we did observe greater runoff from the subalpine compared to the alpine. However, our observation does not account for the discrepancy in soil pool sizes observed between the alpine and subalpine. Additionally, we would assume that most of the THg lost from soil through leaching would be bound up in DOC;

however, we did not find a significant relationship between THg and DOC in the subalpine runoff.

Regardless of uncertainties associated with fluxes of Hg into and from soil, the larger storage of Hg in the alpine appears to be driven by C dynamics in these high-elevation sites, evidenced by the fact that THg normalized to soil organic matter is nearly identical between the alpine (0.33 ± 0.13 μg Hg g C^{-1}) and subalpine (0.33 ± 0.22 μg Hg g C^{-1}). Interestingly, in addition to finding a strong correlation between THg concentrations and soil C across these sites, we also found a positive relationship between soil THg pools and soil C resulting in higher THg concentrations, THg pools, and soil bulk density in the alpine compared to the subalpine. This finding is not typical because areas with higher soil organic matter typically have higher THg concentrations, but lower bulk density, which results in smaller THg pools. We observed this pattern in the subalpine site where wet soils have significantly higher THg concentrations, but due to low bulk density (very peaty soils with high soil organic matter), the THg pools are lower at these sites compared to the dry soil regions. In the case of the alpine and subalpine, however, higher soil organic matter content in the alpine (0.19 ± 0.07 g C g dry $soil^{-1}$) compared to the subalpine (0.15 ± 0.06 g C g dry $soil^{-1}$) does not lead to lower bulk density. In fact, bulk density in the alpine (0.7 ± 0.3 g cm^{-3}) and subalpine (0.7 ± 0.5 g cm^{-3}) are nearly identical. The higher THg concentrations and pools in the alpine are likely due to colder air and soil temperatures in the alpine, compared to the subalpine, which results in slower soil mineralization rates over time and the gradual accumulation of C within the soils.

In many environments, higher soil organic matter is typically driven by greater litter contirbutions, which have much lower bulk density than mineral soils. In contrast, soil organic matter accumulation in the alpine results from slower

decomposition, which does not lead to reduced bulk density. Since Hg binds strongly to C, the buildup of organic matter in the alpine creates more substrate for Hg to accumulate, making is less easily lost in runoff and evasion. Overall, this finding suggests that the larger THg pools in the alpine are a result of soil C dynamics rather than differences in inputs and runoff between the alpine and subalpine. These patterns also raise important questions regarding climate change impacts on rates of C mineralization in high-elevation soils and is discussed further in the final section.

5.5.4 Limitations in Hg Sink Estimates due to Evasion and Climate Change

When only considering runoff of Hg in our study, we find Hg retention rates of atmospheric deposition in soils between 93–99 %, comparable to past values estimated by Mast and colleagues (2005) in Rocky Mountain National Park (82 – 93%). By including evasion estimates in our study, however, annual Hg retention decreases to 24–63 % in the subalpine and ~ 46% in the alpine. The large uncertainty regarding Hg evasion rates from soil back to the atmosphere highlights a major gap in constraining the mass balance of Hg in mountain ecosystems.

Globally, Hg evasion rates remain highly unconstrained with the majority of studies from the past several decades biased toward Hg-enriched sites, daytime, and summertime measurements (Agnan et al., 2016). Past work has demonstrated strong positive relationships between THg fluxes and solar radiation (due to photochemical reduction of Hg(II) to volatile Hg(0)), soil and air temperatures (collinear to radiation and also impacted by lower activation energy) (Eckley et al., 2016; Zhou et al., 2020). While strong correlations exist between Hg fluxes and substrate concentrations at elevated Hg concentrations, this relationship is absent at sites at background levels of Hg (<300 ng g^{-1}) and marks an important knowledge

gap. In forested ecosystems where contributions from leaf-atmosphere exchange is highly uncertain, flux estimates vary widely ranging from -513–1353 Mg yr^{-1} globally (Agnan et al., 2016). Other uncertainties exist regarding the influence of litter cover. Agnan and colleagues (2016) found fluxes from substrate to the atmosphere decreased going from bare soil (1.26 ± 1.89 ng m^{-2} hr^{-1}) to soil covered with litter (1.17 ± 1.64 ng m^{-2} hr^{-1}) to leaf surfaces (-0.06 ± 2.17 ng m^{-2} hr^{-1}). Predicting Hg fluxes in mountain ecosystems that typically have both background Hg concentrations in soils, presence of litter cover, as well as large expanses of forested areas, is therefore a challenge.

Evasion is likely a large flux in mountain ecosystems where there is intense solar radiation, large fluctuations in air and soil temperatures, and strong gradients in soil moisture. By using estimates from past studies, as well as our snowpack data, we demonstrate that evasion may account for a large percent of THg removal from both the alpine and subalpine terrestrial ecosystems, with much larger uncertainty in the latter. Ranges in evasion rate estimates in the subalpine could be due to patchy solar radiation due to areas of dense, year-round canopy cover (Eckley et al., 2016). Low soil pH may also contribute to reduced evasion in the subalpine. Agnan and colleagues (2016) found that soil pH was strongly correlated with Hg fluxes, with only 29 % of soils with a pH < 5 showing net Hg(0) emissions globally. In the subalpine, the dry forest floor had pH values ranging from 3.65–4.34 which may also contribute to varied evasion rates. In general, studies of soils in coniferous forests have found net storage of deposition. Zhou and colleagues (2020) observing evasion rates of -0.04 ± 0.81 ng m^2 h^{-1} in evergreen pine forests of China (Zhou et al., 2020) and Blackwell and colleagues (2014) observed rates of -1.0 μg m^{-2} yr^{-1} in coniferous forests of the Adirondack Mountains. Larger-scale estimates, including coniferous forest-dominated mountain regions, have estimated much higher evasion

rates. For example, Eckley and colleagues (2016) estimated losses of 10.5 ± 1.2 μg m^{-2} yr^{-1} in the southern semi-arid highlands of the U.S., which include sites in the Rocky Mountains (Eckley et al., 2016). Season also appears to be important in driving the direction of Hg transport in coniferous forests. Zhou and colleagues (2020) observed net evasion of THg in the temperate coniferous forest soils during the spring and summer and net storage of atmospheric deposition in the fall and winter.

Our comparison of THg pools in snowpack to precipitation fluxes during the winter is a novel approach to estimating loss of Hg from snow through evasion. Our estimates for the alpine (5.0 ± 1.1 μg m^{-2}) and subalpine (6.3 ± 3.5 μg m^{-2}) fall within the range of fluxes previously measured for snowpack of 7.63 ± 22.87 μg m^{-2} yr^{-1} (Agnan et al., 2016) suggesting that this is a sound method for estimating Hg loss during snow covered periods. Since high-elevation ecosystems experience snow cover for a significant portion of the year, estimating Hg fluxes in these ecosystem pools is important for overall estimations of Hg mass balance. Indeed, past work from Niwot Ridge demonstrates that strong, diurnal patterns of photochemical GEM production in surface snowpack can lead to re-emission losses of deposited Hg back to the atmosphere (LøNne, 2008). Faïn and colleagues (2013) measured enhanced GEM concentrations in interstitial air of surface snowpack reaching as high as 8 ng m^{-3}; for comparison, our air measurements from NWT-LTER were 0.92 ± 0.15 ng m^{-3}. In addition, they observed the highest GEM production following fresh snowfall and that fluxes were not radiation-limited with strong GEM production even on cloudy days. These high rates of GEM production even under cloud cover may explain why the subalpine did not have lower evasion rates in snowpack despite the presence of canopy cover.

While we observed large uncertainties in evasion within this mountain ecosystem, across the range of estimated evasion rates considered in our study, both the alpine and subalpine remain on the "sink" side of the mass balance equation (Fig. 5-5). However, our observed drivers of inputs, storage, and losses suggest that continued climate change may push these ecosystems closer to a steady-state, or even "source", condition in the coming years.

5.6 The Future of Hg Sink-Source Behavior in High-Elevation Ecosystems

Drier, warmer conditions may increase dry deposition to high-elevation ecosystems. Because atmospheric concentrations of Hg(II) are elevated during dry periods with warmer temperatures and more solar radiation (Blackwell & Driscoll, 2015; Lindberg & Stratton, 1998), climate change in the Western U.S. will likely promote greater dry deposition of Hg to canopy surfaces. When precipitation events occur, throughfall concentrations will be higher resulting in greater Hg fluxes into ecosystems, as has been documented in coniferous forests of the Adirondack Mountains (Blackwell et al., 2014). Succession of vegetation due to glacier retreat and soil development has also been shown to increase fluxes of Hg to ecosystems via litterfall (Wang, Luo, et al., 2020). In addition to recently deglaciated terrain, upward shifts in tree cover in mountain ecosystems more broadly will result in greater litterfall fluxes, and, therefore, fluxes of Hg (Cazzolla Gatti et al., 2019; Tourville et al., 2023). Finally, increasing intensity and frequency of wildfire, which remobilizes Hg from soil and vegetation pools, may lead to greater Hg deposition to mountain ecosystems via atmospheric deposition when smoke plumes reach mountain environments (Kumar & Wu, 2019; Zolkos et al., 2024).

Warming air and soil temperatures have the potential to reduce Hg pools in soil by both increasing soil mineralization rates, as well as the potential for soil

erosion. As soils warm, increased microbial mineralization draws down soil C pools (Y. Chen et al., 2024). Since Hg soil storage at our site is strongly driven by C pools, it is likely that warming soil temperatures and increased mineralization will result in greater loss of Hg from soils either via runoff or evasion back to the atmosphere. The lower soil pools of C and Hg in the subalpine likely reflect increased mineralization with warming temperatures since average soil temperatures in the subalpine (2°C) are higher than the alpine (0.3°C), an observation that was also made by D'Alò and colleagues in the Italian Alps (D'Alò et al., 2021). Loss of soil Hg in aqueous transport has already been observed in thawing Arctic permafrost soils (Schaefer et al., 2020), which is the largest pools of Hg globally (Schuster et al., 2018). These losses may lead not only to reduced storage but even to a flipping from sink status to source in the coming decades (Bishop et al., 2020). Increased wildfire activity may also decrease Hg soil pools if the fire occurs within the mountain landscape. Fires release large amounts of Hg bound up in surface soil layers resulting in additional Hg loss to the atmosphere (Biswas et al., 2007; Homann et al., 2015; Webster et al., 2016).

Although soil Hg pools may decrease with warming, shifts in vegetation and tree cover to higher elevations may offset some of this Hg loss. Since vegetation efficiently scavenges and stores Hg from the air (Zhou et al., 2021), greater terrestrial primary productivity at higher elevations may help store more Hg within these ecosystems as has been documented in the Tibetan Plateau (Wang, Yuan, et al., 2020). Shifts in plant type, though, may offset some of this loss. Non-vascular plant species, common of tundra and high-elevation ecosystems, have much higher Hg concentrations compared to vascular plants within the same area (Olson et al., 2019). If warming temperatures promote more growth of plants with lower Hg concentrations, overall storage of Hg within vegetation may decrease.

Finally, climate change may alter losses of Hg from high-elevation ecosystems by changes in hydrology, as well as evasion rates. (Bishop et al., 2020). Loss of Hg from melting glaciers (X. Sun et al., 2022) and thawing permafrost (Mu et al., 2020) has also been documented within the Tibetan Plateau indicating that loss of Hg from mountain environments may increase with continued warming. Glacier melt, however, also initiates vegetation succession within exposed glacier forefields. This behavior creates a dichotomy where melting glaciers release Hg originally stored in ice to the atmosphere and downstream, while vegetation simultaneously takes up Hg from the atmosphere during growth. In the Tibetan Plateau, Wang and colleagues (2020) found that Hg uptake by vegetation is ~ three-fold higher than the total Hg mass lost via meltwater suggesting that this glacier-to-vegetation transition will actually result in high-elevation ecosystems acting as more of sink in coming decades despite loss of Hg within ice (Wang, Luo, et al., 2020)..

Earlier and more rapid snowmelt in high-elevation ecosystems (Clow, 2010) also causes a variety of impacts on Hg transport. Due to higher flow velocities, earlier, faster snowmelt can increase erosion potential and therefore remobilization of Hg in soils (Cache et al., 2023). In addition, thawing permafrost features may connect previously disconnected parts of the landscape to flow paths, thereby increasing losses of Hg downstream (Hermes et al., 2020). Decreasing snowpack, however, can also lead to reduced periods of hydrologic connectivity, which may decrease Hg export by reducing flow of water through surface soils.

Climate impacts on evasion are complex and may cause either increasing or decreasing fluxes. Drier, warmer soils tend to evade more Hg but if these drivers also cause greater vegetation growth, the loss of solar radiation may decrease evasion rates (Eckley et al., 2016). Additionally, changes in extent and depth of

snowpack will alter net Hg evasion with snow-covered soils typically having negative or very low evasion rates (Zhou et al., 2020), while snow and ice efficiently reduce Hg back to the atmosphere (Faïn et al., 2013). One study from a hardwood forest at Hubbard Brook, USA found that increased growing season temperatures and freeze-thaw cycles increased Hg evasion from soils back to the atmosphere adding to the source component of these ecosystems (Y. Yang et al., 2019). To better predict the role of evasion in mountain ecosystems under a changing climate, it is critically important to better constrain baseline drivers of Hg evasion across environmental gradients in high-elevation ecosystems.

5.7 Conclusions

This study highlights the complexities of Hg cycling in high-elevation ecosystems and demonstrates the role they play as sinks of atmospheric Hg deposition under current climate conditions. Open precipitation made up the largest proportion of atmospheric Hg inputs into both the alpine and subalpine, despite 40% canopy cover in the subalpine. Litterfall and throughfall contributed important Hg inputs to the subalpine, but when adjusting for percent canopy cover only contributed 16 % and 32 % of total Hg inputs, respectively. Dust sources of Hg were nominal compared to other atmospheric deposition pathways (~1 %), but these measurements provide an important baseline since future warming and aridification may increase Hg transport in dust globally. Mercury transport in runoff was driven by snowmelt and precipitation events, and, unlike past studies, showed little correlation with DOC concentrations. This lack of correlation suggests greater Hg sourcing from atmospheric deposition rather than surface soils.

Despite greater inputs of THg into the subalpine compared to the alpine, Hg pools were greater in the alpine, likely due to enhanced C storage. The larger pool

size in the alpine cannot be fully explained by larger Hg losses via runoff and evasion in the subalpine. This finding aligns with global observations that coniferous forest ecosystems have low Hg-accumulating soils despite elevated atmospheric inputs and marks an important gap in our understanding of Hg cycling in high-elevation and boreal regions. The degree to which our study sites retain atmospherically deposited Hg decreases from 93–99 % when only considering Hg losses via runoff to 24–63 % when also including evasion. This finding highlights the importance of including evasion estimates when constructing Hg mass balances for mountain ecosystems and the need for a better understanding of how different environmental variables (e.g., soil pH, solar radiation, snow cover, canopy cover) influence Hg volatilization. Broadly, our findings emphasize that mountain ecosystems act as complex regions for Hg cycling and highlight the critical need to constrain the sinks-source nature of these areas in the context of continued climatic change.

CHAPTER VI

CONCLUSIONS

The persistent nature of mercury (Hg) in the environment, as well as the impacts of climate change on Hg biogeochemistry, make it critically important to determine how this contaminant cycles through Earth's spheres. Mountain ecosystems, which are disproportionately influenced by climate change and make up a large percentage of land surfaces, are particularly important areas for this research. With this dissertation, I advance quantitative analysis of: (1) the patterns and drivers of Hg cycling within high-elevation ecosystems, and (2) how climate change may influence the toxicity and mobility of Hg in the coming decades. This research provides baseline quantification of Hg inputs, storage, and losses in high-elevation ecosystems that are hard to access, and, therefore, historically underrepresented in site-specific studies of Hg cycling. I demonstrate how ongoing climate change in mountain landscapes may influence Hg biogeochemistry with implications for Hg bioavailability and storage.

In Chapter II, I present the first comprehensive synthesis of Hg cycling in the Rocky Mountains, identifying key patterns and drivers of Hg inputs, storage, and losses across elevational and climatic gradients. These findings highlight the critical role of climate change-driven shifts in wildfire activity and hydrology in altering Hg dynamics in semi-arid mountain ecosystems of the western U.S. I also outline priority area for future research, including quantifying Hg concentrations and fluxes in dry atmospheric deposition, measuring MeHg production rates in high-elevation aquatic ecosystems, and characterizing the overall sink-source behavior of

these regions. Identifying these knowledge gaps helped shape the direction of the remaining chapters of my dissertation.

Chapter III, is a comprehensive evaluation of Hg cycling across a semi-arid mountain ecosystem elevation gradient in the Colorado Rocky Mountains. I found elevation, as well as patterns in precipitation and tree cover drove Hg cycling. The greatest inputs of Hg were in the mid-elevation zones driven by higher contributions of litterfall and throughfall. Storage of Hg in soils was greatest in the alpine due to elevated soil carbon (C), which suggests continued warming could lead to loss of Hg from these regions via increased soil C mineralization. Bioaccumulation of Hg into terrestrial food webs was highest in the mid-elevations likely driven by higher throughfall and open precipitation Hg fluxes. This suggests that future changes in precipitation may influence Hg toxicity in local wildlife. Altogether, this study provides a valuable baseline investigation of Hg cycling in semi-arid mountain ecosystems, while also highlighting important areas for future research.

In Chapter IV, I assess the potential of increasing sulfate export in alpine streams to stimulate methylmercury (MeHg) formation in high-elevation wetlands. As far as we are aware, this is the first assessment of MeHg production rates, as well as sulfate limitations, in mountain wetlands. Through laboratory incubation experiments, I found MeHg production increased significantly following sulfate additions in subalpine peatlands, with the highest rates at moderate sulfate concentrations that are comparable to those observed in mountain regions. This study is the first to identify sulfate limitation in mountain wetlands, as well as to define soil sulfate-related thresholds for MeHg formation.

In Chapter V, I evaluate the sink-source character of alpine and subalpine regions of the Colorado Rocky Mountains under current climate conditions. Only the

second such study in the Rocky Mountains, and the first in the past 20 years, this research provides a more comprehensive mass balance by including Hg inputs via litterfall and dust, and estimated losses via evasion. I found that alpine regions retain ~46 % of atmospherically deposited Hg, while subalpine regions retain anywhere between 24–63 % depending on different Hg evasion estimates. These findings highlight the need for better quantification of Hg losses via evasion, particularly in subalpine coniferous forest zones that act as complex regions for Hg cycling.

The findings from this dissertation emphasize the critical role of mountain ecosystems in global Hg cycling and provide essential benchmarks for evaluating the effectiveness of initiatives such as the Minamata Convention. As climate change accelerates, these ecosystems are likely to experience significant shifts in their sink-source dynamics, driven by warming temperatures, altered precipitation patterns, and vegetation changes. My research underscores the need for integrative policies that address both legacy Hg contamination and emerging challenges posed by climate change, while also providing actionable data for future research on high-elevation ecosystems. By bridging gaps in our understanding of Hg cycling, this dissertation contributes to the broader goal of mitigating Hg's environmental and health impacts on vulnerable ecosystems and communities.

REFERENCES

Abatzoglou, J. T., & Williams, A. P. (2016). Impact of anthropogenic climate change on wildfire across western US forests. *Proceedings of the National Academy of Sciences of the United States of America*, *113*(42), 11770–11775. https://doi.org/10.1073/pnas.1607171113

Ackerman, J. T., Eagles-Smith, C. A., Herzog, M. P., Hartman, C. A., Peterson, S. H., Evers, D. C., Jackson, A. K., Elliott, J. E., Vander Pol, S. S., & Bryan, C. E. (2016). Avian mercury exposure and toxicological risk across western North America: A synthesis. *Science of the Total Environment*, *568*, 749–769. https://doi.org/10.1016/j.scitotenv.2016.03.071

Adams, D. K., & Comrie, A. C. (1997). The North American Monsoon. *Bulletin of the American Meteorological Society*, *78*(10), 2197–2214. https://doi.org/10.1175/1520-0477(1997)078<2197:TNAM>2.0.CO;2

Agnan, Y., Le Dantec, T., Moore, C. W., Edwards, G. C., & Obrist, D. (2016). New Constraints on Terrestrial Surface-Atmosphere Fluxes of Gaseous Elemental Mercury Using a Global Database. *Environmental Science and Technology*, *50*(2), 507–524. https://doi.org/10.1021/acs.est.5b04013

Alhassan, A., Ozturk, I., AL-Zyoud, M. F., & Bekun, F. V. (2024). Coal consumption-environmental sustainability nexus in developed and developing major coal-consuming economies. *Heliyon*, *10*(4). https://doi.org/10.1016/j.heliyon.2024.e25619

Amos, H. M., Jacob, D. J., Kocman, D., Horowitz, H. M., Zhang, Y., Dutkiewicz, S., Horvat, M., Corbitt, E. S., Krabbenhoft, D. P., & Sunderland, E. M. (2014). Global biogeochemical implications of mercury discharges from rivers and

sediment burial. *Environmental Science and Technology*, *48*(16), 9514–9522. https://doi.org/10.1021/es502134t

Amos, H. M., Jacob, D. J., Streets, D. G., & Sunderland, E. M. (2013). Legacy impacts of all-time anthropogenic emissions on the global mercury cycle. *Global Biogeochemical Cycles*, *27*(2), 410–421. https://doi.org/10.1002/gbc.20040

Andreasen, M., Christiansen, J. R., Sonnenborg, T. O., Stisen, S., & Looms, M. C. (2023). Seasonal dynamics of canopy interception loss within a deciduous and a coniferous forest. *Hydrological Processes*, *37*(4), e14828. https://doi.org/10.1002/hyp.14828

Badger, A. M., Bjarke, N., Molotch, N. P., & Livneh, B. (2021). The sensitivity of runoff generation to spatial snowpack uniformity in an alpine watershed: Green Lakes Valley, Niwot Ridge Long-Term Ecological Research station. *Hydrological Processes*, *35*(9). https://doi.org/10.1002/hyp.14331

Bae, H.-S., Dierberg, F. E., & Ogram, A. (2014). Syntrophs Dominate Sequences Associated with the Mercury Methylation-Related Gene hgcA in the Water Conservation Areas of the Florida Everglades. *Applied and Environmental Microbiology*, *80*(20), 6517–6526. https://doi.org/10.1128/AEM.01666-14

Bank, M. S. (2020). The mercury science-policy interface: History, evolution and progress of the Minamata Convention. *Science of The Total Environment*, *722*, 137832. https://doi.org/10.1016/j.scitotenv.2020.137832

Barbo, N., Stoiber, T., Naidenko, O. V., & Andrews, D. Q. (2023). Locally caught freshwater fish across the United States are likely a significant source of exposure to PFOS and other perfluorinated compounds. *Environmental Research*, *220*. https://doi.org/10.1016/j.envres.2022.115165

Barry, R. G. (1973). A Climatological Transect on the East Slope of the Front Range, Colorado. *Arctic and Alpine Research*, *5*(2), 89–110. https://doi.org/10.1080/00040851.1973.12003684

Bartrons, M., Gratton, C., Spiesman, B. J., & Zanden, M. J. V. (2015). Taking the trophic bypass: Aquatic-terrestrial linkage reduces methylmercury in a terrestrial food web. *Ecological Applications*, *25*(1), 151–159. https://doi.org/10.1890/14-0038.1

Basu, N., Abass, K., Dietz, R., Krümmel, E., Rautio, A., & Weihe, P. (2022). The impact of mercury contamination on human health in the Arctic: A state of the science review. *Science of the Total Environment*, *831*. https://doi.org/10.1016/j.scitotenv.2022.154793

Battaglia, M. A., Gannon, B., Brown, P. M., Fornwalt, P. J., Cheng, A. S., & Huckaby, L. S. (2018). Changes in forest structure since 1860 in ponderosa pine dominated forests in the Colorado and Wyoming Front Range, USA. *Forest Ecology and Management*, *422*, 147–160. https://doi.org/10.1016/j.foreco.2018.04.010

Beniston, M. (2006). Mountain Weather and Climate: A General Overview and a Focus on Climatic Change in the Alps. *Hydrobiologia*, *562*(1), 3–16. https://doi.org/10.1007/s10750-005-1802-0

Benoit, J. M., Gilmour, C. C., Heyes, A., Mason, R. P., & Miller, C. L. (2002). Geochemical and Biological Controls over Methylmercury Production and Degradation in Aquatic Ecosystems. *ACS Symposium Series*, *835*, 262–297. https://doi.org/10.1021/bk-2003-0835.ch019

Bergman, I., Bishop, K., Tu, Q., Frech, W., Åkerblom, S., & Nilsson, M. (2012). The Influence of Sulphate Deposition on the Seasonal Variation of Peat Pore

Water Methyl Hg in a Boreal Mire. *PLOS ONE*, *7*(9), e45547. https://doi.org/10.1371/journal.pone.0045547

Bishop, K., Shanley, J. B., Riscassi, A., de Wit, H. A., Eklöf, K., Meng, B., Mitchell, C., Osterwalder, S., Schuster, P. F., Webster, J., & Zhu, W. (2020). Recent advances in understanding and measurement of mercury in the environment: Terrestrial Hg cycling. *Science of the Total Environment*, *721*. https://doi.org/10.1016/j.scitotenv.2020.137647

Biswas, A., Blum, J. D., Klaue, B., & Keeler, G. J. (2007). Release of mercury from rocky mountain forest fires. *Global Biogeochemical Cycles*, *21*(1). https://doi.org/10.1029/2006GB002696

Blackwell, B. D., & Driscoll, C. T. (2015). Deposition of mercury in forests along a montane elevation gradient. *Environmental Science and Technology*, *49*(9), 5363–5370. https://doi.org/10.1021/es505928w

Blackwell, B. D., Driscoll, C. T., Maxwell, J. A., & Holsen, T. M. (2014). Changing climate alters inputs and pathways of mercury deposition to forested ecosystems. *Biogeochemistry*, *119*(1–3), 215–228. https://doi.org/10.1007/s10533-014-9961-6

Blakowski, M., Rader, S., Aarons, S., Dong, Z., Perala-Dewey, J., Hageman, K., Heim, E., Bartos, A., & Brahney, J. (2021). *Heavy Metals in Dust From the Shrinking Great Salt Lake: Where Do They Come From and Where Do They Go? 2021*, B41A-06. AGU Fall Meeting Abstracts.

Bodner, G. S., & Robles, M. D. (2017). Enduring a decade of drought: Patterns and drivers of vegetation change in a semi-arid grassland. *Journal of Arid Environments*, *136*, 1–14. https://doi.org/10.1016/j.jaridenv.2016.09.002

Brahney, J., Wetherbee, G., Sexstone, G. A., Youngbull, C., Strong, P., & Heindel, R. C. (2020). A new sampler for the collection and retrieval of dry dust

deposition. *Aeolian Research*, *45*, 100600. https://doi.org/10.1016/j.aeolia.2020.100600

Brand, R. F., du Preez, P. J., & Brown, L. R. (2013). High altitude montane wetland vegetation classification of the Eastern Free State, South Africa. *South African Journal of Botany*, *88*, 223–236. https://doi.org/10.1016/j.sajb.2013.07.011

Brearley, F. Q., Sellan, G., McKendry, D., Sumail, S., & van der Ent, A. (2023). Soil Mercury Along an Elevation Gradient in Northern Borneo. In A. Kallel, M. Barbieri, J. Rodrigo-Comino, H. I. Chaminé, B. Merkel, H. Chenchouni, J. Knight, S. Panda, N. Khélifi, A. C. Benim, S. Grab, H. El-Askary, S. Banerjee, R. Hadji, & M. Eshagh (Eds.), *Selected Studies in Environmental Geosciences and Hydrogeosciences* (pp. 99–102). Springer Nature Switzerland. https://doi.org/10.1007/978-3-031-43803-5_22

Brey, S. J., Ruminski, M., Atwood, S. A., & Fischer, E. V. (2018). Connecting smoke plumes to sources using Hazard Mapping System (HMS) smoke and fire location data over North America. *Atmospheric Chemistry and Physics*, *18*(3), 1745–1761. https://doi.org/10.5194/acp-18-1745-2018

Cache, T., Ramirez, J. A., Molnar, P., Ruiz-Villanueva, V., & Peleg, N. (2023). Increased erosion in a pre-Alpine region contrasts with a future decrease in precipitation and snowmelt. *Geomorphology*, *436*. https://doi.org/10.1016/j.geomorph.2023.108782

Calmels, D., Gaillardet, J., Brenot, A., & France-Lanord, C. (2007). Sustained sulfide oxidation by physical erosion processes in the Mackenzie River basin: Climatic perspectives. *Geology*, *35*(11), 1003–1006. https://doi.org/10.1130/G24132A.1

Campbell, D. H., Clow, D. W., Ingersoll, G. P., Mast, M. A., Spahr, N. E., & Turk, J. T. (1995). Processes Controlling the Chemistry of Two Snowmelt-Dominated Streams in the Rocky Mountains. *Water Resources Research*, *31*(11), 2811–2821. https://doi.org/10.1029/95WR02037

Campbell, J. L., Driscoll, C. T., Jones, J. A., Boose, E. R., Dugan, H. A., Groffman, P. M., Jackson, C. R., Jones, J. B., Juday, G. P., Lottig, N. R., Penaluna, B. E., Ruess, R. W., Suding, K., Thompson, J. R., & Zimmerman, J. K. (2022). Forest and Freshwater Ecosystem Responses to Climate Change and Variability at US LTER Sites. *BioScience*, *72*(9), 851–870. https://doi.org/10.1093/biosci/biab124

Cantzler, J. M., & Huynh, M. (2016). Native American Environmental Justice as Decolonization. *American Behavioral Scientist*, *60*(2), 203–223. https://doi.org/10.1177/0002764215607578

Carling, G. T., Rupper, S. B., Fernandez, D. P., Tingey, D. G., & Harrison, C. B. (2017). Effect of Atmospheric Deposition and Weathering on Trace Element Concentrations in Glacial Meltwater at Grand Teton National Park, Wyoming, U.S.A. *Arctic, Antarctic, and Alpine Research*, *49*(3), 427–440. https://doi.org/10.1657/AAAR0016.071

Cazzolla Gatti, R., Callaghan, T., Velichevskaya, A., Dudko, A., Fabbio, L., Battipaglia, G., & Liang, J. (2019). Accelerating upward treeline shift in the Altai Mountains under last-century climate change. *Scientific Reports*, *9*(1), 7678. https://doi.org/10.1038/s41598-019-44188-1

Chai, L., Zhou, Y., & Wang, X. (2022). Impact of global warming on regional cycling of mercury and persistent organic pollutants on the Tibetan Plateau: Current progress and future prospects. *Environmental Science: Processes and Impacts*, *24*(10), 1616–1630. https://doi.org/10.1039/d1em00550b

Chen, C. Y., Driscoll, C. T., Eagles-Smith, C. A., Eckley, C. S., Gay, D. A., Hsu-Kim, H., Keane, S. E., Kirk, J. L., Mason, R. P., Obrist, D., Selin, H., Selin, N. E., & Thompson, M. R. (2018). A Critical Time for Mercury Science to Inform Global Policy. *Environmental Science and Technology*, *52*(17), 9556–9561. https://doi.org/10.1021/acs.est.8b02286

Chen, Y., Qin, W., Zhang, Q., Wang, X., Feng, J., Han, M., Hou, Y., Zhao, H., Zhang, Z., He, J.-S., Torn, M. S., & Zhu, B. (2024). Whole-soil warming leads to substantial soil carbon emission in an alpine grassland. *Nature Communications*, *15*(1), 4489. https://doi.org/10.1038/s41467-024-48736-w

Chételat, J., Ackerman, J. T., Eagles-Smith, C. A., & Hebert, C. E. (2020). Methylmercury exposure in wildlife: A review of the ecological and physiological processes affecting contaminant concentrations and their interpretation. *Science of the Total Environment*, *711*. https://doi.org/10.1016/j.scitotenv.2019.135117

Chiapella, A. M., Eagles-Smith, C. A., & Strecker, A. L. (2021). From forests to fish: Mercury in mountain lake food webs influenced by factors at multiple scales. *Limnology and Oceanography*, *66*(4), 1021–1035. https://doi.org/10.1002/lno.11659

Chignell, S. M., Laituri, M. J., Young, N. E., & Evangelista, P. H. (2019). Afroalpine Wetlands of the Bale Mountains, Ethiopia: Distribution, Dynamics, and Conceptual Flow Model. *Annals of the American Association of Geographers*, *109*(3), 791–811. https://doi.org/10.1080/24694452.2018.1500439

Clow, D. W. (2010). Changes in the timing of snowmelt and streamflow in Colorado: A response to recent warming. *Journal of Climate*, *23*(9), 2293–2306. https://doi.org/10.1175/2009JCLI2951.1

Cohen, J. S., Asce, S. M., Harrison, ;, Zeff, B., & Herman, J. D. (2020). *Adaptation of Multiobjective Reservoir Operations to Snowpack Decline in the Western United States*. https://doi.org/10.1061/(ASCE)

Coleman Wasik, J. K., Mitchell, C. P. J., Engstrom, D. R., Swain, E. B., Monson, B. A., Balogh, S. J., Jeremiason, J. D., Branfireun, B. A., Eggert, S. L., Kolka, R. K., & Almendinger, J. E. (2012). Methylmercury declines in a boreal peatland when experimental sulfate deposition decreases. *Environmental Science and Technology*, *46*(12), 6663–6671. https://doi.org/10.1021/es300865f

Colorado State Forest Service. (n.d.). *Forest Types*. Retrieved October 5, 2024, from https://csfs.colostate.edu/colorado-forests/forest-types/

Cook, B. A., Peterson, B. D., Ogorek, J. M., Janssen, S. E., & Poulin, B. A. (2024). Simulated Sea Level Rise in Coastal Peat Soils Stimulates Mercury Methylation. *ACS Earth and Space Chemistry*, *8*(9), 1784–1796. https://doi.org/10.1021/acsearthspacechem.4c00124

Cooper, D. J., Chimner, R. A., & Merritt, D. M. (2012). *Western Mountain Wetlands*.

Coppola, E., Raffaele, F., & Giorgi, F. (2018). Impact of climate change on snow melt driven runoff timing over the Alpine region. *Climate Dynamics*, *51*(3), 1259–1273. https://doi.org/10.1007/s00382-016-3331-0

Craig, J. R., & Vokes, F. M. (1993). The metamorphism of pyrite and pyritic ores: An overview. *Mineralogical Magazine*, *57*(386), 3–18. https://doi.org/10.1180/minmag.1993.057.386.02

Crawford, J. T., Hinckley, E. L. S., & Neff, J. C. (2020). Long-Term Trends in Acid Precipitation and Watershed Elemental Export From an Alpine Catchment of the Colorado Rocky Mountains, USA. *Journal of Geophysical Research: Biogeosciences*, *125*(11). https://doi.org/10.1029/2020JG005683

Crawford, J. T., Hinckley, E.-L. S., Litaor, M. I., Brahney, J., & Neff, J. C. (2019). Evidence for accelerated weathering and sulfate export in high alpine environments. *Environmental Research Letters*, *14*(12), 124092. https://doi.org/10.1088/1748-9326/ab5d9c

Cristol, D. A., Brasso, R. L., Condon, A. M., Fovargue, R. E., Friedman, S. L., Hallinger, K. K., Monroe, A. P., & White, A. E. (2008). The movement of aquatic mercury through terrestrial food webs. *Science*, *320*(5874), 335. https://doi.org/10.1126/science.1154082

Dahl, T. E. (2011). *Status and Trends of Wetlands in the Conterminous United States 2004 to 2009*. US Department of the Interior, US Fish and Wildlife Services, Fisheries and Habitat Conservation.

Dai, M. Q., Geyman, B. M., Hu, X. C., Thackray, C. P., & Sunderland, E. M. (2023). Sociodemographic Disparities in Mercury Exposure from United States Coal-Fired Power Plants. *Environmental Science & Technology Letters*. https://doi.org/10.1021/acs.estlett.3c00216

D'Alò, F., Odriozola, I., Baldrian, P., Zucconi, L., Ripa, C., Cannone, N., Malfasi, F., Brancaleoni, L., & Onofri, S. (2021). Microbial activity in alpine soils under climate change. *Science of The Total Environment*, *783*, 147012. https://doi.org/10.1016/j.scitotenv.2021.147012

Dangles, O., Rabatel, A., Kraemer, M., Zeballos, G., Soruco, A., Jacobsen, D., & Anthelme, F. (2017). Ecosystem sentinels for climate change? Evidence of wetland cover changes over the last 30 years in the tropical Andes. *PLoS ONE*, *12*(5). https://doi.org/10.1371/journal.pone.0175814

Darmody, R. G., Thorn, C. E., & Dixon, J. C. (2007). Pyrite-enhanced chemical weathering in Kärkevagge, Swedish Lapland. *Bulletin of the Geological Society of America*, *119*(11–12), 1477–1485. https://doi.org/10.1130/B26228.1

Dastoor, A., Angot, H., Bieser, J., Christensen, J. H., Douglas, T. A., Heimbürger-Boavida, L.-E., Jiskra, M., Mason, R. P., McLagan, D. S., Obrist, D., Outridge, P. M., Petrova, M. V., Ryjkov, A., St. Pierre, K. A., Schartup, A. T., Soerensen, A. L., Toyota, K., Travnikov, O., Wilson, S. J., & Zdanowicz, C. (2022). Arctic mercury cycling. *Nature Reviews Earth & Environment*, *3*(4), 270–286. https://doi.org/10.1038/s43017-022-00269-w

Day, N. K., Schmidt, T. S., Roberts, J. J., Osmundson, B. C., Willacker, J. J., & Eagles-Smith, C. A. (2020). Mercury and selenium concentrations in fishes of the Upper Colorado River Basin, southwestern United States: A retrospective assessment. *PLoS ONE*, *15*(1). https://doi.org/10.1371/journal.pone.0226824

Demers, J. D., Driscoll, C. T., Fahey, T. J., & Yavitt, J. B. (2007). Mercury cycling in litter and soil in different forest types in the Adirondack region, New York, USA. *Ecological Applications*, *17*(5), 1341–1351. https://doi.org/10.1890/06-1697.1

DiMiceli, C., Sohlberg, R., & Townshend, J. (2022). *MODIS/Terra Vegetation Continuous Fields Yearly L3 Global 250m SIN Grid V061* [Dataset]. NASA EOSDIS Land Processes Distributed Active Archive Center. https://doi.org/10.5067/MODIS/MOD44B.061

DiMiceli, C., Townshend, J., Carroll, M., & Sohlberg, R. (2021). Evolution of the representation of global vegetation by vegetation continuous fields. *Remote Sensing of Environment*, *254*, 112271. https://doi.org/10.1016/j.rse.2020.112271

Dohnal, M., Černý, T., Votrubová, J., & Tesař, M. (2014). Rainfall interception and spatial variability of throughfall in spruce stand. *Journal of Hydrology and Hydromechanics*, *62*(4), 277–284. https://doi.org/10.2478/johh-2014-0037

Domagalski, J., Majewski, M. S., Alpers, C. N., Eckley, C. S., Eagles-Smith, C. A., Schenk, L., & Wherry, S. (2016). Comparison of mercury mass loading in streams to atmospheric deposition in watersheds of Western North America: Evidence for non-atmospheric mercury sources. *Science of the Total Environment*, *568*, 638–650. https://doi.org/10.1016/j.scitotenv.2016.02.112

Dong, Z., Driscoll, C. T., Campbell, J. L., Pourmokhtarian, A., Stoner, A. M. K., & Hayhoe, K. (2019). Projections of water, carbon, and nitrogen dynamics under future climate change in an alpine tundra ecosystem in the southern Rocky Mountains using a biogeochemical model. *Science of the Total Environment*, *650*, 1451–1464. https://doi.org/10.1016/j.scitotenv.2018.09.151

Donovan, V. M., Wonkka, C. L., & Twidwell, D. (2017). Surging wildfire activity in a grassland biome. *Geophysical Research Letters*, *44*(12), 5986–5993. https://doi.org/10.1002/2017GL072901

Drenner, R. W., Chumchal, M. M., Jones, C. M., Lehmann, C. M. B., Gay, D. A., & Donato, D. I. (2013). Effects of Mercury Deposition and Coniferous Forests on the Mercury Contamination of Fish in the South Central United States. *Environmental Science & Technology*, *47*(3), 1274–1279. https://doi.org/10.1021/es303734n

Driscoll, C. T., Han, Y.-J., Chen, C. Y., Evers, D. C., Lambert, K. F., Holsen, T. M., Kamman, N. C., & Munson, R. K. (2007). Mercury Contamination in Forest and Freshwater Ecosystems in the Northeastern United States. *BioScience*, *57*(1), 17–28. https://doi.org/10.1641/b570106

Driscoll, C. T., Mason, R. P., Chan, H. M., Jacob, D. J., & Pirrone, N. (2013). Mercury as a Global Pollutant: Sources, Pathways, and Effect. *Environmental Science and Technology*, *47*, 4967–4983. https://doi.org/10.1021/es305071v

Duncan, F. T., Jacob, D. J., & Park, R. J. (2007). The impact of transpacific transport of mineral dust in the United States. *Atmospheric Environment*, *41*(6), 1251–1266. https://doi.org/10.1016/j.atmosenv.2006.09.048

Duniway, M. C., Pfennigwerth, A. A., Fick, S. E., Nauman, T. W., Belnap, J., & Barger, N. N. (2019). Wind erosion and dust from US drylands: A review of causes, consequences, and solutions in a changing world. *Ecosphere*, *10*(3). https://doi.org/10.1002/ecs2.2650

Eagles-Smith, C. A., Ackerman, J. T., Willacker, J. J., Tate, M. T., Lutz, M. A., Fleck, J. A., Stewart, A. R., Wiener, J. G., Evers, D. C., Lepak, J. M., Davis, J. A., & Pritz, C. F. (2016). Spatial and temporal patterns of mercury concentrations in freshwater fish across the Western United States and Canada. *Science of the Total Environment*, *568*, 1171–1184. https://doi.org/10.1016/j.scitotenv.2016.03.229

Eagles-Smith, C. A., Wiener, J. G., Eckley, C. S., Willacker, J. J., Evers, D. C., Marvin-DiPasquale, M., Obrist, D., Fleck, J. A., Aiken, G. R., Lepak, J. M., Jackson, A. K., Webster, J. P., Stewart, A. R., Davis, J. A., Alpers, C. N., & Ackerman, J. T. (2016). Mercury in western North America: A synthesis of environmental contamination, fluxes, bioaccumulation, and risk to fish and wildlife. *Science of the Total Environment*, *568*(October 2016), 1213–1226. https://doi.org/10.1016/j.scitotenv.2016.05.094

Eagles-Smith, C. A., Willacker, J. J., Nelson, S. J., Flanagan Pritz, C. M., Krabbenhoft, D. P., Chen, C. Y., Ackerman, J. T., Campbell Grant, E. H., & Pilliod, D. S. (2020). A national-scale assessment of mercury bioaccumulation in United States national parks using dragonfly larvae as biosentinels through a citizen-science framework. *Environmental Science and Technology*, *54*(14), 8779–8790. https://doi.org/10.1021/acs.est.0c01255

Eckley, C. S., Luxton, T. P., Goetz, J., & McKernan, J. (2017). Water-level fluctuations influence sediment porewater chemistry and methylmercury production in a flood-control reservoir. *Environmental Pollution*, *222*, 32–41. https://doi.org/10.1016/j.envpol.2017.01.010

Eckley, C. S., Tate, M. T., Lin, C. J., Gustin, M., Dent, S., Eagles-Smith, C., Lutz, M. A., Wickland, K. P., Wang, B., Gray, J. E., Edwards, G. C., Krabbenhoft, D. P., & Smith, D. B. (2016). Surface-air mercury fluxes across Western North America: A synthesis of spatial trends and controlling variables. *Science of the Total Environment*, *568*, 651–665. https://doi.org/10.1016/j.scitotenv.2016.02.121

Ekino, S., Susa, M., Ninomiya, T., Imamura, K., & Kitamura, T. (2007). Minamata disease revisited: An update on the acute and chronic manifestations of methyl mercury poisoning. *Journal of the Neurological Sciences*, *262*(1–2), 131–144. https://doi.org/10.1016/j.jns.2007.06.036

Everett, K. R. (2014). Mercury and air toxics standards. *Environmental Policy on Ballotpedia*.

Fahnestock, M. F., Bryce, J. G., McCalley, C. K., Montesdeoca, M., Bai, S., Li, Y., Driscoll, C. T., Crill, P. M., Rich, V. I., & Varner, R. K. (2019). Mercury reallocation in thawing subarctic peatlands. *Geochemical Perspectives Letters*, 33–38. https://doi.org/10.7185/geochemlet.1922

Faïn, X., Helmig, D., Hueber, J., Obrist, D., & Williams, M. W. (2013). Mercury dynamics in the Rocky Mountain, Colorado, snowpack. *Biogeosciences*, *10*(6), 3793–3807. https://doi.org/10.5194/bg-10-3793-2013

Fisher, L. S., & Wolfe, M. H. (2012). Examination of mercury inputs by throughfall and litterfall in the Great Smoky Mountains National Park. *Atmospheric Environment*, *47*, 554–559. https://doi.org/10.1016/j.atmosenv.2011.10.017

Fleck, J. A., Marvin-DiPasquale, M., Eagles-Smith, C. A., Ackerman, J. T., Lutz, M. A., Tate, M., Alpers, C. N., Hall, B. D., Krabbenhoft, D. P., & Eckley, C. S. (2016). Mercury and methylmercury in aquatic sediment across western North America. *Science of the Total Environment*, *568*, 727–738. https://doi.org/10.1016/j.scitotenv.2016.03.044

Flocke, F., Pfister, G., Crawford, J. H., Pickering, K. E., Pierce, G., Bon, D., & Reddy, P. (2020). Air Quality in the Northern Colorado Front Range Metro Area: The Front Range Air Pollution and Photochemistry Éxperiment (FRAPPÉ). *Journal of Geophysical Research: Atmospheres*, *125*(2), e2019JD031197. https://doi.org/10.1029/2019JD031197

French, B. J., Hope, G. S., Pryor, L. D., & Bowman, D. M. J. S. (2016). The vulnerability of peatlands in the Australian Alps. *Australasian Plant Conservation: Journal of the Australian Network for Plant Conservation*, *24*(4), 16–18. https://doi.org/10.5962/p.373646

Fu, X., Marusczak, N., Wang, X., Gheusi, F., & Sonke, J. E. (2016). Isotopic Composition of Gaseous Elemental Mercury in the Free Troposphere of the Pic du Midi Observatory, France. *Environmental Science & Technology*, *50*(11), 5641–5650. https://doi.org/10.1021/acs.est.6b00033

Fu, X. W., Feng, X., Dong, Z. Q., Yin, R. S., Wang, J. X., Yang, Z. R., & Zhang, H. (2010). Atmospheric gaseous elemental mercury (GEM) concentrations and mercury depositions at a high-altitude mountain peak in south China. *Atmospheric Chemistry and Physics*, *10*(5), 2425–2437. https://doi.org/10.5194/acp-10-2425-2010

Gerson, J. R., Driscoll, C. T., Demers, J. D., Sauer, A. K., Blackwell, B. D., Montesdeoca, M. R., Shanley, J. B., & Ross, D. S. (2017). Deposition of mercury in forests across a montane elevation gradient: Elevational and

seasonal patterns in methylmercury inputs and production. *Journal of Geophysical Research: Biogeosciences*, *122*, 131–144. https://doi.org/10.1002/2016JG003721.Received

Gilmour, C. C., & Henry, E. A. (1991). Mercury methylation in aquatic systems affected by acid deposition. *Environmental Pollution*, *71*(2), 131–169. https://doi.org/10.1016/0269-7491(91)90031-Q

Gilmour, C. C., Henry, E. A., & Ralph, M. (1992). Sulfate Stimulation of Mercury Methylation in Freshwater Sediments. *Environmental Science and Technology*, *26*(11), 2281–2287. https://doi.org/10.1021/es00035a029

Goudie, A. (2018). *Dust storms and ephemeral lakes*. http://desert.ut.ac.ir

Greenland, D., & Losleben, M. (2001). *Ch. 2 climate in structure and function of an alpine ecosystem*. (W. D. Bowman & W. D. Seastedt, Eds.). Oxford University Press.

Grigal, D. F. (2003). Mercury Sequestration in Forests and Peatlands. *Journal of Environmental Quality*, *32*(2), 393–405. https://doi.org/10.2134/jeq2003.3930

Gu, J., Pang, Q., Ding, J., Yin, R., Yang, Y., & Zhang, Y. (2020). The driving factors of mercury storage in the Tibetan grassland soils underlain by permafrost. *Environmental Pollution*, *265*, 115079. https://doi.org/10.1016/j.envpol.2020.115079

Gustin, M. S., Amos, H. M., Huang, J., Miller, M. B., & Heidecorn, K. (2015). Measuring and modeling mercury in the atmosphere: A critical review. *Atmospheric Chemistry and Physics*, *15*(10), 5697–5713. https://doi.org/10.5194/acp-15-5697-2015

Halofsky, J. E., & Peterson, D. L. (2018). *Climate Change and Rocky Mountain Ecosystems*. http://www.springer.com/series/5588

Han, J., Dai, H., & Gu, Z. (2021). Sandstorms and desertification in Mongolia, an example of future climate events: A review. *Environmental Chemistry Letters*, *19*(6), 4063–4073. https://doi.org/10.1007/s10311-021-01285-w

Hannoun, D., & Tietjen, T. (2022). Lake management under severe drought: Lake Mead, Nevada/Arizona. *Journal of the American Water Resources Association*. https://doi.org/10.1111/1752-1688.13090

He, M., Tian, L., Braaten, H. F. V., Wu, Q., Luo, J., Cai, L. M., Meng, J. H., & Lin, Y. (2019). Mercury–Organic Matter Interactions in Soils and Sediments: Angel or Devil? *Bulletin of Environmental Contamination and Toxicology*, *102*(5), 621–627. https://doi.org/10.1007/s00128-018-2523-1

Heil, E., Warix, S., Singha, K., & Navarre-Sitchler, A. (2022). Decadal trends in solute concentrations, mass flux, and discharge reveal variable hydrologic and geochemical response to climate change in two alpine watersheds. *Applied Geochemistry*, *144*, 105402. https://doi.org/10.1016/j.apgeochem.2022.105402

Heindel, R. C., Putman, A. L., Murphy, S. F., Repert, D. A., & Hinckley, E. L. S. (2020). Atmospheric Dust Deposition Varies by Season and Elevation in the Colorado Front Range, USA. *Journal of Geophysical Research: Earth Surface*, *125*(5). https://doi.org/10.1029/2019JF005436

Heiri, O., Lotter, A. F., & Lemcke, G. (2001). Loss on ignition as a method for estimating organic and carbonate content in sediments: Reproducibility and comparability of results. In *Journal of Paleolimnology* (Vol. 25, pp. 101–110).

Helmrich, S., Vlassopoulos, D., Alpers, C. N., & O'Day, P. A. (2022). Critical review of mercury methylation and methylmercury demethylation rate constants in aquatic sediments for biogeochemical modeling. *Critical Reviews in*

Environmental Science and Technology, *52*(24), 4353–4378. https://doi.org/10.1080/10643389.2021.2013073

Hermes, A. L., Wainwright, H. M., Wigmore, O., Falco, N., Molotch, N. P., & Hinckley, E. L. S. (2020). From Patch to Catchment: A Statistical Framework to Identify and Map Soil Moisture Patterns Across Complex Alpine Terrain. *Frontiers in Water*, *2*. https://doi.org/10.3389/frwa.2020.578602

Hintelmann, H., Douglas Evans, R., & Y. Villeneuve, J. (1995). Measurement of mercury methylation in sediments by using enriched stable mercury isotopes combined with methylmercury determination by gas chromatography–inductively coupled plasma mass spectrometry. *Journal of Analytical Atomic Spectrometry*, *10*(9), 619–624. https://doi.org/10.1039/JA9951000619

Hintelmann, H., & Evans, R. D. (1997). Application of stable isotopes in environmental tracer studies—Measurement of monomethylmercury (CH 3 Hg +) by isotope dilution ICP-MS and detection of species transformation. *Fresenius' Journal of Analytical Chemistry*, *358*(3), 378–385. https://doi.org/10.1007/s002160050433

Hock, R., & Rasul, G. (2019). High Mountain Areas. In *Bert Wouters*. Elizabeth Jimenez Zamora.

Hock, R., Rasul, G., Adler, C., Caceres, B., Gruber, S., Hirabayashi, Y., Jackson, M., Kääb, A., Kang, S., Kutuzov, S., Milner, A., Molau, U., Morin, S., Orlove, B., Steltzer, H., Allen, S., Arenson, L., Baneerjee, S., Barr, I., … Zhang, Y. (2019). High Mountain Areas. In *IPCC special report on the ocean and cryosphere in a changing climate* (pp. 131–202). STATI UNITI D'AMERICA. https://iris.unito.it/handle/2318/1803038

Hoffmann, U., Hoffmann, T., Johnson, E. A., & Kuhn, N. J. (2014). Assessment of variability and uncertainty of soil organic carbon in a mountainous boreal

forest (Canadian Rocky Mountains, Alberta). *Catena*, *113*, 107–121. https://doi.org/10.1016/j.catena.2013.09.009

Homann, P. S., Darbyshire, R. L., Bormann, B. T., & Morrissette, B. A. (2015). Forest Structure Affects Soil Mercury Losses in the Presence and Absence of Wildfire. *Environmental Science and Technology*, *49*(21), 12714–12722. https://doi.org/10.1021/acs.est.5b03355

Hornbrook, R., Orlando, J., & Lee, S. (2017). *Process-Based and Regional Source Impact Analysis for FRAPPÉ and DISCOVER-AQ 2014*.

Houde, M., Krümmel, E. M., Mustonen, T., Brammer, J., Brown, T. M., Chételat, J., Dahl, P. E., Dietz, R., Evans, M., Gamberg, M., Gauthier, M. J., Gérin-Lajoie, J., Hauptmann, A. L., Heath, J. P., Henri, D. A., Kirk, J., Laird, B., Lemire, M., Lennert, A. E., … Whiting, A. (2022). Contributions and perspectives of Indigenous Peoples to the study of mercury in the Arctic. *Science of the Total Environment*, *841*. https://doi.org/10.1016/j.scitotenv.2022.156566

Hu, J., Moore, D. J. P., Burns, S. P., & Monson, R. (2010). Longer growing seasons lead to less carbon sequestration by a subalpine forest. *Global Change Biology*, *16*(2), 771–783. https://doi.org/10.1111/j.1365-2486.2009.01967.x

Huang, J., & Gustin, M. S. (2015). Use of passive sampling methods and models to understand sources of mercury deposition to high elevation sites in the Western United States. *Environmental Science and Technology*, *49*(1), 432–441. https://doi.org/10.1021/es502836w

Huang, J., Kang, S., Yin, R., Ram, K., Liu, X., Lu, H., Guo, J., Chen, S., & Tripathee, L. (2020). Desert dust as a significant carrier of atmospheric mercury. *Environmental Pollution*, *267*. https://doi.org/10.1016/j.envpol.2020.115442

Huang, J., Kang, S., Zhang, Q., Yan, H., Guo, J., Jenkins, M. G., Zhang, G., & Wang, K. (2012). Wet deposition of mercury at a remote site in the Tibetan Plateau: Concentrations, speciation, and fluxes. *Atmospheric Environment*, *62*, 540–550. https://doi.org/10.1016/j.atmosenv.2012.09.003

Huber, M. E. (2021). *Patterns of Sulfur and Carbon Biogeochemistry in Alpine Wetlands of Niwot Ridge, Colorado (Master's thesis, University of Colorado Boulder)* [Dissertation]. https://www.proquest.com/docview/2634589406?pq-origsite=gscholar&fromopenview=true&sourcetype=Dissertations%20&%20Theses

Iqbal, A., & Shang, Z. (2020). Wetlands as a Carbon Sink: Insight into the Himalayan Region. In Z. Shang, A. A. Degen, M. K. Rafiq, & V. R. Squires (Eds.), *Carbon Management for Promoting Local Livelihood in the Hindu Kush Himalayan (HKH) Region* (pp. 125–144). Springer International Publishing. https://doi.org/10.1007/978-3-030-20591-1_7

Jackson, A., Evers, D. C., Eagles-Smith, C. A., Ackerman, J. T., Willacker, J. J., Elliott, J. E., Lepak, J. M., Vander Pol, S. S., & Bryan, C. E. (2016). Mercury risk to avian piscivores across western United States and Canada. *Science of the Total Environment*, *568*, 685–696. https://doi.org/10.1016/j.scitotenv.2016.02.197

Jane, S. F., Hansen, G. J. A., Kraemer, B. M., Leavitt, P. R., Mincer, J. L., North, R. L., Pilla, R. M., Stetler, J. T., Williamson, C. E., Woolway, R. I., Arvola, L., Chandra, S., DeGasperi, C. L., Diemer, L., Dunalska, J., Erina, O., Flaim, G., Grossart, H. P., Hambright, K. D., … Rose, K. C. (2021). Widespread deoxygenation of temperate lakes. *Nature*, *594*(7861), 66–70. https://doi.org/10.1038/s41586-021-03550-y

Janssen, S. E., Kotalik, C. J., Eagles-Smith, C. A., Beaubien, G. B., Hoffman, J. C., Peterson, G., Mills, M. A., & Walters, D. M. (2023). Mercury Isotope Values in Shoreline Spiders Reveal the Transfer of Aquatic Mercury Sources to Terrestrial Food Webs. *Environmental Science & Technology Letters*. https://doi.org/10.1021/acs.estlett.3c00450

Janssen, S. E., Kotalik, C. J., Willacker, J. J., Tate, M. T., Pritz, C. M. F., Nelson, S. J., Krabbenhoft, D. P., Walters, D. M., & Eagles-Smith, C. A. (2024). Geographic Drivers of Mercury Entry into Aquatic Food Webs Revealed by Mercury Stable Isotopes in Dragonfly Larvae. *Environmental Science & Technology*, *58*(30), 13444–13455. https://doi.org/10.1021/acs.est.4c02436

Janssen, S. E., Tate, M. T., Dantoin, E. D., Filstrup, C. T., Reavie, E. D., Stewart, R. M., Robinson, C., Allan, C. J., Robertson, D. M., & Krabbenhoft, D. P. (2025). Connecting tributary mercury loads to nearshore and offshore sediments in Lake Superior. *Journal of Great Lakes Research*, *51*(1), 102381. https://doi.org/10.1016/j.jglr.2024.102381

Janssen, S. E., Tate, M. T., Poulin, B. A., Krabbenhoft, D. P., DeWild, J. F., Ogorek, J. M., Varonka, M. S., Orem, W. H., & Kline, J. L. (2022). Decadal trends of mercury cycling and bioaccumulation within Everglades National Park. *Science of the Total Environment*, *838*. https://doi.org/10.1016/j.scitotenv.2022.156031

Jeremiason, J. D., Engstrom, D. R., Swain, E. B., Nater, E. A., Johnson, B. M., Almendinger, J. E., Monson, B. A., & Kolka, R. K. (2006). Sulfate addition increases methylmercury production in an experimental wetland. *Environmental Science and Technology*, *40*(12), 3800–3806. https://doi.org/10.1021/es0524144

Jiskra, M., Wiederhold, J. G., Skyllberg, U., Kronberg, R. M., Hajdas, I., & Kretzschmar, R. (2015). Mercury Deposition and Re-emission Pathways in Boreal Forest Soils Investigated with Hg Isotope Signatures. *Environmental Science and Technology*, *49*(12), 7188–7196. https://doi.org/10.1021/acs.est.5b00742

Khan, A., Said, A., & Ullah, I. (2020). Landsat based distribution mapping of high-altitude peatlands in Hindu Kush Himalayas—A case study of Broghil Valley, Pakistan. *Journal of Mountain Science*, *17*(1), 42–49. https://doi.org/10.1007/s11629-019-5384-0

Kittel, T. G. F., Williams, M. W., Chowanski, K., Hartman, M., Ackerman, T., Losleben, M., & Blanken, P. D. (2015). Contrasting long-term alpine and subalpine precipitation trends in a mid-latitude North American mountain system, Colorado Front Range, USA. *Plant Ecology and Diversity*, *8*(5–6), 607–624. https://doi.org/10.1080/17550874.2016.1143536

Krabbenhoft, D., Olson, M., Dewild, J., Clow, D., Striegl, R., Dornblaser, M., & VanMetre, P. (2002). Mercury Loading and Methylmercury Production and Cycling in High-Altitude Lakes from the Western United States. *Water, Air and Soil Pollution: Focus*, *2*(2), 233–249. https://doi.org/10.1023/A:1020162811104

Krabbenhoft, D. P., & Sunderland, E. M. (2013). Global Change and Mercury. *Science*, *341*(6153), 1457–1458. https://doi.org/10.1126/science.1242838

Ku, P., Tsui, M. T. K., Nie, X., Chen, H., Hoang, T. C., Blum, J. D., Dahlgren, R. A., & Chow, A. T. (2018). Origin, Reactivity, and Bioavailability of Mercury in Wildfire Ash. *Environmental Science and Technology*, *52*(24), 14149–14157. https://doi.org/10.1021/acs.est.8b03729

Kumar, A., & Wu, S. (2019). Mercury Pollution in the Arctic from Wildfires: Source Attribution for the 2000s. *Environmental Science and Technology*. https://doi.org/10.1021/acs.est.9b01773

Kumar, A., Wu, S., Huang, Y., Liao, H., & Kaplan, J. O. (2018). Mercury from wildfires: Global emission inventories and sensitivity to 2000–2050 global change. *Atmospheric Environment*, *173*(October 2017), 6–15. https://doi.org/10.1016/j.atmosenv.2017.10.061

Landis, J. D., Obrist, D., Zhou, J., Renshaw, C. E., McDowell, W. H., Nytch, C. J., Palucis, M. C., Del Vecchio, J., Montano Lopez, F., & Taylor, V. F. (2024). Quantifying soil accumulation of atmospheric mercury using fallout radionuclide chronometry. *Nature Communications*, *15*(1), 5430. https://doi.org/10.1038/s41467-024-49789-7

Larson, R. P., Byrne, J. M., Johnson, D. L., Kienzle, S. W., & Letts, M. G. (2011). Modelling climate change impacts on Spring Runoff for the Rocky Mountains of Montana and Alberta II: Runoff change projections using future scenarios. *Canadian Water Resources Journal*, *36*(1), 35–52. https://doi.org/10.4296/cwrj3601035

Lawson, S. T., Scherbatskoy, T. D., Malcolm, E. G., & Keeler, G. J. (2003). Cloud water and throughfall deposition of mercury and trace elements in a high elevation spruce–fir forest at Mt. Mansfield, Vermont. *J. Environ. Monit.*, *5*(4), 578–583. https://doi.org/10.1039/B210125D

Lee, L. Y., Kerry, R., Ingram, B., Golden, C. S., & LeMonte, J. J. (2024). Investigating the Spatial Patterns of Heavy Metals in Topsoil and Asthma in the Western Salt Lake Valley, Utah. *Environments*, *11*(10), 223.

Lehner, B., Reidy Liermann, C., Revenga, C., Vorosmarty, C., Fekete, B., Crouzet, P., Doll, P., Endejan, M., Frenken, K., Magome, J., Nilsson, C., Robertson, J.

C., Rodel, R., Sindorf, N., & Wisser, D. (2011). Global Reservoir and Dam Database, Version 1 (GRanDv1): Reservoirs, Revision 01. *Global Water System Project*.

Li, F., Ma, C., & Zhang, P. (2020). Mercury Deposition, Climate Change and Anthropogenic Activities: A Review. *Frontiers in Earth Science*, *8*. https://doi.org/10.3389/feart.2020.00316

Li, X., Wang, X., Yuan, W., Lu, Z., & Wang, D. (2022). Increase of litterfall mercury input and sequestration during decomposition with a montane elevation in Southwest China. *Environmental Pollution*, *292*. https://doi.org/10.1016/j.envpol.2021.118449

Lin, C. J., Shetty, S. K., Pan, L., Pongprueksa, P., Jang, C., & Chu, H. W. (2012). Source attribution for mercury deposition in the contiguous United States: Regional difference and seasonal variation. *Journal of the Air and Waste Management Association*, *62*(1), 52–63. https://doi.org/10.1080/10473289.2011.622066

Lindberg, S. E., & Stratton, W. J. (1998). Atmospheric Mercury Speciation: Concentrations and Behavior of Reactive Gaseous Mercury in Ambient Air. *Environmental Science & Technology*, *32*(1), 49–57. https://doi.org/10.1021/es970546u

Littell, J. S., Peterson, D. L., & Tjoelker, M. (2008). Douglas-Fir Growth in Mountain Ecosystems: Water Limits Tree Growth from Stand to Region. *Ecological Monographs*, *78*(3), 349–368. https://doi.org/10.1890/07-0712.1

LøNne, I. (2008). Faint traces of high Arctic glaciations: An early Holocene ice-front fluctuation in Bolterdalen, Svalbard. *Boreas*, *34*(3), 308–323. https://doi.org/10.1111/j.1502-3885.2005.tb01103.x

Lovett, G. M., & Kinsman, J. D. (1990). Atmospheric pollutant deposition to high-elevation ecosystems. *Atmospheric Environment Part A, General Topics*, *24*(11), 2767–2786. https://doi.org/10.1016/0960-1686(90)90164-I

Lyman, S. N., Cheng, I., Gratz, L. E., Weiss-Penzias, P., & Zhang, L. (2020). An updated review of atmospheric mercury. *Science of The Total Environment*, *707*, 135575. https://doi.org/10.1016/j.scitotenv.2019.135575

Ma, H., Cheng, H., Guo, F., Zhang, L., Tang, S., Yang, Z., & Peng, M. (2022). Distribution of mercury in foliage, litter and soil profiles in forests of the Qinling Mountains, China. *Environmental Research*, *211*, 113017. https://doi.org/10.1016/j.envres.2022.113017

Ma, Y., Chen, S., Shang, L., Zhang, W., Yan, Y., Huang, Z., Hu, Y., Liang, J., Ji, S., Zhao, Z., Zhou, Z., & Hu, H. (2023). Small mammals as a bioindicator of mercury in a biodiversity hotspot – The Hengduan Mountains, China. *Ecological Indicators*, *154*. https://doi.org/10.1016/j.ecolind.2023.110892

Ma, Y., Shang, L., Hu, H., Zhang, W., Chen, L., Zhou, Z., Singh, P. B., & Hu, Y. (2021). Mercury distribution in the East Himalayas: Elevational patterns in soils and non-volant small mammals. *Environmental Pollution*, *288*, 117752. https://doi.org/10.1016/j.envpol.2021.117752

Manning, A. H., Verplanck, P. L., Caine, J. S., & Todd, A. S. (2013). Links between climate change, water-table depth, and water chemistry in a mineralized mountain watershed. *Applied Geochemistry*, *37*, 64–78. https://doi.org/10.1016/j.apgeochem.2013.07.002

Marchese, M. J., Gerson, J. R., Berky, A. J., Driscoll, C., Fernandez, L. E., Hsu-Kim, H., Lansdale, K. N., Letourneau, E., Montesdeoca, M., Pan, W. K., Robie, E., Vega, C., & Bernhardt, E. S. (2024). Diet choices determine mercury exposure

risks for people living in gold mining regions of Peru. *Environmental Research: Health*, *2*(3), 035001. https://doi.org/10.1088/2752-5309/ad3d79

Mason, G. T., Arndt, R. E., & The Survey. (1996). Mineral Resources Data System (MRDS). In *Data Series*. https://doi.org/10.3133/ds20

Mast, M. A., Campbell, D. H., Krabbenhoft, D. P., & Taylor, H. E. (2005). Mercury transport in a high-elevation watershed in Rocky Mountain National Park, Colorado. *Water, Air, and Soil Pollution*, *164*(1–4), 21–42. https://doi.org/10.1007/s11270-005-1657-z

Mast, M. A., Drever, J. I., & Baron, J. (1990). Chemical Weathering in the Loch Vale Watershed, Rocky Mountain National Park, Colorado. *Water Resources Research*, *26*(12), 2971–2978. https://doi.org/10.1029/WR026i012p02971

Mast, M. A., Manthorne, D. J., & Roth, D. A. (2010). Historical deposition of mercury and selected trace elements to high-elevation National Parks in the Western U.S. inferred from lake-sediment cores. *Atmospheric Environment*, *44*(21–22), 2577–2586. https://doi.org/10.1016/j.atmosenv.2010.04.024

McCabe, G. J., & Wolock, D. M. (2010). Long-term variability in Northern Hemisphere snow cover and associations with warmer winters. *Climatic Change*, *99*(1), 141–153. https://doi.org/10.1007/s10584-009-9675-2

McGuire, C. R., Nufio, C. R., Bowers, M. D., & Guralnick, R. P. (2012). Elevation-Dependent Temperature Trends in the Rocky Mountain Front Range: Changes over a 56- and 20-Year Record. *PLoS ONE*, *7*(9). https://doi.org/10.1371/journal.pone.0044370

McLagan, D. S., Stupple, G. W., Darlington, A., Hayden, K., & Steffen, A. (2021). Where there is smoke there is mercury: Assessing boreal forest fire mercury emissions using aircraft and highlighting uncertainties associated with

upscaling emissions estimates. *Atmospheric Chemistry and Physics*, *21*(7), 5635–5653. https://doi.org/10.5194/acp-21-5635-2021

Miller, C. (2021). *Saving a Sacred Lake: A Century of Pollution Haunts the Haudenosaunee*. NMAI Magazine. https://www.americanindianmagazine.org/story/saving-a-sacred-lake

Miller, H. R., Driscoll, C. T., & Hinckley, E.-L. S. (2023). Mercury cycling in the U.S. Rocky Mountains: A review of past research and future priorities. *Biogeochemistry*. https://doi.org/10.1007/s10533-023-01108-w

Mu, C., Schuster, Paul. F., Abbott, Benjamin. W., Kang, S., Guo, J., Sun, S., Wu, Q., & Zhang, T. (2020). Permafrost degradation enhances the risk of mercury release on Qinghai-Tibetan Plateau. *Science of The Total Environment*, *708*, 135127. https://doi.org/10.1016/j.scitotenv.2019.135127

Murphy, R., & Strongin, D. R. (2009). Surface reactivity of pyrite and related sulfides. *Surface Science Reports*, *64*(1), 1–45. https://doi.org/10.1016/j.surfrep.2008.09.002

Murphy, S. F., Verplanck, P. L., & Barber, L. B. (2003). *Comprehensive water quality of the Boulder Creek Watershed, Colorado, during high-flow and low-flow conditions, 2000*. https://doi.org/10.3133/wri034045

Murphy, S. F., Writer, J. H., McCleskey, R. B., & Martin, D. A. (2015). The role of precipitation type, intensity, and spatial distribution in source water quality after wildfire. *Environmental Research Letters*, *10*(8), 084007. https://doi.org/10.1088/1748-9326/10/8/084007

Musselman, K. N., Lehner, F., Ikeda, K., Clark, M. P., Prein, A. F., Liu, C., Barlage, M., & Rasmussen, R. (2018). Projected increases and shifts in rain-on-snow flood risk over western North America. *Nature Climate Change*, *8*(9), 808–812. https://doi.org/10.1038/s41558-018-0236-4

NADP. (2025). *National Atmospheric Deposition Program Monitoring Network*. https://nadp.slh.wisc.edu/

NatureServe Explorer. (n.d.). *Southern Rocky Mountain Dry-Mesic Montane Mixed Conifer Forest and Woodland*. Retrieved October 5, 2024, from https://explorer.natureserve.org/Taxon/ELEMENT_GLOBAL.2.722850/Southern_Rocky_Mountain_Dry-Mesic_Montane_Mixed_Conifer_Forest_and_Woodland

NEON. (n.d.). *Como Creek NEON | NSF NEON | Open Data to Understand our Ecosystems*. Retrieved December 24, 2024, from https://www.neonscience.org/field-sites/como

NEON. (2025). *Litterfall and fine woody debris production and chemistry (DP1.10033.001): RELEASE-2025* (Version RELEASE-2025, p. 444.1 MB) [Csv]. National Ecological Observatory Network (NEON). https://doi.org/10.48443/11HX-C586

NOAA Physical Sciences Laboratory. (2024). *Boulder Colorado monthly precipitation 1893-present*. Boulder Monthly Climate Data: Precipitation. https://psl.noaa.gov/boulder/Boulder.mm.precip.html

Obrist, D., Pearson, C., Webster, J., Kane, T., Lin, C.-J., Aiken, G. R., & Alpers, C. N. (2016). Terrestrial mercury in the Western United States: Spatial distribution defined by land cover and plant productivity. *Science of the Total Environment*, *568*(775), 522–535.

Olson, C. I., Fakhraei, H., & Driscoll, C. T. (2020). Mercury Emissions, Atmospheric Concentrations, and Wet Deposition across the Conterminous United States: Changes over 20 Years of Monitoring. *Environmental Science and Technology Letters*, *7*(6), 376–381. https://doi.org/10.1021/acs.estlett.0c00185

Olson, C. I., Geyman, B. M., Thackray, C. P., Krabbenhoft, D. P., Tate, M. T., Sunderland, E. M., & Driscoll, C. T. (2022). Mercury in soils of the conterminous United States: Patterns and pools. *Environmental Research Letters*, *17*(7). https://doi.org/10.1088/1748-9326/ac79c2

Olson, C. L., Jiskra, M., Sonke, J. E., & Obrist, D. (2019). Mercury in tundra vegetation of Alaska: Spatial and temporal dynamics and stable isotope patterns. *Science of the Total Environment*, *660*, 1502–1512. https://doi.org/10.1016/j.scitotenv.2019.01.058

Olund, S. D., DeWild, J. F., Olson, M. L., & Tate, M. T. (2004). Methods for the preparation and analysis of solids and suspended solids for total mercury. In *Techniques and Methods* (5-A8). U.S. Geological Survey. https://doi.org/10.3133/tm5A8

O'Toole, C. (2012). *Onondaga Lake cleanup continues; next up: Dredging, capping contaminated lake bottom*. Syracuse.Com. https://www.syracuse.com/news/2012/03/onondaga_lake_cleanup_continue.html

Outridge, P. M., Mason, R. P., Wang, F., Guerrero, S., & Heimbürger-Boavida, L. E. (2018). Updated Global and Oceanic Mercury Budgets for the United Nations Global Mercury Assessment 2018. *Environmental Science and Technology*, *52*(20), 11466–11477. https://doi.org/10.1021/acs.est.8b01246

Overpeck, J. T., & Udall, B. (2020). Increased drought severity tracks warming in the United States' largest river basin. *Proceedings of the National Academy of Sciences of the United States of America*, *117*(21). https://doi.org/10.1073/pnas.1916208117

Packer, B. N., Carling, G. T., Veverica, T. J., Russell, K. A., Nelson, S. T., & Aanderud, Z. T. (2020). Mercury and dissolved organic matter dynamics

during snowmelt runoff in a montane watershed, Provo River, Utah, USA. *Science of the Total Environment*, *704*, 135297. https://doi.org/10.1016/j.scitotenv.2019.135297

Parks, J. M., Johs, A., Podar, M., Bridou, R., Hurt, R. A., Smith, S. D., Tomanicek, S. J., Qian, Y., Brown, S. D., Brandt, C. C., Palumbo, A. V., Smith, J. C., Wall, J. D., Elias, D. A., & Liang, L. (2013). The genetic basis for bacterial mercury methylation. *Science*, *339*(6125), 1332–1335. https://doi.org/10.1126/science.1230667

Pelletier, J. D. (2009). The impact of snowmelt on the late Cenozoic landscape of the southern Rocky Mountains, USA. *GSA Today*, *19*(7), 4–11. https://doi.org/10.1130/GSATG44A.1

Pepin, N. C., Arnone, E., Gobiet, A., Haslinger, K., Kotlarski, S., Notarnicola, C., Palazzi, E., Seibert, P., Serafin, S., Schöner, W., Terzago, S., Thornton, J. M., Vuille, M., & Adler, C. (2022). Climate Changes and Their Elevational Patterns in the Mountains of the World. *Reviews of Geophysics*, *60*(1), e2020RG000730. https://doi.org/10.1029/2020RG000730

Peterson, B. D., Krabbenhoft, D. P., McMahon, K. D., Ogorek, J. M., Tate, M. T., Orem, W. H., & Poulin, B. A. (2023). Environmental formation of methylmercury is controlled by synergy of inorganic mercury bioavailability and microbial mercury-methylation capacity. *Environmental Microbiology*. https://doi.org/10.1111/1462-2920.16364

Pleijel, H., Klingberg, J., Nerentorp, M., Broberg, M. C., Nyirambangutse, B., Munthe, J., & Wallin, G. (2021). Mercury accumulation in leaves of different plant types – the significance of tissue age and specific leaf area. *Biogeosciences*, *18*(23), 6313–6328. https://doi.org/10.5194/bg-18-6313-2021

Pokharel, A. K., & Obrist, D. (2011). Fate of mercury in tree litter during decomposition. *Biogeosciences*. https://doi.org/10.5194/bg-8-2507-2011

Polk, M. H., Young, K. R., Baraer, M., Mark, B. G., McKenzie, J. M., Bury, J., & Carey, M. (2017). Exploring hydrologic connections between tropical mountain wetlands and glacier recession in Peru's Cordillera Blanca. *Applied Geography*, *78*, 94–103. https://doi.org/10.1016/j.apgeog.2016.11.004

Poulin, B. A., Gerbig, C. A., Kim, C. S., Stegemeier, J. P., Ryan, J. N., & Aiken, G. R. (2017). Effects of Sulfide Concentration and Dissolved Organic Matter Characteristics on the Structure of Nanocolloidal Metacinnabar. *Environmental Science & Technology*, *51*(22), 13133–13142. https://doi.org/10.1021/acs.est.7b02687

Quimby, B., Crook, S. E., Miller, K. M., Ruiz, J., & Lopez-Carr, D. (2020). Identifying, defining and exploring angling as urban subsistence: Pier fishing in Santa Barbara, California. *Marine Policy*, *121*. https://doi.org/10.1016/j.marpol.2020.104197

R Core Team. (2023). *R: A language and environment for statistical computing* (Version Version 2023.03.0+386) [Computer software]. R Foundation for Statistical Computing. https://www.r-project.org/

Richter, L., Amouroux, D., Tessier, E., & Fostier, A. H. (2023). Impact of forest fire on the mercury stable isotope composition in litter and soil in the Amazon. *Chemosphere*, *339*, 139779. https://doi.org/10.1016/j.chemosphere.2023.139779

Rimmer, C. C., Miller, E. K., McFarland, K. P., Taylor, R. J., & Faccio, S. D. (2010). Mercury bioaccumulation and trophic transfer in the terrestrial food web of a montane forest. *Ecotoxicology*, *19*(4), 697–709. https://doi.org/10.1007/s10646-009-0443-x

Rocca, M. E., Brown, P. M., MacDonald, L. H., & Carrico, C. M. (2014). Climate change impacts on fire regimes and key ecosystem services in Rocky Mountain forests. *Forest Ecology and Management*, *327*, 290–305. https://doi.org/10.1016/j.foreco.2014.04.005

Rodenhouse, N. L., Lowe, W. H., Gebauer, R. L. E., McFarland, K. P., & Bank, M. S. (2019). Mercury bioaccumulation in temperate forest food webs associated with headwater streams. *Science of the Total Environment*, *665*, 1125–1134. https://doi.org/10.1016/j.scitotenv.2019.02.151

Roe, A. (2003). Fishing for identity: Mercury contamination and fish consumption among indigenous groups in the United States. *Bulletin of Science, Technology and Society*, *23*(5), 368–375. https://doi.org/10.1177/0270467603259787

Ross, M. R. V., Nippgen, F., Hassett, B. A., McGlynn, B. L., & Bernhardt, E. S. (2018). Pyrite Oxidation Drives Exceptionally High Weathering Rates and Geologic CO2 Release in Mountaintop-Mined Landscapes. *Global Biogeochemical Cycles*, *32*(8), 1182–1194. https://doi.org/10.1029/2017GB005798

Rühland, K., Phadtare, N. R., Pant, R. K., Sangode, S. J., & Smol, J. P. (2006). Accelerated melting of Himalayan snow and ice triggers pronounced changes in a valley peatland from northern India. *Geophysical Research Letters*, *33*(15). https://doi.org/10.1029/2006GL026704

Santofimia, E., López-Pamo, E., Palomino, E. J., González-Toril, E., & Aguilera, Á. (2017). Acid rock drainage in Nevado Pastoruri glacier area (Huascarán National Park, Perú): Hydrochemical and mineralogical characterization and associated environmental implications. *Environmental Science and Pollution Research*, *24*(32), 25243–25259. https://doi.org/10.1007/s11356-017-0093-0

Sauer, A. K., Driscoll, C. T., Evers, D. C., Adams, E. M., & Yang, Y. (2020). Mercury exposure in songbird communities along an elevational gradient on Whiteface Mountain, Adirondack Park (New York, USA). *Ecotoxicology*, *29*(10), 1830–1842. https://doi.org/10.1007/s10646-020-02175-7

Schaefer, K., Elshorbany, Y., Jafarov, E., Schuster, P. F., Striegl, R. G., Wickland, K. P., & Sunderland, E. M. (2020). Potential impacts of mercury released from thawing permafrost. *Nature Communications*, *11*(1), 4650. https://doi.org/10.1038/s41467-020-18398-5

Schofield, R. K., & Taylor, A. W. (1955). The Measurement of Soil pH. *Soil Science Society of America Journal*, *19*(2), 164–167. https://doi.org/10.2136/sssaj1955.03615995001900020013x

Schuster, P. F., Schaefer, K. M., Aiken, G. R., Antweiler, R. C., Dewild, J. F., Gryziec, J. D., Gusmeroli, A., Hugelius, G., Jafarov, E., Krabbenhoft, D. P., Liu, L., Herman-Mercer, N., Mu, C., Roth, D. A., Schaefer, T., Striegl, R. G., Wickland, K. P., & Zhang, T. (2018). Permafrost Stores a Globally Significant Amount of Mercury. *Geophysical Research Letters*, *45*(3), 1463–1471. https://doi.org/10.1002/2017GL075571

Scott, A. F., & Black, F. J. (2020). *Great Salt Lake Biology: Mercury bioaccumulation and Biomagnification in Great Salt Lake Ecosystems*.

Seaber, P. R. (1988). Hydrostratigraphic units. In W. Back, J. S. Rosenshein, & P. R. Seaber (Eds.), *Hydrogeology: Vol. O-2* (p. 0). Geological Society of America. https://doi.org/10.1130/DNAG-GNA-O2.9

Seigneur, C., Vijayaraghavan, K., Lohman, K., Karamchandani, P., & Scott, C. (2004). Global Source Attribution for Mercury Deposition in the United States. *Environmental Science and Technology*, *38*(2), 555–569. https://doi.org/10.1021/es034109t

Selin, N. E. (2009). Global Biogeochemical Cycling of Mercury: A Review. *Annual Review of Environment and Resources*, *34*(1), 43–63. https://doi.org/10.1146/annurev.environ.051308.084314

Selin, N. E., & Jacob, D. J. (2008). Seasonal and spatial patterns of mercury wet deposition in the United States: Constraints on the contribution from North American anthropogenic sources. *Atmospheric Environment*, *42*(21), 5193–5204. https://doi.org/10.1016/j.atmosenv.2008.02.069

Selin, N. E., Jacob, D. J., Yantosca, R. M., Strode, S., Jaeglé, L., & Sunderland, E. M. (2008). Global 3-D land-ocean-atmosphere model for mercury: Present-day versus preindustrial cycles and anthropogenic enrichment factors for deposition. *Global Biogeochemical Cycles*, *22*(2). https://doi.org/10.1029/2007GB003040

Shanley, J. B., Alisa Mast, M., Campbell, D. H., Aiken, G. R., Krabbenhoft, D. P., Hunt, R. J., Walker, J. F., Schuster, P. F., Chalmers, A., Aulenbach, B. T., Peters, N. E., Marvin-DiPasquale, M., Clow, D. W., & Shafer, M. M. (2008). Comparison of total mercury and methylmercury cycling at five sites using the small watershed approach. *Environmental Pollution*, *154*(1), 143–154. https://doi.org/10.1016/j.envpol.2007.12.031

St. Louis, V. L., Rudd, J. W. M., Kelly, C. A., Beaty, K. G., Bloom, N. S., & Flett, R. J. (1994). Importance of Wetlands as Sources of Methyl Mercury to Boreal Forest Ecosystems. *Canadian Journal of Fisheries and Aquatic Sciences*, *51*(5), 1065–1076. https://doi.org/10.1139/f94-106

Stankwitz, C., Kaste, J. M., & Friedland, A. J. (2012). Threshold increases in soil lead and mercury from tropospheric deposition across an elevational gradient. *Environmental Science and Technology*, *46*(15), 8061–8068. https://doi.org/10.1021/es204208w

Streets, D. G., Horowitz, H. M., Lu, Z., Levin, L., Thackray, C. P., & Sunderland, E. M. (2019). Global and regional trends in mercury emissions and concentrations, 2010–2015. *Atmospheric Environment*, *201*(December 2018), 417–427. https://doi.org/10.1016/j.atmosenv.2018.12.031

Sun, J., Gallego-Sala, A., & Yu, Z. (2023). Topographic and climatic controls of peatland distribution on the Tibetan Plateau. *Scientific Reports*, *13*(1), 14811. https://doi.org/10.1038/s41598-023-39699-x

Sun, R., Sun, G., Kwon, S. Y., Feng, X., Kang, S., Zhang, Q., Huang, J., & Yin, R. (2021). Mercury biogeochemistry over the Tibetan Plateau: An overview. *Critical Reviews in Environmental Science and Technology*, *51*(6), 577–602. https://doi.org/10.1080/10643389.2020.1733894

Sun, X., Wang, K., Kang, S., Guo, J., Zhang, G., Huang, J., Cong, Z., Sun, S., & Zhang, Q. (2017). The role of melting alpine glaciers in mercury export and transport: An intensive sampling campaign in the Qugaqie Basin, inland Tibetan Plateau. *Environmental Pollution*, *220*, 936–945. https://doi.org/10.1016/j.envpol.2016.10.079

Sun, X., Zhang, Q., Zhang, G., Li, M., Li, S., Guo, J., Dong, H., Zhou, Y., Kang, S., Wang, X., & Shi, J. (2022). Melting Himalayas and mercury export: Results of continuous observations from the Rongbuk Glacier on Mt. Everest and future insights. *Water Research*, *218*. https://doi.org/10.1016/j.watres.2022.118474

Szopka, K., Karczewska, A., & Kabała, C. (2011). Mercury accumulation in the surface layers of mountain soils: A case study from the Karkonosze Mountains, Poland. *Chemosphere*, *83*(11), 1507–1512. https://doi.org/10.1016/j.chemosphere.2011.01.049

Tague, C., & Dugger, A. L. (2010). Ecohydrology and Climate Change in the Mountains of the Western USA - A Review of Research and Opportunities.

Geography Compass, *4*(11), 1648–1663. https://doi.org/10.1111/j.1749-8198.2010.00400.x

Tan, Z., Mclaren, R., & Cameron, K. (1994). Forms of sulfur extracted from soils after different methods of sample preparation. *Soil Research*, *32*(4), 823. https://doi.org/10.1071/SR9940823

Tate, M. T., Janssen, S. E., Lepak, R. F., Flucke, L., & Krabbenhoft, D. P. (2023). National-Scale Assessment of Total Gaseous Mercury Isotopes Across the United States. *Journal of Geophysical Research: Atmospheres*, *128*(8), e2022JD038276. https://doi.org/10.1029/2022JD038276

Tjerngren, I., Karlsson, T., Björn, E., & Skyllberg, U. (2012). Potential Hg methylation and MeHg demethylation rates related to the nutrient status of different boreal wetlands. *Biogeochemistry*, *108*(1–3), 335–350. https://doi.org/10.1007/s10533-011-9603-1

Todd, A. S., Manning, A. H., Verplanck, P. L., Crouch, C., McKnight, D. M., & Dunham, R. (2012). Climate-Change-Driven Deterioration of Water Quality in a Mineralized Watershed. *Environmental Science & Technology*, *46*(17), 9324–9332. https://doi.org/10.1021/es3020056

Tourville, J., Publicover, D., & Dovciak, M. (2023). Forests on the move: Tracking climate-related treeline changes in mountains of the northeastern United States. *Journal of Biogeography*, *50*(12), 1993–2007. https://doi.org/10.1111/jbi.14708

Townsend, J. M., Driscoll, C. T., Rimmer, C. C., & Mcfarland, K. P. (2014). Avian, salamander, and forest floor mercury concentrations increase with elevation in a terrestrial ecosystem. *Environmental Toxicology and Chemistry*, *33*(1), 208–215. https://doi.org/10.1002/etc.2438

Trant, A., Higgs, E., & Starzomski, B. M. (2020). A century of high elevation ecosystem change in the Canadian Rocky Mountains. *Scientific Reports*, *10*(1), 9698. https://doi.org/10.1038/s41598-020-66277-2

Tripathee, L., Guo, J., Kang, S., Paudyal, R., Huang, J., Sharma, C. M., Zhang, Q., Rupakheti, D., Chen, P., Sharma Ghimire, P., & Gyawali, A. (2019). Concentration and risk assessments of mercury along the elevation gradient in soils of Langtang Himalayas, Nepal. *Human and Ecological Risk Assessment*, *25*(4), 1006–1017. https://doi.org/10.1080/10807039.2018.1459180

UCAR. (2023). *Why did Boulder, CO look like this on May 20, 2023? | Atmospheric Chemistry Observations & Modeling*. https://www2.acom.ucar.edu/news/why-did-boulder-co-look-may-20-2023

UN Environment. (2019). Minamata Convention on Mercury. *International Legal Materials*, *55*(3), 582. https://doi.org/10.5305/intelegamate.55.3.0582

UNEP. (2018). *GLOBAL MERCURY ASSESSMENT*.

U.S. EPA. (1998). *Method 1630: Methyl Mercury in Water by Distillation, Aqueous Ethylation, Purge and Trap, and Cold Vapor Atomic Fluorescence Spectrometry*.

U.S. EPA. (2002). *Method 1631, Revision E: Method 1631: Mercury in Water by Oxidation, Purge and Trap, and Cold Vapor Atomic Fluorescence Spectrometry*. https://www.epa.gov/sites/default/files/2015-08/documents/method_1631e_2002.pdf

U.S. EPA. (2007). *Method 7473: Mercury in Solids and Solutions by Thermal Decomposition, Amalgamation, and Atomic Absorption Spectrophotometry*. https://www.epa.gov/sites/default/files/2015-07/documents/epa-7473.pdf

US EPA. (2015, September 15). *Environmental Laws that Apply to Mercury* [Overviews and Factsheets]. https://www.epa.gov/mercury/environmental-laws-apply-mercury

US EPA, O. (2014, November 10). *Fish and Shellfish Advisories and Safe Eating Guidelines* [Announcements and Schedules]. https://www.epa.gov/choose-fish-and-shellfish-wisely/fish-and-shellfish-advisories-and-safe-eating-guidelines

USEPA. (2018). Minamata Convention on Mercury. *EPA*, *April*.

Val Martin, M., Heald, C. L., Ford, B., Prenni, A. J., & Wiedinmyer, C. (2013). A decadal satellite analysis of the origins and impacts of smoke in Colorado. *Atmospheric Chemistry and Physics*, *13*(15), 7429–7439. https://doi.org/10.5194/acp-13-7429-2013

van der Knaap, W. O., Lamentowicz, M., van Leeuwen, J. F. N., Hangartner, S., Leuenberger, M., Mauquoy, D., Goslar, T., Mitchell, E. A. D., Lamentowicz, Ł., & Kamenik, C. (2011). A multi-proxy, high-resolution record of peatland development and its drivers during the last millennium from the subalpine Swiss Alps. *Quaternary Science Reviews*, *30*(23), 3467–3480. https://doi.org/10.1016/j.quascirev.2011.06.017

Wang, X., Luo, J., Yuan, W., Lin, C. J., Wang, F., Liu, C., Wang, G., & Feng, X. (2020). Global warming accelerates uptake of atmospheric mercury in regions experiencing glacier retreat. *Proceedings of the National Academy of Sciences of the United States of America*, *117*(4), 2049–2055. https://doi.org/10.1073/pnas.1906930117

Wang, X., Yuan, W., Lin, C.-J., Luo, J., Wang, F., Feng, X., Fu, X., & Liu, C. (2020). Underestimated Sink of Atmospheric Mercury in a Deglaciated Forest Chronosequence. *Environmental Science & Technology*, *54*(13), 8083–8093. https://doi.org/10.1021/acs.est.0c01667

Weathers, K. C., Simkin, S. M., Lovett, G. M., & Lindberg, S. E. (2006). Empirical modeling of atmospheric deposition in mountainous landscapes. *Ecological Applications*, *16*(4), 1590–1607. https://doi.org/10.1890/1051-0761(2006)016[1590:EMOADI]2.0.CO;2

Webster, J. P., Kane, T. J., Obrist, D., Ryan, J. N., & Aiken, G. R. (2016). Estimating mercury emissions resulting from wildfire in forests of the Western United States. *Science of the Total Environment*, *568*, 578–586. https://doi.org/10.1016/j.scitotenv.2016.01.166

Weiss-Penzias, P., Jaffe, D. A., Swartzendruber, P., Dennison, J. B., Chand, D., Hafner, W., & Prestbo, E. (2006). Observations of Asian air pollution in the free troposphere at Mount Bachelor Observatory during the spring of 2004. *Journal of Geophysical Research Atmospheres*, *111*(10), 1–15. https://doi.org/10.1029/2005JD006522

Weiss-Penzias, P. S., Gay, D. A., Brigham, M. E., Parsons, M. T., Gustin, M. S., & ter Schure, A. (2016). Trends in mercury wet deposition and mercury air concentrations across the U.S. and Canada. *Science of the Total Environment*, *568*, 546–556. https://doi.org/10.1016/j.scitotenv.2016.01.061

Willacker, J. J., Eagles-Smith, C. A., Lutz, M. A., Tate, M. T., Lepak, J. M., & Ackerman, J. T. (2016). Reservoirs and water management influence fish mercury concentrations in the western United States and Canada. *Science of the Total Environment*, *568*, 739–748. https://doi.org/10.1016/j.scitotenv.2016.03.050

Wilson, J. J., Reyes Rivera, L., & Garayar S., J. (1967). Geología de los cuadrángulos de Mollebamba, Tayabamba, Huaylas, Pomabamba, Carhuaz y Huari (Hojas 17-h, 17-i, 18-h, 18-i, 19-h, 19-i)—[Boletín A 16]. *Instituto*

Geológico, Minero y Metalúrgico - INGEMMET. https://repositorio.ingemmet.gob.pe/handle/20.500.12544/133

Witherow, R. A., & Lyons, W. B. (2008). Mercury deposition in a polar desert ecosystem. *Environmental Science and Technology*, *42*(13), 4710–4716. https://doi.org/10.1021/es800022g

Woolf, A. D. (2022). Chapter 1.2—Three methylmercury poisoning disasters. In A. D. Woolf (Ed.), *History of Modern Clinical Toxicology* (pp. 15–33). Academic Press. https://doi.org/10.1016/B978-0-12-822218-8.00037-5

Wright, P. L., Zhang, L., & Marsik, F. J. (2016). Overview of mercury dry deposition, litterfall, and throughfall studies. *Atmospheric Chemistry and Physics*, *16*(21), 13399–13416. https://doi.org/10.5194/acp-16-13399-2016

Yang, Y., Meng, L., Yanai, R. D., Montesdeoca, M., Templer, P. H., Asbjornsen, H., Rustad, L. E., & Driscoll, C. T. (2019). Climate change may alter mercury fluxes in northern hardwood forests. *Biogeochemistry*, *146*(1), 1–16. https://doi.org/10.1007/s10533-019-00605-1

Yang, Z., Gao, X., Lei, J., Meng, X., & Zhou, N. (2022). Analysis of spatiotemporal changes and driving factors of desertification in the Africa Sahel. *Catena*, *213*. https://doi.org/10.1016/j.catena.2022.106213

Yu, R.-Q., Reinfelder, J. R., Hines, M. E., & Barkay, T. (2018). Syntrophic pathways for microbial mercury methylation. *The ISME Journal*, *12*(7), 1826–1835. https://doi.org/10.1038/s41396-018-0106-0

Zaremehrjardy, M., Victor, J., Park, S., Smerdon, B., Alessi, D. S., & Faramarzi, M. (2022). Assessment of snowmelt and groundwater-surface water dynamics in mountains, foothills, and plains regions in northern latitudes. *Journal of Hydrology*, *606*, 127449. https://doi.org/10.1016/j.jhydrol.2022.127449

Zhang, C., Gao, R., Wu, J., & Yang, Z. (2019). *Combating Climate Change, Desertification and Sandstorms: A Collaborative Approach*. http://www.springer.com/series/13571

Zhang, H., Yin, R. S., Feng, X. B., Sommar, J., Anderson, C. W. N., Sapkota, A., Fu, X. W., & Larssen, T. (2013). Atmospheric mercury inputs in montane soils increase with elevation: Evidence from mercury isotope signatures. *Scientific Reports*, *3*, 1–8. https://doi.org/10.1038/srep03322

Zhang, J., Li, C., Tang, W., Wu, M., Chen, M., He, H., Lei, P., & Zhong, H. (2023). Mercury in wetlands over 60 years: Research progress and emerging trends. *Science of the Total Environment*, *869*. https://doi.org/10.1016/j.scitotenv.2023.161862

Zhang, L., Kok, J. F., Henze, D. K., Li, Q., & Zhao, C. (2013). Improving simulations of fine dust surface concentrations over the western United States by optimizing the particle size distribution. *Geophysical Research Letters*, *40*(12), 3270–3275. https://doi.org/10.1002/grl.50591

Zhang, Q., Sun, X., Sun, S., Yin, X., Huang, J., Cong, Z., & Kang, S. (2019). Understanding Mercury Cycling in Tibetan Glacierized Mountain Environment: Recent Progress and Remaining Gaps. *Bulletin of Environmental Contamination and Toxicology*, *102*(5), 672–678. https://doi.org/10.1007/s00128-019-02541-0

Zhang, Y., Zhang, P., Song, Z., Huang, S., Yuan, T., Wu, P., Shah, V., Liu, M., Chen, L., Wang, X., Zhou, J., & Agnan, Y. (2023). An updated global mercury budget from a coupled atmosphere-land-ocean model: 40% more re-emissions buffer the effect of primary emission reductions. *One Earth*, *6*(3), 316–325. https://doi.org/10.1016/j.oneear.2023.02.004

Zhang, Yanxu., Jacob, D. J., Horowitz, H. M., Chen, Long., Amos, H. M., Krabbenhoft, D. P., Slemr, F., St. Louis, V. L., & Sunderland, E. M. (2016). Observed decrease in atmospheric mercury explained by global decline in anthropogenic emissions. *Proceedings of the National Academy of Sciences of the United States of America*, *113*(3), 526–531. https://doi.org/10.1073/pnas.1516312113

Zhou, J., Obrist, D., Dastoor, A., Jiskra, M., & Ryjkov, A. (2021). Vegetation uptake of mercury and impacts on global cycling. *Nature Reviews Earth & Environment*, *0123456789*, 1–16. https://doi.org/10.1038/s43017-021-00146-y

Zhou, J., Wang, Z., Zhang, X., Driscoll, C. T., & Lin, C.-J. (2020). Soil–atmosphere exchange flux of total gaseous mercury (TGM) at subtropical and temperate forest catchments. *Atmospheric Chemistry and Physics*, *20*(24), 16117–16133. https://doi.org/10.5194/acp-20-16117-2020

Zhu, B. Q., Zhang, J. X., & Sun, C. (2022). Potential links of gobi, dust, and desertification: A comprehensive understanding from aeolian landform evolution in a middle-latitude desert. *Sedimentary Geology*, *428*. https://doi.org/10.1016/j.sedgeo.2021.106049

Zolkos, S., Geyman, B. M., Potter, S., Moubarak, M., Rogers, B. M., Baillargeon, N., Dey, S., Ludwig, S. M., Melton, S., Navarro-Pérez, E., McElvein, A., Balcom, P. H., Natali, S. M., Sistla, S., & Sunderland, E. M. (2024). Substantial Mercury Releases and Local Deposition from Permafrost Peatland Wildfires in Southwestern Alaska. *Environmental Science & Technology*, *58*(46), 20654–20664. https://doi.org/10.1021/acs.est.4c08765

APPENDICES

A. Supplemental Materials for Chapter III

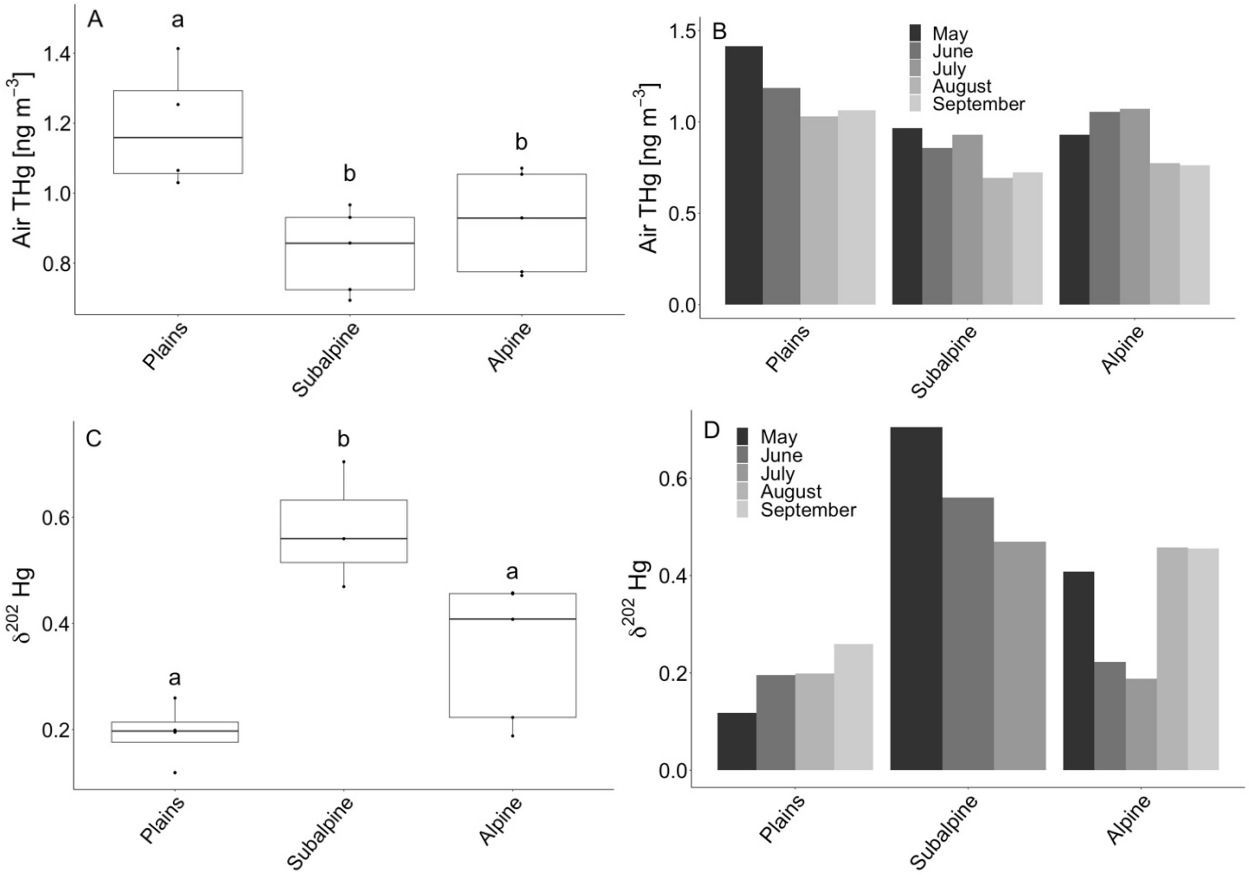

Figure S3-1: Atmospheric air concentrations averaged across all months (A) and for each month separately (B) for each elevation zone. δ^{202}Hg averaged across all months (C) and for each month separately (D).

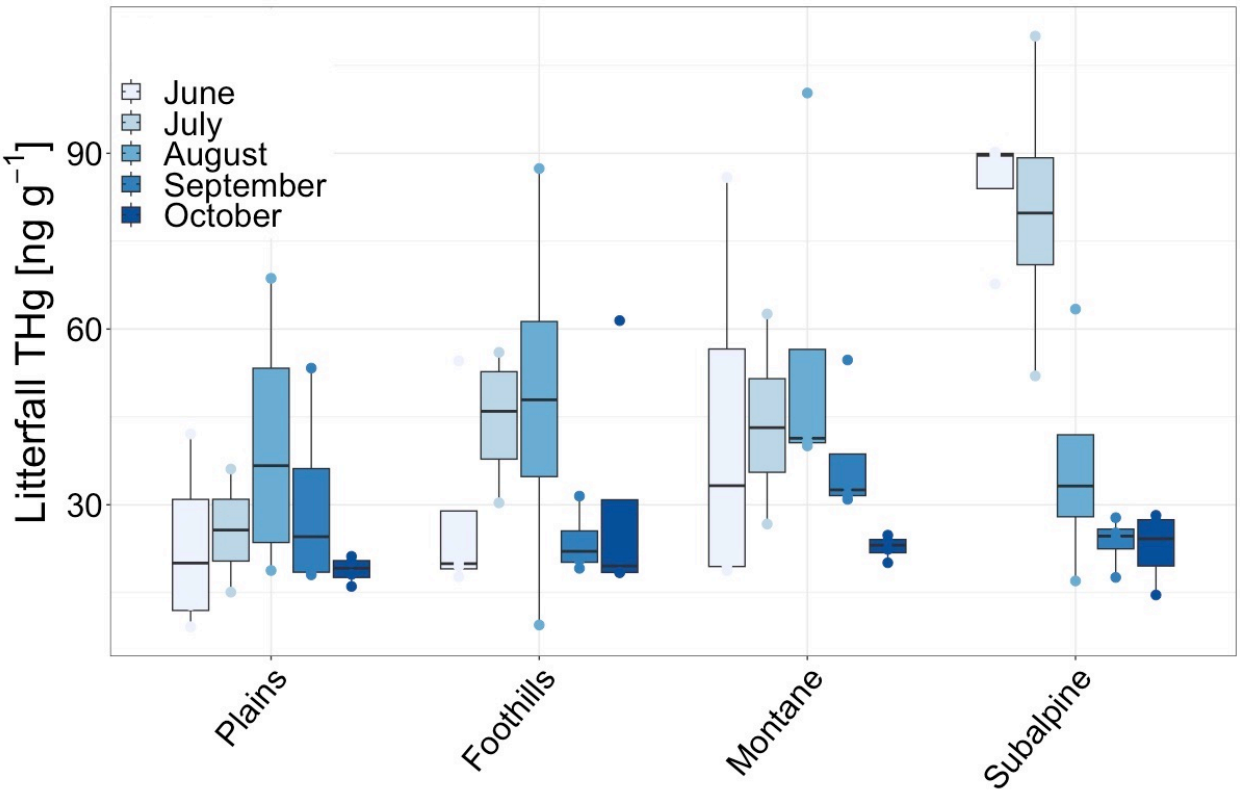

Figure S3-2: Monthly litterfall concentrations along the elevation gradient.

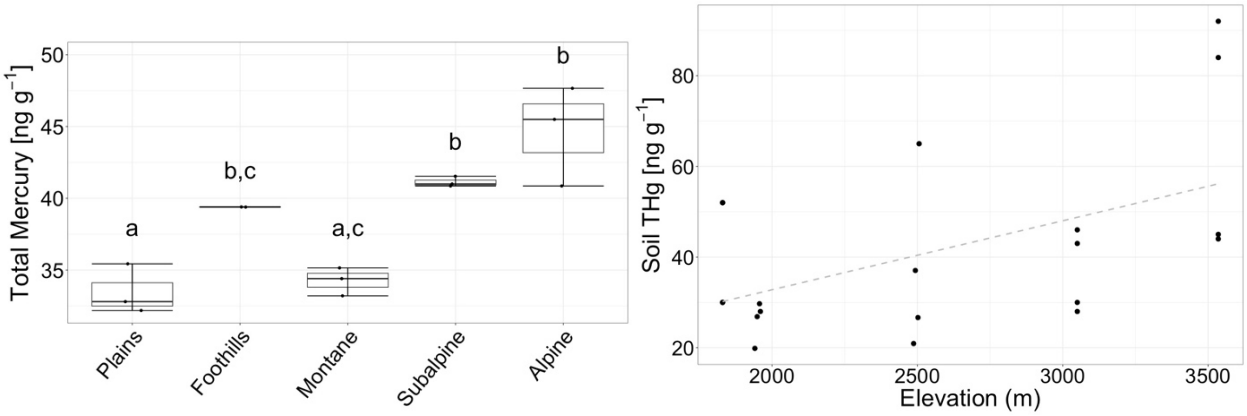

Figure S3-3: Soil litter layer THg concentrations for each elevation zone (A) and plotted against elevation (B).

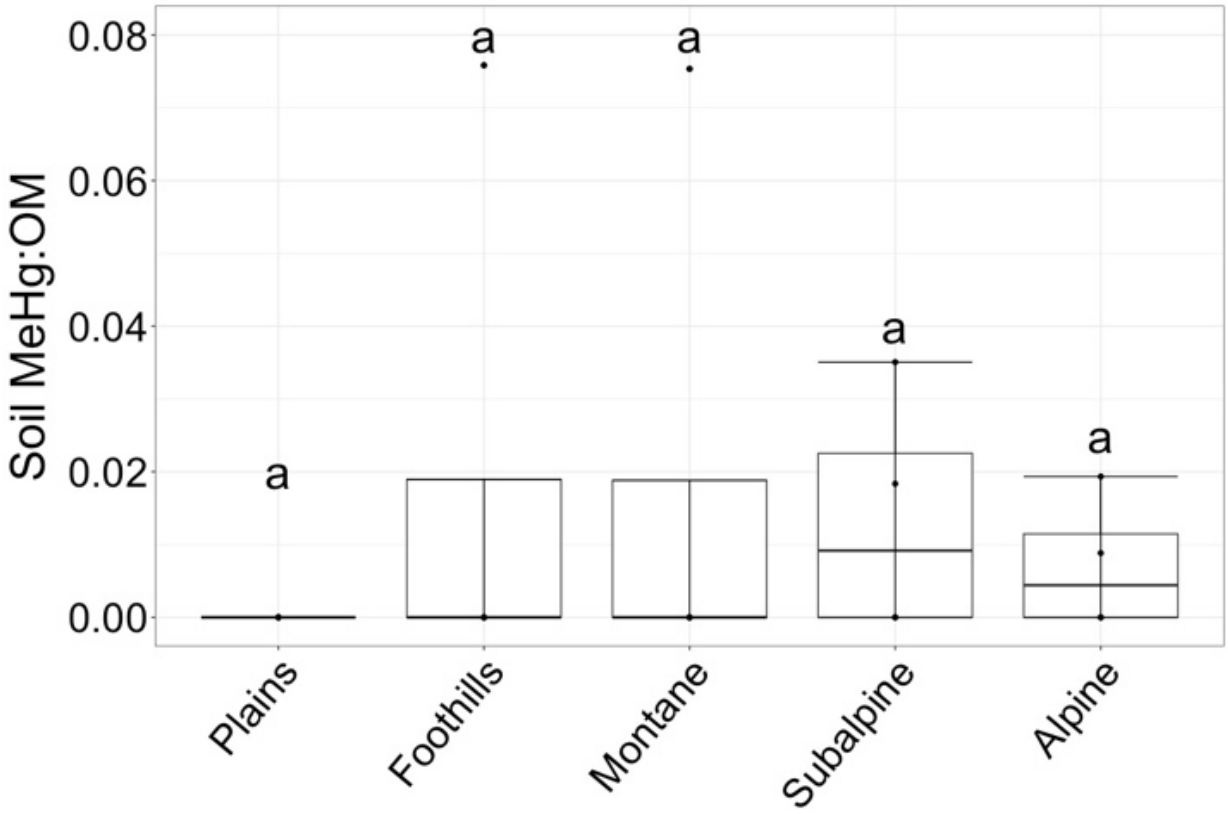

Figure S3-4: Soil MeHg concentrations normalized to soil organic matter.

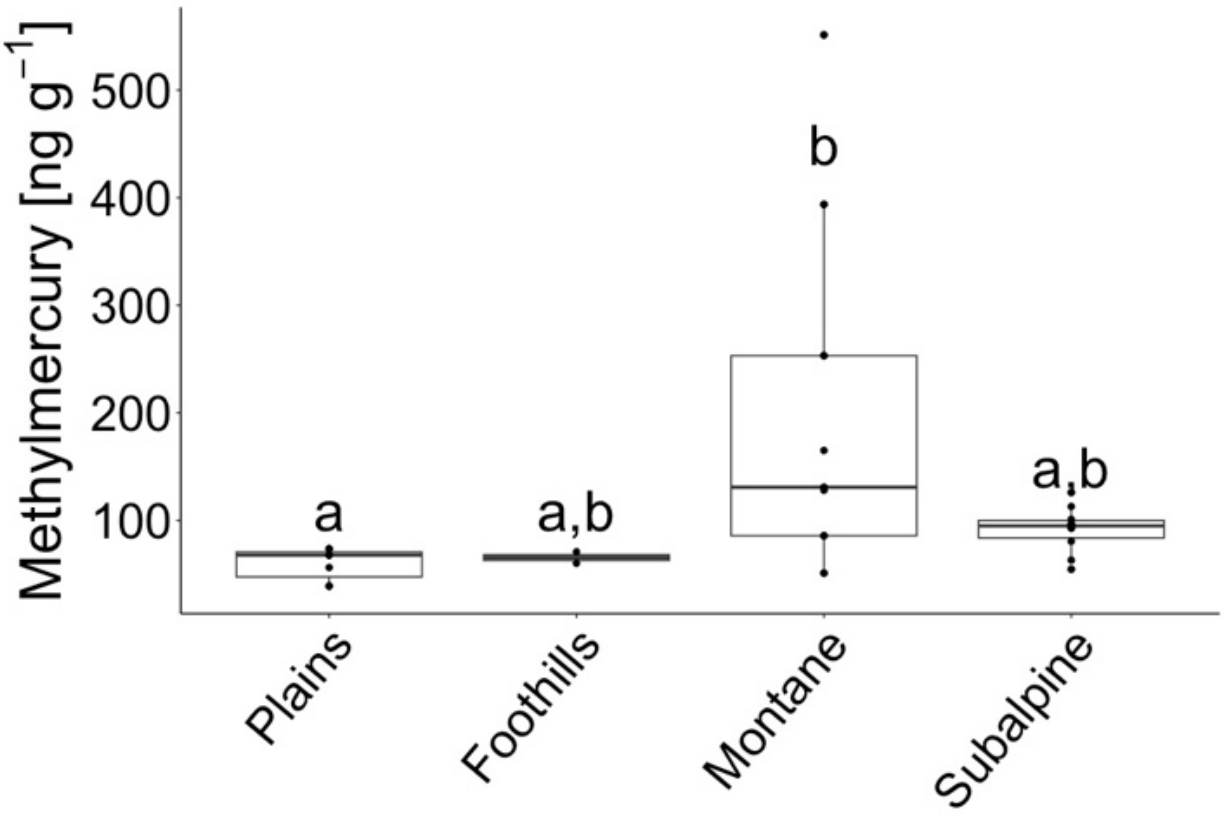

Figure S3-5: Chickadee MeHg concentrations across the elevation gradient (lower case letters indicate significance).

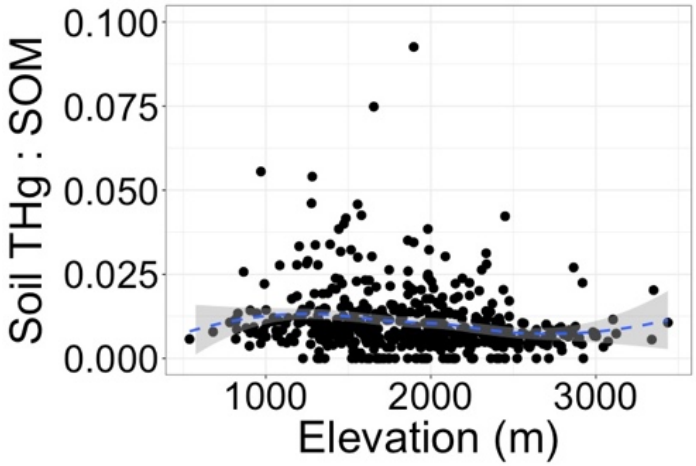

Figure S3-6: Rocky Mountain soil total mercury (THg) normalized to soil organic matter (SOM) plotted against elevation from USGS soil samples.

Table S3-1: Table of average open precipitation and throughfall volumes used to calculate a weighted average throughfall coefficient.

Site	*Open Volume*	*Throughfall Volume*	*Open / Through Coefficient*
Plains	40.60	22.73	0.56
Plains	33.00	20.45	0.62
Foothills	79.80	22.50	0.28
Foothills	38.90	12.05	0.31
Foothills	43.90	16.21	0.37
Montane	44.50	18.18	0.41
Montane	33.10	15.91	0.48
Montane	34.80	18.18	0.52
Montane	50.00	10.91	0.22
Subalpine	51.10	21.59	0.42
Subalpine	32.80	24.24	0.74
Subalpine	25.90	20.45	0.79
Subalpine	38.60	11.36	0.29
Subalpine	33.23	25.00	0.75

Site	*Average Coefficient*	*Weighted average coefficient*
Plains	0.59	**0.48**
Foothills	0.32	
Montane	0.41	
Subalpine	0.60	

Table S3-2: Table of predictive models used in the study.

Model type	Model	p-value	R2	AIC	Coefficient
GLM	Precip THg conc ~ Elevation	< 0.01		336	-0.01
LM	Throughfall THg conc ~ poly(Elevation)	0.02	0.13		-53
LM	Litterfall THg conc ~ Elevation * Month	< 0.01	0.21		< 0.01
LM	Litterfall THg conc ~ poly(Elevation)	< 0.01	0.09		-1.3
LM	Litterfall THg conc ~ poly(Elevation) * Month	< 0.01	0.27		-1.9
LM	Litterfall THg conc ~ Elevation (no alpine) * Month	< 0.01	0.41		< 0.01
LM	Soil Litter THg conc ~ Elevation	< 0.01	0.57		< 0.01
LM	Soil THg conc ~ % Nitrogen	< 0.01	0.69		1.15
LM	Soil THg conc ~ Elevation	0.02	0.21		< 0.01
LM	Soil THg conc ~ % Water	< 0.01	0.45		0.03
LM	Soil THg conc ~ SOM	< 0.01	0.49		0.04
LM	Soil THg conc ~ % Nitrogen	< 0.01	0.69		1.15
LM	Soil THg conc ~ Sulfate	0.01	0.29		7.6
LM	Soil THg conc ~ Precip flux canopy	0.02	0.24		0.14
LM	Soil THg pools ~ % water	0.02	0.23		0.02
LM	Soil THg pools ~ SOM	< 0.01	0.41		0.03
LM	Soil THg pools ~ % nitrogen	< 0.01	0.63		1.01
LM	Soil THg pools ~ Precip flux	0.02	0.25		0.12
GLM	Chickadee MeHg ~ poly(Elevation)	< 0.01		36	-0.41
GLM	Chickadee MeHg ~ THg:SOM	0.07		23	0.04
GLM	Chicakdee MeHg ~ Precip THg flux	0.01		20	0.2
GLM	Chicakdee MeHg ~ Throughfall conc	0.03		21	< 0.01
GLM	Chicakdee MeHg ~ Throughfall flux	< 0.01		7	0.05

Table S3-3: Percent tree cover, total precipitation, and litterfall mass for the sampling period

Elevation Zone	Percent Tree Cover	Total Annual Precipitation (L/m2)	Total Annual Litterfall (g/m2)
Plains	13	590.8	122.2
Foothills	32	548.9	101.4
Montane	35	603.8	101.4
Subalpine	40	832.1	162.2
Alpine	12	719.6	13.1

B. Supplemental Materials for Chapter IV

Supplementary Text

Extended description of soil analyses

For physicochemical analysis, soils were divided into subsamples based on drying technique: one subsample was dried at 105°C to calculate gravimetric water content and loss on ignition (LOI), one subsample was dried at 60°C to determine total carbon (C) and nitrogen (N), and the remaining soil was air-dried and used to measure pH and extractable sulfate (SO_4^{2-}). Loss on ignition was used as a proxy for total soil organic matter (SOM). Briefly, dried soils were combusted at 550°C for 4-h following methods outlined byHeiri et al. (Heiri et al., 2001). To measure pH, ~10 g of air-dried soil was suspended in 20 mL of 0.01 M calcium chloride ($CaCl_2$) for 1 h and measured with a benchtop pH probe (Schofield & Taylor, 1955). Extractable SO_4^{2-} concentrations were determined by shaking ~30 g of air-dried soil in 100mL of 0.006 M calcium dihydrogen phosphate ($Ca(H_2PO_4)^2*H_2O$) solution and measuring the filtrate for SO_4^{2-} using ion chromatography (Metrohm 930 Compact IC Flex; detection limit 0.1 mg L^{-1} SO_4^{2-}) (Tan et al., 1994). For total C and N, dried and pulverized soil was packed into tins and measured on a Thermo Finnigan elemental analyzer at the University of Wyoming Stable Isotope Facility.

Extended description of soil total mercury (THg) and methylmercury (MeHg) concentration analysis

Soil samples were lyophilized with a FreeZone Labconco at -50°C under 0.1 mm Hg pressure for a minimum of 72 h. Soils were analyzed for THg using atomic adsorption followed by direct combustion on a Nippon MA-3000 Mercury analyzer. Analytical quality control was verified by an instrument calibration linearity > 0.995, as well as a method blank (< 0.05 ng/boat), certified reference material

(CRM) IAEA-475 (Marine Sediment, THg concentration = 29.9 ± 1.5 ng g^{-1}), and a triplicate every 10 samples. IAEA-475 recovery averaged 98 ± 5 % and the relative standard deviation of the triplicates was < 6 % across analyses.

Samples were analyzed for excess $T^{201}Hg$ and ambient THg concentrations per EPA Method 1631 (Cook et al., 2024; Peterson et al., 2023; U.S. EPA, 2002). Samples ranging from 50 – 150 mg were weighed into Teflon bombs and 6 ml hydrochloric acid (HCl) and 2 ml concentrated nitric acid (HNO_3 OmniTrace) were added to each sample. Samples were then brought up to 30 ml total volume with a 5% bromine monochloride (BrCl) solution and heated to 50°C for at least 8 h. Just prior to analysis, the BrCl was neutralized by the addition of hydroxylamine hydrochloride and all Hg(II) species were reduced to Hg^0 by the addition of stannous chloride ($SnCl_2$). Volatile Hg^0 was then purged from the sample and captured on gold coated bead traps, desorbed, and detected by cold vapor atomic fluorescence. Sample analysis was then conducted with the Brooks-Rand "MERX-T" automated Hg analytical system coupled to the Thermo iCAP inductively plasma-mass spectrometer (ICP-MS) with a detection limit of 0.014 ng g^{-1}. The CRM IAEA 456 (coastal sediment, THg = 77 ± 5 ng g^{-1}) recovery averaged 100 ± 10 % and the relative standard deviation of the triplicates was 3.9 ± 0.1 %. Quality assurance acceptance criteria can be found in Table S4-3 and S4-4.

Ambient MeHg and excess $Me^{201}Hg$ concentrations were determined by distillation and isotope dilution per the USGS Techniques and Methods 5A-7 (Helmrich et al., 2022; Hintelmann et al., 1995; Hintelmann & Evans, 1997; U.S. EPA, 1998). Samples were enriched with a MeHg spike, acidified with potassium chloride / cupric sulfate solution, and distilled by heating to 120-125°C while being purged with nitrogen gas. The resulting distillate was then buffered with sodium acetate/acetic acid, ethylated with sodium tetraethylborate (NaTEB), and analyzed

on the Brooks-Rand "MERX-M" automated MeHg analytical system coupled to the ICP-MS. MeHg concentrations were calculated using isotopic dilution. Analytical quality control was performed with a mass bias correction (< 5%) and isotope dilution correction (< 5%) at instrument calibration, as well as an instrument calibration check standard every six samples (85 – 115% recovery), a method triplicate (< 25% relative standard deviation of MeHg concentration) every fifteen samples, and a CRM IAEA 405 (Estuarine Sediment, MeHg concentration = 5.49 ± 0.53 ng g^{-1}, 80 – 120%) every 15 samples. IAEA-405 recovery averaged 93 ± 12 % and the relative standard deviation of the triplicates was < 8 % across our analyses. Quality assurance acceptance criteria can be found in Table S3-4.

Extended description of MeHg production potential:

Since this is the first time such an incubation experiment has been conducted in a high elevation environment, we tested two different water sources for the Hg isotope tracer solution. For all sites we collected nearby stream runoff representative of a recent precipitation event and called this "runoff". For the subalpine peatland and solifluction lobe, we additionally collected porewater by sampling soil directly into plastic bags that were later centrifuged for porewater extraction in the lab. Porewater and runoff were deoxygenated using ultra high-purity nitrogen (N_2) prior to preparation of the Hg isotope tracer solution (see description below). Overlying water from an alpine wet meadow, representative of recent snowmelt, was collected to saturate the alpine dry meadow soil during the incubation experiments.

The enriched isotope used to amend the environmental samples was purchased from Oak Ridge National Laboratories (batch 176506) with the fraction of ^{201}Hg certified at 98.11%. The $^{201}Hg(II)$ tracer was preequilibrated with both type

of filtered waters (runoff and porewater) for a minimum of 4 h after an initial purge with N_2 for 20 min. To match the ^{201}Hg(II) signal from the soil at each site with the isotope spike, we targeted ^{201}Hg(II) amendments that were ~ 13% of the ambient total THg concentrations, since the natural abundance of ^{201}Hg(II) is ~ 13 % of the total Hg mass. This addition resulted in ^{201}Hg(II) abundance double that of the natural isotope abundance.

All samples were processed within an anoxic environment in a N_2-purged glove bag. All soils were homogenized; soils from the alpine dry meadow and solifluction lobe were thoroughly mixed with a clean plastic spoon. Soils from the subalpine peatland were homogenized in a blender due to high organic content. For the subalpine peatland and solifluction lobes, 50-60 g of field wet soil were placed into incubation jars. For the alpine dry meadow, 25-30 g of soil were placed into incubation jars followed by 25 - 30 ml N_2-purged overlying water to saturate the sediments, representative of precipitation, or snowmelt, events. All incubation jars were then sealed and removed from the glove bag for Hg isotope and sulfate additions.

Isotope spikes and sulfate amendments were added by injecting samples with syringes through the incubation jar septum. For the alpine dry meadow site, all samples were spiked with 0.5 ml of 250 ng ml^{-1} T^{201}Hg of the runoff spiking solution. For the solifluction lobe, half the samples were spiked with 0.5 ml of 359 ng ml^{-1} T^{201}Hg of the runoff spiking solution and the other half were spiked with the same concentration of the porewater spiking solution. For the subalpine peatland, half the samples were spiked with 0.5 ml of 1248 ng ml^{-1} T^{201}Hg of the runoff spiking solution and the other half were spiked with the same concentrations of the porewater spiking solution. To assess sulfate controls on MeHg production in the subalpine peatland, additional triplicate soil samples were amended with the runoff

spiking solution, as well as 50 µM (5 mg sulfate L^{-1}), 100 µM (10 mg sulfate L^{-1}), and 200 µM (20 mg sulfate L^{-1}) of a 0.5 M sodium sulfate solution to mimic enhanced sulfate concentrations in runoff. These amendments resulted in a 50 to 280% increase in soil sulfate concentrations comparable to ~200 % increase in sulfate concentrations detected within the watershed (Crawford et al., 2020). Triplicates from each site and each treatment were frozen at time 0h, 24 h, 48 h, and 72 h to halt the incubation. Samples were stored at room temperature (21.0 - 22.5°C) in dark boxes to prevent photochemical degradation of Hg species throughout the experiment.

Supplemental Figures

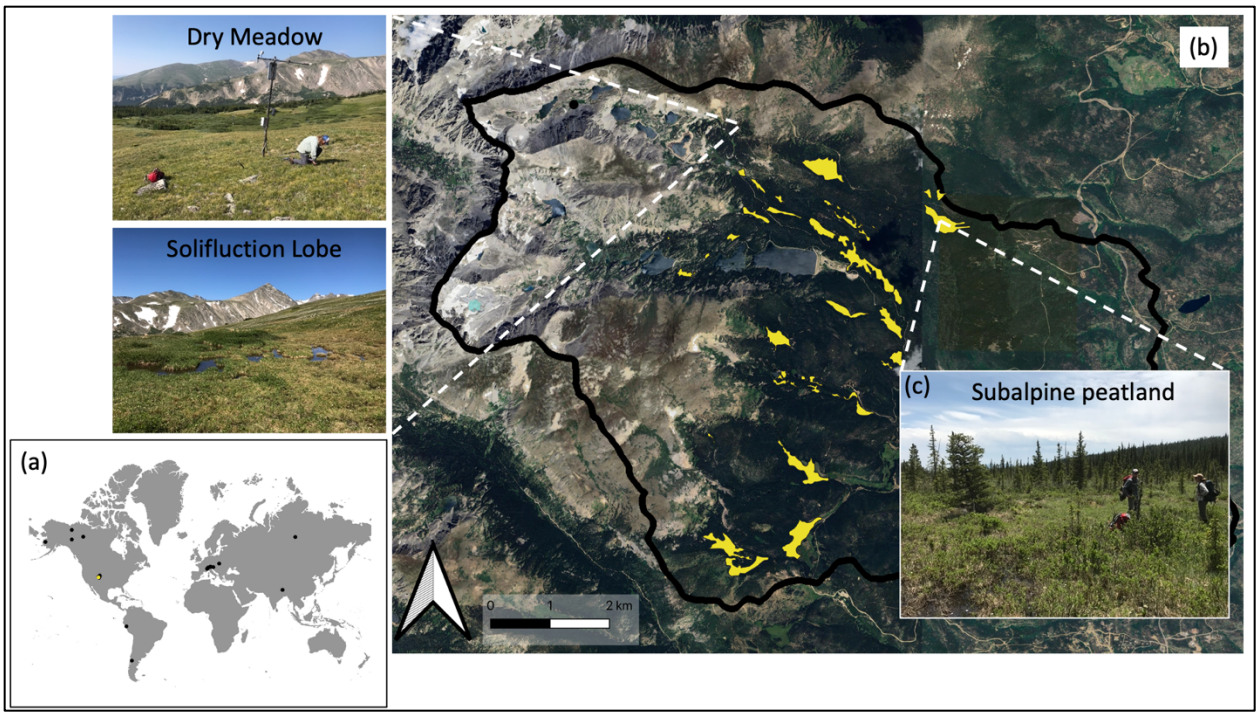

Figure S4-1: Global locations where mobilization of sulfate from thawing ice features has increased over the past several decades with our study site highlighted in yellow (a). The North Boulder Watershed extent outlined in black with subalpine peatlands highlighted in yellow and insets of dry meadow, solifluction lobe, and subalpine peatland (c) sites.

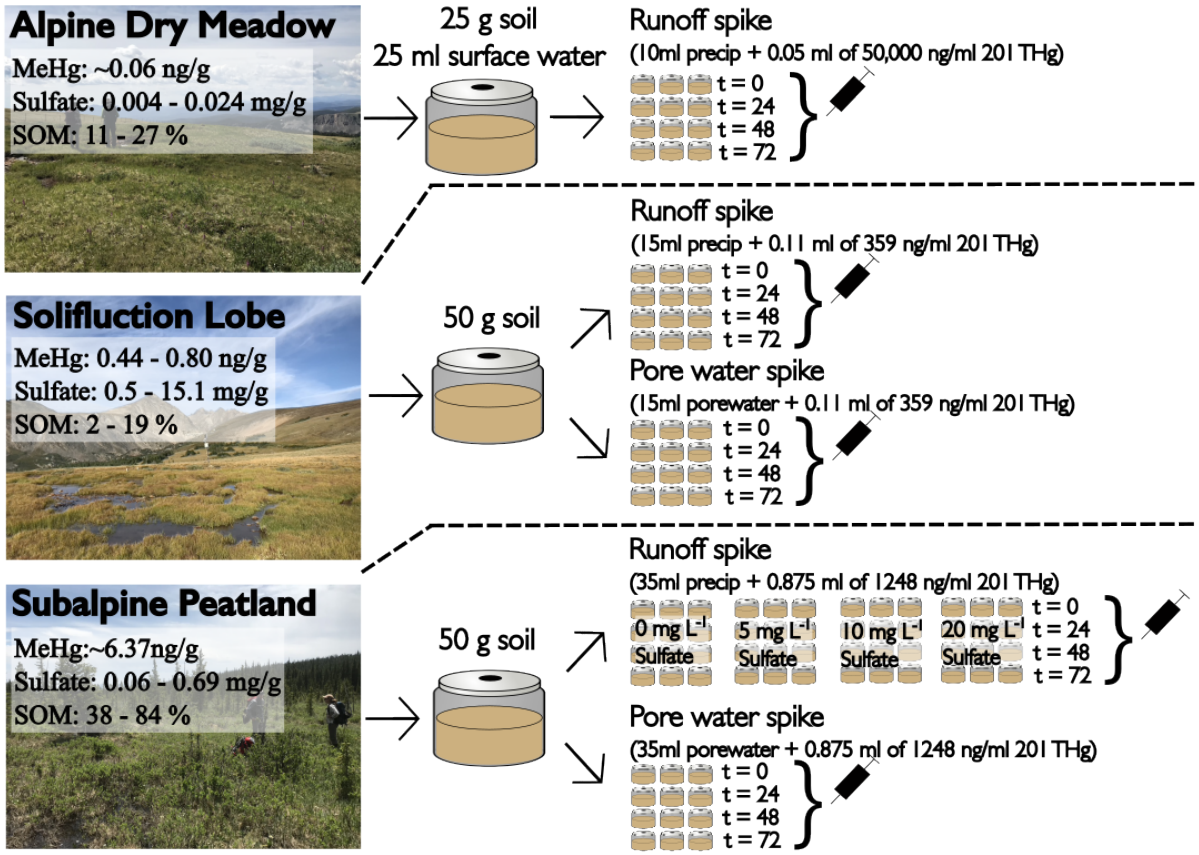

Figure S4-2: Schematic of methylmercury (MeHg) production assays in soils from alpine dry meadows, solifluction lobes, and subalpine peatlands. Ambient MeHg and extractable sulfate concentrations, as well as soil organic matter (SOM) percentages are indicated over the site photo in the left panel. Total mercury (THg) concentrations and spike volumes are noted in parentheses for each set of incubations.

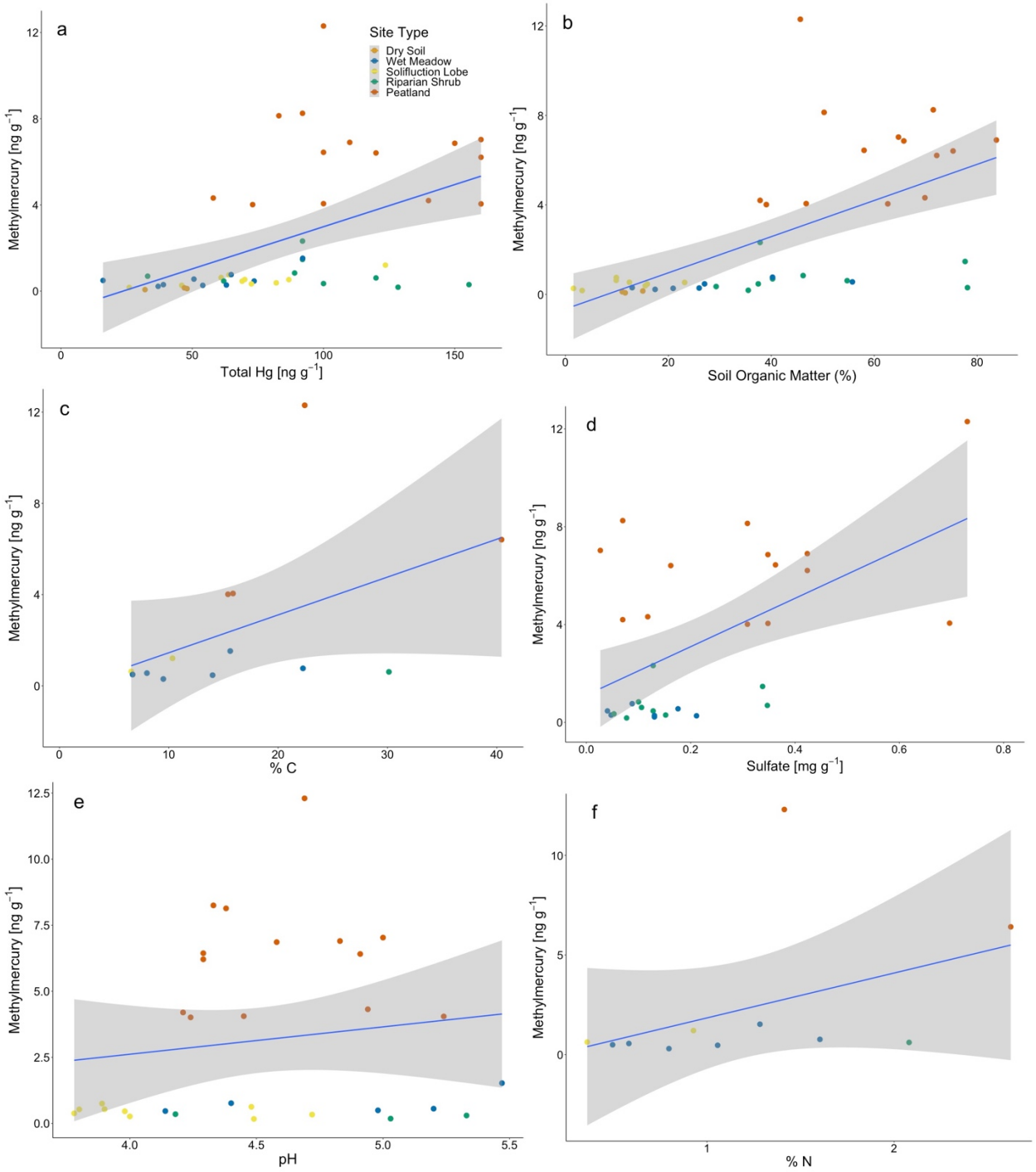

Figure S4-3: Relationships between MeHg and THg (a), soil organic matter (b), total percent carbon (c), extractable sulfate (d), pH (e), and percent total nitrogen (f). A significant relationship ($p < 0.05$) was only observed for a – d.

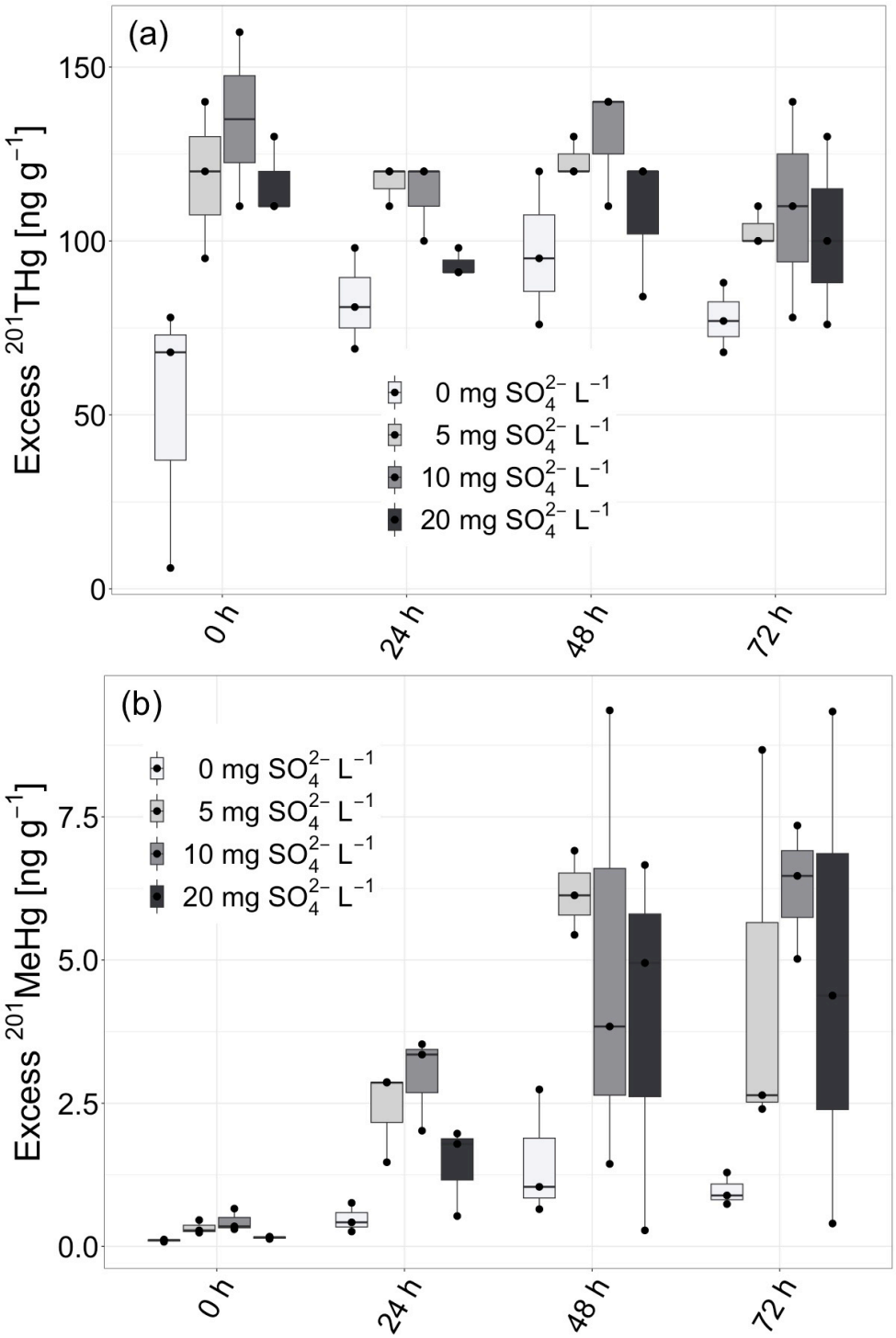

Figure S4-4: Excess total mercury ($T^{201}Hg$) (a) and methylmercury ($Me^{201}Hg$) (b) concentrations across the duration of the incubation experiment in sulfate amended subalpine peatland soils. The interquartile range is represented by the box, the median is represented by the horizontal line, 1.5 interquartile range is represented by the whiskers, and measured data points are represented by the black dots.

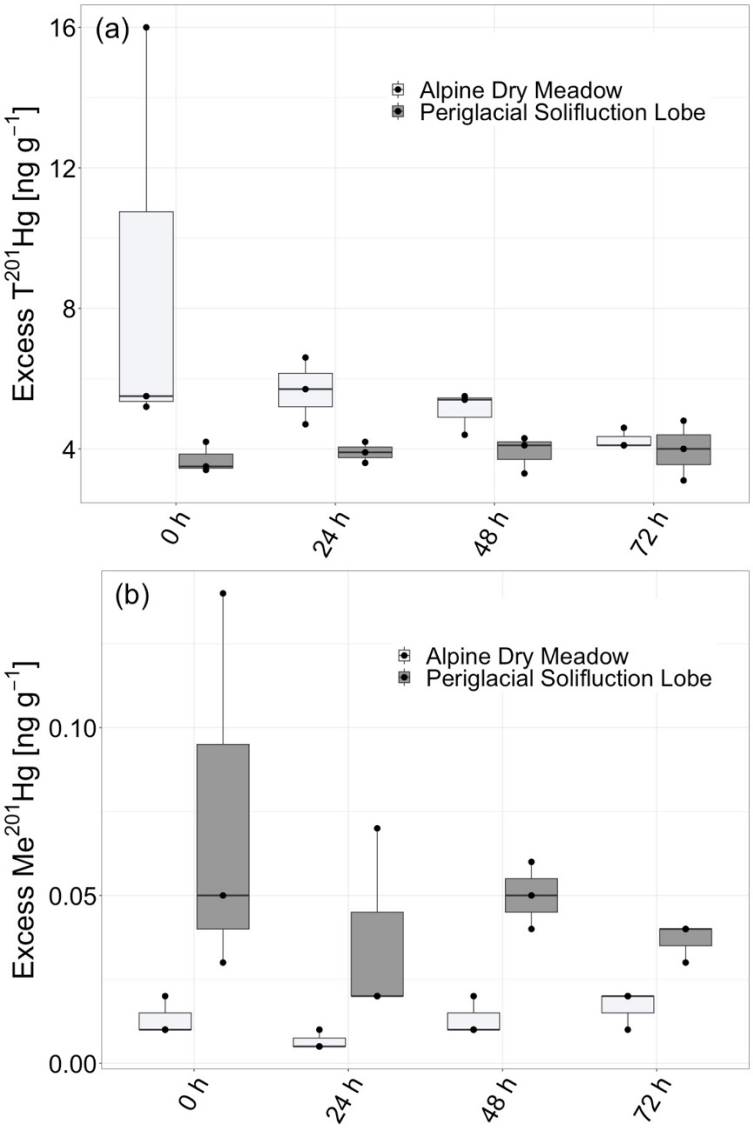

Figure S4-5: Excess total mercury ($T^{201}Hg$) (a) and methylmercury ($Me^{201}Hg$) (b) concentrations across the duration of the incubation experiment in alpine dry meadow and solifluction lobe soils. The interquartile range is represented by the box, the median is represented by the horizontal line, 1.5 interquartile range is represented by the whiskers, and measured data points are represented by the black dots.

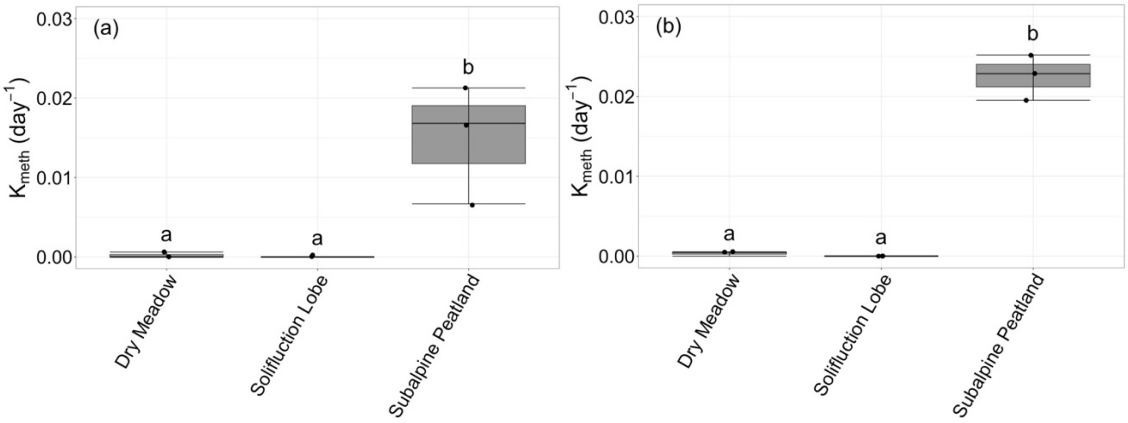

Figure S4-6: Mercury methylation rates (K_{meth}) for alpine dry meadow, solifluction lobe, and subalpine peatland soils for (a) 48 h and (b) 72 h. Lower case letters indicate significance. The interquartile range is represented by the box, the median is represented by the horizontal line, 1.5 interquartile range is represented by the whiskers, and measured data points are represented by the black dots.

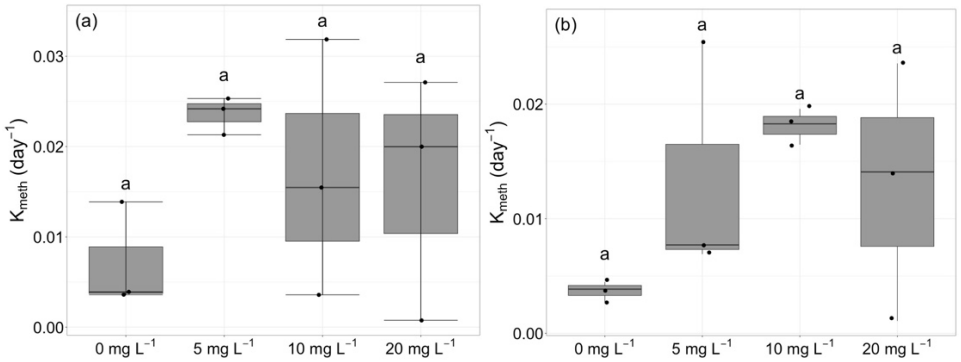

Figure S4-7: Mercury methylation rates (K_{meth}) for subalpine peatland soils for 48 h (a) and 72 h (b) of the sulfate treatment (0, 5, 10, and 20 mg SO_4^{2-} L^{-1}) incubation experiment. No significant differences were observed among the treatments (p > 0.05). The interquartile range is represented by the box, the median is represented by the horizontal line, 1.5 interquartile range is represented by the whiskers, and measured data points are represented by the black dots.

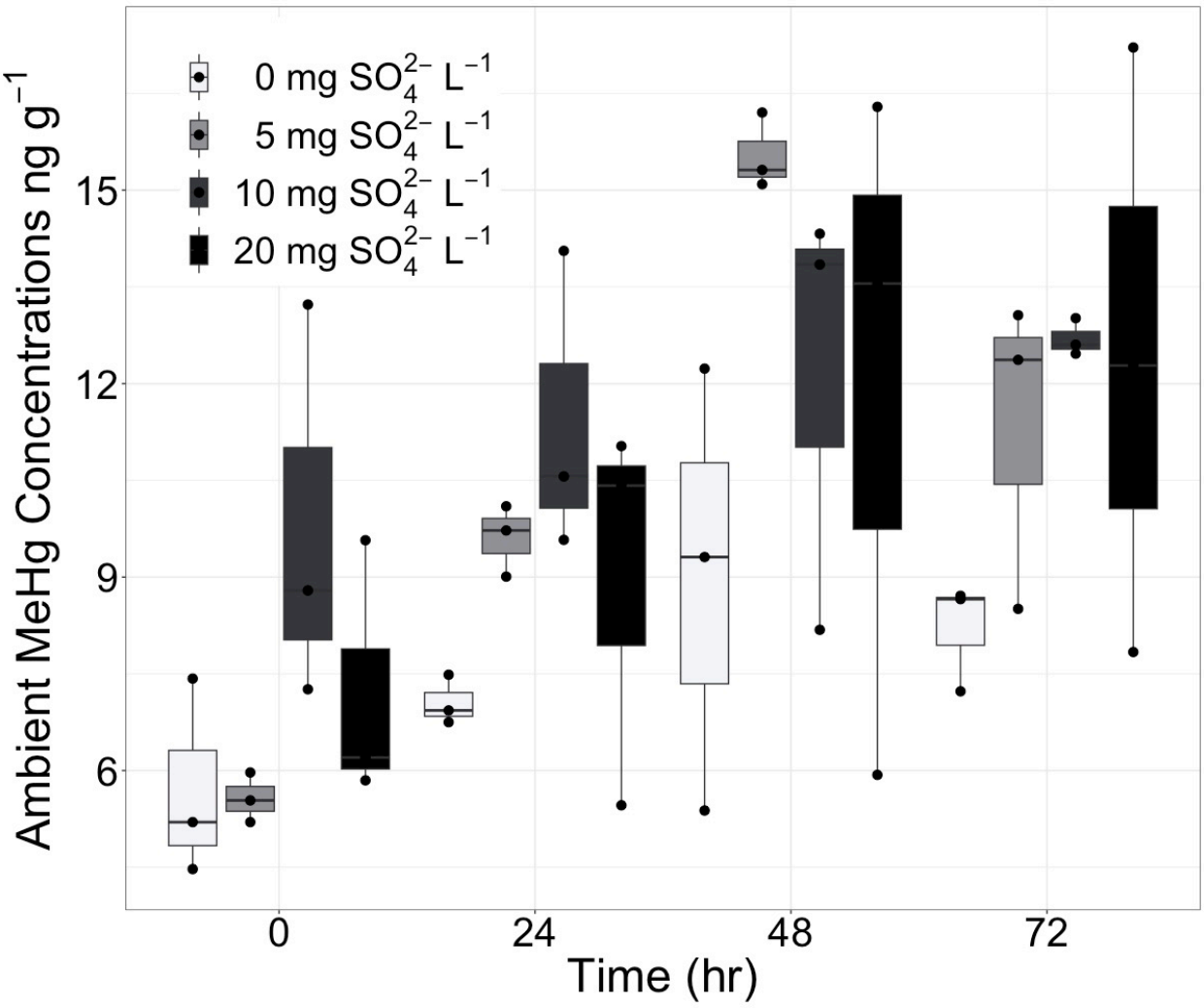

Figure S4-8: Ambient methylmercury (MeHg) concentrations for subalpine peatlands soils at each time point for all sulfate treatments (0, 5, 10, 20 mg SO_4^{2-} L^{-1}).

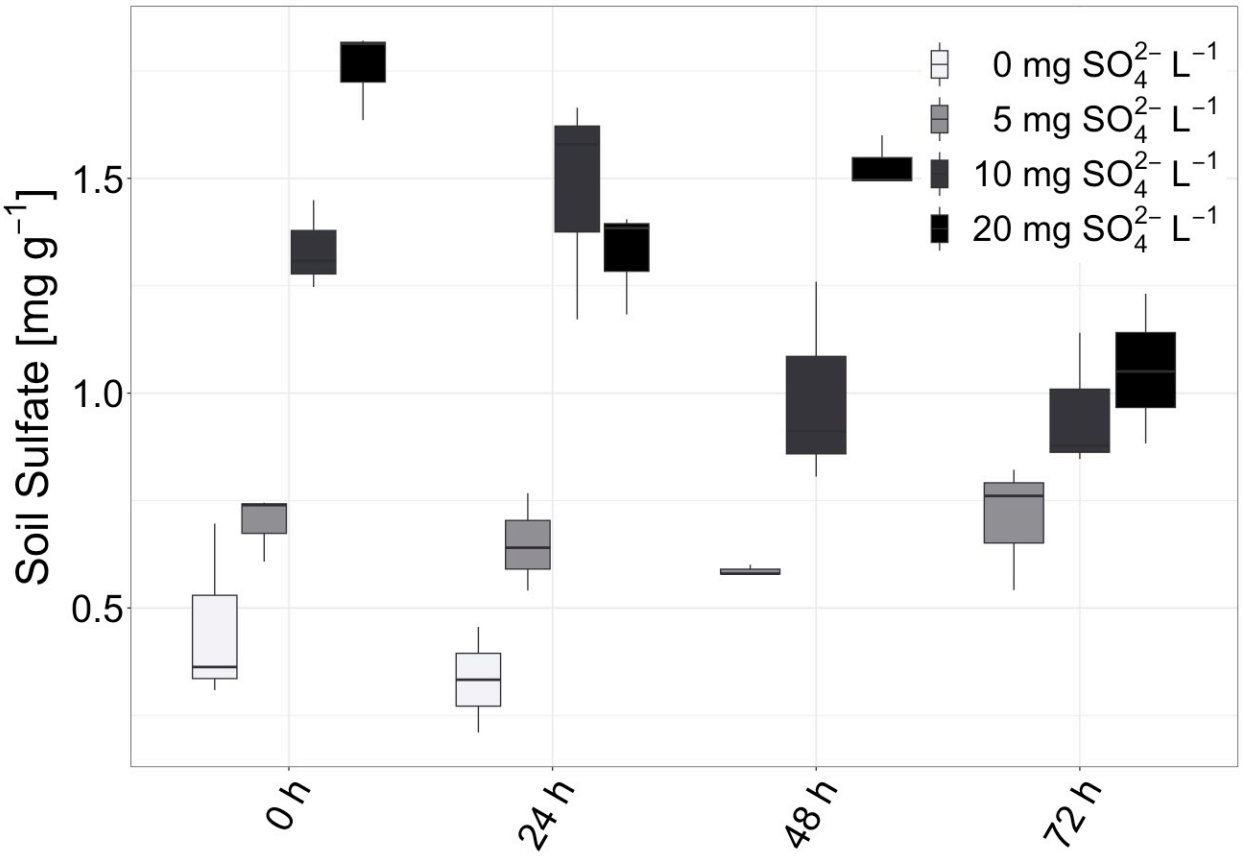

Figure S4-9: Subalpine peatland extractable soil sulfate concentrations in mg SO_4^{2-} per g dry soil for each sulfate treatment across the 3-day incubation experiment. The interquartile range is represented by the box, the median is represented by the horizontal line, and the 1.5 interquartile range is represented by the whiskers. For the 0 mg L^{-1} sulfate amendments, sulfate concentrations were only measured for the 0 h and 24 h time points.

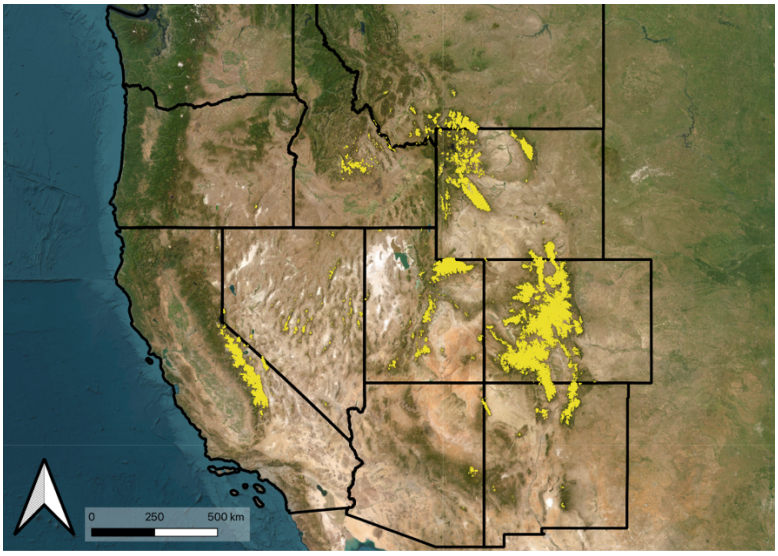

Figure S4-10: Spatial extent of alpine and subalpine wetlands (yellow highlight) across the western U.S. (data extracted from the U.S. Fish and Wildlife Services National Wetlands Inventory). The total land cover of these wetlands is ~ 2,230 km^2.

Supplemental Tables

Table S4-1: Previously documented trends in sulfate concentration in runoff from high elevation ecosystems globally. NA indicates not available.

Site Name	Lat	Long	Reference	Bedrock	Increase sulfate export rate (kg ha-1 yr-1)*	Sulfate concentration range (mg L-1)*	Sulfate flux range (kg ha-1 yr-1)*	# Sites	Site type
Colorado Rockies	40.29	-105.66	Baron et al., 2009	Biotite gneiss (80%) and silver plume granite (20%)	33.2% increase from 1991-1999 period to 2000-2006 period in export (~10 -> 30)	0.5 ± 0.19 - 0.86 ± 0.28	3.64 - 4.85	1	Streams
Argentine Andes	-41.16	-71.89	Chillrud et al., 1994	NA	NA	0.28 - 17.10	NA	1	Catchments
Italian Alps	45.74	7.40	Colombo et al., 2019	Metamorphic rocks	NA	0.29 - 21.87	NA	4	Ponds
Colorado Rockies	40.05	-105.63	Crawford et al., 2019	Precambrian Sillimanite-biotite gneiss and granite	> 200% increase between 1984 - 2015 for fluxes	2.88 - 4.80	10 - 30	1	Streams
Swiss Alps	46.42	8.68	Del Siro et al., 2023	NA	NA	0.3 - 45.0	NA	2	Streams
Iceland	NA	NA	Gislason et al., 2009	NA	NA	NA	NA		Catchments
Colorado Rockies	40.29	-105.66	Heil et al., 2022	Andrews: Precambrian gneiss and silver plume granite; GLV: Precambrian sillimanite-biotite gneiss and granite	Concentrations increased at both sites but only fluxes increased in GLV and not in Andrews	0.80 - 7.88	NA	2	Catchments
Central Siberian Plateau	64.27	100.21	Kolosov et al., 2018	basalts	~150% increase between 1960 to 2011	NA	11.3 to 27.9	2	Catchments
Tatra Mtns	49.22	20.04	Kopacek et al., 2019	Granodiorite, granite, felsic gneiss, and mica schist	Concentrations decreasing across all sites and at higher rates with more soil cover	NA	NA	1	Catchments

Himalayas	27.93	86.7	Lami et al., 2010	Late Tertiary Granites	>200% increase in sulfate concentrations from 1990 to 2008 (~50 - 200 ueq/L)	2.76 - 20.16	NA	2	Lakes
Colorado Rockies	39.48	-105.81	Manning et al., 2013	Precambrian metamorphic rocks (gneiss, schist, amphibolite)	Increased by 29 m/L per decade from 1980 to 2011 (~200% increase from 1980 to 2011)	50 - 150	NA	2	Catchments
Colorado Rockies	38.6	-106.4	Manning et al., 2024	NA	~2% site median increase every year for sulfate concentrations (doubling over the past 30 y)	NA	NA	8	Catchments
Colorado Rockies	39.12	-107.19	Mast et al., 2011	Precambrian granite and gneiss, Tertiary basalt flows, Precambrian quartzite	Increasing by 0.87 - 3.82 ueq/L/yr from 1985-2008 across the 6 lakes	NA	NA	6	Lakes
Colorado Rockies	39.12	-107.19	Mast et al., 2011	Precambrian granite and gneiss, Tertiary basalt flows, Precambrian quartzite	Decreasing trends at two locations (Flat Tops and Mount Zirkel) and increasing in Weminuche	0.24 - 8.4	NA	7	Lakes
Italian Alps	46.45	8.44	Rogora et al., 2020	Gneiss, limestone, dolomite, and calcshists	~300% increase from 1984 to 2017	2.4 - 9.6	NA	2	Lakes
Himalayas	27.9	86.81	Salerno et al., 2016	sillimanite gneisses calc-silicates, amphibolites, and K-feldspar augen gneisses	Up to 400% increase from 1990 to 2000	3.84 ± 6.2 - 6.1 ± 11.8	NA	20	Lakes
Peruvian Andes	-9.17	-77.58	Santofimia et al., 2016	NA	NA	2.0 - 600	NA	9	Lagoons
Austrian Alps	47.1	10.86	Schreder et al., 2023	Crystalline bedrock	200-500% increase in sulfate concentrations from 1982 to 2020 across small to strong rock	NA	NA	3	Lakes

					glacier metlwater influence lakes				
Austrian Alps	47.1	10.86	Schreder et al., 2023	Crystalline bedrock	No clear increasing trend in areas with no rock glacier input	0.2 - 12.5	NA	3	Lakes
Austrian Alps	46.74	13.84	Sommaruga Wograth et al., 1997	Varied bedrock	Between 1985 and 1995 sulfate has increased by ~150% in 57 lakes	1.9 to 4.8	NA	57	Lakes
Central Alps	46.47	8.72	Steingruber et al., 2021	Pre-Triassic basement and metamorphosed sedimentary {aleozoic and Early Mesozoic	~350% increase in concentrations from 1980 to 2020	2.4 - 10.8	NA	1	Lakes
Northwest Territories	64.38	-123.11	Tank et al., 2016	Varied bedrock: Precambrian basment, volcanic, metamorphic, siliciclastic, mixed sedimentary, carbonate, alluvial deposits	~75% increase in sulfate loads from 1970 to 2010	NA	~9.08 - 18.0 kg/ha/yr (~17 - 35 Gmol/yr)	1	Rivers
Austrian Alps	46.97	10.95	Thies et al., 2007	Oetztal metamorphic complex	700-2000% increase in sulfate concentrations (RAS = 9.1 to 216 mg/L, SOS = 1.2 to 9.6 ueq/L)	1.2 - 216	NA	2	Lakes
Italian Alps	45.52	7.32	Tiberti et al., 2019	NA	Sulfate increased significantly across all lakes but don't have a percentage change value	NA	NA	25	Lakes
Colorado Rockies	39.6	-105.88	Todd et al., 2012	Precambrian metamorphic rocks (gneiss, schist, amphibolite)	29.1 mg/L increase in sulfate concentrations per decade. (~200% increase from 1975 to 2015)	~50 - 150	NA	1	Rivers

Alaska	61.94	-162.88	Toohey et al., 2016	NA	~65% increase in sulfate fluxes Gg/yr) between 1982 to 2014 in Yukon	NA	52.8 - 88.0 kg/ha/yr (4500 - 7500 Gg/yr)	1	Rivers
Yukon Territory	63.11	-135.11	Van Stempvoort et al., 2023	NA	0.05 to 3.32 mg/L increase per year from 1190s to 2020s (60-150% increase in concentration across those decades)	~30 - 140 mg/L	NA	8	Streams
Central Eastern Alps	46.84	10.52	Wanner et al., 2023	Polymetamorphic paragneisses and micashists	NA	NA	NA	6	Streams
Colorado Rockies	38.86	-107.06	Zhi et al., 2020	Primary sandstone and mudstone also with plutonic rock and glacial drift	~20% increase in sulfate concentrations from 2016 to 2019	8 to 9.5 mg/L	NA	1	Streams
Northwest Territories	67.33	-135.12	Zolkos et al., 2018	Carbonate and sulfide-bearing units containing carbonates, sulfides, and silicates	~100% increase in sulfate fluxes from 1980 to 2015	NA	95 - 205 (7 to 15 Gmol/yr)	8	Streams

*Units unless otherwise noted.

Table S4-2: Soil physiochemical variables for North Boulder Watershed sites used in this study. ND indicates not determined.

Site	Bulk density (g/cm^3)	THg (ng/g)	MeHg (ng/g)	Sulfate (mg/g)	SOM (%)	Water content (%)	pH	Total C (%)	Total N (%)	K_{meth} (day^{-1})
Alpine dry meadow	0.76	48.2 ± 15.8	0.08 ± 0.09	0.01 ± 0.002	22.9 ± 21.6	15.9 ± 9.9	4.7 ± 0.2	14.6 ± 7.4	0.8 ± 0.2	-0.001 ± 0.001
Solifluction lobe	1.06	79.3 ± 25.8	0.62 ± 0.43	6.18 ± 5.43	15.7 ± 11.8	55.4 ± 21.6	4.3 ± 0.5	11.5 ± 6.1	0.8 ± 0.3	-0.009 ± 0.007
Peatland	0.16	98.3 ± 21.1	6.77 ± 3.06	0.36 ± 0.27	70.6 ± 7.3	84.5 ± 2.5	4.4 ± 0.2	18.9 ± 5.0	2.0 ± 0.9	0.027 ± 0.004
Alpine wet meadow	0.48	54.5 ± 22.4	0.54 ± 0.41	0.09 ± 0.06	32.1 ± 18.6	64.4 ± 15.0	4.8 ± 0.1	13.4 ± 5.4	1.0 ± 0.4	ND
Riparian shrub	0.31	96.9 ± 36.0	0.80 ± 0.69	0.14 ± 0.09	50.8 ± 19.6	41.4 ± 16.2	4.7 ± 0.5	32.0 ± 1.6	0.3 ± 0.1	ND

Table S4-3: Methodological details for sediment analysis of total mercury (THg) established by the USGS Mercury Research Laboratory (Peterson et al., 2023; U.S. EPA, 2002). Quality assurance acceptance criteria reported for analytical methods.

Analyte, Matrix, and Method	**Quality Control Objective**	**Acceptance Criteria (Result)**	**Description**	**Frequency**	**Instrumentation**
THg in Soil by Acid Digestion	Quality Check Standards	< 5%	Average ongoing check of instrument calibration		Brooks Rand MERX-M Automated Methylmercury System Thermo Scientific iCAP RQ
	Method Triplicate	< 20%	Relative standard deviation of THg concentration for triplicate analysis of a sample.	Once every 15 samples	
	Certified Reference Material (IAEA-475)	80 - 120%	Certified Reference Material prepared and analyzed similar to samples.	Once every 15 samples	

Table S4-4: Methodological details for sediment analysis of methylmercury (MeHg) established by the USGS Mercury Research Laboratory (Hintelmann et al., 1995; Hintelmann & Evans, 1997; U.S. EPA, 1998). Quality assurance acceptance criteria reported for analytical methods.

Analyte, Matrix, and Method	Quality Control Objective	Acceptance Criteria (Result)	Description	Frequency	Instrumentation
MeHg in Soil by Distillation and Isotope Dilution	Mass Bias Correction	< 5%	Correction for instrument mass bias for the isotope used for dilution ($Me^{199}Hg$) relative to $Me^{202}Hg$. Relative standard deviation for five analyses.	At instrument calibration	Brooks Rand MERX-M Automated Methylmercury System Thermo Scientific iCAP RQ
	Isotope Dilution Calibration	< 5%	Calibration of mass of isotope addition to samples ($Me^{199}Hg$ or $Me^{204}Hg$). Relative standard deviation for five analyses.	At instrument calibration	
	Instrument Calibration Check Standard	85 - 115%	Percent recovery for the analysis of a MeHg standard by isotope dilution during sample analysis.	Once every 6 samples	
	Method Triplicate	< 25%	Relative standard deviation of MeHg concentration for triplicate analysis of a sample.	Once every 15 samples	
	Certified Reference Material (IAEA-405, estuarine sediment)	80 - 120%	Certified Reference Material prepared and analyzed similar to samples.	Once every 15 samples	

C. Supplemental Materials for Chapter V

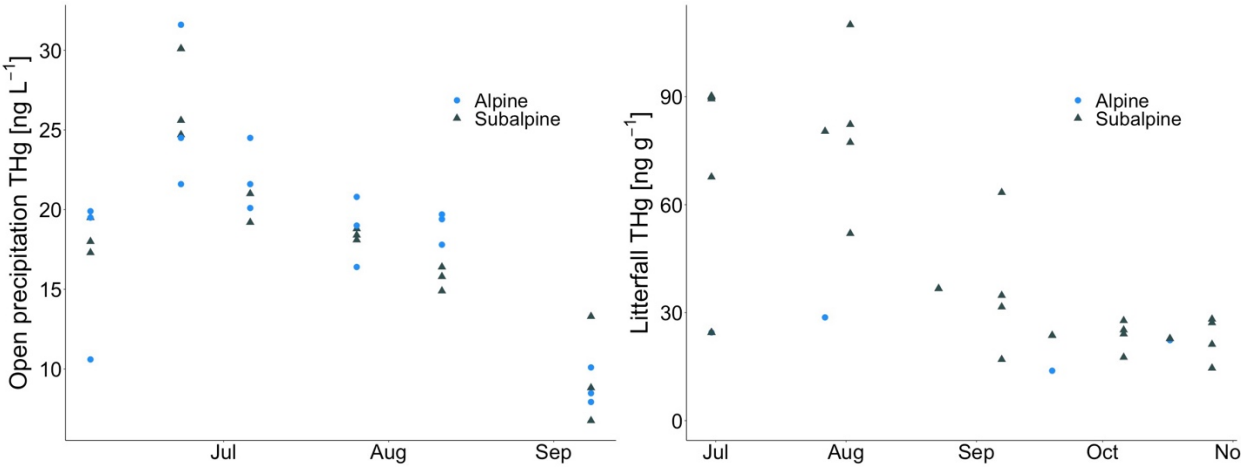

Table S5-1: Open precipitation and litterfall total mercury (THg) concentrations across the sampling period.

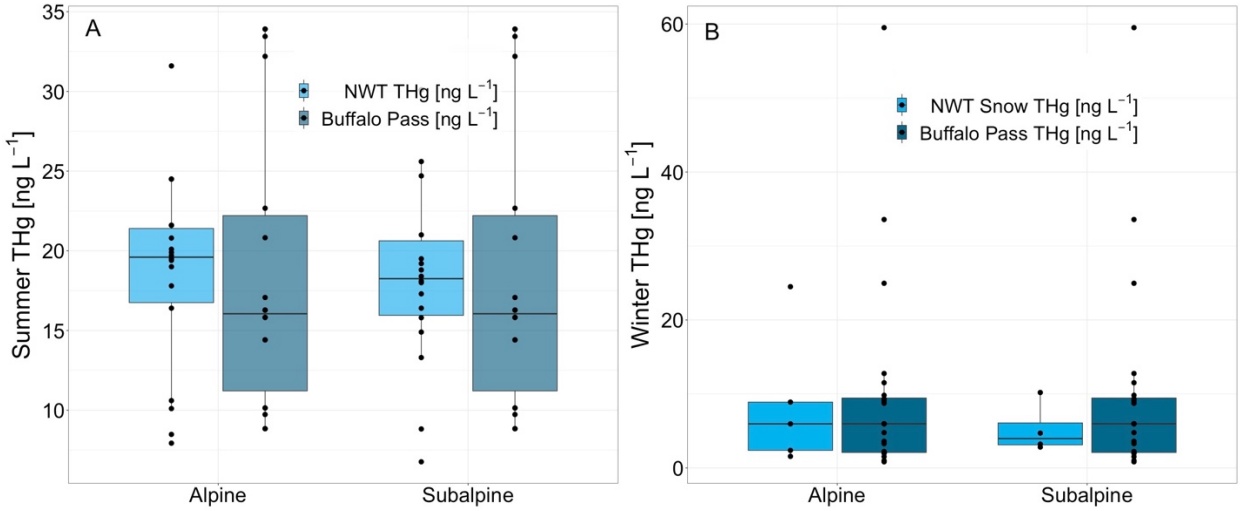

Table S5-2: Comparison of open precipitation total mercury (THg) concentrations from June – September at NWT ridge and Buffalo Pass (A) and comparison of snow concentrations at NWT Ridge to Buffalo Pass winter deposition concentrations (B). Concentrations were not significantly different between the two locations for either the alpine or the subalpine for either the summer or winter period (Wilcoxon test, $p > 0.05$).

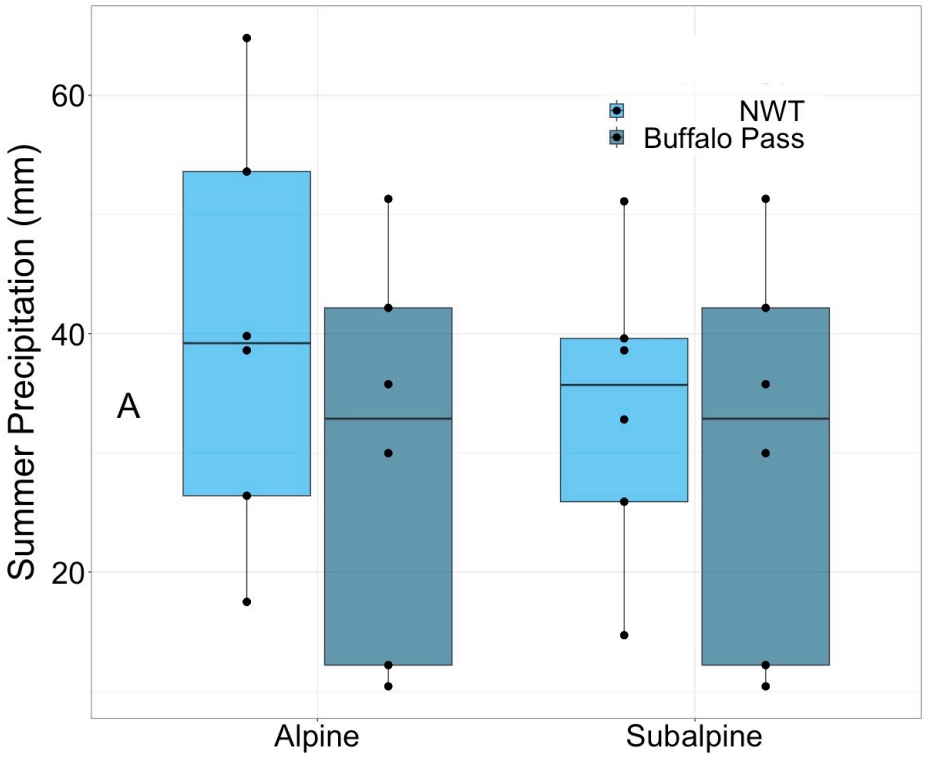

Table S5-3: Comparison of summer precipitation volumes between NWT-LTER and Buffalo Pass.

While NWT Ridge had higher precipitation volumes on average compared to Buffalo Pass, the difference between location was not significant for either the alpine or the subalpine (Wilcoxon test, $p > 0.05$).

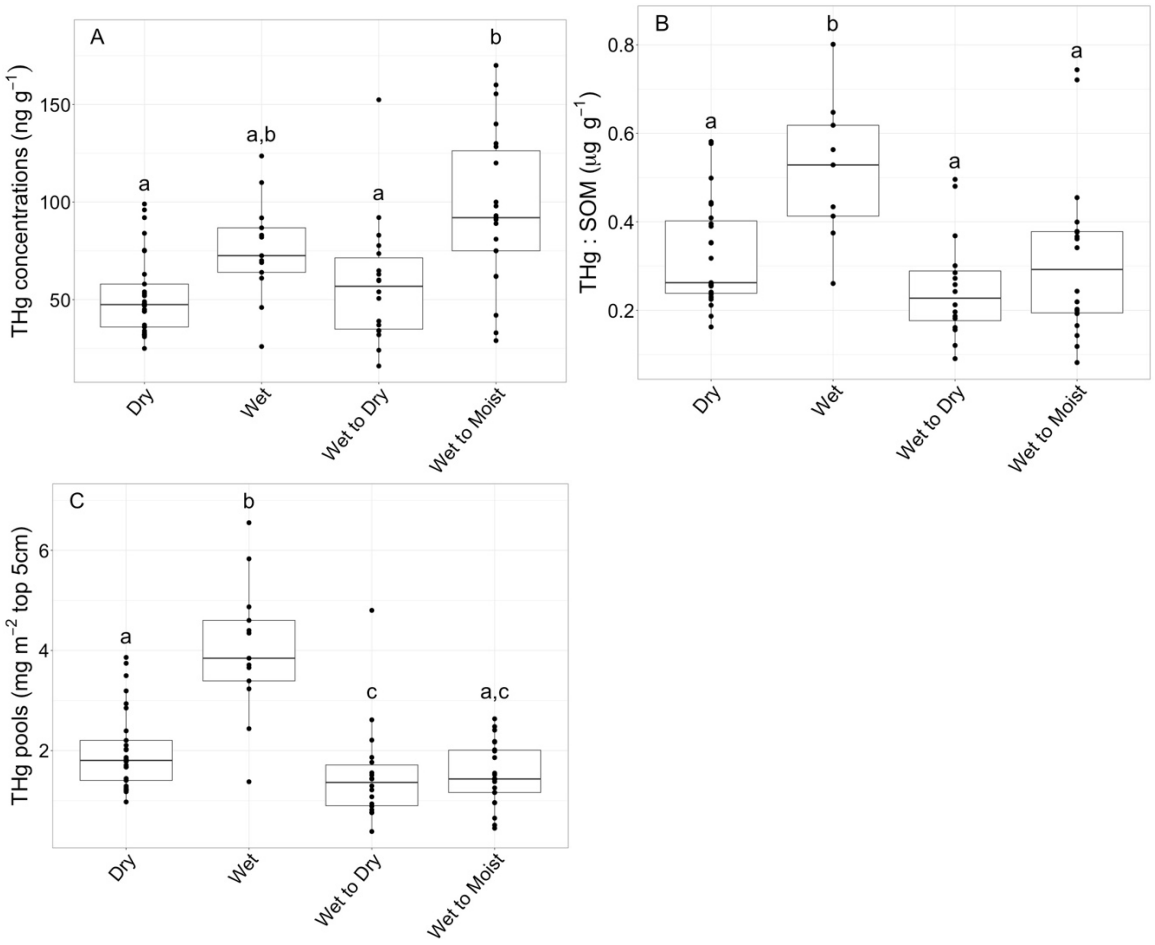

Table S5-4: Soil total mercury (THg) concentrations (A), THg concentrations normalized to soil organic matter (SOM) (B), and THg pools (C) across different soil moisture groups in the alpine. Lower case letters indicate significance among soil moisture groups.

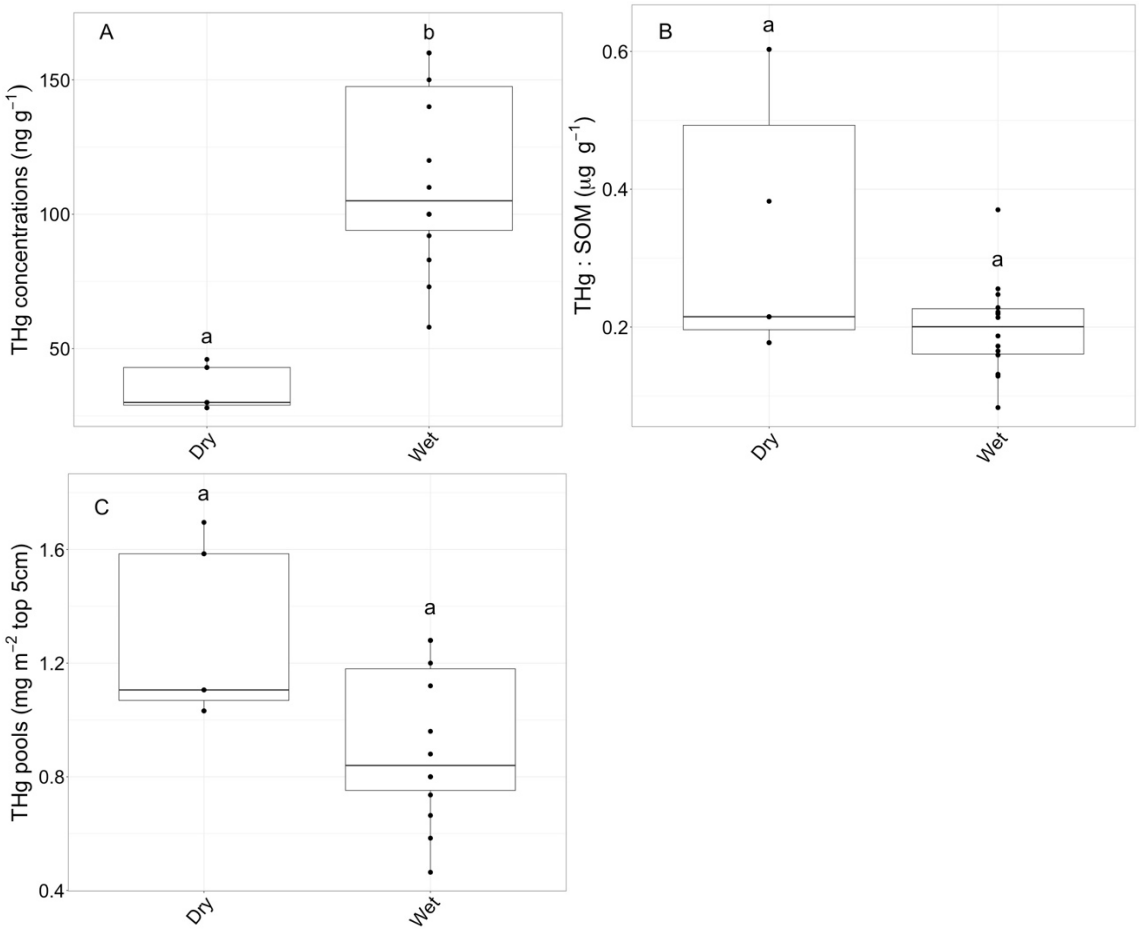

Table S5-5: Soil total mercury (THg) concentrations (A), THg concentrations normalized to soil organic matter (SOM) (B), and THg pools (C) across different soil moisture groups in the subalpine. Lower case letters indicate significance between soil moisture groups.